Gönnert, Gabriele; Dube, Shishir K.; Murty, Tad; Siefert, Winfried

6. Storm Surges generated by Tropical Cyclones - Case Studies

Die Küste

Zur Verfügung gestellt in Kooperation mit/Provided in Cooperation with:
Kuratorium für Forschung im Küsteningenieurwesen (KFKI)

Verfügbar unter/Available at: https://hdl.handle.net/20.500.11970/101446

Vorgeschlagene Zitierweise/Suggested citation:
Gönnert, Gabriele; Dube, Shishir K.; Murty, Tad; Siefert, Winfried (2001): 6. Storm Surges generated by Tropical Cyclones - Case Studies. In: Die Küste 63 Sonderheft. Heide, Holstein: Boyens. S. 291-454.

6. Storm Surges generated by Tropical Cyclones – Case Studies

6.1 North America

6.1.1 East Coast of U.S.A.

HARRIS (1956) summarized the status of research on hurricane-generated storm surges in the United States up to the early 1950's. He mentioned the study of CLINE (1926) as typical of that period.

Much of the research on storm surges has never been formally published, largely because the people performing the work in relative isolation have not been satisfied with the results. Much of the material, which has been published, contains a number of questionable statements, mainly in the nature of oversimplification. After the tremendous losses in the northeastern United States due to hurricanes in 1954, congress directed both the U. S. Army Corps of Engineers and the weather bureau to conduct an intensified study of the causes, behaviour and methods of forecasting these storms. A large fraction of the available funds are to be spent in studying methods of protection against inundation from the sea.

Thus, one can consider this as the beginning of systematic studies on the storm surges due to hurricanes on the East Coast of the United States. First, some factual information will be considered before proceeding to models.

WIEGEL (1964) stated that during the period 1900–55 there was more than 11, 750 deaths caused by hurricanes in the United States. The worst storm surge (from the point of view of loss of life) in United States history occurred in September 1900 when more than 6000 people drowned, most of them at Galveston, Texas (Price 1956). During the 14-year period 1940–53, the loss of life due to hurricane-generated surges over the globe was 3744; 590 of those deaths occurred in the United States (WIEGEL, 1964).

DUNN (1958) mentioned the years and the locations of some of the greatest storm surges on the east coast of United States: Galveston (1900 and 1915), Tampa Bay (1921), Miami (1926), Palm Beach and Lake Okeechobee (1928 and 1949), Florida Keys (1953), and New England, particularly Narragansett Bay (1938 and 1954). The maximum storm surge from these was about 12.5 ft (3.8 m) above mean low water.

HARRIS (1956) and DUNN (1958) mentioned forerunners to storm surges and also resurgence. REDFIELD and MILLER (1957) studied these phenomena in detail and these will be considered now. Also, these authors provided a review of the literature up to 1957; some pertinent information will be extracted.

Between 1635 and 1938 there were at least six major hurricanes on the coast of New England (TANNEHILL, 1950) and between 1938 and 1957 there were at least another six. Since 1874 at least 40 hurricanes passed within 200 nautical miles (370 km) of Rhode Island. NAMIAS (1955) analyzed the tracks of hurricanes and showed that the region most frequently traversed during 1935–55 near the Gulf of Maine was at 40° N, 65° W. One important point made by REDFIELD and MILLER (1957) is that although more than three quarters of the deaths due to hurricanes are caused by the storm surge, until the mid-1950's little attention was paid to the water level problem and all the consideration was given to meteorological problem.

The database for the study by REDFIELD and MILLER (1957) is the following: (1) September 21, 1938, (2) September 14–15, 1944, (3) August 31, 1954 (Carol), (4) September 11, 1954 (Edna), (5) October 15–16, 1954 (Hazel). The tracks of these hurricanes are shown in Fig. 6.1. The three phenomena studied were forerunners, hurricane surge, and resurgence.

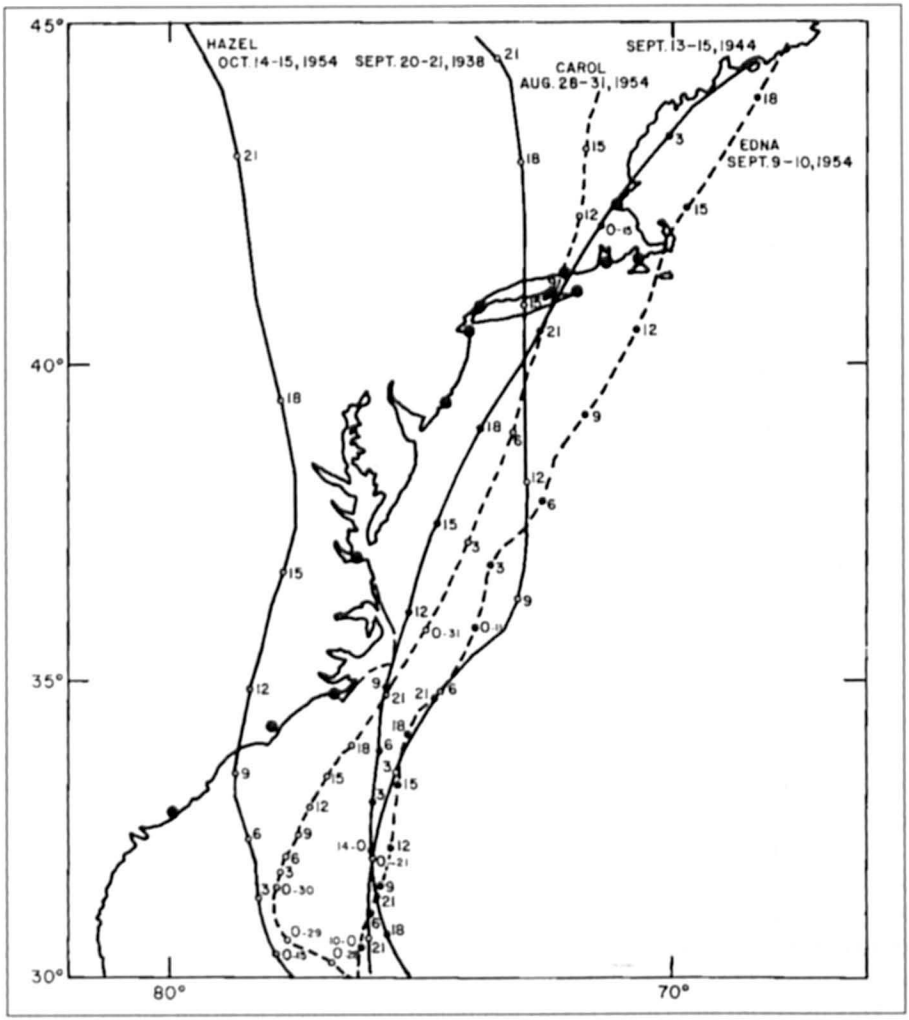

Fig. 6.1: Tracks of some of the hurricanes that affected the New England States. Solid circles show the locations of the tide gauges. Circles on the tracks represent the hours (GMT) and the small numbers denote the dates (REDFIELD and MILLER, 1957)

A forerunner is the gradual rise in sea level along the coast that precedes the arrival of the hurricane, and which may occur while the storm center is at a great distance from the coast regardless of whether or not it reaches the point of observation. The hurricane surge is the sudden and substantial rise in water level that accompanies the violent winds of the storm. Resurgences include a number of phenomena that occur after the passage of a storm center. They may be attributed in general to the free motion of water in returning to the normal level but are augmented in some cases by wind blowing in a changing direction.

CLINE (1920, 1926 and 1933) noticed forerunners in the Gulf of Mexico and called attention to their importance in the prediction of the storm arrival. The sea level began to rise (above the predicted tide) 1 or 2 d before the arrival of the storm. Elevations of several feet were noticed before the rapid rise due to the storm surge itself. Cline explained the forerunners as being due to transport of water by the swell that arrives in advance of the hurricanes.

Table 6.1: Relation of duration of surge to size and speed of storm (REDFIELD and MILLER, 1957)

Storm	Time (h) half level Preceded maximum Level	Speed at Coast ($km \cdot h^{-1}$)	Diameter of 980-mb Isobar (km)	Time (h) Pressure < 980 mb
1938	1.0–1.5	96	270	3.2
1944	2.1–2.2	67	241	4.2
1954 (Carol)	1.1–1.3	74	183	2.9
1954 (Edna)	2.0–2.3	63	261	4.8
1954 (Hazel)	3.0–5.0	46	261	6.5

Observations showed that if the tide gauge was within 50 nautical miles (93 km) to the left (in the Northern Hemisphere) of the storm track, or 100 nautical miles (185 km) to its right, the rate of rise of water level increased to more than 1 ft h^{-1} beginning 3 or 4 h before the passage of the center. (This rapid rise is the surge whereas the slow gradual rise before this is the forerunner).

Examples of the forerunners can be found in the storm surge records at Atlantic City and Sandy Hook. At Atlantic City during Hurricane Carol of September 1954, the water level began to increase even before the storm passed Cape Hatteras (260 nautical miles or 481 km to the south). This rise continued for 8–12 h at which time the storm center passed over Atlantic City and the wind shifted. Then the water level dropped abruptly and this was followed by resurgences. The hurricane of September 14–15, 1944, traveled close to the coast and the forerunner was not significant. REDFIELD and MILLER (1957) discounted the fall in barometric pressure as the cause of the forerunners. They cited wind as the main agent responsible. The fact that the water levels decreased abruptly when the wind shifted is another piece of evidence, according to them.

After the storm surge itself, on the outer coast, surges up to 8–9 ft (2.4–2.7 m) occurred. At Long Island, and along the coasts of Rhode Island and Massachusetts, water level deviation up to 18-ft (5.5 m) occurred (but part of this were wind-generated waves). However in Buzzards Bay, Narragansett Bay, Long Island Sound, etc., surges up to 15-ft (4.6 m) have occurred many times. These authors introduced the term „half-level time" to define the time required to develop from one half the maximum to the maximum water level achieved. For hurricanes crossing the coast of New England this time varied from 1.25 to more than 2 h (Table 6.1.). This half-level time that defines the sharpness of the surge varies in proportion with the storm speed at the time the storm crosses the coast, as can be seen from Table 6.1. This Table also lists the size of the storm as typified by the diameter of the 980-mb isobar and the time during which the pressure was less than 980 mb. This time is roughly twice the half-level time.

The storm surge amplitude (meters) along the ordinate versus distance (nautical miles) from the storm center along the abscissa is given in Fig. 6.2. It can be seen that maximum water levels occurred some 50–70 nautical miles (93–130 km) to the right of the storm center. However, REDFIELD and MILLER (1957) pointed out that the highest water levels following Hurricane Hazel of 1954 occurred close to the storm center, and 40 nautical miles (74 km) to

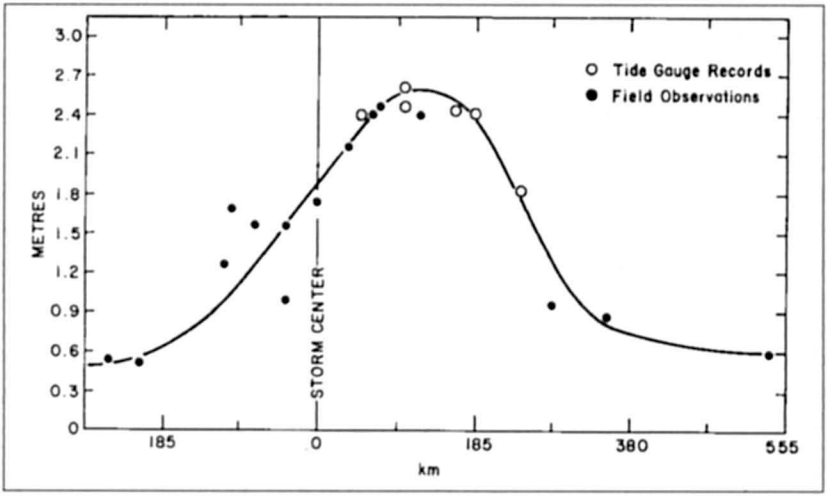

Fig. 6.2: Storm surge amplitude (ordinate) versus distance from storm center (abscissa) (REDFIELD and MILLER, 1957)

the right they were small. HUBERT and CLARK (1955) mentioned that for the coast of the Gulf of Mexico the maximum water levels occurred close to the storm center slightly to its right.

The time of occurrence of the maximum surges with reference to the passage of the storm center differed from one storm to another and from one location to another. If the storm center passed close to a tide gauge, usually, maximum surges occurred within 1 h before or after the storm passage. The differences in the time of occurrence of the maximum surges can be explained by differences in the exposure of the gauges and also by the fact that the wind and pressure centers of a hurricane need not coincide (MYERS, 1954).

The maximum surges on the southern New England Coast and their times of occurrence following the hurricane of September 21, 1938, are shown in Fig. 6.3 and 6.4 respectively. Similar information for Hurricane Carol of August 31, 1954, is given in Fig. 6.5 and 6.6. Large surges on the coast of southern New England might to some extent be accounted for by the presence of a wide and shallow shelf. This topographic effect is most noticeable between Montauk Point (at the eastern tip of Long Island) and Martha's Vineyard. However, greatest surges and most property damage occurred on the Narragansett Bay coast. Extreme surges

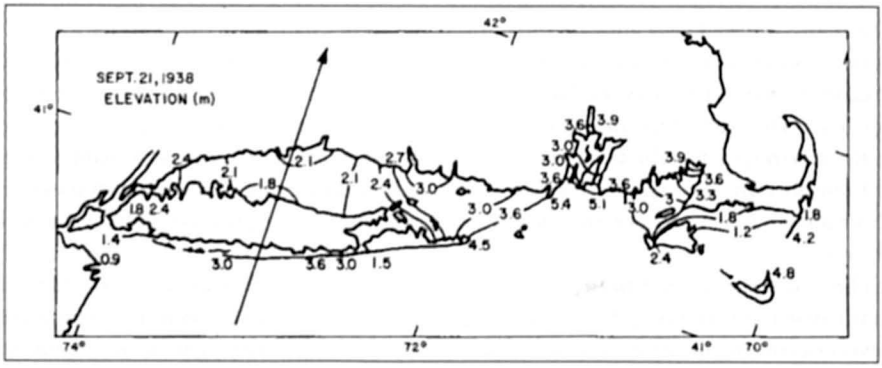

Fig. 6.3: Storm surge heights (meters) on the coast of the southern New England States. The arrow shows the track of the storm of September 21, 1938, that caused this surge (REDFIELD and MILLER, 1957)

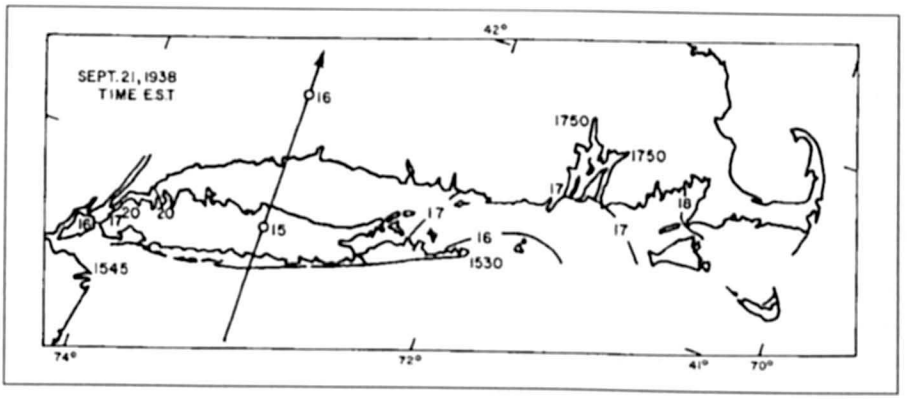

Fig. 6.4: Times of occurrence of maximum surge along the coast of the southern New England States on September 21, 1938 (REDFIELD and MILLER, 1957)

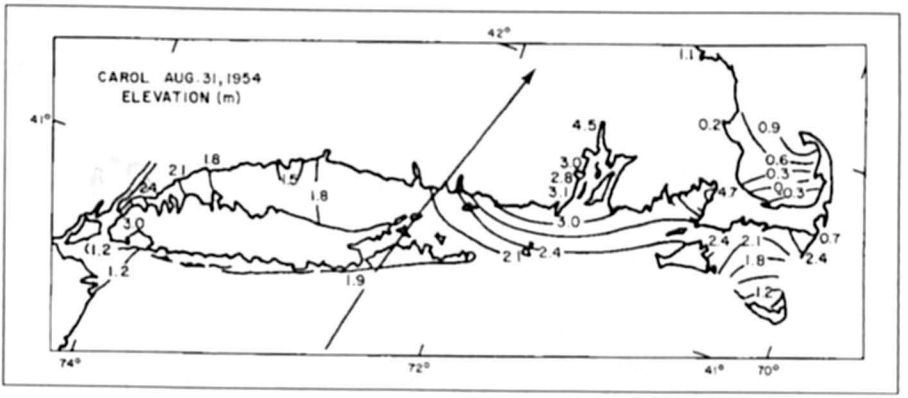

Fig. 6.5: Storm surge heights (meters) along the coast of the southern New England States following Hurricane Carol of August 31, 1954 (REDFIELD and MILLER, 1957)

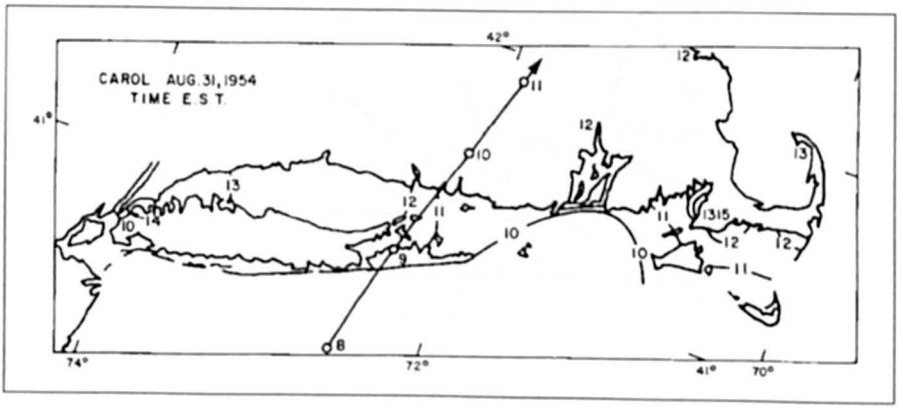

Fig. 6.6: Times of occurrence of maximum surge along the coast of the southern New England States following Hurricane Carol of August 31, 1954. The arrow shows the hurricane track (REDFIELD and MILLER, 1957)

up to 13 ft (4 m) were noted at Providence, Rhode Island, in water of depth less than 20 ft (6.1 m).

According to REDFIELD and MILLER (1957), Providence is among the most frequently flooded (due to surges) in the United States. Surges up to 11 ft (3.4 m) were observed in 1944 (but little damage occurred because the maximum surge coincided with low tide); 15 ft (4.6 m) surges were recorded on August 31, 1954, and there was evidence of 12 to 14 ft (3.7–4.3 m) surges in 1815. In Buzzards Bay, surges of 13 ft (4m) occurred in 1938 and 15 ft (4.6 m) surges were recorded following Hurricane Carol in 1954. A diary entry by Governor Bradford in 1635 (MORRISON, 1952) describes a 20 ft (6.1 m) surge on August 14–15 of that year. There is evidence of negative surges of 1–3 ft (0.3–0.9 m) in Cape Cod Bay and Nantucket Sound. Surges up to 4 ft (1.2 m) were noted at Boston and Portland. North of Cape Cod the amplitudes of surges become small and amount to about 1 ft at Eastport (Miane).

REDFIELD and MILLER (1957) paid particular attention to the resurgences, which are basically free oscillations of the water in trying to return to its normal level. Following Hurricane Carol of August 31, 1954, the damage at the Cape Cod area was a result of the resurgence. In Buzzards Bay, although the main surge had amplitudes of about 12 ft (3.7 m) along the western shore, resurgences with amplitudes up to 15 ft (4.6 m) occurred on the eastern shore. The resurgence following a 1938 hurricane in Buzzards Bay caused great damage and loss of life at Woodshole. In Long Island Sound, resurgences occurred following the hurri-

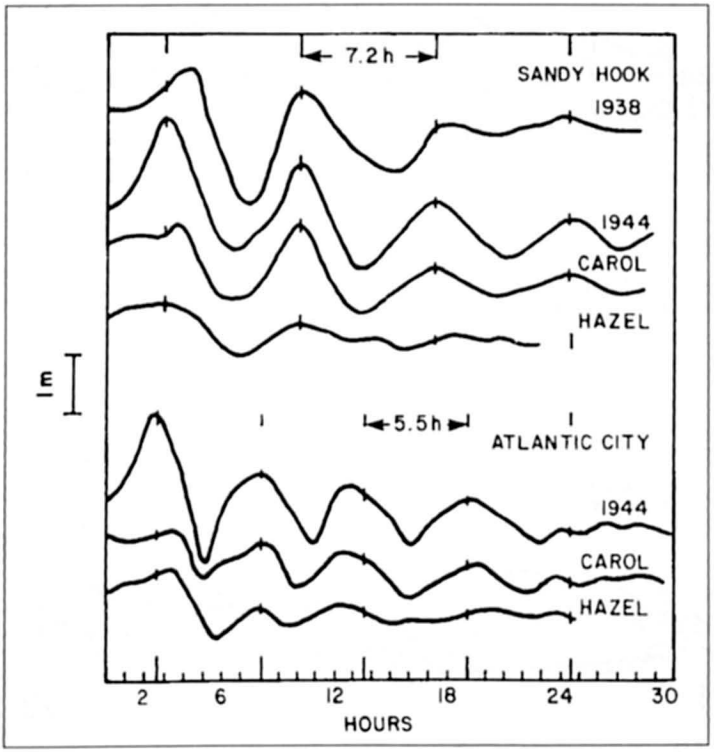

Fig. 6.7: Comparison of resurgences following the passage of several storms at Sandy Hook and Atlantic City. The times were adjusted (for each station) so that the time of occurrence of the first resurgence for the different storms coincide. Vertical ticks denote time separation of 7.2 h for Sandy Hook and 5.5 h for Atlantic City. Ordinate: water level (meters); abscissa: duration of surge (hours) (REDFIELD and MILLER, 1957)

canes of September 21, 1938, and August 31, 1954. Tide gauges at Atlantic City and Sandy Hook showed prominent resurgences (Fig. 6.7.). After the original surge reaches a maximum, the water level drops abruptly to low values and then increases again in a series of undulations with periods of several hours. These resurgences periods are about 5.5 h at Atlantic City and 7.2 h at Sandy Hook. The attenuation rate of the resurgences at Sandy Hook is about 0.07 h^{-1}. MUNK et al. (1956) explained these resurgences as due to edge waves.

Storm surges on the east Coast of the United States also occur as a result of extra-tropical cyclones. Some differences between storm surges due to tropical and extra-tropical storms on the east Coast of the United States are listed in Table 6.2.

Some models that were developed with the aim of hindcasting and eventually predicting storm surges will now be considered. The so-called bathystrophic storm surge (FREEMAN et al., 1957) was discussed earlier. PARARAS-CARAYANNIS (1975) used this approach to hind-

Table 6.2: Differences between hurricane-generated and extratropical storm generated surges

Parameter	Tropical system	Extratropical system
Size of storm	Small	Large
Representation on weather charts	Some times difficult to position on weather charts using ordinary weather reports. The vigorous portion of the storm may lie between two observing stations	Easier
Requirement of specialized observations such as satellite, weather, reconnaissance, radar, aircraft	Needed	Usually not required. Standard weather reports usually adequate unless mesoscale systems are embedded
Amplitude of surges	Greater The Maximum surge generated in the United States was at Gulfport, MS, following Hurricane Camille in August 1969: 7.5 m	Smaller surges of amplitudes up to 5 m can occur infrequently
Duration of surge	Short (Several hours to 1/2 d)	Long (usually 2–5 d). Severe erosion of coastline can occur
Inland inundation	Large	Little
Length of coastline affected by the surge	Less (usually < 160 km)	Several hundred kilometers
Geometry of the storm	Compact and nearly symmetrical	Ill-defined and sprawling geometry
Speed of movement of the storm	Variable	Slow motion generally along a regular track
Pressure gradients and wind stress associated with the storm	Easy to model the driving forces could be represented analytically	Difficult to model the driving fields

cast surges on the East Coast and Gulf of Mexico coast of the United States. The observed and computed surges at three locations are compared in Fig. 6.8. PARARAS-CARAYANNIS (1975) simulated surges due to the hurricanes listed in Table 6.3. Pertinent meteorological information is also listed in this table, which is used in the above calculations.

KAJIURA (1959) examined analytically, as well as empirically, hurricane-generated surges on continental shelves. Using dimensional analysis he showed that the surge is determined by the following two dimensionless ratios: V/c and L_2/L_1 where V is the speed of movement of the storm, c is the speed of long gravity waves on the shelf, L_2 is the scale of the storm and L_1 is the width of the shelf, the dynamic response of the water level is significantly influenced by the natural modes of oscillation on the shelf (the dynamic amplification for a one-dimensional case is between 1 and 2). The free oscillations again become important when one considers the transient aspects. Coriolis force becomes relevant if the scale of the disturbance is significant relative to c/f, where f is the Coriolis parameter. When the scale of the shelf is comparable with the scale of storm, the two-dimensional aspects of hurricanes must be considered.

Other important results from KUJIURA'S (1959) study are the following. If the storm moves perpendicular to the coastline from the sea, then the maximum surge always occurs a little later than the time of the nearest approach of the storm center to the water level station. For any other type of track, the maximum surge can occur either before or after the storm center approaches nearest to the observing station. When the storm moves inland from the sea, the maximum surge is found to the right of the track. The dynamic amplification of the surge is maximum when the track is parallel to the coast and the amplification depends on the duration of the storm as well as V/c.

Actual data of hurricane-generated surges along the Atlantic coast showed that significant surges (up to one third of the maximum surge) occur within 70 nautical miles (130 km) to the left and 110 nautical miles (204 km) to the right of storm track. The maximum surge usually occurs about 25 nautical miles (46 km) to the right of the track. Unless the storm center is very close to the station, usually the water levels are greater south of Sandy Hook than on the New England coast.

Table 6.3: Hurricane parameters in the bathystrophic storm surge study (PARARAS-CARAYANNIS, 1975)

Hurricane	Central pressure (mb)	Peripheral pressure (mb)	Radius of maximum winds (km)	Speed of movement ($km \cdot h^{-1}$)	Maximum gradient wind speed ($km \cdot h^{-1}$)
Hurricane of Oct. 3–4, 1949	963.4	1014.2	27.8	20.4	141.6
Carol of Aug. 30–31, 1954	971.6	1013.2	46.3	61.7	152.9
Audrey of June 26–27, 1957	946.5	1005.8	35.2	24.1	152.9
Carla of Sept. 7–12, 1961	936.0	1013.2	85.2	5.6	160.9
Camille of Aug. 15–16, 1969	905.2	1013.2	25.9	24.1	201.2

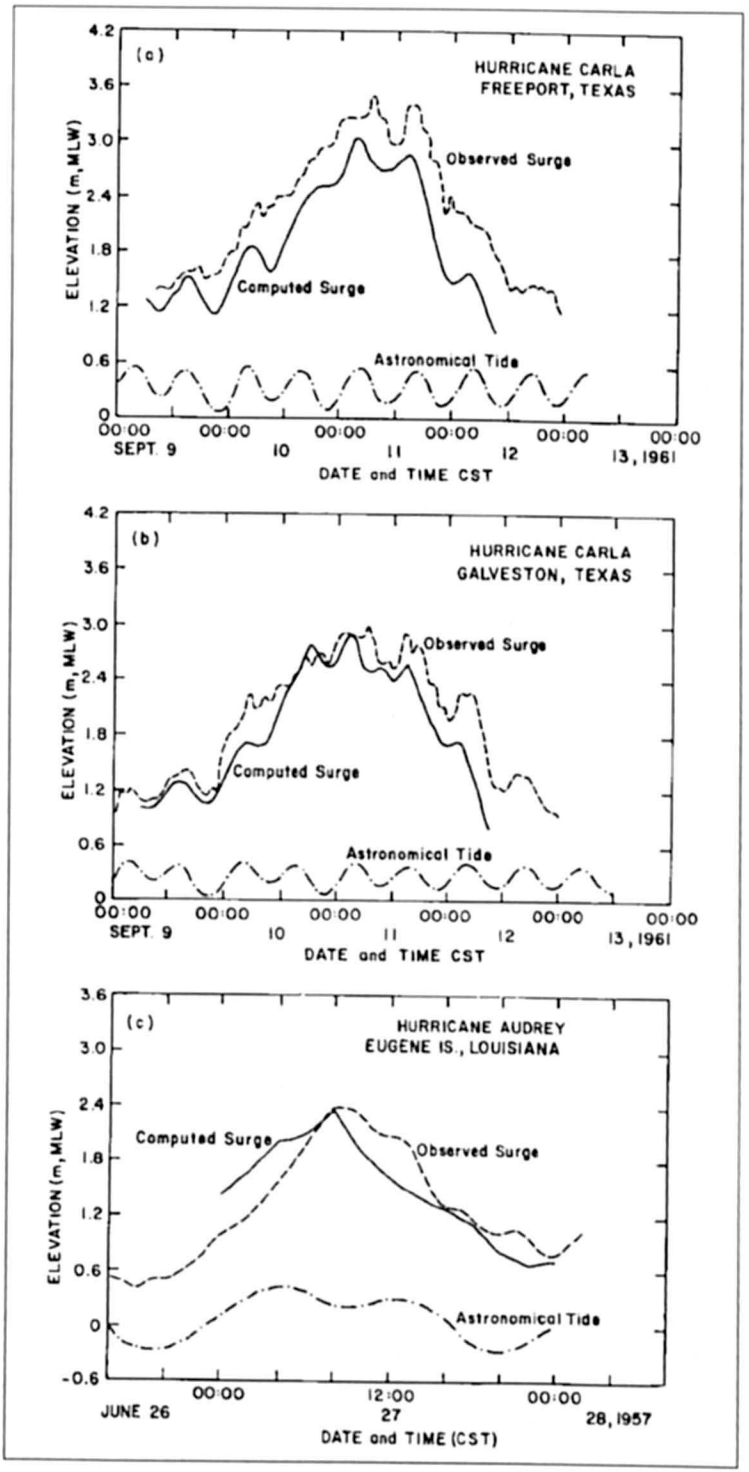

Fig. 6.8: Computed surge (using bathystrophic approach), observed surge, and tide due to (a) Hurricane Carla at Freeport, Texas, (b) Hurricane Carla at Galveston, Texas, and (c) Hurricane Audrey at Eugene Island, Louisiana (PARARAS-CARAYANNIS, 1975)

SPLASH *Models*

SPLASH is an acronym for "special program to list amplitudes of surges from hurricanes." SPLASH I deals with landfalling hurricanes and SPLASH II takes care of situations in which the hurricanes need not go over land. These models were developed at the Techniques Development Laboratory of the U.S. National Weather Service (JELESNIANSKI 1972, 1974, 1976; JELESNIANSKI and BARRIENTOS 1975; BARRIENTOS and JELESNIANSKI 1976, 1978). This computer program is operationally used at the National Hurricane Center in Miami and is applied to the Atlantic coast and the Gulf of Mexico coast of the United States. The stretch of coast for which these models are used extends about 3000 mi (4827 km) from Brownsville, Texas, to Long Island, New York. Along this coastal stretch, reference stations (for use in hurricane landfall determination) are established with an approximate spacing of 100 mi (161 km).

SPLASH is a numerical storm surge model that involves a linearized version of the transport equations. The geometry of the model is idealized into a rectangle with variable depth. One side of the rectangle is the coast and the other three sides are open boundaries. At the coast the normal transport is zero and at the deepwater open boundary static height is prescribed (this height is zero in the absence of an atmospheric pressure gradient). On the two lateral open boundaries the normal derivative of transport is prescribed to be zero. Depth contours are analysed on overlapping 600 mi × 72 mi (965 km × 116 km) basins. The basins are centerd 50 mi apart.

In SPLASH I, which applies to landfalling hurricanes only, the following meteorological input is required: (1) pressure drop $\Delta p = p_\infty - p_0$ where p_∞ is the ambient pressure outside the storm and p_0 is the central pressure of the hurricane, (2) the radius R of maximum winds, (3) the vector storm motion U_s/θ where U_s is the storm speed and θ is the storm direction of motion, and (4) point of landfall. This program assumes that the conditions are steady state, i. e., the size, intensity, and speed of movement are constants.

SPLASH II deals with an unsteady storm. The storm track could have any orientation and the storms need no landfall. The input data consist of (among other things) a 24-h track segment, which is defined by latitude and longitude for five points on the track staggered 6 h apart for a 24-h period. These latitude and longitude data not only define the track but also the speed of movement of the storm. Other input data are the radius of maximum winds and pressure drop, which can vary with time.

One very important component in SPLASH is a normalized shoaling correction, which is used to correct the computed surge along the coast if the landfall point is shifted. Shoaling corrections were prepared for the Atlantic and the Gulf coasts by using landfall storms normal to the coast at 16-mi (25.8 km) intervals using a storm speed of 15 mi $\cdot$ h^{-1} (24 km $\cdot$ h^{-1})

The SPLASH models were verified generally against data from 43 hurricanes during five hurricane seasons. These cases, the dates of occurrence, location of the peak surge, and computed and observed peak surges are listed in Table 6.4. The varying location of the peak surge, depending on the nature of the bathymetry, is shown quantitatively in Fig. 6.9.

Whereas SPLASH I can deal with landfalling hurricanes only, SPLASH II can be applied to a general storm track. Especially the following three types of tracks are considered: (1) landfall storm with its track perpendicular to a straight-line coast, (2) an alongshore moving storm (i.e. constant abeam distance of the track from the coast), and (3) a recurving storm (non-landfall). Slow-moving storms are treated as a special case and a hypothetical storm with the following properties is used: (1) the storm traverses the continental shelf with the speed of less than 8 mi $\cdot$ h^{-1} (12.9 km $\cdot$ h^{-1}), (2) the storm's closest approach to the coast occurs

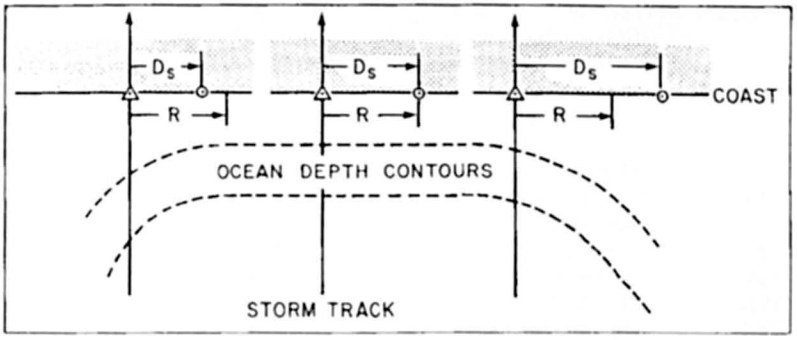

Fig. 6.9: Qualitative illustration showing the varying positions of peak surge on the coast as compared with two-dimensional bathymetry. ⊙, location of peak surge; △, landfall point; R, radius of maximum winds; Ds, distance to peak surge. (JELESNIANSKI, 1972)

near Miami where there is hardly any continental shelf, and (3) the storm's strength and size (Δp = 100 mb, R = 15 mi · h^{-1} [24 km · h^{-1}]) do not change along the track.

Calculations using SPLASH II gave the following results. The maximum surge is not highly sensitive to storm size for landfall storms. However, for non-landfall storms, the storm size is important because the surge is a function of distance from the coast relative to storm size. When the storm is on the shelf, if the component of the track on the coast is large, the length of the coastline affected by the surge could be very long. For a storm travelling perpendicular to the coast, the component of the track on the coast degenerates to a point, and surges occur only along a small length of the coastline.

One of the main drawbacks of SPLASH II (although it is an improvement over SPLASH I) is that it treats the coast as a straight line and cannot include the curvature of the coastline. To remove this restriction, JELESNIANSKI (1976) developed a sheared coordinate system. In this model, a mildly curving coastline (which does not include bays, estuaries, sounds, deltas, capes, spits, etc.) is sheared into a straight-line. A surface plane, beginning at the ocean shelf and containing the curved coast as one of the boundaries, is fitted with a curve, nonorthogonal grid. The plane with curved boundaries is then transformed via a sheared coordinate system onto an image rectangle. In this transformed system, one deals with a Cartesian, orthogonal, equally spaced grid in which the coast coincides with grid lines. JELESNIANSKI (1976) used such a model incorporating the linearized storm surge equations for a 3000 mi (4827 km) coastline beginning at the United States-Mexico border in the Gulf of Mexico to the eastern tip of Long Island in New York. The storm tracks could be curved and the intensity, the size of the storms, and its speed of movement could be variable.

The somewhat idealized SPLASH models are being replaced with a new generation of models referred to as SLOSH (sea, lake and overland surges from hurricanes). These models are being developed for the east and gulf coasts of the United States. Specifically, the following coastal stretches are being modelled: New Orleans Area, Lake Okeechobee, Tampa Bay, Mobile Bay, Galveston area, Charlotte Harbour (Florida), Florida Bay, Biscayne Bay, Florida Keys, Long Island Sound, Chesapeake Bay, Charleston Harbour (South Carolina), Narragansett Bay, Buzzards Bay, Delaware Bay, Palmico Sound, Massachusetts Bay, Corpus Christi (Texas), Lower Laguna Madre (Texas), Matagorda Bay (Texas), Lake Sabine (Texas), and Pensacola (Florida). Some testing of the SLOSH model during Hurricane Bob in July 1979 showed that the results are quite satisfactory.

Table 6.4: Comparison of observed maximum surges (m) in the United States with those computed from the nomograms using SPLASH (JELESNIANSKI, 1972)

Date	Location of peak surge	Computed peak surge	Observed peak surge
Oct. 2, 1893	Mobile, AL	3.32	2.83
Sept.27, 1894	Charleston, NC	1.59	1.62
Sept. 8, 1900	Galveston, TX	4.60	4.45
Aug. 14, 1901	Mobile, AL	2.07	2.26
July 21, 1909	Galveston, TX	3.54	3.05
Sept. 13, 1912	Mobile, AL	0.91	1.34
Aug. 16, 1915	High Island, TX	3.60	4.24
Sept. 29, 1915	Grand Isle, LA	3.41	2.74
Oct. 18, 1916	Pensacola, FL	1.59	0.91
Sept. 28, 1917	Fort Barrancas, FL	1.77	2.16
Sept. 9, 1919	Key West, FL	2.23	1.98
Oct. 25, 1921	Punta Rassa, FL	3.29	3.32
Aug. 26, 1926	Timbalier Island, LA	3.02	2.99
Sept. 18, 1926	Miami Beach, FL	3.57	3.17
Sept. 20, 1926	Pensacola, FL	2.19	2.74
Sept. 16, 1928	West Palm Beach, FL	2.74	2.96
Sept. 28, 1929	Key Largo, FL	2.23	2.68
Sept. 7, 1933	Brownsville, TX	3.02	3.96
July 25, 1934	Galveston, TX	2.07	1.80
Nov. 4, 1935	Miami Beach, FL	2.01	2.74
July 31, 1936	Panama City, FL	1.71	1.83
Aug. 7, 1940	Colcasieu Pass, LA	1.62	1.62
Aug. 11, 1940	Beaufort, SC	2.44	2.44
Sept. 23, 1941	Sargent, TX	2.35	2.59
Oct. 7, 1941	St. Marks, FL	3.08	1.86
Aug. 30, 1942	Matagorda, TX	2.90	4.27
July 27, 1943	Galveston, TX	1.77	1.10
Oct. 19, 1944	Naples, FL	3.26	3.23
Oct. 20, 1944	Charleston, FL	1.22	1.22
Aug. 27, 1945	Matagorda, TX	1.89	1.95
Aug. 24, 1947	Safine Pass, LA	0.87	0.76
Aug. 17, 1947	Hillsboro Beach, FL	1.95	2.90
Sept. 19, 1947	Biloxi, MS	3.41	3.32
Oct. 15, 1947	Quarantine Station, GA	2.13	1.77
Sept. 4, 1948	Biloxi, MS	1.59	1.55
Aug. 26, 1949	New Jupiter In., FL	1.65	1.25
Oct. 4, 1949	Freeport, TX	3.17	2.74
Aug. 30, 1950	Pensacola, FL	1.16	1.55
Sept. 5, 1950	St. Petersburg, FL	2.10	1.92
Oct. 15, 1954	Southport, NC	3.81	3.90
Aug. 17, 1955	Holden Beach, NC	1.62	1.65
Sept. 24, 1956	Laguna Beach, FL	1.43	2.16
June 27, 1957	Calcasieu Pass, LA	4.82	3.81

Earlier we referred to the SLOSH models of N.O.A.A., U.S.A. More recent information on these can be found in JELESNIANSKI et al., (1992). One of the strongest Hurricanes to make a landfall on the East Coast of U.S.A. was Hurricane Hugo of September 11–25, 1989 causing a total damage in excess of 7 billion US dollars. The track is shown in Fig. 6.10.

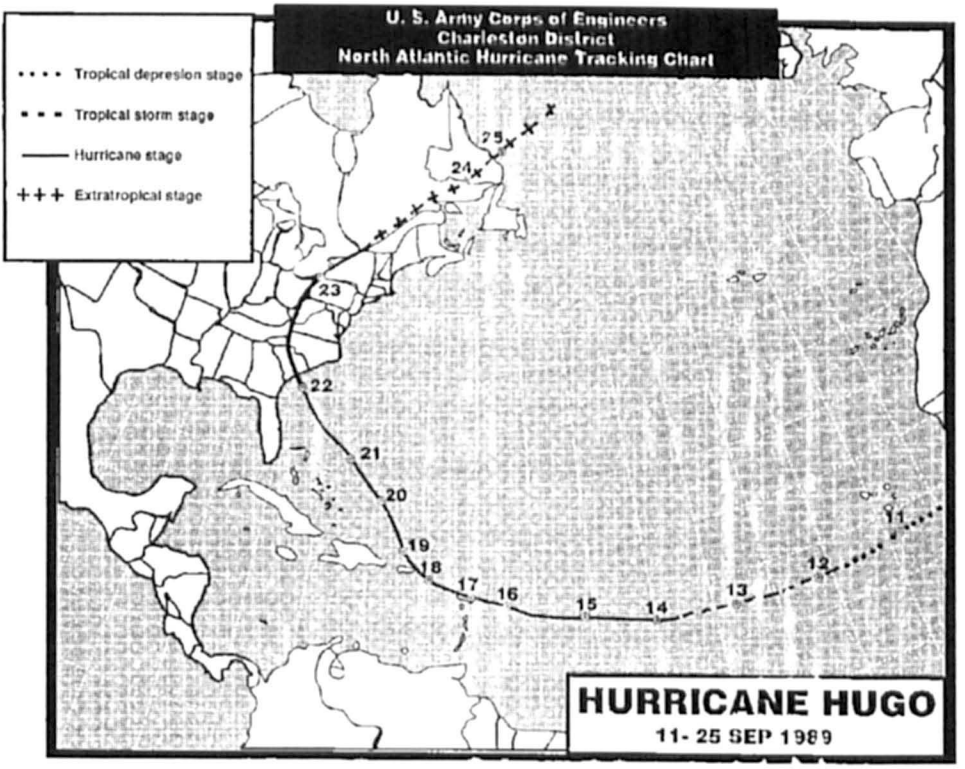
U. S. Army Corps of Engineers
Charleston District
North Atlantic Hurricane Tracking Chart
Tropical depresion stage
Tropical storm stage
Hurricane stage
Extratropical stage
25
24
23
22
21
20
19
18
17
16
15
14
13
12
11
HURRICANE HUGO
11- 25 SEP 1989

Fig. 6.10

6.1.2 Gulf of Mexico Coast (Excluding Florida Coast)

Up to this point, storm surges along the Atlantic Coast and the Gulf of Mexico have been studied. The gulf coast will now be considered in some detail. CLINE (1920) discussed the storm surges in the Gulf of Mexico due to hurricanes during the 20-yr period 1900–19. The pertinent information for these hurricanes and the storm surges generated are given in Table 6.5.

Following are some results of the study by CLINE (1920). During 1900–19, about 7225 people were killed and about $ 106 million in property damage occurred as a result of hurricanes in the Gulf of Mexico. The storm surges need not be symmetric about the hurricane track because the wind velocities to the left side of the track are much smaller (and less persistent) than on the right side. Peak surges occur a few kilometers to the right and at about the time of the passage of the center of the hurricane. The high water extends for only a short distance to the left of the point where the center of the storm moves inland. High water, however, occurs to the right of the center for a distance of 100–200 mi (161–322 km).

CONNER et al. (1957) gave a table of hurricanes and associated surges during the period 1893–1950. This table is reproduced here as Table 6.6. Although this table bears some resemblance to an earlier table (Table 6.4), certain entries are different. Also, in Table 6.8 only the observed surge is included (there is no calculated surge). In addition, the lowest pressure in the hurricane is also listed. Two empirical relations best fit these data. One is

$$h_{max} = 0.867(1005 - p_0)^{0.618} \tag{6.1}$$

where, h_{max} is the surge height (feet) and p_0 is the lowest central pressure (millibars). The correlation coefficient between h_{max} calculated and p_0 is 0.66. Another is

$$h_{max} = 0.154(1019 - p_0) \tag{6.2}$$

In this case the correlation coefficient is 0.68. The difference in the values for the observed surges for the same storms listed in Tables 6.4 and 6.6 are mainly due to different sources.

Hurricane Audrey of 1957 was the first hurricane that caused major storm surges since the organization of the National Hurricane Research Project by the U.S. Weather Bureau. This hurricane crossed the shore near the Texas–Louisiana border on the morning of June 27, 1957. HARRIS (1958a, 1958b) studied the storm surges associated with this hurricane and gave detailed diagrams of the surge height distribution along the coast.

MARINOS and WOODWARD (1968) used the bathystrophic theory to compute storm surges on the Texas-Louisiana coast. They made use of three storms to calibrate their model and checked it against several other storms. Using several synthetic hurricanes, 100-yr surge hydrographs were also constructed.

MIYAZAKI (1965) computed the storm surge in Gulf of Mexico due to Hurricane Carla of September 7–11, 1961, using a time-dependent linearized two-dimensional model. He first used a coarse grid of 48 nautical miles (89 km) for the entire Gulf and then developed a fine-grid model (grid spacing of 9.6 nautical miles or 17.8 km) for the northwestern part where the storm surge was the most significant. In the coarse-mesh model, bottom friction was ignored whereas quadratic bottom friction was used in the fine-mesh model.

Hurricane Carla is an exceptional hurricane in the sense that it moved very slowly (about 7 knots or 13 km · h^{-1}). The maximum wind speed was 85–95 knots (137–176 km · h^{-1}) and the radius of maximum winds was about 50 nautical miles (93 km). Another remarkable feature of this hurricane is in the generated surge. Along the Texas-Louisiana coast the storm surge occurred for almost a 6-d period (September 7–12, 1961). Maximum surge height of about 10ft. (3.1 m) was estimated on September 10 at Galveston. The calculated surge was compared with the observed surge by MIYAZAKI (1965) at the following stations: Port Isabel (Texas), Port Aransas (Texas), Freeport (Texas), Pier 21 and Pleasure Pier (both in the Galveston area), Fort Point (Texas), Sabine Pass (Texas), Bayou Rigaud (Louisiana), Humble Oil Platform A (Louisiana) and Pensacola (Florida).

Hurricane Betsy struck the southeastern Louisiana coast on September 9, 1965. It was the most destructive (economically) ever to hit the United States coast up to that time (GOUDEAU and CONNER, 1968). Winds reaching up to 125 mi · h^{-1} (201 km · h^{-1}) caused a great storm surge resulting in extensive flooding in the Metropolitan area of New Orleans. Goudeau and Conner 1968 also gave detailed diagrams for the storm surge height distribution and flooded areas on the Mississippi River and also in Lake Pontchartrain.

PEARCE (1972) developed a two-dimensional, time-dependent numerical model for studying storm surges in the Gulf of Mexico. He used two different mesh sizes: 16 nautical miles (29.6 km) and 6 nautical miles (11.1 km). These were applied to the surge generated by Hurricane Camille of August 17–22, 1969. There was no significant difference in the results between the smaller grid and larger grid models. Inclusion of the nonlinear advective terms made only a difference of 2 % in the surge heights. The model results were insensitive to bottom friction coefficients between 0.005 and 0.02. PEARCE (1972) also used a one-dimensional model as well as an analytical model. The distribution of surge heights computed for August 17 at 23:40 is shown in Fig. 6.11. Although in this subsection the Gulf of Mexico was considered as a whole, later subsections will consider parts of this system such as Galveston Bay, Mobile Bay, etc. in detail.

Howard Elgison made the following comments in ANNON (1992) on page 60. Hopefully there will never be another storm with the destructive power of Hurricane Andrew. Certainly, there will never be another hurricane named Andrew. Like the great athletes whose numbers have been retired, the great hurricanes, those that were particularly severe or destructive, have their names retired.

Currently, a total of 33 names are enshrined in the Hurricane Hall of Infamy. They are listed below in chronological order:

1954 Carol-Edna – Hazel
1955 Connie – Diane – Ione – Janet
1957 Audrey
1959 Gracie
1960 Donna
1961 Carla
1963 Flora
1964 Cleo – Dora – Hilda
1965 Betsy
1967 Beulah
1969 Camille
1970 Celia
1972 Agnes
1974 Carmen
1975 Eloise
1977 Anita
1979 David - Frederic
1980 Allen
1983 Alicia
1985 Elena – Gloria
1988 Gilbert – Joan
1989 Hugo
1991 Bob

Table 6.5: Hurricanes and storm surges in the Gulf of Mexico during 1900-19.

Date(s) of hurricane	Hurricane	Storm surge
Sept. 1–12, 1900	Hurricane reached Florida Straits on Sept. 5 and moved in a northwesterly direction across the gulf a distance of about 1600 km. Maximum winds observed were 193 km-h^{-1}.	Surge of 4.6 m at Galveston on Sept. 8; over 6000 people killed; $ 30 million damage (in 1920 currency)
July 5–10, 1901	Storm of small extent and moderate intensity moved through the Yucatan channel into the Gulf of Mexico on July 7 and reached the Texas coast west of Galveston on July 10.	Surge of 1.4 m at Galveston; no damage
Aug. 9–15, 1901	Hurricane first appeared to the north of Cuba on Aug. 9. It moved across southern Florida and into the Gulf of Mexico on the morning of Aug. 11, continued its course westward to 90° W when, during Aug. 14, it recurved and on the morning of Aug. 15 passed northeastward between New Orleans and Port Eads. Hurricane had small diameter but great intensity and its track was unusual.	Surge of 1.3 m at Port Eads, 1.7 m at New Orleans, and 2.5 m at Mobile; 10 persons killed; $ 1 million damage
Sept. 23–27, 1906	Disturbance passed through the Yucatan channel on the morning of Sept. 24, travelled roughly in a straight line, and moved in on the Mississippi coast on the morning of Sept. 27. Hurricane was of large extent and of unusual intensity.	Surge of 1.2 m at Port Eads, 3.3 m at Pensacola. At Pensacola 32 people killed and near Mobile 31 killed (it is not known whether some of these deaths were due to hurricane and not the surge)
July 18–21, 1909	Hurricane moved from the Caribbean Sea though the Yucatan Channel on July 18 and moved inland on the Texas coast with its centre near Velasco.	Surges (amplitude not known) occurred to the right of the storm center up to Galveston; 4 people killed
Sept. 12–21, 1909	Storm of great extent and unusual intensity. Its effect was felt from east of Pensacola to the west of Galveston. Hurricane passed through the Yucatan channel during Sept. 17 and moved inland on the Louisiana coast on Sept. 20.	353 people killed; $ 6.4 million damage
Oct. 13–18, 1910	Disturbance moved into the Florida Straits on Oct. 14, moved towards the northwest during Oct. 15, southward during Oct. 16, and then eastward to the Florida Straits by the morning of Oct. 17 after which it moved northward over Florida on Oct. 18.	Negative surge of 2 m at Tampa
Aug. 13–17, 1915	Storm moved across the western end of Cuba into the Gulf of Mexico during the morning of Aug. 14, travelled in a direct line, and passed inland on the Texas coast a short distance to the left of Galveston on the morning of Aug. 17.	$ 21 million damage

Sept. 2–4, 1915	Disturbance of considerable intensity crossed western Cuba, moved into the east Gulf, and recurving slowly, moved inland near the mouth of the Apalachicola River during early morning of Sept. 4.	Surge of at least 1.5 m at St. Petersburg
Sept. 22–30, 1915	One of the most intense hurricanes in the history of the Gulf coast. Hurricane moved through the Yucatan channel during the night of Sept. 27 and, travelling northwestward, moved inland on the Louisiana coast to the left of and near Grand Isle during Sept. 29. Disturbance recurved slowly after crossing latitude 27° N and moved slowly northward.	275 persons killed; $ 13 million damage. Surge heights up to 3.7 m on the coast of Lake Pontchartrain and 3–3.4 m on the Louisiana and Mississippi coasts. Inside Lake Pontchartrain, surges up to 4 m
July 1–6, 1916	Disturbances first appeared in the Caribbean Sea on the afternoon of July 1, moved almost in a straight line through the Yucatan channel on July 3, and reached the Mississippi coast late in the afternoon of July 5. Storm covered considerable area and was of great intensity.	Damage at Mobile and along the Albama coast of $ 2.5 million; 12 people killed. Damage at Pensacola of $ 1 million. Maximum surge up to 3.5 m.
Aug. 12–19, 1916	Disturbances passed through the Yucatan channel into the Gulf during the night of Aug. 16, advanced northwesterly in nearly a straight line, and moved inland on the Texas coast midway between Corpus Cristi and Brownsville during the afternoon of Aug.	15 people killed; $ 1.8 million damage. Surges greater than 2.1m at Mobile.
Sept. 21–29, 1917	Disturbance moved through the Yucatan channel into the Gulf during the night of Sept. 25 and advanced in a direction a little west of north towards the mouth of the Mississippi river. When within about 80 km of Port Eads the storm began recurving to the right and center, passing about 80 km to the right of Port Eads, and moved inland to the right of Pensacola.	Surge of 0.86 m at Pensacola. Surge of 1.77 m at Fort Barancas. Negative surge of 1.52 at Mobile.
Aug. 1–6, 1918	Disturbances moved through the Yucatan channel into the Gulf of Mexico during the night of Aug. 4, travelled in a northwesterly direction, and passed inland over Lake Charles during Aug. 6. Hurricane was small but of marked intensity.	$ 5 million damage and 34 people killed due to the hurricane. Surge of 0.91 m at Morgan City. Surge of 0.86 at Johnson Bayou
Sept. 6–14, 1919	Storm moved through the Yucatan channel into the Gulf towards the mouth of the Mississippi River. Then it moved more or less parallel to the coast.	284 people killed; more than $ 20 million damage. Surges of up to 3.7 m occurred

Table 6.6: Lowest central pressures and highest surges of Gulf of Mexico hurricanes (CONNOR et al., 1957)

Date	Location of highest surge on open coast	Lowest Pressure (mb)	Peak Surge (m)
Oct. 2, 1983	Mobile, AL	956	2.56
Sept. 8, 1900	Galveston, TX	936	4.42
Aug. 14, 1901	Mobile, AL	973	2.26
Sept. 27, 1906	Fort Barrancas, FL	965	3.29
July, 21, 1909	Galveston, TX	959	3.05
Sept. 20, 1909	Mobile, AL	980	2.38
Sept. 13, 1912	Mobile, AL	993	1.34
Aug. 16, 1915	High Island, TX	953	4.24
Sept. 29, 1915	Grand Isle, LA	944	2.74
July 5, 1916	Fort Morgan, AL	961	1.43
Sept. 28, 1917	Fort Barrancas, FL	964	2.16
Sept. 14, 1919	Port Aransas, TX	948	3.38
Oct. 25, 1921	St. Petersburg, FL	958	2.38
Aug. 25, 1926	Timbalier Bay, LA	959	3.05
Sept. 20, 1926	Pensacola, FL	955	2.32
Sept. 5, 1933	Brownsville, TX	949	3.96
July 25, 1934	Galveston, TX	975	1.80
July 31, 1936	Panama City, FL	964	1.83
Aug. 7, 1940	Calcasieu Pass, LA	974	1.46
Sept. 23, 1941	Sargent, TX	959	3.02
Oct. 7, 1941	St. Marks, FL	981	2.44
Aug. 30, 1942	Matagorda, TX	951	4.51
July 27, 1943	Galveston, TX	975	1.22
Aug. 27, 1945	Matagorda, TX	968	2.23
Aug. 24, 1947	Sabine Pass, LA	992	1.10
Sept. 19, 1947	Biloxi, MS	968	3.38
Sept. 4, 1948	Biloxi, MS	987	1.71
Oct. 4, 1949	Freeport, TX	978	3.17
Aug. 30, 1950	Pensacola, FL	979	1.68
Sept. 5, 1950	Cedar Key, FL	958	1.55

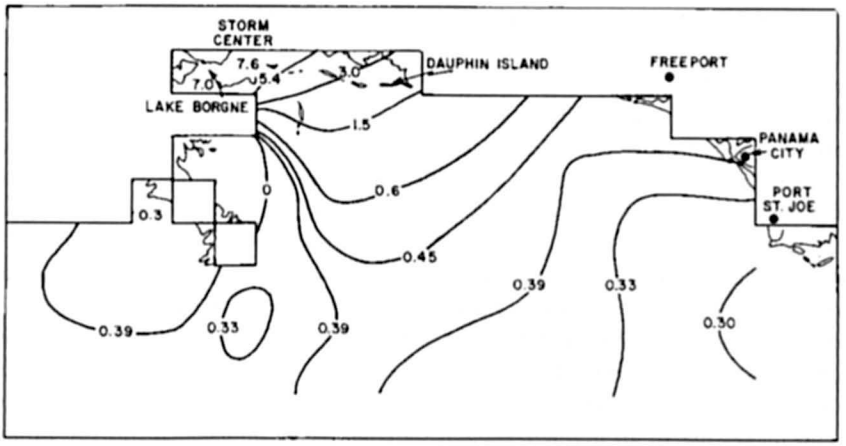

Fig. 6.11: Distribution of the water levels (storm surge with a 0.25 m tide superimposed) along parts of the coasts of Louisiana, Mississippi, and Alabama due to Hurricane Camille of 1969 (PEARCE, 1972)

There are many ways to measure the destructive power of hurricanes. The method chosen by the National Hurricane Center (NHC) is to calculate the total dollar value of property losses in the United States and adjust for inflation. Using this method, the top six hurricanes of all time are listed below. The damage Figs. are given in 1990 dollars. Needless to say, Hurricane Andrew sits atop the list with monetary damages greater than the combined total of the next three most costly storms. Table 6.7 lists the damage from some intense Hurricanes that affected the U.S.A.

Table 6.7: Damage in Billions of U.S. Dollars (at 1990 prices) by the Topio Hurricanes affecting the U.S.A. (ANON, 1993)

Rank	Hurricane	Year	Damage in Billions of US Dollars at 1990 price levels
1	Andrew	1992	30.0
2	Hugo	1989	7.0
3	Frederic	1979	2.3
4	Agnes	1972	2.1
5	Alicia	1983	2.0
6	Iniki	1992	1.8
7	Juan	1985	1.5
8	Camille	1969	1.427
9	Betsy	1965	1.425
10	Elena	1985	1.25

Even though only 53 people died in the wake of Hurricane Andrew, it is the single most natural disaster in U.S. history in terms of damage up to that time.

6.1.3. Storm Surges along the Coast of Florida

In this subsection, storm surges along the Gulf of Mexico coast and the Atlantic coast of Florida will be considered. Storm surges in Lake Okeechobee will be considered in the next subsection. DAMSGAARD and DINSMORE (1975) used a two-dimensional numerical model to study storm surges in Biscayne Bay, Florida. Their model allows for overtopping of low-lying barrier islands as well as inundation of flood plains. They tested their model against the storm surge generated by Hurricane Betsy of September 8, 1965.

VERMA and DEAN (1969) also used a two-dimensional model to study storm surges in Biscayne Bay. Their model allows for the inclusion of rainfall. ROSS and JERKINS (1977) used two different models to study storm surges in Tampa Bay, Florida. The first model (referred to as USF) was developed at the University of South Florida and is based on the explicit model by REID and BODINE (1968). The second model is based on the Rand model (LEENDERTSE, 1967) and makes use of an implicit-explicit scheme. Based on calculations for Tampa Bay, these authors concluded that the USF model provides a more accurate simulation than the Rand model.

By far the most comprehensive study of storm surges on the Florida coast (which this author could find) is one by BRUUN et al. (1962), in which they studied the storm surges in relation to coastal topography. Forty hurricanes during the period 1900–60 that caused significant storm surges along Florida coast are listed in Table 6.8.

Table 6.8: Major Hurricanes affecting Florida, 1903–65. The last four entries are taken from TETRA TECH INC. (1978) coastal flooding storm surge model, Part I. Methodology prepared by Tetra Tech Inc. for U.S. Dep. Of Insurance Administration, Washington, DC, May 1978 (BRUUN et al., 1962)

Index No.	Date of occurrence	Coastal area affected
1	Sept. 10–16, 1903	Fort Lauderdale and Tampa Bay
2	Oct. 10–23, 1904	West Palm Beach
3	Oct. 11–20, 1906	Florida Keys and Miami
4	Oct. 6–15, 1909	Florida Keys and Miami
5	Oct. 11–13, 1910	Key West to Tampa Bay and Jacksonville
6	Sept. 2–14, 1919	Florida Keys
7	Sept. 27–Oct. 1, 1920	Cedar Keys and St. Augustine
8	Oct. 21–23, 1921	Tampa Bay and Daytona Beach
9	July 22–Aug. 2, 1926	Entire east coast
10	Sept. 6–22, 1926	Miami and Everglades to Tampa Bay
11	Aug. 7–10, 1928	Fort Pierce and Cedar Key
12	Sept. 6–20, 1928	West Palm Beach to Jacksonville
13	Sept. 22–Oct. 4, 1929	Florida Keys to Tampa Bay
14	Aug. 31–Sept. 7, 1933	West Palm Beach to Cedar Key
15	Aug. 31–Sept. 8, 1935	Florida Keys to Cedar Key
16	Oct. 30–Nov. 8, 1935	West Palm Beach to Miami and Key West to Fort Myers
17	July 27–Aug. 1, 1936	Miami and Everglades to Tampa Bay
18	Oct. 4–12, 1941	Miami to Florida Keys and Everglades to Cedar Key
19	Oct. 13–21, 1944	Key West to Tampa Bay and Jacksonville
20	Sept. 12–19, 1945	Florida Keys to Miami and northeast coast
21	Oct. 7–9, 1946	Fort Myers to Cedar Key and Jacksonville
22	Sept. 11–19, 1947	Fort Lauderdale and Fort Myers
23	Oct. 9–15, 1947	Key West to Miami
24	Sept. 19–25, 1948	Key West to Fort Myers and Fort Pierce
25	Oct. 4–8, 1948	Florida Keys to Fort Lauderdale
26	Aug. 24–29, 1949	West Palm Beach and Cedar Key
27	Sept. 1–7, 1950	Key West to Cedar Key
28	Oct. 15–19, 1950	Entire east coast
29	Sept. 30–Oct. 7, 1951	Fort Myers and Fort Pierce
30	Oct. 8–10, 1953	Fort Myers and Fort Pierce
		Florida Panhandle
31	Sept. 10–30, 1906	Pensacola
32	Aug. 9–14, 1911	Key West to Pensacola
33	Sept. 11–23, 1912	Tampa Bay to Pensacola
34	Sept. 4, 1915	Key West to Apalachicola
35	July 5, 1916	Pensacola
36	Oct. 12–21, 1916	Pensacola
37	Sept. 21–29, 1917	Pensacola
38	Sept. 13–20, 1924	Panama City of Apalachicola
39	Sept. 24–26, 1953	Pensacola to Panama City
40	Sept. 9–12, 1960 (Donna)	Florida Keys and South Gulf Coast
41	Aug. 26–29, 1964 (Cleo)	Southeast Florida
42	Sept. 7–11, 1964 (Dora)	Northeast Florida
43	Oct. 8–16, 1964 (Isabell)	Southern Florida
44	Sept. 6–9, 1965 (Betsy)	Southern tip of Florida

6.1.4 Lake Okeechobee

In an earlier section a storm surge study by REID et al. (1977a, 1977b) was considered, which treated the extensive vegetation areas of Lake Okeechobee as a canopy. MYERS (1954) studied in detail the data from the hurricanes that were pertinent for levee design for this lake. Here, some studies on storm surges in this lake will be considered. KIVISILD (1954) made an extensive study of storm surges in shallow bodies of water and applied this to Lake Okeechobee storm surges.

During the period 1886–1950, the average number of hurricanes reaching Florida was 1.28 per year. The probability that the Okeechobee area would be subjected to winds greater that 75 mi · h^{-1} (121 km · h^{-1}) in any given year is 1 in 7. Several tide gauges were located during the Lake Okeechobee project that was organized during the early 1950s. The north-south extent (maximum) of the lake is 30 mi (48 km), the east-west extent (maximum) is 25 mi (40 km), and the total area is 730 mi^2 (1891 km^2). Extensive marsh and vegetation covers the western portion of the lake. The south shore of the lake from St. Lucie Canal to Fisheating Creek is enclosed by levees constructed to an average crown height of 32.5 ft (9.8 m) above mean sea level. On the north shore a levee of the same height extends from 2 mi (3.2 km) southeast of Taylor Creek to Kissimmee River, and this levee protects the town of Okeechobee. The northwest portion of the lake, bordering low, saw grass marshes, and the northeast shore, bordering comparatively high ground, are unprotected. Ritta, Kreamer, and Torry islands at the southern end of the lake are partially protected by levees but these are insufficient against storm surges such as the hurricane of August 26–27, 1949.

KIVISILD (1954) used simple analytical formulae to calculate the surges in Lake Okeechobee. However, for better resolution of the geometry of the lake, he divided it into triangular elements. The pertinent information of the five hurricanes studied by KIVISILD (1954) and the related surges is summarised in Table 6.9.

LANGHAAR (1951) calculated the storm surges in Lake Okeechobee using simple analytical formulae. These values agreed well with observed surges, which ranged from 3.5 to 10.2 ft (1.1–3. 1 m). In this calculation, Langhaar considered the surge at the leeward end of the lake as a superposition of the surge due to seiches and a statical surge that the wind would maintain if it persisted indefinitely. The surge due to seiche is referred to as the "dynamical surge" and the total surge is the sum of the dynamical and statical surges. FARRER (1958) also used simple analytical formulae to compute storm surges in Lake Okeechobee for the hurricane of August 26, 1949. The water level distribution in the lake at three different times is shown in Fig. 6.12. The shaded area represents the marsh.

DANARD and MURTHY (1994) re-examined the work of REID and WHITAKER (1976) on the effect of vegetation in Lake Okeechobee on the storm surges.

Their assumptions on the equality of various drag coefficients are replaced by more realistic calculations. A new method for calculating wind stress on water is presented for the case when the vegetation extends above the water surface.

For the case of vanishingly small water-depth, it is shown that the horizontal stress is approximately constant in the vertical. This results in a diagnostic relationship for the water current as a function of the wind stress and bottom roughness.

A new expression for the vertically averaged frictional force per unit mass is derived on the assumption that the friction velocity varies linearly with height. The vertical rate of change of friction velocity depends on the mean water current, the wind stress, the bottom roughness, and the water depth.

For coastal defenses against storm surges, traditionally concrete sea walls have been in

Table 6.9. Five hurricanes and storm surges in Lake Okeechobee studied by KIVISILD (1954)

Date(s) of Hurricane	Meteorological information	Storm surge information
Sept. 15–16, 1945	Storm first noted east of the Leeward Islands on Sept. 11; it passed north of Puerto Rico on Sept. 13 and near Turks Island on the night of Sept. 13–14. It began a slow curvature over the great Bahamas Banks during the night of Sept. 14–15 and struck Florida with its center passing over the northern end of Key Largo. Highest measured wind velocity was 222 $km \cdot h^{-1}$ at Carysfort Reef, at the southern tip of Florida. Path of the hurricane-intensity winds was only 32–48 km wide, so that only the southwestern shores of Lake Okeechobee received winds of a velocity greater that 121 $km \cdot h^{-1}$. Storm was, in general, of moderate intensity.	Maximum surge recorded was about 1.8 m in range
Sept. 16–18, 1947	Hurricane center developed on Sept. 5 in the vicinity of Daker (French West Africa). It moved about 27 $km \cdot h^{-1}$ on a west-northwest course to the Bahamas where on Sept. 15 it became almost stationary for about 24 h. Center reached the Florida coast at Fort Lauderdale on Sept. 17. Highest recorded wind velocity in Florida was 250 $km \cdot h^{-1}$ at Hillsboro Light near Pompano. Center moved westward across the state at about 16 $km \cdot h^{-1}$ and entered the Gulf of Mexico just north of Naples. Hurricane force winds were experienced along about 386 km of the Florida east coast, while winds of 160 $km \cdot h^{-1}$ were recorded in a 113-km stretch between Miami and Palm Beach. Hurricane was one of the great storms. Lowest barometric pressure recorded in the Lake Okeechobee area was about 985 mb at Moore Haven.	Maximum positive surge of about 2.13 m and a maximum negative surge of 1.22 m
Sept. 21–22, 1948	Hurricane center developed on Sept. 18 between Jamaica and Grand Cayman Islands and moved slowly in a northerly direction passing over Cuba on Sept. 20 with winds greater than 160 $km \cdot h^{-1}$. When the storm center passed over Florida on Sept. 21–22 there appeared to have been several centers, with lulls reported from 64 to 129 km apart normal to the path of the storm. Speed of movement of the storm was 13-16 $km \cdot h^{-1}$. Strongest wind recorded was in gusts of 196 $km \cdot h^{-1}$ at Boca airport near Key West. By the time the Lake Okeechobee region was reached, wind velocities diminished to gusts of about 145 $km \cdot h^{-1}$. Lowest barometric pressure recorded in the Lake Okeechobee area was 962.8 mb.	Calculated values much bigger because the bottom friction due to the marsh grass was not taken into account
Aug. 26–27, 1949	Storm was noticed on Aug. 23 in its formative stage, 201 km northeast of Leeward Islands. Center was well organized by the time it passed North Nassau on Aug. 26 and it intensified as it approached the Florida coast. Strongest winds occurred some distance to the right of the center near Jupiter, FL, where the anemometer failed after reaching an extreme of 246 $km \cdot h^{-1}$. Center passed the northern part of Lake Okeechobee during the early part of the evening of Aug. 26 with wind velocities ranging from 160 to 203 $km \cdot h^{-1}$. In the Lake Okeechobee section it was the worst hurricane felt since the great disastrous hurricane of September 1928.	Storm surges with ranges up to 4.27 m were recorded
Oct. 17–18, 1950	Storm formed over the northwestern Caribbean Sea on Oct. 15 and moved northeastward and then northward across Cuba as a small hurricane. Center of the hurricane, about 8 km in diameter passed directly over Miami on the midnight of Oct.17–18. Highest recorded wind speed was 201 $km \cdot h^{-1}$. Center crossed northward over Lake Okeechobee during the morning of Oct. 18 with wind gust up to 153 $km \cdot h^{-1}$. In general, the diameter of this storm was smaller than that of most hurricanes, and sustained wind velocities were barely above the minimum hurricane	Surges with a maximum range of 2.74 m were recorded

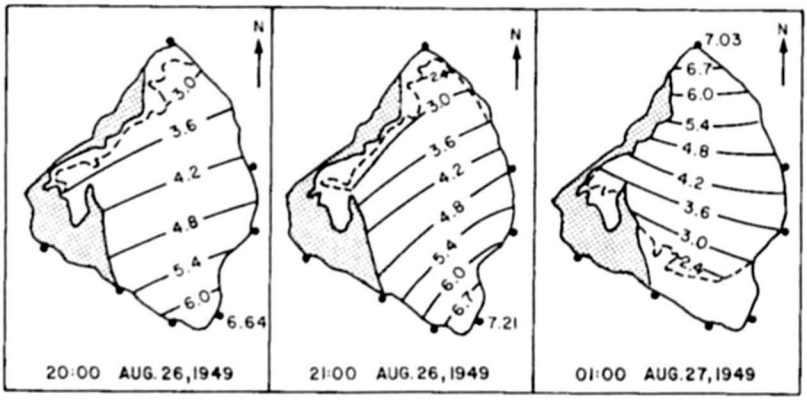

Fig. 6.12: Storm surge height (meters) distribution at three different times in Lake Okeechobee, Florida, due to the hurricane of August 26–27, 1949. (FARRER, 1958)

use. Even such prohibitively expensive structures might not be able to withstand the full force of impact from the incoming surge. Indeed during the 29 April 1991 storm surge in Bangladesh, two-foot thick concrete walls were taken out by the surge.

Earlier it was noticed (REID and WHITAKER, 1976) that surges were of smaller amplitude in those parts of Lake Okeechobee in Florida, wherever there was tall reed grass extending above the water surface. Thus there is observational evidence that a vegetation canopy can reduce storm surges significantly. However, it should be noted that this type of moderation by vegetation would occur more for the locally generated surge by a local wind field, than for that part of the surge that is generated outside and propagates into the region under discussion. This is because for a locally generated surge, the wind speed and therefore wind stress on the water surface are reduced by vegetation protruding above the water. Generally, the locally generated surge accounts for 50 to 80 % of the total surge; hence possible reduction of storm surges by vegetation canopies id of great practical interest.

The case where the water completely covers the canopy is shown in Fig. 6.13. D is the undisturbed total depth of the water and b is the height of the canopy. The velocity of the water above the canopy ($b \le z \le D$) is u_1, τ_a is the stress (force per unit area) that the atmosphere exerts on the water surface, τ_c is the stress the upper layer exerts on the lower, and τ_b is the stress lower layer exerts on the bottom.

Ignoring atmospheric pressure gradients, the linearized, vertically integrated equation of motion for the lower (canopy) layer is

$$\rho \frac{\partial \mathbf{U}_1}{\partial t} + \rho g b \nabla h = \hat{\mathbf{o}}_c - \hat{\mathbf{o}}_b - \mathbf{F}_c - \rho f \, \mathbf{k} \times \mathbf{U}_1 \qquad (6.3)$$

Where

$$\mathbf{U}_1 = b\mathbf{u}_1$$

h is the perturbation height of the free surface and $\mathbf{F}_c$ is the resistance (force per unit horizontal area) due to the canopy elements. Since the fluid is hydrostatic and homogeneous, the horizontal pressure gradient force is independent of z and is proportional to the gradient of the perturbation height of the free surface even in the lower layer. Let N be the number of

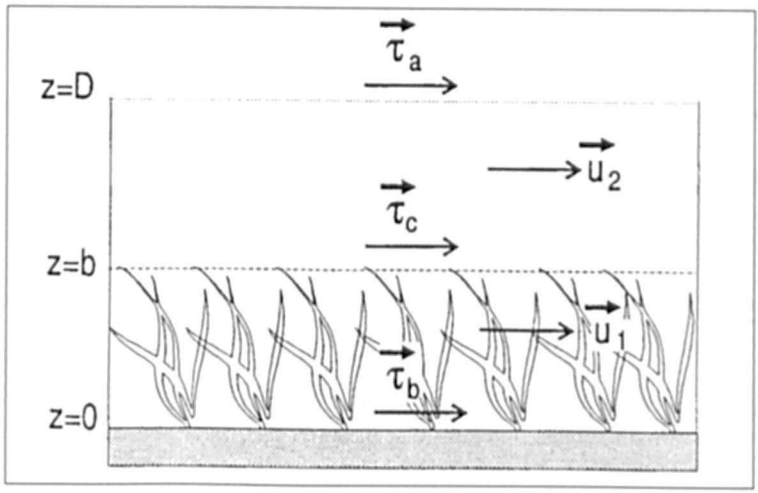

Fig. 6.13: Schematic diagram of stresses and water velocities in case where water completely covers the canopy (DANARD and MURTY, 1994)

canopy elements per unit horizontal area of width w. Then the vertical area obstructing the flow is bw for each canopy element, so the total obstructing area (per unit horizontal area) is Nbw. Thus

$$\mathbf{F}_c = \rho C_d \, Nbw |\mathbf{u}_1| \mathbf{u}_1 \tag{6.4}$$

where, C_d is the drag coefficient for the vertical surface of the canopy elements. For rigid canopy elements presenting a flat surface perpendicular to the water flow, the velocity should be zero or nearly so immediately behind the canopy elements. The dynamic pressure force per unit horizontal area opposing $\mathbf{u}_1$ is

$$F_c = \frac{1}{2} \rho u_1^2 Nbw \tag{6.5}$$

Equating (6.4) and (6.5) gives

$$C_d = 1/2 \tag{6.6}$$

This is of course an upper limit. In general, C_d will be smaller.
Reid and Whitaker write τ_c as

$$\hat{o}_c = \rho f_1 |\mathbf{U}_2 - \mathbf{u}_1| (\mathbf{u}_2 - \mathbf{u}_1) \tag{6.7}$$

where, f_1 is a non-dimensional coefficient. An alternate expression to (6.7) may be derived using reasoning similar to that of CRESSMAN (1960). Let ϵ ($\perp$ b) be the top part of canopy that u_2 senses. The vertical area of the canopy obstructing $\mathbf{u}_2$ is Nwϵ per unit horizontal area. Assuming zero velocity immediately behind the canopy elements, the dynamic pressure force opposing $\mathbf{u}_2$ is Nwϵ < 1/2 ρu_2^2 Let k (< 1) be an efficiency factor representing the efficiency of the top of the canopy in blocking $\mathbf{u}_2$. Then

$$\hat{\mathbf{o}}_c = kNw\epsilon \cdot \frac{1}{2}\rho|\mathbf{u}_2|\mathbf{u}_2 \tag{6.8}$$

We can write (6.8) as

$$\hat{\mathbf{o}}_c = \rho C|\mathbf{u}_2|\mathbf{u}_2 \tag{6.9}$$

where,

$$C = \frac{kNw\epsilon}{2} \tag{6.10}$$

is the drag coefficient of the top of the canopy. CRESSMAN (1960) estimates k ~1/4 for air flowing over mountain ridges. For k = 0.25, N = 100 m^{-2}, w = 0.1 m and ϵ = 0.1 m, (6.10) gives

$$C = 0.125 \tag{6.11}$$

The equation of motion for the upper layer is

$$\frac{\partial \mathbf{U}_2}{\partial t} + \rho g(D-b)\nabla h = \hat{\mathbf{o}}_a - \hat{\mathbf{o}}_c - \rho f\,\mathbf{k}\times\mathbf{U}_2 \tag{6.12}$$

Where

$\mathbf{U}_2 = (D-b)\mathbf{u}_2$

Write τ_a as

$$\hat{\mathbf{o}}_a = \rho_a C_w|\mathbf{W}|\mathbf{W} \tag{6.13}$$

where, ρ_a is the air density, C_w is the drag coefficient of the water surface, and $\mathbf{W}$ is the anemometer level wind. A typical value for C_w is (ROLL, 1965)

$$C_w = 2x103, \tag{6.14}$$

although SIMONS (1978) points out that storm surge modellers frequently must use higher values.

Now consider the case where the canopy extends above the water surface as shown in Fig. 6.14. τ_w is the stress the wind exerts on the top of the canopy, $\mathbf{W}_1$ is the mean wind within canopy, and τ_s is the stress the wind (i.e., $\mathbf{W}_1$) exerts on the water surface. Clearly, $|\mathbf{W}_1| < |\mathbf{W}|$ so $|\tau_s| < |\tau_a|$. Let $\mathbf{R}$ be the stress (force per unit horizontal area) exerted by $\mathbf{W}_1$ on the vertical canopy elements. By analogy to equation (6.4),

$$\mathbf{R} = \rho_a C_d N(b-D)w|\mathbf{W}_1|\mathbf{W}_1 \tag{6.15}$$

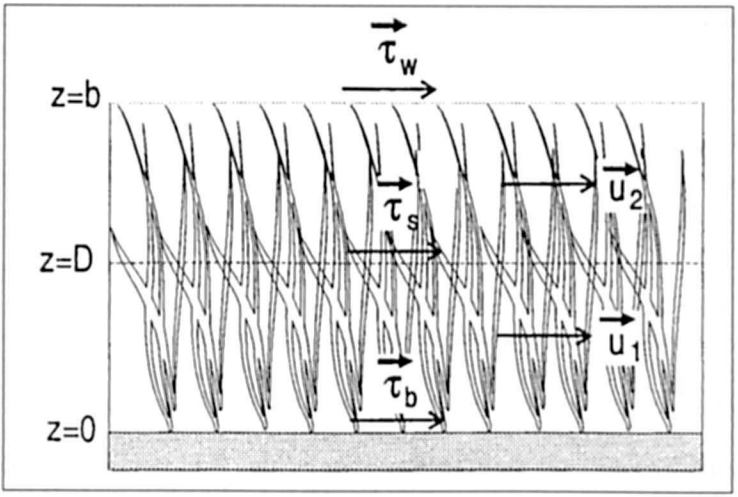

Fig. 6.14: Schematic diagram of stresses in case where canopy extends above the water surface (DANARD and MURTY, 1994)

The same drag coefficient is used in (6.4) and (6.15) since C_d is a function of the roughness of the surface and does not depend on the fluid (water or air) flowing over the surface. By analogy to (6.9),

$$\hat{\mathbf{o}}_w = \rho_a C |\mathbf{W}| \mathbf{W} \tag{6.16}$$

The same drag coefficient applies to (6.9) and (6.16) since they both represent fluid moving over the top of the canopy. By analogy to (6.13)

$$\hat{\mathbf{o}}_S = \rho_a C_w |\mathbf{W}_1| \mathbf{W}_1 \tag{6.17}$$

From the balance of forces in the layer $D \le z \le b$,

$$\hat{\mathbf{o}}_S = \hat{\mathbf{o}}_w \cdot \mathbf{R} \tag{6.18}$$

Each term in (6.18) is in the direction of **W**. Substituting (6.15) – (6.17) in (6.18) gives

$$W_1^2 = \left[\frac{C}{C_w + C_d N(b-D)w}\right] W^2 \tag{6.19}$$

This enables one to calculate τ_s from (6.17). Reid and Whitaker assume that $C = C_w = C_d$. However, C refers to flow over the top of the canopy whereas C_w refers to flow over a water surface. Clearly, then, $C \neq C_w$. Also, C_d refers to the obstruction to flow of the vertical surface of the canopy elements. Obviously between $C_w \neq C_d$ and $C \neq C_d$. The values given by (6.6), (6.11) and (6.14) show the differences between C_d, C and C_w.
The equation of motion for the water layer is (6.3)

$$\rho \frac{\partial \mathbf{U}_1}{\partial t} + \rho g D \nabla h = \hat{\mathbf{o}}_S - \hat{\mathbf{o}}_b - \mathbf{R} - \rho f \, \mathbf{k} \times \mathbf{U}_1 \tag{6.20}$$

The magnitude of the wind stress on the water is

$$\hat{o}_S = \rho_a C_w W_1^2 \tag{6.21}$$

where, W_1^2 is evaluated from (6.19). Substituting (6.19) in (6.21) yields

$$\hat{o}_S = \left[\frac{\rho_a C_w C}{C_w + C_d N(b-D)w}\right] W^2 \tag{6.22}$$

Using Reid and Whitaker's assumption ($C_w = C = C_d$), $\rho_a = 1.2$ kgm^{-3}, $C_w = 2 \times 10^{-3}$, $N = 100$ m^{-2}, $b = 2$ m, $D = 1$ m and $w = 0.1$ m, (6.22) gives

$$\hat{o}_S = 2.2 \times 10^{-4} W^2 \tag{6.23}$$

for τ_s on Pa and W in ms^{-1}. On the other hand if we employ (6.6), (6.11) and (6.14) in (6.1.50), we obtain

$$\hat{o}_S = 6.0 \times 10^{-6} W^2 \tag{6.24}$$

There is clearly a significant difference between (6.23) and (6.24), due to the fact that Reid and Whitaker predict a much higher wind speed at the water surface.

Comparison of equations (6.23) derived by Reid and Whitaker and (6.24) derived here shows that for the situation where the vegetation extends above the water surface, the effective wind stress is an order of magnitude smaller. This explains why a vegetation canopy (especially in the situation where the vegetation extends above the water surface) can moderate storm surges quite significantly.

It is well known that most of damage to coastal structures during a storm surge occurs from water currents and wind waves and not from the high water levels themselves. Hence, it is important to compute the water currents and wind waves for building design purposes.

Consider now the case of wind-driven water flow without a canopy. The linearized equation of motion is

$$\frac{\partial \mathbf{u}}{\partial t} + g\nabla h + \frac{1}{\rho}\nabla \rho_a = \frac{1}{\rho}\frac{\partial \hat{o}}{\partial z} - f\,\mathbf{k}\times\mathbf{u} \tag{6.25}$$

where, ρ_a is atmospheric pressure. Tides may be included in (6.25) by imposing boundary conditions on $\mathbf{u}$ and h at the seaward boundary of the computational domain. The non-linear advective acceleration is omitted from (6.25) although this may be important. Take the vertical average of (6.25) to yield

$$\frac{\partial \bar{\mathbf{u}}}{\partial t} + g\nabla h + \frac{1}{\rho}\nabla \rho_a = \mathbf{F} - f\,\mathbf{k}\times\bar{\mathbf{u}} \tag{6.26}$$

where, ($\bar{\mathbf{u}}$ is the vertically averaged water velocity,

$$\mathbf{F} = \frac{(\hat{o}_a - \hat{o}_b)}{\rho H} \tag{6.27}$$

is the vertically averaged friction force per unit mass and H = D + h is the total water depth. τ_a is usually calculated from (6.13). τ_b is frequently computed from a similar expression

$$\hat{o}_b = \rho c |\bar{u}| \bar{u} \tag{6.28}$$

where, c is the drag coefficient of the bottom surface. FLATHER (1979) and GREENBERG (1977) use

$$c = 2.5 \times 10^{-3} \tag{6.29}$$

However, (6.13) and (6.28) are calculated essentially independently, (6.4) therefore has a singularity as the denominator approaches zero. FLATHER and HEAPS (1975) avoid this singularity by specifying a minimum depth D_0 = 1m for use in (6.27). While this is preferable to having the model blow up, a better way is needed.

As the water depth becomes smaller, one would expect $\tau_b \rightarrow \tau_a$. Given the dimensionless number δ (≤ 0.1), there exists a depth d (δ) such that

$$\frac{|\hat{o}_a - \hat{o}_b|}{|\hat{o}_a|} \leq \delta \tag{6.30}$$

for $H \leq d$. However, (6.30) simply implies a constant flux layer through which $\tau \approx \tau_a$. For a neutral stratification this means

$$u = \frac{u_{*w}}{k_v} \ln\left(\frac{z}{z_0}\right) \tag{6.31}$$

where u_{*w} is the (constant) water friction velocity, k_v is von Karman's constant, and z_0 is the roughness length of the bottom surface. The vertical average of (6.31) is

$$\bar{u} = \frac{1}{(H - z_0)} \int_{z_0}^{H} u dz \tag{6.32}$$

Substituting (6.31) in (6.32) gives

$$\bar{u} = \frac{u_{*w}}{(H - z_0) k_v} \left\{ H \left[\ln\left(\frac{H}{z_0}\right) - 1 \right] + z_0 \right\} \tag{6.33}$$

For $z_0 \leq H$, (6.33) simplifies to

$$\bar{u} = \frac{u_{*w}}{k_v} \left[\ln\left(\frac{H}{z_0}\right) - 1 \right] \tag{6.34}$$

Note that (6.33) and (6.34) are diagnostic expressions for the water current. The direction of $\bar{u}$ is the same as τ_a or **W**. This will be discussed further in the paragraph following equation (6.41).

To find u_{*w}, note that the stress the water surface exerts on the atmosphere is equal in magnitude and opposite in direction to the stress the atmosphere exerts on the water. This is:

$$\varrho u_{*w}^{2} = \tau_a$$

or

$$u_{*w} = \left[\frac{\tau_a}{\varrho}\right]^{1/2} \tag{6.35}$$

An alternate to (6.33) and (6.34) may be obtained by setting $\tau_b = \tau_a$ in (6.28) and solving for $\bar{\mathbf{u}}$ to give

$$\bar{u} = \left(\frac{\tau_a}{c\rho}\right)^{1/2} \tag{6.36}$$

Let's obtain a numerical value for $\bar{\mathbf{u}}$ from (6.36). For $\rho_a = 1.2$ kgm^{-3}, $C_w = 2 \times 10^{-3}$ and $W = 10$ ms^{-1}, (6.13) gives $\tau_a = 0.24$ Pa. Substitute this value in (6.36) along with $c = 2.5 \times 10^{-3}$ and $\rho = 10^3$ kg m^{-3} to obtain ($\bar{u} = 0.31$ ms^{-1}.

An attempt will now be made to estimate the critical depth d following the method of DANARD (1981). Integrate (6.25) from z = 0 to z = d and write as

$$\frac{\left|\hat{\mathbf{o}}_a - \hat{\mathbf{o}}_b\right|}{\hat{\mathbf{o}}_a} = \frac{\varrho d\left|\partial \mathbf{u}/\partial t + g\nabla h + \varrho^{-1}\nabla \varrho_1 + f\,\mathbf{k}\times\bar{\mathbf{u}}\right|}{\left|\hat{\mathbf{o}}_a\right|} \tag{6.37}$$

Equating the right side of (6.37) to (and solving for *d* gives

$$d = \frac{\delta\left|\hat{\mathbf{o}}_a\right|}{\varrho\left|\partial \mathbf{u}/\partial t + g\nabla l + \varrho^{21}\nabla \varrho_a + f\,\mathbf{k}\times\bar{\mathbf{u}}\right|} \tag{6.38}$$

Suppose the water velocity decreases by 0.1 ms^{-1} in 10^3 s. Then for $\rho = 10^3$ kg m^{-3}, $\rho|\partial \mathbf{u}/\partial t| \sim 0.1$ Pa m^{-1}. The terms $g\nabla h$ and $f\mathbf{k} \times \bar{\mathbf{u}}$ frequently offset each other and do so exactly if the current is geostrophically balanced. The sum of these terms should be the same order of magnitude as $\partial \bar{\mathbf{u}}/\partial t$. Now

$$\left|\nabla \varrho_a\right| = \varrho_a f\left|\mathbf{W}_g\right| \tag{6.39}$$

where, $\mathbf{W}_g$ is the geostrophic wind. For $\rho = 1.2$ kg m^{-3}, $f = 10^{-4}$ s^{-1} and $|\mathbf{W}_g| = 15$ ms^{-1}, (6.39) gives $|\nabla \rho_a| = 1.8 \times 10^{-3}$ Pa m^{-1}. This is two orders of magnitude smaller than $\rho|\partial \bar{\mathbf{u}}/\partial t|$ so we will approximate (6.38) by

$$d = \frac{\delta\left|\hat{\mathbf{o}}_a\right|}{\rho\left|\partial \bar{\mathbf{u}}/\partial t\right|} \tag{6.40}$$

In the previous paragraph we calculated $|\tau_a| = 0.24$ Pa. Setting $\delta = 0.1$ in (6.40) yields Larger accelerations attainable in small mesh models would result in smaller values of d.

$$d = 0.24 \text{ m} \tag{6.41}$$

To show that $\bar{\mathbf{u}}$ is in the same direction as τ_a or $\mathbf{W}$, it has just been demonstrated that if $H \le d$, then τ_a and τ_b are approximately parallel. One would expect $\bar{\mathbf{u}}(H)$ to be parallel to τ_a.

For small z, one would expect $\bar{\mathbf{u}}(z)$ to be parallel to τ_b (6.28). It follows that the direction of $\bar{\mathbf{u}}(z)$ is approximately constant for all z and therefore $\bar{\mathbf{u}}$ is parallel to τ_a.

It is proposed that the prognostic calculation of $\bar{\mathbf{u}}$ using equation (6.26) be replaced by a diagnostic calculation using equation (6.36), when the total water depth falls below a critical value *d*. Here *d* may be estimated from (6.38) or (6.10) using the nearest available data, or replaced by a constant which varies directly with grid size.

One shortcoming of the diagnostic approach is that the water current is always in the direction of the wind. Thus an ebbing tide with an onshore wind of any magnitude would result in onshore water current. Similarly, an incoming tide with zero wind stress would have zero water velocity. However, this is only for points nearest the shore whose depths are less than d.

Next we describe a new method for calculating **F**, which may be used for smaller depths than equation (6.37). Consider 2-dimensional flow (u, w) in the vertical x–z plane. The following derivation in this paragraph [equations (6.42)–(6.49)] is similar to classical boundary layer theory (see e.g., HALTINER and MARTIN, 1957). However, the rest of the derivation is new. The horizontal stress is

$$\tau = -\rho u' w' \tag{6.42}$$

where, the primes denote perturbation velocities (departures from time-average values) and the carat signifies a time average. Assume that

$$u' = \ell\left(\frac{\partial u}{\partial z}\right) \tag{6.43}$$

where, ℓ is the mixing length. Assume also that

$$u' = -w'\,\mathrm{sign}\left(\frac{\partial u}{\partial z}\right) \tag{6.44}$$

where, sign($\partial u/\partial z$) has the sign of $\partial u/\partial z$ and a unit magnitude. Substituting (6.43) and (6.44) in (6.42) yields

$$\tau = \rho\left(\ell\frac{\partial u}{\partial z}\right)^2 \mathrm{sign}\left(\frac{\partial u}{\partial z}\right) \tag{6.45}$$

A negative sign ($\partial u/\partial z$) means that τ is in the -x direction. Now assume that

$$\ell = k_v z \tag{6.46}$$

Substituting (6.46) in (6.45) gives

$$\tau = \rho\left(k_v z\frac{\partial u}{\partial z}\right)^2 \mathrm{sign}\left(\frac{\partial u}{\partial z}\right) \tag{6.47}$$

Define the friction velocity u_* from the equation

$$\tau = \rho u_*^2 \operatorname{sign}(u_*) \tag{6.48}$$

where, sign (u_*) = sign$(\partial u/\partial z)$. Then from (6.47) and (6.48),

$$u_0 = k_v z \frac{\partial u}{\partial z} \tag{6.49}$$

If

$$u_* = u_{*w} = \text{constant}, \tag{6.50}$$

where, u_{*w} is given by (6.35), then (6.31) is obtained. However, to obtain a more general result, instead of (6.50) it will be assumed that the friction velocity varies linearly with height, i.e.,

$$u_* = u_{*w} - a(H - z) \tag{6.51}$$

where, a is a constant, which may be positive or negative. Substituting (6.51) in (6.49) yields

$$u = \frac{(u_{*w} - aH)}{k_v} \ln\left(\frac{z}{z_0}\right) + \frac{b(z - z_0)}{k_v} \tag{6.52}$$

Note that (6.52) is similar to the 'log-linear' profile of stable flows (see, e.g. DEARDROFF, 1972, eq. [13]). The mean velocity is obtained by substituting (6.52) in (6.32), assuming $z_0 \perp H$. and integrating to give

$$\bar{u} = \frac{(u_{*w} - aH)}{k_v}\left[\ln\left(\frac{H}{z_0}\right) - 1\right] + \left(\frac{aH}{2K_v}\right) \tag{6.53}$$

Since aH is unknown, (6.53) is not a diagnostic equation for $\bar{u}$. However, (6.34) and (6.36) are diagnostic equations.
The vertically averaged frictional force per unit mass is

$$F = \frac{u_{*w}^2 \operatorname{sign}(u_{*w}) - u_{*0}^2 \operatorname{sign}(u_{*0})}{H} \tag{6.54}$$

where, from (6.51),

$$u_{*0} = u_{*w} - aH \tag{6.55}$$

The quantity aH is obtained diagnostically from the mean water velocity using (6.53):

$$aH = \frac{u_{*w}\left[\ln\left(\frac{H}{z_0}\right)-1\right]-k_v\bar{u}}{\left[\ln\left(\frac{H}{z_0}\right)-\frac{3}{2}\right]} \tag{6.56}$$

This expression has a singularity for

$$\ln\left(\frac{H}{z_0}\right)=\frac{3}{2}$$

or

$$\frac{H}{z_0}=4.5 \tag{6.57}$$

In deriving (6.56) it was assumed that $H/z_0 \pi 1$, although if this assumption were not made, all that would result would be the appearance of additional terms. If use of (6.56) is limited to cases where $H > d$ (see eq. [6.38]) or $H > 10z_0$, whichever is larger, then the singularity (6.57) will pose no problem. This limitation on H will also help avoid the singularity in (6.54) for $H = 0$. The numerator of the right side of (6.56) won't necessarily become small for small H, nor will the numerator of (6.54).

Equations (6.54)–(6.56) provide a diagnostic procedure for evaluating F given u_{*w}, H, z_0 and $\bar{u}$. If tides are included, they will affect $\bar{u}$.

It was shown above that a vegetation canopy, especially one that projects above the water surface can significantly dissipate storm surges. This has practical importance because instead of erecting prohibitively expensive sea walls, one can use reed grass whose expense will be orders of magnitude less. A method has been proposed to compute the horizontal currents, which account for most of the damage. A prior knowledge of the possible maximum value of such currents for each surge prone location can help in the design of coastal engineering structures.

6.1.5 Galveston Bay

REID and BODINE (1968) developed a two-dimensional numerical model for computing storm surges in Galveston Bay. They also allowed for rainfall by including it in the continuity equation. The observed and computed surges at different locations for two different hurricanes are compared in Fig. 6.15 and 6.16. BUTLER (1979) also developed a two-dimensional numerical model for storm surge computations in Galveston bay. The time dependence is treated implicitly in this model. Spatially varying and time-dependent wind fields and rainfall are included. Flooding of low-lying areas is simulated by treating the location of land-water boundary as a function of the time-varying local water depth. Subgrid barrier effects are also included. Exposed, submerged, and overtopping barriers can be represented in the mesh system; thus, one can allow for the surge waters breaching narrow barriers such as elevated highway, control structures, etc.

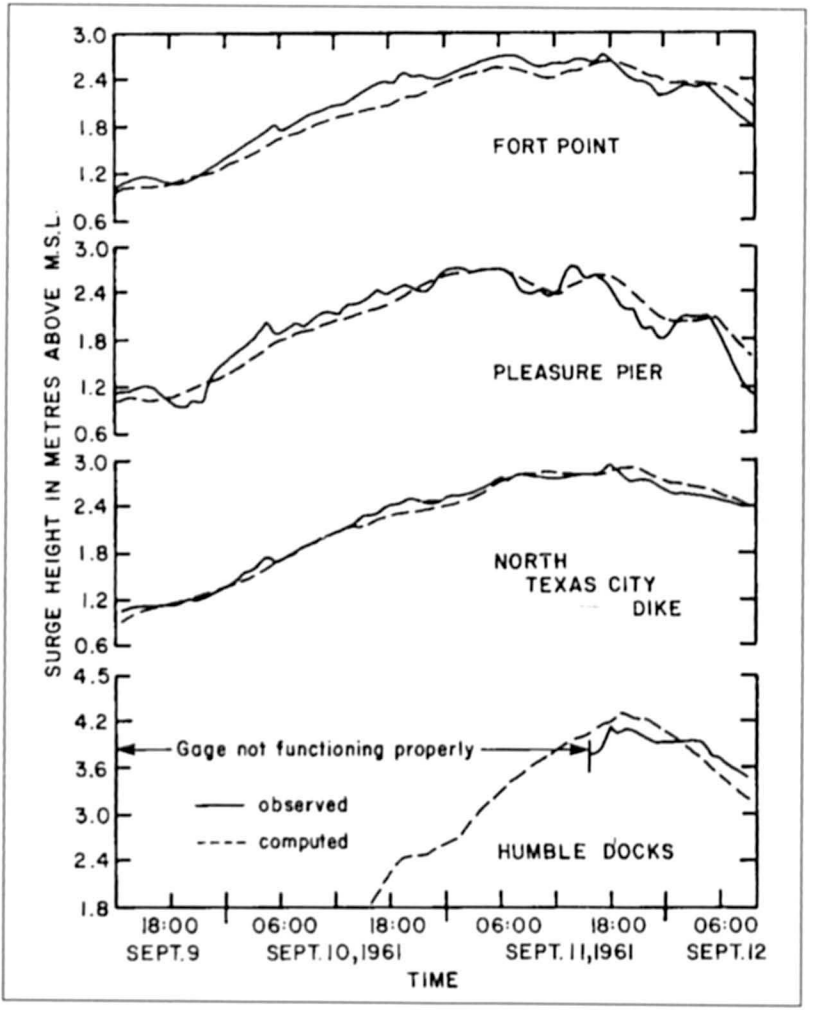

Fig. 6.15: Comparison of observed and computed surges at four locations in Galveston Bay due to Hurricane Carla of September 9–12, 1961 (REID and BODINE, 1968)

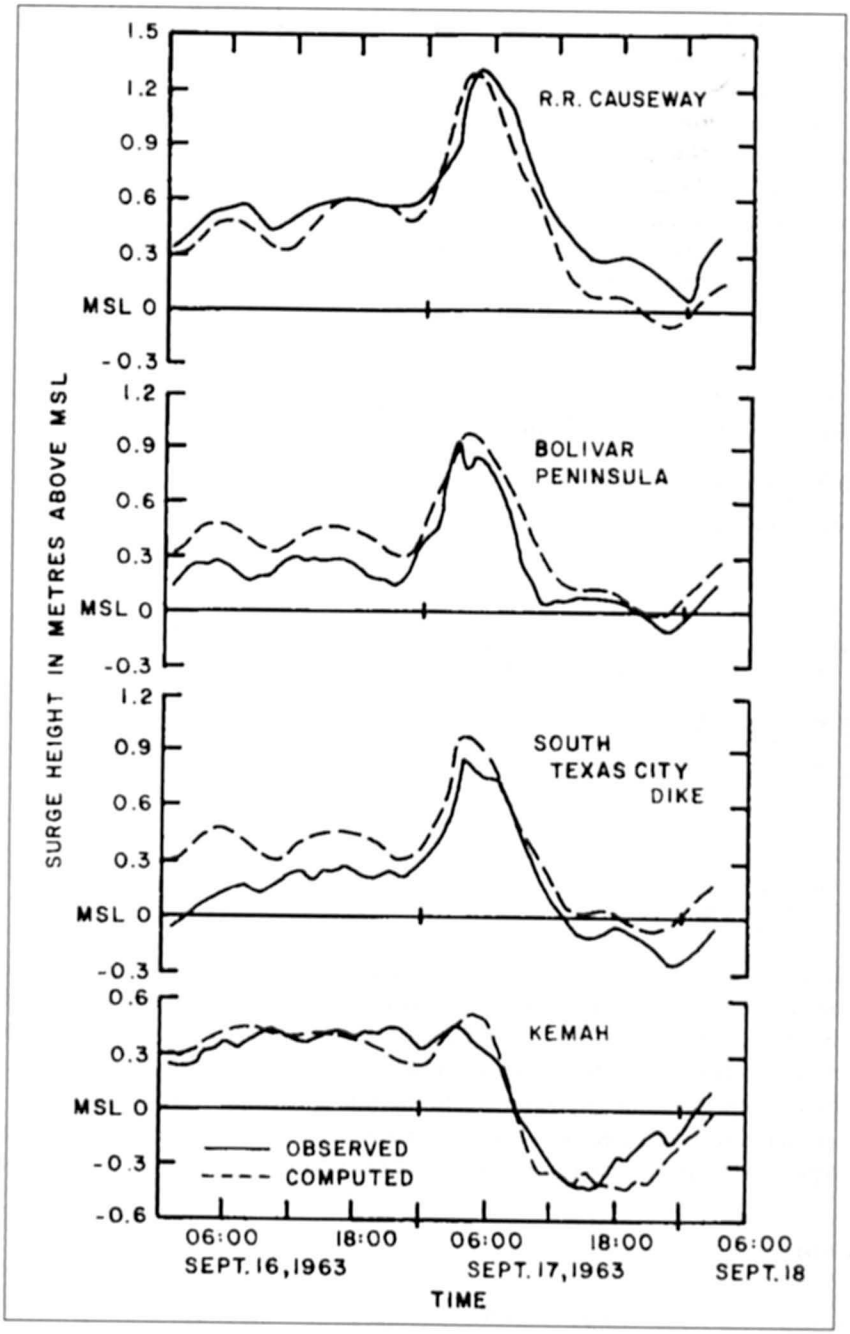

Fig. 6.16: Comparison of computed and observed surges at four locations in Galveston Bay due to Hurricane Cindy of September 16–18, 1963 (REID and BODINE, 1968)

One special feature of this model is the employment of a coordinate transformation in the form of a piecewise exponential stretch. This transformation maps prototype space, discretized with a smoothly varying grid, into computational space with a regularly spaced grid, and in the computational space all the derivatives are cantered. Through this transformation one can simulate a complex domain by locally increasing grid resolution and also by aligning coordinates along physical boundaries. A smoothly varying grid with continuous first derivatives eliminates the problem usually associated with variable grids. Indeed, BUTLER (1979) used expansions of grid length in prototype space by a factor of 10. BUTLER (1979) wrote the vertically integrated two-dimensional equations of motion and continuity as follows:

$$\frac{\partial U}{\partial t}+\frac{\partial}{\partial x}\left(\frac{U^2}{d}\right)+\frac{\partial}{\partial y}\left(\frac{UV}{d}\right)-fV+gd\frac{\partial}{\partial x}(\eta-\eta_a)+F_x+\frac{gU}{c^2d^2}\left(U^2+V^2\right)^{1/2}$$
$$-de\left(\frac{\partial^2 U}{\partial x^2}+\frac{\partial^2 U}{\partial y^2}\right)=0 \qquad (6.58)$$

$$\frac{\partial V}{\partial t}+\frac{\partial}{\partial x}\left(\frac{UV}{d}\right)+\frac{\partial}{\partial y}\left(\frac{V^2}{d}\right)+fU+gd\frac{\partial}{\partial y}(\eta-\eta_a)+F_y+\frac{gV}{c^2d^2}\left(U^2+V^2\right)^{1/2}$$
$$-de\left(\frac{\partial^2 V}{\partial x^2}+\frac{\partial^2 V}{\partial y^2}\right)=0 \qquad (6.59)$$

$$\frac{\partial \eta}{\partial t}+\frac{\partial U}{\partial x}+\frac{\partial V}{\partial v}=0 \qquad (6.60)$$

Here, h is the still-water elevation, $d = h + \eta$ is the total water depth, c is the Chezy friction coefficient, e is a generalized eddy viscosity coefficient, R is the rate at which additional water is introduced into or taken out of the water body (rainfall, evaporation), F_x and F_y represent external forcing functions such as wind stress, η is the water surface elevation, and η_a is the hydrostatic elevation corresponding to the atmospheric pressure anomaly.

For each direction a piecewise reversible transformation is independently used to map prototype into computational space. The transformation is of the form

$$x = a + b\alpha^c \qquad (6.61)$$

where, a, b, and c are arbitrary constants. The equations of motion in the α-space are

$$\frac{\partial U}{\partial t}+\frac{1}{\mu_1}\frac{\partial}{\partial \alpha_1}\left(\frac{U^2}{d}\right)+\frac{1}{\mu_2}\frac{\partial}{\partial \alpha_2}\left(\frac{UV}{d}\right)-fV+\frac{gd}{\mu_1}\frac{\partial}{\partial \alpha_1}(\eta-\eta_a)+F_{\alpha_1}$$
$$+\frac{gU}{C^2d^2}\left(U^2+V^2\right)^{1/2}-T_1=0 \qquad (6.62)$$

$$\frac{\partial V}{\partial t}+\frac{1}{\mu_1}\frac{\partial}{\partial \alpha_1}\left(\frac{UV}{d}\right)+\frac{1}{\mu_2}\left(\frac{V^2}{d}\right)+fU+\frac{gd}{\mu_2}\frac{\partial}{\partial \alpha_2}(\eta-\eta_a)+F_{\alpha_2}$$

$$+\frac{gV}{C^2d^2}\left(U^2+V^2\right)^{1/2}-T_2=0 \qquad (6.63)$$

$$\frac{\partial \eta}{\partial t}+\frac{1}{\mu_1}\frac{\partial U}{\partial \alpha_1}+\frac{1}{\mu_2}\frac{\partial V}{\partial \alpha_2}=R \qquad (6.64)$$

where,

$$\mu_1=\frac{\partial x}{\partial \alpha_1}=b_1c_1\alpha^{c_1-1} \qquad (6.65)$$

$$\mu_2=\frac{\partial y}{\partial \alpha_2}=b_2c_2\alpha^{c_2-1} \qquad (6.66)$$

Table 6.10: Comparison of computed and observed surges (m) at several locations in Galveston Bay due to Hurricane Carla of 1961 (mean absolute error = 0.18 m). (BUTLER, 1979)

Gauge Location	Observed	Computed	Difference
Oyster Creek	3.11	3.29	+0.18
San Luis Pass	3.29	3.05	−0.24
Sea Isle Beach	3.69	3.05	−0.64
Bermuda Beach	3.20	2.99	−0.21
Scholes Field	2.59	2.93	+0.33
Bolivar Beach	2.83	2.83	+0.00
Crystal Beach	2.68	2.87	+0.18
Rollover Beach	2.93	2.83	−0.09
Halls Bayou	4.36	4.30	−0.06
Highway Six	3.84	3.87	+0.03
Sievers Cove	3.23	2.83	−0.39
Dickinson Bayou	3.47	3.60	+0.12
Carbide Docks	3.35	3.17	−0.18
Kemah	4.33	3.90	−0.43
Smith Point	2.99	3.17	+0.18
Oyster Bayou	3.20	3.35	+0.15
Scott Bay	4.33	4.30	−0.03
Humble Docks	4.18	3.84	−0.34
Ananuac	3.78	3.87	+0.09
Wallisville	4.27	4.26	+0.00
Pleasure Pier	2.83	2.87	+0.03
Fort Point	2.74	2.90	+0.15
Pier 21	2.68	2.90	+0.21
Pelican Bridge	2.74	2.87	+0.12
Texas City Dyke (south)	2.90	3.05	+0.15
Texas City Dyke (north)	2.96	3.05	+0.09

The parameters μ_1 and μ_2 define stretching of the regular grid into α-space to approximate the study area of real space. The terms T_1 and T_2 represent the transformed flux terms (which are not included in the application to Galveston Bay).

The above model is applied to storm surge computation in Galveston Bay (which is a large shallow bay of area greater than 1000 km^2) due to Hurricane Carla of 1961. The model was calibrated by reproducing the tides. The observed and computed surges at 26 different locations are compared in Table 6.10.

6.1.6 Pamlico Sound and Cape Fear Estuary

Two important water bodies along the coast of North Carolina are Palmico Sound in the north and Cape Fear Estuary in the south In Palmico sound the astronomical tides are small (5-cm range) but storm surges could be significant. ROELOFS and BUMPUS (1953) calculated the surges in this water body using the following simple relation of KEULEGAN (1951):

$$\frac{S}{L} = 3.3\times10^{-6}\left[1+63\left(\frac{H}{L}\right)^{1/2}\right]\frac{V^2}{gH} \qquad (6.67)$$

where, S is the setup (i.e. $h_2 - h_1$, where h_2 and h_1 are the windward and leeward displacements of water level), L is the length of the water body, V is the wind velocity, and H is the mean depth of the water body. From this formula it was calculated that a southwest wind of about 13 knots (24 km $\cdot$ h^{-1}) is needed to generate a setup of about 1 feet (0.3 m) and a 40-knot (74 km $\cdot$ h^{-1}) wind could produce a surge of 9.8 ft (3 m). This result does not include the funnelling effect due to the geometry of the sound. Northeasterly winds will cause a similar rise along the southwest shore.

MYERS (1975) used a one-dimensional numerical model to calculate the storm surges in Cape Fear Estuary. Some recent dredging operations increased the tidal range at Wilmington, North Carolina. Hence, they used two different depth profiles: the first corresponding to the early 1950's and the second corresponding to the present depths. They generated time histories of the open coast surge from the SPLASH II model for an ensemble of hurricanes, each storm being related to a frequency of occurrence. These time histories are linearly combined with appropriate phases of the astronomical tide at the entrance to Cape Fear River. Three hurricanes were selected: Hazel of 1954, Diane of 1955, and Helene of 1958. The pertinent information for these hurricanes is listed in Table 6.11.

Table 6.11: Meteorological data for Hurricanes Hazel of 1954, Diane of 1955, and Helene of 1958 (MYERS, 1975)

Hurricane	Central pressure depression (mb)	Radius of maximum winds (km)	Speed of movement (km·h^{-1})	Maximum wind speed (km·h^{-1})
Hazel	66	38.9	53.2	166.7
Diane	30	31.5	22.8	110.4
Helene	65	38.9	24.1	165.9

Table 6.12: Pertinent information about selected hurricanes affecting Chesapeake Bay. (BRETSCHNEIDER, 1959)

Parameter	Hurricane of Aug. 22–24, 1933	Connie of Aug. 11–13, 1955	Diane of Aug. 15–18, 1955	Hazel of Oct. 14–17, 1957
Track	Just west of Chesapeake Bay's west coast	Just west of Chesapeake Bay's east coast	About 160 km west of Chesapeake Bay's west coast	About 160 km west of Chesapeake Bay's west coast
Radius of maximum winds ($km \cdot h^{-1}$)	86.9	72.4	72.4	57.9
Central pressure anomaly (mb)	28.8	46.4	24.0	56.2
Speed of movement over ocean ($km \cdot h^{-1}$)	46.2	22.2	38.9	101.9
Speed of movement over Chesapeake Bay ($km \cdot h^{-1}$)	24.1	18.5	22.2	66.6
Maximum wind speed over ocean ($km \cdot h^{-1}$)	98.2	115.9	86.9	148.1
Maximum wind speed over Chesapeake Bay ($km \cdot h^{-1}$)	80.5	72.4	56.3	112.7
Peak surge (m) at Hampton Roads, VA	2.01	1.34	0.18	0.55
Peak surge (m) at Gloucester Point, VA	–	1.37	0.70	0.88
Peak surge (m) at Solomon's Island, MD	–	1.28	0.67	0.85
Peak surge (m) at Annapolis, MD	1.77	1.49	0.98	1.28
Peak surge (m) at Baltimore, MD	2.20	1.59	1.13	1.46

6.1.7 Chesapeake Bay

Hurricane-generated storm surges in this water body were studied by BRETSCHNEIDER (1959). Of all the hurricanes that generated surges in Chesapeake Bay up to 1959, only four are sufficiently well documented: August 22–24, 1933, August 11–13, 1955 (Connie), August 15–18, 1955 (Diane), and October 14–17, 1954 (Hazel).

The pertinent information for the meteorological aspects of these hurricanes as well as the storm surges recorded is given in Table 6.12. Some typical surge profiles in Chesapeake Bay are illustrated in Fig. 6.17 and 6.18.

For computing the surges outside Chesapeake Bay on the open coast, two model hurricanes were selected. The first (referred to as A) is the September 14, 1944, hurricane transposed to the Chesapeake Bay area but not adjusted for filling. For this hurricane, the radius R of maximum winds is 33.5 nautical miles (62 km); the atmospheric pressure anomaly at the center is 2.2 in. Hg (74.5 mb), and the maximum sustained wind speed at R is 105 $mi \cdot h^{-1}$ (169 $km \cdot h^{-1}$). The path of movement over the open ocean was assumed to be perpendicular to the coast and the speed of travel was 15–25 $mi \cdot h^{-1}$ (24–40 $km \cdot h^{-1}$). After crossing the coast, the path of movement curves and proceeds northward along the west side of Chesapeake Bay, and the speed of movement reduces to 12–15 $mi \cdot h^{-1}$ (19–24 $km \cdot h^{-1}$). The second storm (referred to as B) is exactly the same as A, except that all wind speeds are 5 $mi \cdot h^{-1}$ (8 $km \cdot h^{-1}$) larger. The results for the surges due to hurricanes A and B are summarized in Table 6.13. The prediction curves for hurricane surges at Washington, DC, are given in Fig. 6.19.

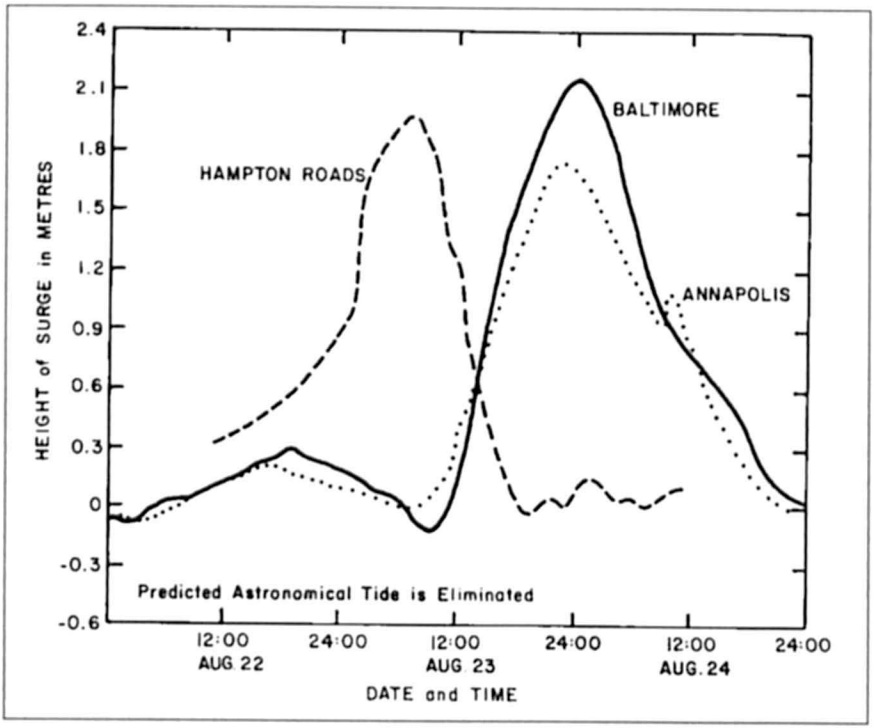

Fig. 6.17: Storm surges at three locations in Chesapeake Bay due to the hurricane of August 22–24, 1933 (BRETSCHNEIDER, 1959)

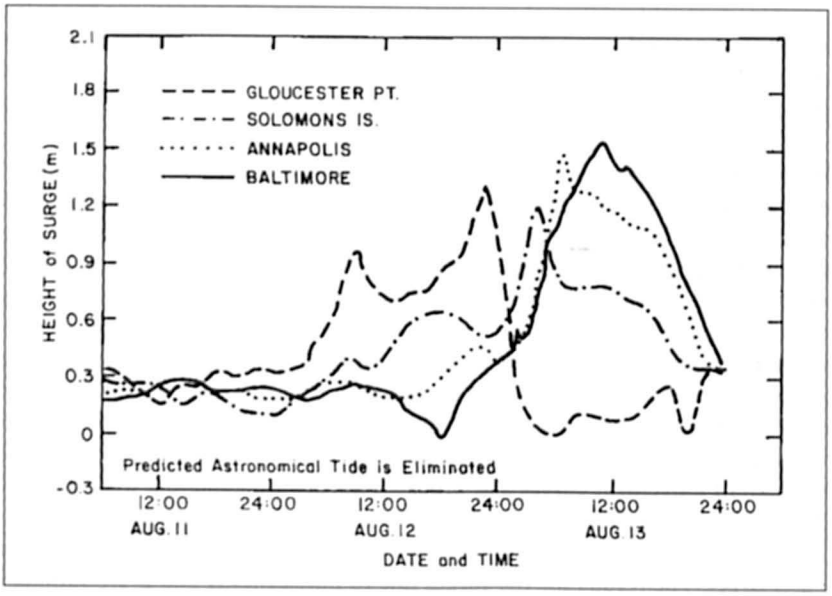

Fig. 6.18: Storm surges at four locations in Chesapeake Bay due to Hurricane Connie of August 11–13, 1955 (BRETSCHNEIDER, 1959)

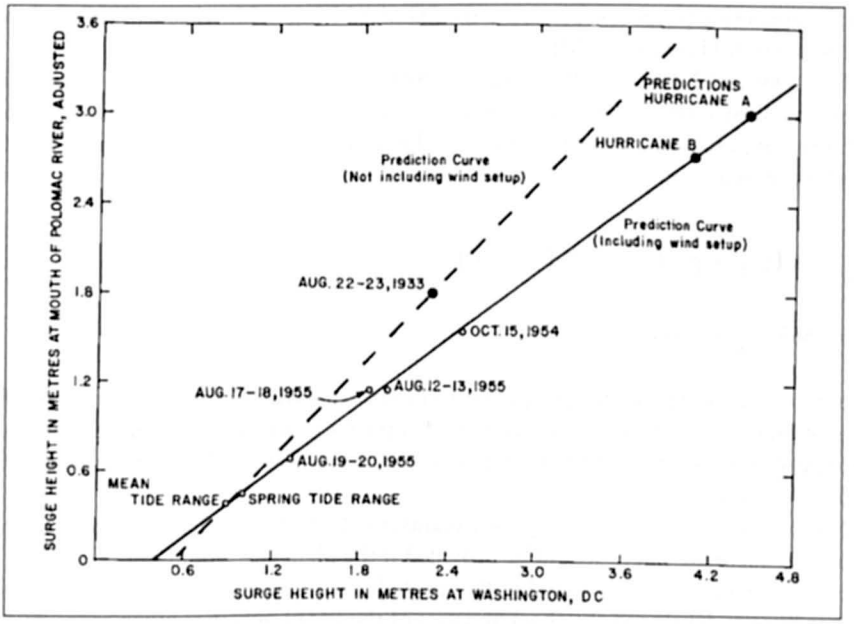

Fig. 6.19: Storm surges prediction curves for hurricane generated storm surges at Washington D.C. (BRETSCHNEIDER, 1959)

BODINE (1971) used the bathystrophic theory to compute storm surges on an open coast and applied this to the Chesapeake Bay area. In this connection, he pointed to the important effect of interaction between tide and surge, especially when it is recognized that the tidal range can vary from 18.2 ft (5.5 m) at East Port, Maine, to 1.3 ft (0.4 m) at Key West, Florida, and that, generally, the tides along the Atlantic coast of the United States are semidiurnal whereas along the Gulf of Mexico coast they are mainly diurnal.

Table 6.13: Computed storm surges in Chesapeake Bay due to hurricanes A and B. These values have an uncertainty of 0.12 m (BRETSCHNEIDER, 1959)

Location	Maximum surge (m) due to	
	Hurricane A	Hurricane B
Hampton Roads, VA	3.29	3.57
Mouth of York River	3.14	3.44
Mouth of Rappahanock River	2.99	3.26
Mouth of Potomac River	2.77	3.05
Mouth of Severn River	2.53	2.77
Mouth of Patapaco River	2.87	3.11

To give the most probable degree of protection required for any given area, the standard practice is to select a hurricane with a given set of characteristics for the particular geographical location. This will be called a "hypothetical" or "hypohurricane". Also, for such a hurricane the characteristics are taken as invariant and the track is assumed to follow a prescribed path. The U.S. Weather Bureau and the U.S. Army Corps of Engineers jointly established two design storms (which depend on the geographical location) for practical use for

coastal engineering purposes. These are the Standard Project Hurricane (SPH) and the Probable Maximum Hurricane (PMH).

GRAHAM and NUNN (1959) defined the SPH as a hypohurricane that is intended to represent the most severe combination of hurricane parameters that is reasonably characteristic of a region, excluding extremely rare combinations. The maximum gradient wind speed in the belt of maximum winds (miles per hour) was determined by the following formulae:

$$V_{gx} = K(p_n - p_0)^{1/2} - R(0.575f) \tag{6.68}$$

$$V_x = 0.865V_{gx} + 0.5V_F \tag{6.69}$$

where K = 73, p_n and p_0 are the peripheral and central pressures in inches of mercury, R is the radius of maximum winds in nautical miles, f is the Coriolis parameter in units per hour, V_F is the speed of movement of the hurricane in miles per hour, and V_x is the maximum wind speed 30 ft (9.1 m) above the water.

For protection of the nuclear power plants, the U. S. Atomic Energy Commission concluded that adequate safety would be provided if the plant site would not be flooded by the surge and surface waves associated with a probable maximum hurricane (PMH). The U. S. Weather Bureau developed the characteristics of the PMH, which is much more severe than the SPH. The PMH was defined as a hypothetical hurricane having that combination of characteristics that will make it the most severe storm that can probably occur in the particular region involved. The hurricane should approach the point under study along a critical path and at an optimum rate of movement. Development of the isovel fields is basically the same for the PMH as for the SPH. The difference essentially is that whereas p_n is taken as the standard sea level pressure of 29.92 in. Hg. (1013.2 mb) for the SPH, it is treated as a function of the latitude for the PMH. Also, K is treated as a function of latitude for the PMH whereas it is a constant for SPH. At times it may be desirable to select a design storm other than the SPH or PMH based on the risk or economy factors for a particular location or coastal structure. Using bathystrophic theory, BRETSCHNEIDER (1959) estimated the peak surge (for a selected storm) at the mouth of Chesapeake Bay to be 13.4-ft (4.1 m).

PORE (1965) studied hurricane-generated storm surges in Chesapeake Bay. He made a distinction between western-type (i.e. hurricanes passing west of the bay) and eastern-type (hurricane travelling east of the bay) storms. His study showed that the western-type storms create greater surges in the northern part of the bay whereas the eastern-type storms generate greater surges in the southern portion of the bay. The storm surges resulting from these two types of hurricanes are listed in Tables 6.14 and 6.15.

Table 6.14: Storm surges data for western type storms in the Chesapeake Bay region (PORE, 1965)

Date	Surge amplitudes (m) at						Time lag (h) from Norfolk to Baltimore	Storm movement (km) northward in 12 h
	Baltimore	Annapolis	Cambridge	Solomon's point	Gloucester point	Hampton Roads		
Oct. 2, 1929	1.19	1.10	–	–	–	0.73	18	352
Aug. 23, 1933	2.13	1.68	–	–	–	1.86	18	315
June 19, 1934	–	–	–	–	–	0.24	–	148
Sept. 18, 1945	0.82	0.73	0.70	0.64	–	0.73	17	389
Aug. 29, 1949	0.52	0.43	0.46	0.24	–	–0.06	–	519
Sept. 1, 1952	1.04	0.88	–	0.49	0.15	0.12	13	241
Oct. 15, 1954	1.40	1.19	–	0.85	0.34	0.46	14	945
Aug. 18, 1955	1.88	0.73	–	0.52	0.52	0.30	21	241

Table 6.15: Storm surge amplitudes (m) for eastern type storms in the Chesapeake Bay region. For certain cases, maximum positive and negative surges are listed (PORE, 1965)

Date	Baltimore	Annapolis	Cambridge	Solomon's point	Gloucester point	Hampton Roads	Portsmouth
Sept. 16, 1933	0.27	0.30	–	–	–	1.55	–
Sept. 8, 1934	–	–	–	–	–	0.24	–
Sept. 18, 1936	–1.74, 0.40	–1.28, 0.37	–	–	–	1.49	–
Sept. 21, 1938	–0.98, 0.06	–0.67, 0.03	–	–0.43	–	–	0.55
Oct. 24, 1938	0.21	0.21	–	1.8	–	–	0.21
Sept. 1, 1940	0.06	0.06	–	0.06	–	–	0.09
Sept. 14, 1944	–0.64, 0.27	–0.49, 0.21	–0.27, 0.24	–0.18, 0.18	–	1.13	–
June 26, 1945	–0.34, 0.18	–0.24, 0.24	–0.18, 0.27	0.15	–	0.79	–
Aug. 20, 1950	0.21	0.21	0.15	0.18	–	0.24	–
Aug. 14, 1953	–0.79, 0.40	–0.73, 0.34	–	–0.46, 0.34	0.94	1.13	–
Aug. 31, 1954	–0.18, 0.21	0.24	–	0.24	0.49	0.79	–
Sept. 11, 1954	–0.43, 0.15	–0.30, 0.12	–	–0.12, 0.15	0.67	0.88	–
Sept. 27, 1956	0.34	0.58	–	0.64	–	1.13	–
Aug. 28, 1958	–0.37, 0.18	–	–	0.18	–	0.34	–

6.1.8 Coast of New Jersey

The greatest loss of life and property, damage on the coast of New England occurred during September 21–22, 1938, as a result of storm surge generated by a West Indian hurricane coupled with river flooding (due to excessive rainfall). The storm surge amplitude was maximum in Rhode Island with values exceeding 17-ft. (5.2) m, and the amplitudes reached record levels all along the coast between New York City and Cape Cod. More than 500 people died (PAULSEN et al., 1940) and the property damage exceeded $ 0.3 billion (at 1938 prices).

The storm surge amplitudes at Sandy Hook on the coast of New Jersey and at three other locations are listed as a function of time in Table 6.16. The surge profiles at Forest Hills and Rockway Park, both in New York State, are shown in Fig. 1.2 and 1.3.

Table 6.16: Storm surge amplitudes (m) as a function of time on the Massachusetts-New York-New Jersey coast during Sept. 21–22, 1938. Time is local time. (PAULSEN et al., 1940)

Hour	Sandy Hook, NJ		The Battery, NY		Boston, MA		Mill Neck, NY
	Sept. 21	Sept. 22	Sept. 21	Sept. 22	Sept. 21	Sept. 22	Sept. 21
01	0.40	–0.49	0.27	–0.21	0.30	0.85	–
02	0.85	–0.37	0.73	–0.18	–0.18	–0.03	–
03	1.19	–0.03	1.13	–0.12	–0.03	–0.49	–
04	1.55	0.58	1.46	0.64	0.49	–0.12	–
05	1.71	1.52	1.59	1.34	1.16	0.24	–
06	1.62	1.74	1.62	1.71	1.92	0.91	–
07	1.34	1.59	1.46	1.71	2.65	1.89	–
08	1.04	1.16	1.22	1.43	3.14	2.80	–
09	0.76	0.76	0.88	1.10	3.20	3.23	–
10	0.49	0.34	0.61	0.61	2.80	2.23	–
11	0.30	0.09	0.37	0.34	2.19	2.80	–
12	0.30	0	0.15	0.09	1.55	2.16	–
13	0.55	–0.03	0.18	0	0.79	1.34	–
14	1.07	0.12	0.55	0	0.21	0.43	–
15	1.80	0.55	1.34	0.30	0.18	–0.24	–
16	2.38	1.01	2.47	0.91	0.91	–0.37	–
17	1.55	1.46	2.04	1.37	1.62	0.15	–
18	0.91	1.74	1.16	1.65	2.13	0.82	–
19	0.24	1.77	1.01	1.74	2.68	1.71	3.54
20	0.09	1.43	0.73	1.65	3.23	2.53	4.60
21	0.76	0.98	0.70	1.34	3.35	3.17	4.02
22	0.79	0.58	1.22	0.91	3.05	3.35	3.78
23	0.24	0.24	0.49	0.52	2.50	3.05	3.69
24	–0.37	0	–0.03	0.21	1.86	2.44	3.66

PAGENKOPF and PEARCE (1975) developed several storm models and applied these to the New Jersey coast. In particular, these authors compared two-dimensional finite-difference and finite-element methods and concluded that, at least for storm surge calculations, there is no particular advantage to preferring one to the other. They also compared their results with bathystrophic storm surge calculations. All these calculations were made for the hurricane of

September 14, 1974. The results from bathystrophic calculations are not satisfactory in certain circumstances. The horizontal distributions of storm surge heights computed by the finite-difference and finite-element models are compared in Fig. 6.20.

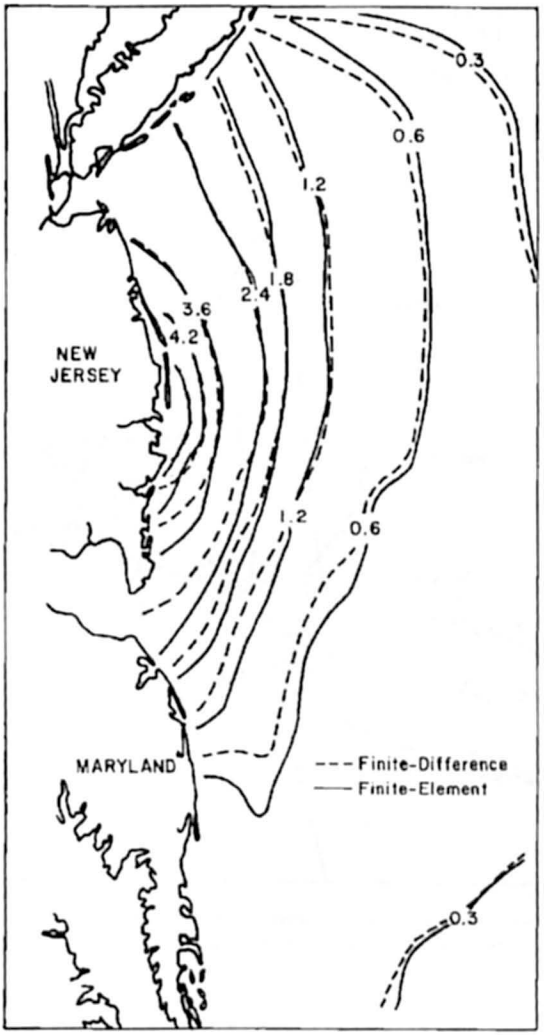

Fig. 6.20: Calculated storm surge heights (meters) along the coast of New Jersey (PAGENKOPF and PEARCE, 1975)

6.1.9 Storm Surges in the New York Bight

PORE and BARRIENTOS (1976) studied storm surges in the New York Bight due to hurricanes and extra-tropical cyclones. This subsection will be confined to only hurricane-generated storm surges (extratropical cyclone generated surges will be discussed later). PORE and BARRIENTOS (1976) selected five major hurricanes that affected the New York Bight area: September 21–22, 1938, September 13–15, 1955, August 30–31, 1954 (Carol), September 10–12, 1954 (Edna), and September 12, 1960 (Donna). The storm surge height distributions for the third and fifth hurricanes are given in Fig 6.21 and 6.22, respectively.

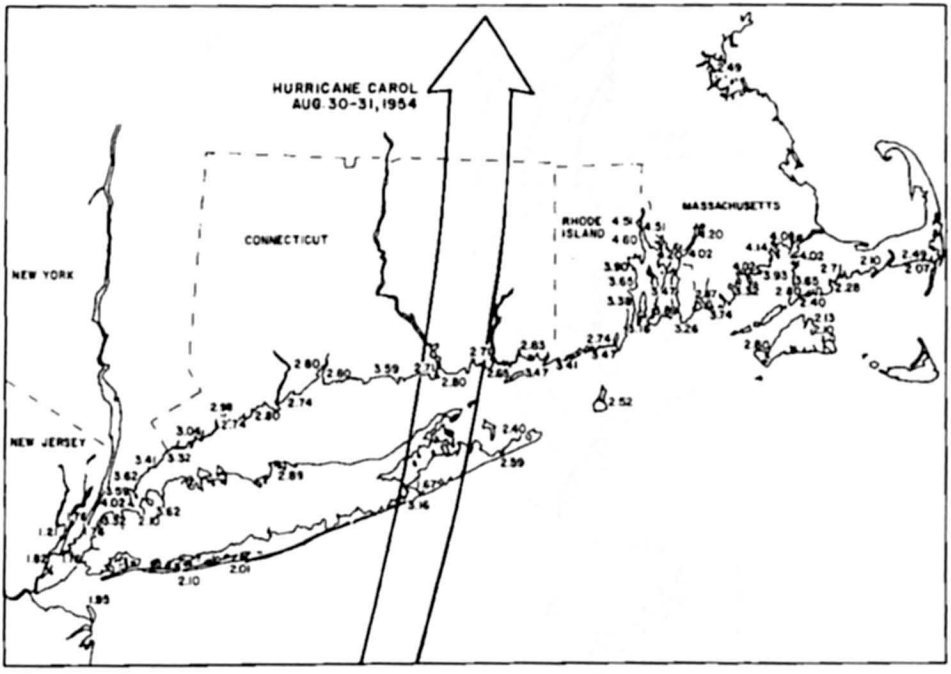

Fig. 6.21: Distribution of storm surge heights (meters) in the New York Bight due to Hurricane Carol of August 30–31, 1954. The arrow shows the hurricane track (PORE and BARRIENTOS, 1976)

SETHURAMAN (1979) studied the storm surge due to Hurricane Belle of august 8–10, 1976. The surge at Shinnecock Inlet (Long Island) is shown in Fig. 6.23. This surge occurred near the time of low tide; hence damage was minimal.

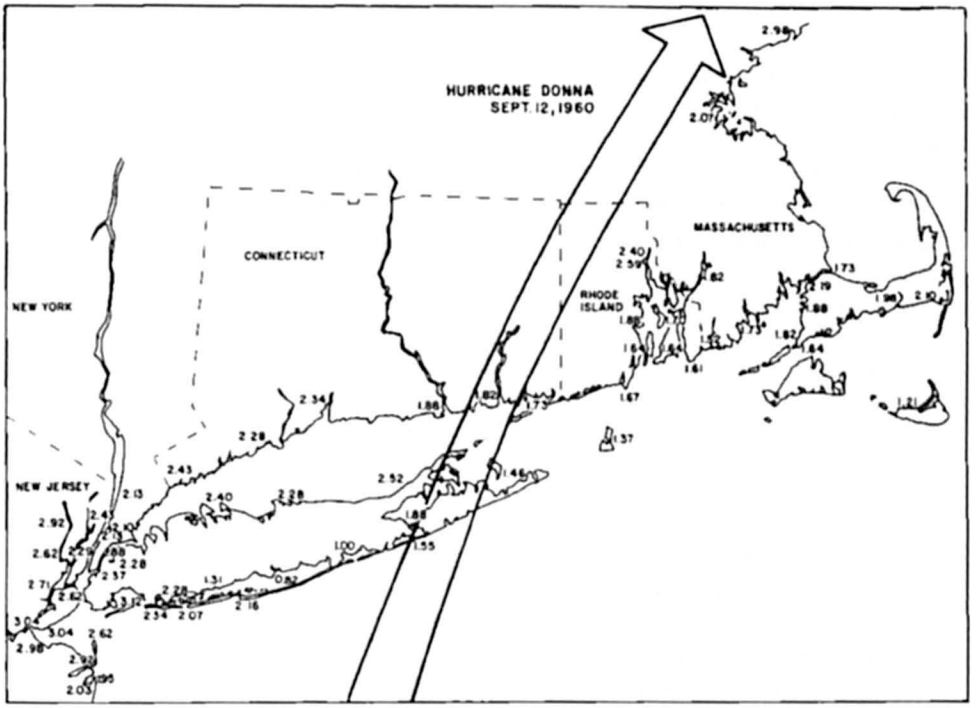

Fig. 6.22: Distribution of storm surge heights (meters) due to Hurricane Donna of September 12, 1960. The arrow shows the hurricane track (PORE and BARRIENTOS, 1976)

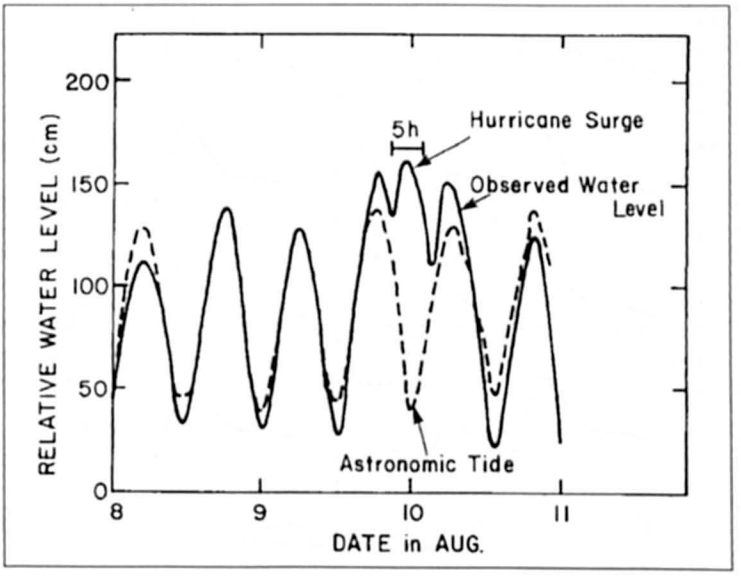

Fig. 6.23: Storm surge and predicted tide at Shinnecock Inlet on Long Island, New York (SETHURAMAN, 1979)

6.1.10 Storm Surges in New York Bay

KUSSMAN (1957) examined the storm surge problem for New York City and surrounding area. The storm amplitudes at several locations due to nine hurricanes are listed in Table 6.17.

The arrow shows the hurricane track. (PORE and BARRIENTOS, 1976)

WILSON (1959, 1961) did a comprehensive study of the hurricane generated storm surge problem in New York Bay. The technique of this study was as follows (WILSON, 1961, p. 548):

> A recursion formula is evolved, using the method of finite differences for time increments of $^1/_3$ hour, which relates tide elevation at the bay-mouth with two values of the elevation at $^1/_3$ and $^2/_3$ hour earlier and with values of wind-stress and pressure-gradient driving force components (directed towards New York Bay from several remote two dimensionally spaced off-shore-stations on the continental shelf) at times earlier by the periods taken for free long gravity waves to travel from the stations to the bay-mouth. The formula includes a cumulative forcing function term, which allows for the geostrophic influence of the earth's rotation and also for an "edge wave" effect northward along the eastern seaboard. Moreover it takes into account the observed tendencies of hurricane storm tides in New York Bay to develop resurgences at periods of 7 hours with decay rates of 50 % amplitude decrease per cycle. The coefficients of the "forcing functions", determined by correlation, tend to represent the storm size and speed and also the dynamic augmentation of the forced wave.

The predicted surge curves at selected locations for a design storm moving with a speed of 35 knots (65 km · h^{-1}) are shown in Fig. 6.24. The maximum storm surge amplitude and resurgence amplitude at several locations, due to a designed hurricane, are given in Table 6.18.

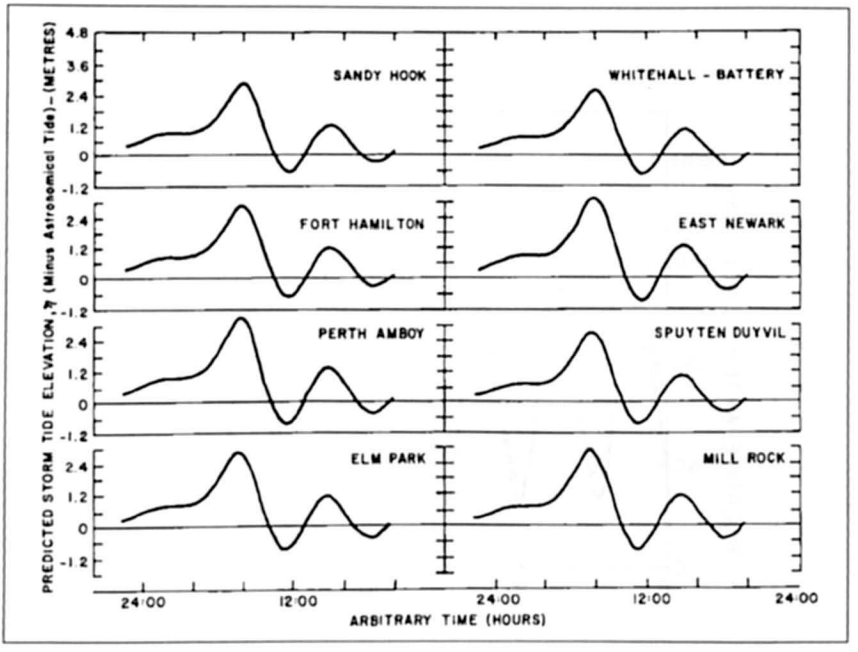

Fig. 6.24: Predicted storm surge heights at various locations in New York Bay for a design hurricane moving with a speed of 65 km · h^{-1}. (WILSON, 1959)

Table 6.17: Maximum storm surge amplitudes (m) in the New York City area and vicinity due to hurricanes during the period 1938–55 (KUSSMAN, 1957)

Location	Sept. 21, 1938	Sept. 15, 1944	Nov. 25, 1950	Nov. 7, 1953	Aug. 31, 1954	Sept. 11, 1954	Oct. 15, 1954	Aug 12–13 1955	Oct. 14–16 1955
Fort Hamilton, NY	1.95	2.04	2.29	2.35	1.80	1.31	–	1.37	1.95
Perth Amboy, NJ	2.01	2.26	2.90	2.68	1.77	1.46	1.68	1.62	2.35
Spuyten Duyvil, NY	1.62	1.83	2.13	2.04	1.59	1.22	1.28	1.34	1.80
Lawrence Point, NY	–	–	3.05	3.17	3.32	1.89	1.80	1.59	2.26
The Battery, NY	1.95	1.95	2.26	2.32	1.71	1.16	1.37	1.28	1.80
Sandy Hook, NJ	1.80	2.56	–	2.41	1.86	1.34	1.40	1.25	1.89
Willets Point, NY	3.66	–	–	2.65	3.47	1.95	1.86	1.62	2.38
Montauk (Fort Pond Bay), NY	4.82	2.41	–	1.65	2.41	1.10	0.94	0.64	1.19
New London, CT	2.99	1.86	2.19	1.80	2.65	0.91	1.22	0.76	1.28

Table 6.18: Predicted maximum storm surge heights due to hurricanes in New York Bay (WILSON, 1959)

Station	Maximum storm surge height (m)			Maximum first resurgence height (m)
	Surge	Probable error (90 %) confidence limits	Resurgence	Probable error (90 %) confidence limits
Sandy Hook	2.71	± 0.21	1.04	± 0.21
Fort Hamilton	2.68	± 0.21	1.04	± 0.21
Perth Amboy	3.20	± 0.30	1.25	± 0.30
Elm Park	2.87	± 0.46	1.16	± 0.46
Whitehall (Battery)	2.53	± 0.18 – 0.24	1.01	± 0.18 – 0.24
East Newark	3.11	± 0.49	1.25	± 0.49
Spuyten Duyvil	2.65	± 0.30	1.04	± 0.30
Mill Rock	2.99	± 1.37[a] –0.91[a]	1.19	± 1.37[a] –0.91[a]

[a] The 90 % confidence limits are probably better than these for the main surge.

6.1.11 Narragansett Bay

MCALEER (1964) studied hurricane-generated storm surges in Narragansett Bay and particularly examined the role of barriers in reducing storm surge levels. The results were arrived at through hydraulic model investigations. Storm surges of up to 10–14 ft (3.0–4.3 m) in amplitude have been observed in Narragansett Bay. A hurricane storm surge in September of 1938 caused $ 100 million damage and killed 110 people. Ten people were killed in another storm surge during 1954. For some of the major hurricane tracks, Narragansett Bay lies in the dangerous northeast quadrant of the storm.

While some of the major hurricanes move relatively slowly along the southern part of the east coast of the United States, they may move faster when they approach the northern part of the coast. Hence, some storms that were reported as having stalled (or as moving

slowly) along the southern east coast suddenly accelerated and caused surges in Narragansett Bay some 8–10 h later.

Numerical and hydraulic models have been used to study the effects of barriers on storm surge amplitudes. The barriers are envisaged as rock fill barriers with large ungated navigation openings across the three entrances to Narragansett Bay. The results indicated tat the barriers would reduce the surge amplitudes by 6–7 ft (1.83–2.13 m) over the 120-mi^2 (311km^2) bay. These barriers will also decrease the mean tidal range somewhat.

PARARAS-CARAYANNIS (1975) used the bathystrophic model to compute the surges at Narragansett Pier, Rhode Island, generated by Hurricane Carol of 1954. This hurricane had a radius of maximum winds of 25 nautical miles (46.3 km) and moved with an average speed of over 33 knots (61 km.h^{-1}). Hurricane Carol arrived over Rhode Island at about 10:30 EST on August 31, 1954,with sustained wind speeds up to 90 mi · h^{-1} (145 km · h^{-1}) and gusts up to 105 mi · h^{-1} (169 km^{-1}). At Block Island, gusts up to 130 mi · h^{-1} (209 km · h^{-1}) were measured.

Because of its intensity, speed of movement, and arrival at the time of high tide, exceptionally large surges and great destruction occurred. About a third of the city of Providence was under 8–10 ft (2.4–3.0 m) of water for several hours. PARARAS-CARAYANNIS (1975) mentioned waves up to 40-ft (12.2 m) in height. Maximum surge at Narragansett Pier was about 12.8-ft (3.9 m). Observed and computed surge profiles at Narragansett Pier are compared in Fig. 6.25.

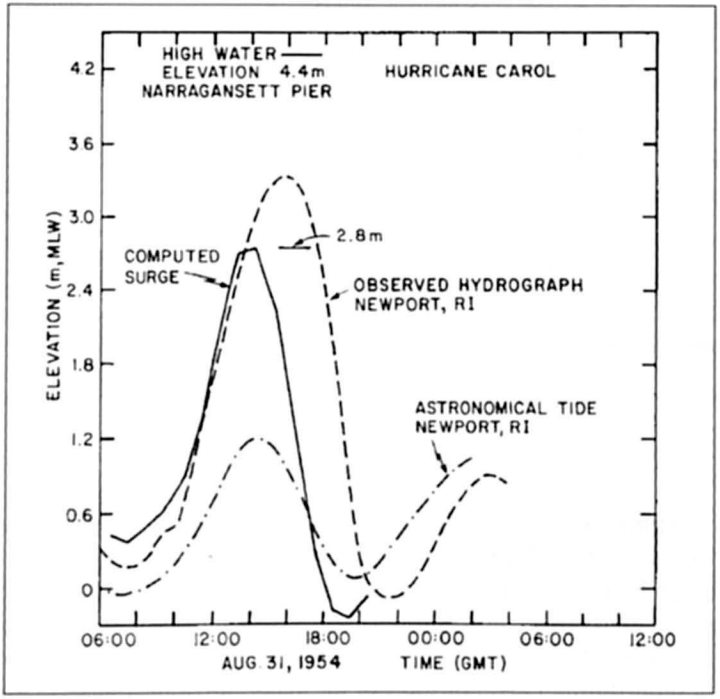

Fig. 6.25: Computed and observed surges at Narragansett Pier due to Hurricane Carol of 1954 (PARARAS-CARAYONNIS, 1975)

6.1.12 Hawaii

The Hawaiian Islands are not frequently subjected to storm surges. However, in November 1982 the storm surge caused by Hurricane Eva resulted in extensive damage to the islands of Kaui and Oahu and a few people died. Another major surge occurred in February 1983. Prior to these two surges, major surges occurred in the mid-1950s and some minor ones occurred in the 1970's.

Even though hurricanes are common over the eastern pacific and annually are seen in parts of central pacific, they are not found over Hawaii only. Four hurricanes impacted Hawaii during 1950 to 1992. Hurricane Iniki of September 6–13, 1992 with winds up to 160 mpH (258 kpH) was by far the strongest and most destructive. Fig. 6.26 shows the track of Hurricane Iniki and Fig. 6.27 shows that the passage of the eye over Kauai. Fig. 6.28 shows the wind field.

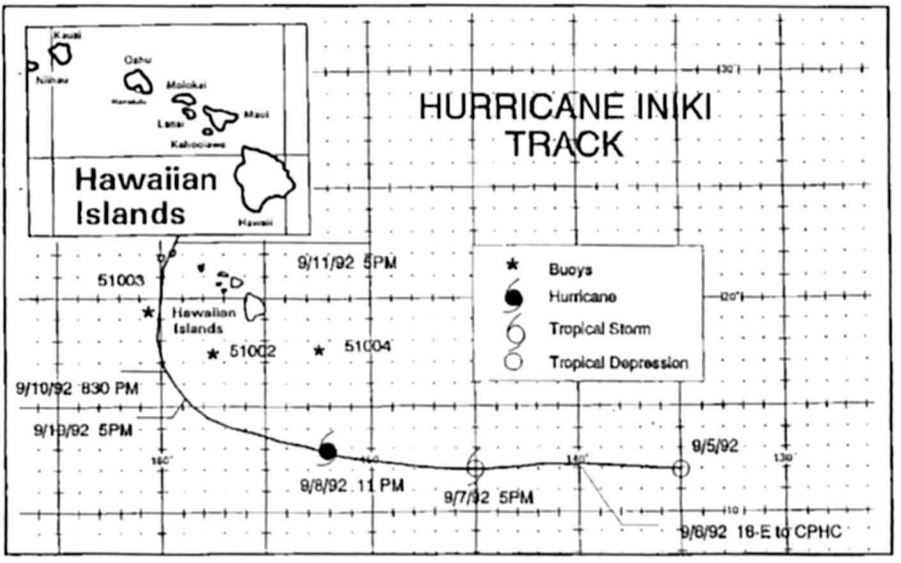

Fig. 6.26: Track of hurricane Iniki (ANON, 1993)

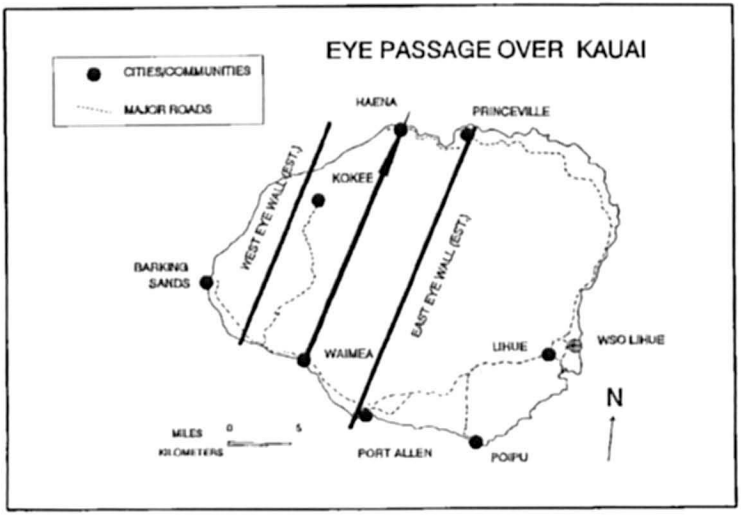

Fig. 6.27: Estimated Iniki Eye Passage over Kauai (ANON, 1993)

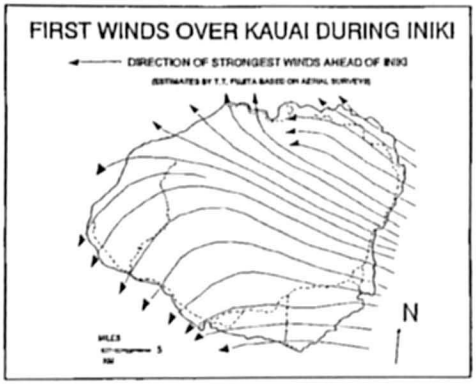

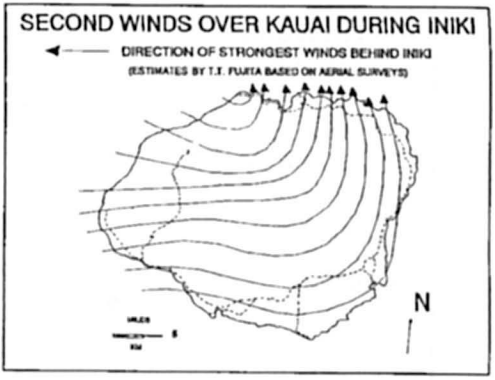

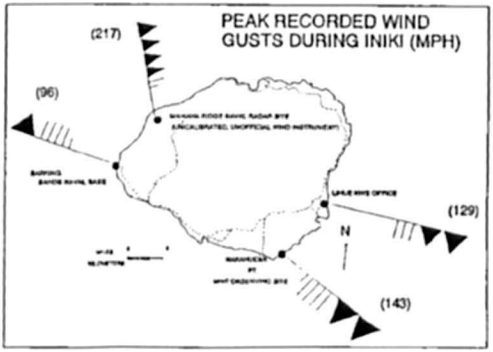

Fig. 6.28: Winds on Kauai from Iniki (ANON, 1993)

Die Küste, 63 Global Storm Surges (2001), 1-623

6.1.13 Mexico

Mexico is affected by storm surges on its Gulf of Mexico coast. Usually, the hurricane tracks over the Gulf of Mexico are such that they strike the United States rather than Mexico. However, on rare occasions, storm surges do occur on the Mexican coast also. On the Pacific coast of Mexico, also, storm surges occur rather infrequently. The storm surge due to Hurricane Paul of September 30, 1982 killed 24 people and caused considerable damage on the Baja California coast. In this hurricane, winds up to 240 $km \cdot h^{-1}$ were reported.

6.2 Central and South America Including the Caribbean

6.2.1 Caribbean Sea Region

Hurricanes and storm surges cause significant death and damage in the nations of the Caribbean Sea region. Of the four nations Haiti, Cuba, The Dominican Republic, and Honduras, maximum effects occurred in Haiti (FUNK, 1980) where about 8400 people were killed in the twentieth century. In 1963 alone, Hurricane Flora caused 5000 deaths. Hurricane David of August 29, 1979, killed 56 people in Dominica.

Hurricanes originating in the Caribbean Sea south of 15° N, especially in the month of August, are a potential threat to Jamaica (BLAKE, 1981). Winds of up to 45 $m \cdot s^{-1}$ generated storm surges with amplitudes up to 12 m at Manchioneal and Galina. Most of the northern coast of Jamaica was struck by surges of amplitudes between 4 and 8 m. There is evidence that the surge penetrated several kilometres inland. The damage was estimated to be about $ 126 million. About 75 % of the banana crop, 95 % of the fishing industry equipment on the north coast, and more than 800 houses were destroyed.

The storm surge of June 12, 1979, made people aware of what to expect and this helped in the safe evacuation of people during the 1980 surge.

6.2.2 Barbados

Barbados and other island of the Lesser Antilles are not usually subjected to storm surges, but they do have severe problems from swell and wind waves. There is a broad reef shelf surrounding Barbados and this makes the problem worse. The swell action is not associated with local storms from the Caribbean Sea but is due to intense extratropical cyclones in the North Atlantic Ocean (DONN and MCGUINNESS, 1959).

Swell with amplitudes up to 20 ft (6.1 m) can occur quite frequently. Between December 1957 and October 1958, at least four occasions of major swell activity occurred.

READING (1990) analysed the annual and decadal frequency of cyclones throughout the Caribbean region. For the "Historical Period" (i.e. period before weather charts were made) the Caribbean has been divided into ten sub-regions as shown in Fig. 6.29 for the modern period (i.e. chated period) a 5° latitude-longitude grid were used as shown in Fig. 6.30. Fig. 6.31 show the mean decadal frequency. Here cyclones are defined as warm cored systems of storm force or above while hurricanes are similar systems of hurricane intensity as defined by the U.S. Weather Bureau.

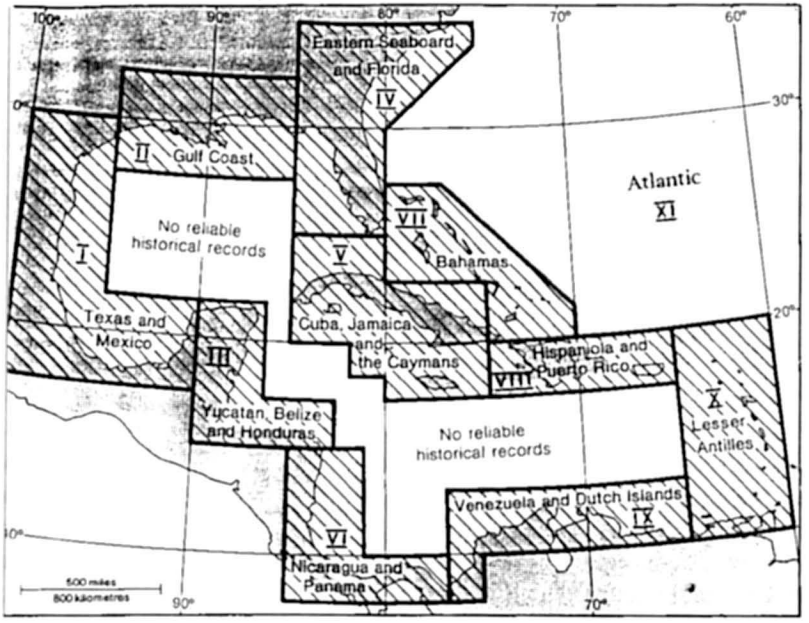

Fig. 6.29: Subregions of the Caribbean: historical data analysis (READING, 1990)

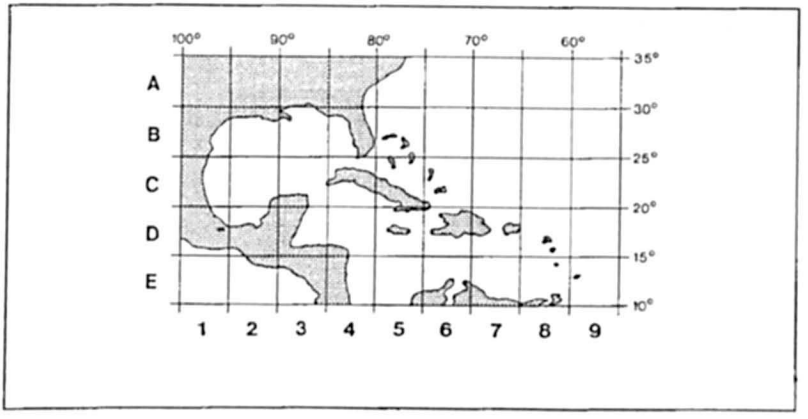

Fig. 6.30: Grid map of Caribbean area: modern data analysis (READING, 1990)

Fig. 6.31 shows that cyclone frequencies are greatest around the Western Bahamas, Eastern Seaboard of U.S and adjacent Atlantic. This can be explained by the fact that this area is within the favoured path of the two types of cyclones that affect this region; the Capeverde (CV) type systems, which recurve around the periphery of the sub-tropical high pressure cell to the north and the western Caribbean (WC) type which, after developing in the warm waters of the western Caribbean, almost immediately become affected by the westerly mid-latitude circulation and move steeply towards higher latitudes. Cyclone frequencies decrease from this northeastern core-region in roughly concentric circles. Areas of anomalously high frequencies between 15° N and 20° N east of 70° W reflect the strong preference of CV

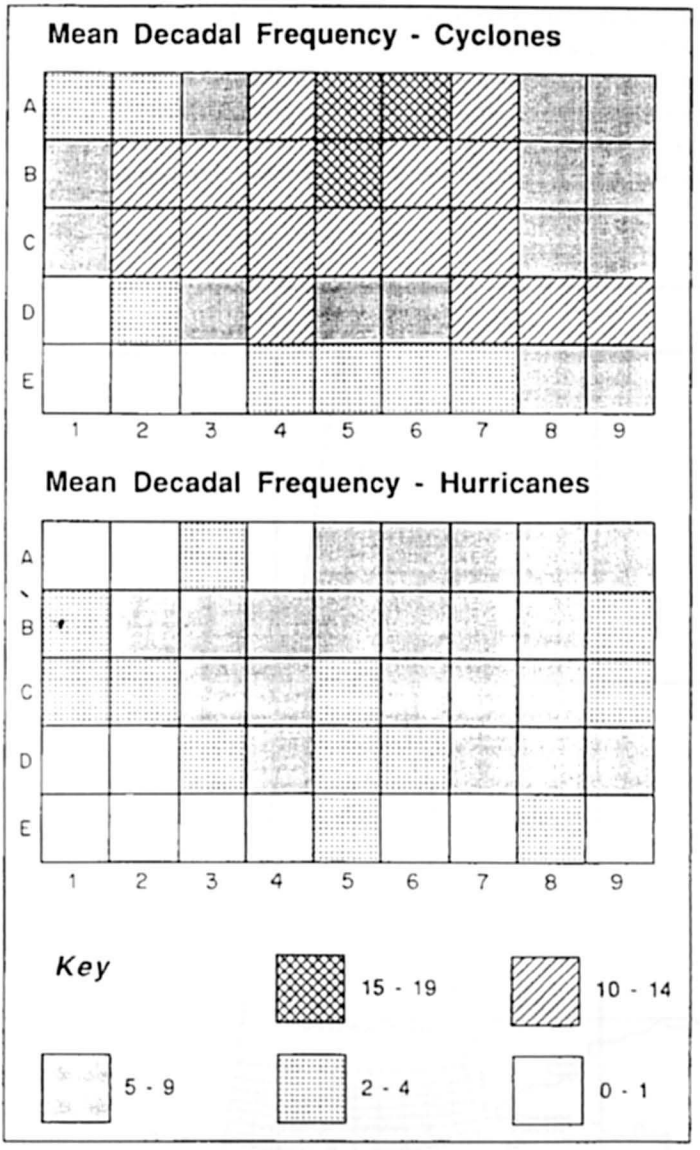

Fig. 6.31: Mean decadal frequency of cyclones and hurricanes: per 5° grid square (READING, 1990)

systems to enter the Caribbean at this latitude. Square D4 represents the major area of intensification for WC type systems.

Areas of relatively high hurricane frequencies (5–9 per decade) occur as two distinct bands. The western band represents the favoured track of WC type systems and the eastern band that of recurving CV type systems. These bands join over the north-central Caribbean, representing an area where both types of system frequently pass.

There is a strong latitudinal and longitudinal preference by the cyclones that develop, possibly a reflection of changes in the relative positions and intensity of the subtropical high pressure cell and the inter-tropical convergence zone. Another important result is that the

proportion of cyclones intensifying to hurricane status within the Caribbean has risen from 45 % in the 1970's to about 63 % in the 1990's.

MERCADO (1994) modelled storm surges in Puerto Rico using the SLOSH model. Fig. 6.32 shows the grid for the SLOSH basin. The grid on which the surge computations and inundation are made has a resolution of approximately 2 x 2 miles (3.2 x 3.2 km). The model was tested against hurricane Hugo storm surge with amplitudes up to 3.5 m.

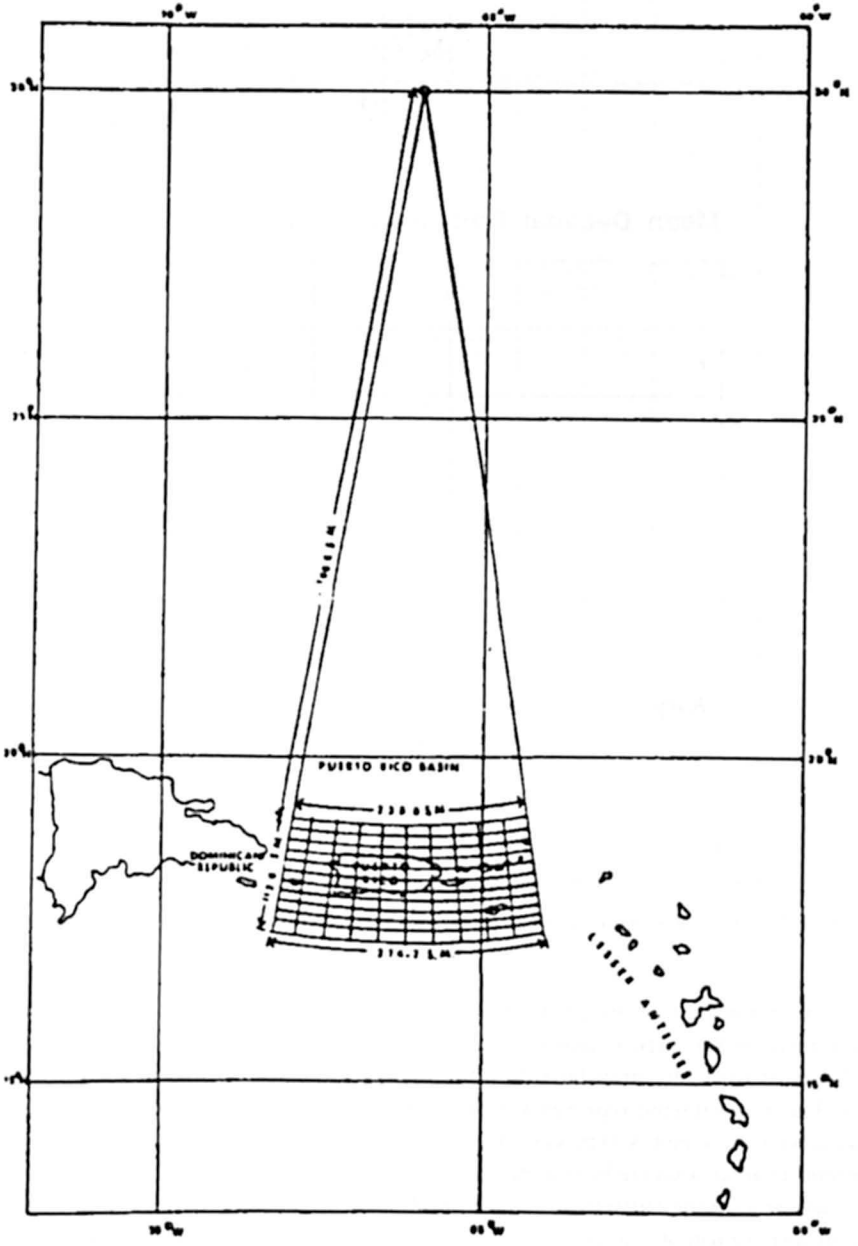

Fig. 6.32: Puerto Rico SLOSH Basin and grid system used (MERCADO, 1994)

Die Küste, 63 Global Storm Surges (2001), 1-623

6.3 North Indian Ocean

Discussion in this section will mainly concentrate on the storm surges in the Bay of Bengal and Arabian Sea. Although the frequency of the tropical cyclones in the North Indian Ocean is not quite high, the coastal regions of India, Bangladesh and Myanmar suffer most in terms of loss of life and property caused by the surges. The reason besides the inadequate accurate prediction, are the low lands all along the coasts and considerably low-lying huge deltas, such as, Gangetic delta and Ayeyarwady delta.

6.3.1 Bay of Bengal

Storm surges are extremely serious hazards along the east coast of India, Bangladesh, Myanmar and Sri Lanka. Although Sri Lanka is affected only occasionally by the storm surge, however tropical cyclones of November 1964, November 1978 and the recent cyclone of November 1992 have caused extensive loss of life and property in the region. Storm surges affecting Myanmar are also to much less extent in comparison with Bangladesh and India. Notable storm surges, which have affected Myanmar, have been during May 1967, May 1968, May 1970 and May 1975, of which May 1975 was the worst cyclone. The storm surge due to the May 1975 event penetrated at least 100 km into the Ayeyarwady river system and caused serious inland flooding (LWIN, 1980)

A detailed review of the problem of storm surges in the Bay of Bengal is given by RAO (1982), ROY (1984), MURTY (1984), MURTY et al. (1986), DAS (1994 a, b), DUBE (1998a), DUBE et al. (1997, 1999b, 2000c) and CHITTIBABU (1999). In this section, a brief account of the problem of storm surges in Bangladesh, east coast of India, Myanmar and Sri Lanka would be given. Of all the countries surrounding the Bay of Bengal, Bangladesh suffers most from storm surges.

(a) Bangladesh

It is probably not incorrect to say that Bangladesh suffered more from storm surges than any other country. ALI (1979) summarized the main factors contributing to the disastrous storm surges on the coast of Bangladesh: (1) shallow water, (2) convergence of the bay, (3) high astronomical tide, (4) thickly populated low-lying islands, (5) favorable cyclone track, and (6) innumerable number of inlets and few large estuaries and rivers. Except in the eastern and southeastern parts of the country (where there are hills) most of the land is flat. Many places, although 160 km from the sea are not more than 9.1 m above sea level. A rise of a few meters in sea level can bring large areas of land under water (GILL, 1975).

Another peculiar problem is the topographical changes that appear to occur in decadal periods in the courses of the rivers and tributaries. The storm surge problem became worse after the Assam earthquake of August 1950 because millions of tons of material from the mountains was dislodged by the earthquake, which ultimately found its way into the river system and caused raising of the bottom by as much as 4.3 m in certain locations.

The approximate number of people killed in Bangladesh because of storm surges is listed in Table 6.19. For comparison, a storm surge in 1881 in China supposedly killed 300,000 people. A surge in Japan in 1923 killed 250 000 people. Another surge in Japan in 1960 killed

Table 6.19: Number of people killed in Bangladesh due to storm surges. Only those cases in which the number is more than 5000 are included

Year	Estimated approximate No. of deaths
1822	40, 000
1876	1,00, 000
1897	1,75, 000
1912	40, 000
1919	40, 000
1960	15, 000
1963	11, 520
1965	19, 279
1970	3,00, 000
1985	11,069
1991	1,40,000

Table 6.20: Damage in Bangladesh (in addition to human death toll) due to the November 1970 cyclone and storm surge (FRANK and HUSSAIN, 1971)

Damage	Toll
Population affected	4.7 million
Crop loss	U.S.$ 63 million
Loss of cattle	280 000
Loss of Poultry	500 000
Houses damaged	400 000
School damaged	3 500
Fishing boats (marine) destroyed	9 000
Fishing boats (inland waters) destroyed	90 000

5000 people. A surge in 1780 in the Antilles killed 22 000 people and one in the Cuba-Haiti area in 1963 killed 7196 people (FRANK and HUSSAIN, 1971).

The November 13, 1970, storm surge was supposed to be the worst on record in Bangladesh. The death toll was initially estimated to be over a million people. Later estimates brought it down to 500,000, then 300,000, and finally 200,000. Whatever the correct toll my be, this storm surge event created a new awareness of tropical cyclones in general and of storm surges in particular, not only in Bangladesh but all over the world. In a storm surge event of this magnitude, there is not only the human death toll but there are other damages as well. The damage in Bangladesh due to this storm surge is listed in Table 6.20. The salt water from the sea flooded the land during the surge event, leaving much salt on the land, which for 4–5 years after the event affected crops until rains finally washed away the salt.

There are more than 40 known cases of storm surges in Bangladesh during the period 1800–1999. A partial list is given in Table 6.21 for the period 1876–1999. It is quite probable that some of the entries in the table are wrong. Also, sometimes the total water level (i.e. tide + surge) is reported as surge. The observed water levels during storm surge events at six different locations in Bangladesh during the period 1965–76 are listed in Table 6.22. The storm surge and the pertinent meteorological and tidal information at Chittagong for the period 1960–70 are given in Table 6.23. ALI (1980b) summarized the numerical models that have

Table 6.21: List of storm surges in Bangladesh (1582–1999)

No.	Date	Location	Damage
1	1582	Near Backergunge, Bangladesh	200,000 deaths, Destruction reported due to surge
2	1699	Sundarban coast, Bangladesh	50,000 deaths
3	1760	Sundarban coast, Bangladesh	Extensive damage
4	1765	Chittagong coast, Bangladesh	Extensive damage
5	1767	Barisal,Bangladesh	13.03 m surge,30,000 deaths
6	May–June, 1797	Chittagong, Bangladesh	2 ships sank. No estimate of deaths
7	6 June, 1822	Barisal/Backergunge, Bangladesh	50,000 deaths, storm wave swept the region
8	16 May, 1869	Khulna	Surge entered through the Pussur and Haringhata Rivers and inundated a vast area causing damage of life and property. 250 people died in Morelganj
9	31 October, 1876	Backergunge, Bangladesh	This was the infamous Backergunge cyclone. Peak water levels in Bangladesh varied from 3 to 13.6 m, including tide and wind waves. 100,000 deaths in Bangladesh (then part of India). This India Meteorological Department was expanded following this surge. GILL (1975), but this could be an over-estimate lot of destruction. Inundation subsided in 2 hours
10	27 October, 1893	Noakhali	
11	October, 1895	Sunderban/Bagerhat, Subdivision, Bangladesh	Damage estimates not available
12	24 October, 1897	Chittagong, Kutubdia Island, Bangladesh	175,000 deaths. Thousands died in the epidemic which followed the calamity
13	May, 1898	Taknaf, Bangladesh	Surge caused huge damage
14	November, 1901	Western Sunderbans, Bangladesh	Damage estimate not available
15	15–18 October, 1909	Backerganj, Bangladesh	172 deaths, extensive damage
16	2–6, December, 1909	Cox's Bazar, Bangladesh	Storm surge caused heavy damage
17	April, 1911	Teknaf, Bangladesh	Damage estimate not available
18	May, 1917	Sunderbans, Bangladesh	Damage estimate not available
19	20–25 September, 1919	Barisal, Bangladesh	3,500 deaths in Bangladesh
20	19–24 April, 1922	Cox Bazar, Bangladesh	Damage to ships, No deaths
21	3–7 May, 1923	Teknaf, Bangladesh	25000 houses damaged
22	19–23 May, 1926	Cox's Bazar, Bangladesh	2700 deaths
23	22–26 May, 1941	Between Barisal and Noakhali, Bangladesh	3.03–3.64 m surge. 5000 deaths due to storm surge
24	21–24 October, 1947	Between Chittagong and Barisal, Bangladesh	500 deaths
25	17–19 May, 1948	Between Chittagong and Noakhali, Bangladesh	Damage estimate not available
26	15–20 November, 1950	Patuakhali, Bangladesh	Damage estimate not available
27	16–19 May, 1958	East Meghna Estuary, Bangladesh	Cargo and country boats capsized, Sandwip island badly affected
28	21–24 October, 1958	Noakhali and West Meghna Estuary, Bangladesh	Up to 2 m suges in Bangladesh and West Bengal State of India, 500 deaths
29	29 May, 1960	Sunderbans, Bangladesh	3.2 m surge, extensive damage

Table 6.21 (continued)

No.	Date	Location	Damage
30	8–10 October, 1960	Noakhali, Meghna Estuary, Bangladesh	6 m surge. 6,000 deaths in offshore island of Noakhali, Barisal, Chittagong.
31	30–31 October, 1960	Nathalie, Chittagong, Bangladesh	6.6 m surge. 5,149 deaths
32	9 May, 1961	Noakhali West Mehgna Estuary, Bangladesh	3 m surges. 11,468 deaths
33	29–30 May, 1961	Chittagong, Cox's Bazaar, Noakhali, offshore islands, Bangladesh	2.6–4.5 m surge. Peak water levels up to 9 m.
34	26–30 October, 1962	Feni, Bangladesh	Damage estimate not available
35	28–29 May, 1963	Noakhali, Chittagong, Bangladesh	Peak water levels up to 8.1 m. 11,520 deaths
36	5–8 June, 1963	Jessore, Bangladesh	Peak surge 3.1 m
37	25–27 October, 1963	Teknaf, Bangladesh	Damage estimate not available
38	11 April, 1964	Bangladesh	196 deaths
39	9–12 May, 1965	Barisal and Noakhlai, Bangladesh	3–6 m surge. 19,279 deaths
40	26 April – 1 May, 1965	Hatia, Bangladesh	Up to 7.6 surges. 12,000 deaths
41	5 November, 1965	Bangladesh	Up to 3.7 m surges
42	11–15 December, 1965	Cox's Bazaar, Bangladesh	2.4 –3.6 m surge. 873 deaths
43	23 September– 1 October, 1966	Noakhali, Bangladesh	6.0 – 6.7 m surge. 850 deaths
44	1 November, 1966	Bangladesh	Peak water levels up to 10 m
45	7–12 December, 1966	Cox's Bazaar, Bangladesh	Damage estimate not available
46	8–11 October, 1967	Khulna, Bangladesh	Peak water levels up to 9.3 m
47	20–24 October, 1967	Cox's Bazaar, Bangladesh	Up to 7.6 m surge, 51 deaths
48	17 April, 1969	Bangladesh	75 deaths
49	10 October, 1969	Khulna, Bangladesh	Peak water levels up to 8 m.
50	2–7 May, 1970	Cox's Bazaar, Bangladesh	Up to 5 m surge
51	18–23 October, 1970	Chandpur, Bangladesh	4.7 m surge. 300 deaths
52	8–13 November, 1970	Between Noakhali and Chittagong, Bangladesh	3–10 m surge, 300,000 deaths, 2,80,000 cattle killed, 44,00,000 houses destroyed, 18,000 boats destroyed, unofficial estimation of deaths more than 500,000
53	8 May, 1971	Khulna to Chittagong and offshore islands, Bangladesh	2.4–4.2 m surge. Other information not available
54	28–30 September, 1971	Chandpur, Bangladesh	Surge plus tide of 5 m
55	5–6 November, 1971	Chittagong, Bangladesh	Water levels up to 5.5 m
56	28–30 November, 1971	Sunderban coast, Khulna, Bangladesh	1 m surge
57	14–18 November, 1973	Barisal, Bangladesh	1.0 m surge. Peak water level including wind waves 3.8 m
58	5–9 December, 1973	Patuakhali coast and offshore islands, Bangladesh	Peak water level 6.2 m. Peak surge 4.5 m. 183 deaths

59	13–15 August, 1974	Khulna, Bangladesh	6.7 m surge
60	24–28 November, 1974	Chittagong, Bangladesh	3.0–5.1 m surge. 20 deaths, 50 injured, 280 persons missing, 1,000 cattle killed, 2,300 house destroyed
61	9–12 May, 1975	Bhola, Cox's Bazaar, Khulna, Bangladesh	5 deaths. 4 injured. 36 fishermen missing
62	4–8 June, 1975	Chittagong, Bangladesh	Peak surge 4.0 m, 50 deaths
63	24–28 June, 1975	Bangladesh	Tide and surge 4.8 m
64	7–11 Nov, 1975	Barisal, Noakhali, Bangladesh	Maximum surge 3.1 m
65	15–21 October, 1976	Meghna Estuary, Bangladesh	Tide plus surge 5.0 m at Comapaniganj
66	20 November, 1976	Chittagong, Bangladesh	1.0 m surge. 2.1 m tide
67	9–13 May, 1977	Noakhali, Bangladesh	0.6 m surge. 0.7 m tide
68	1–3 October, 1978	Khulna and Sunderban coast, Bangladesh	Damage estimate not available
69	6–10 December, 1981	Khulna, Bangladesh	2–4.5 m surge 72 deaths and 200 deaths in India.
70	14–15 October, 1983	Chittagong coast near the Feni River, Bangladesh	43 deaths. Substantial damage
71	5–9 November, 1983	Chittagong, Cox's Bazaar, Bangladesh	1.5 m surge, 300 deaths. Substantial damage
72	20–25 May, 1985	Cox's Bazaar, Chittagong, Sandwip, Bangladesh	4.55 m surge. 11,069 deaths. 94,000 houses destroyed
73	7–9 November, 1986	Chittagong, Bangladesh	0.61 m surge, 50 deaths. Substantial damage
74	January 30– Februar–4, 1987	Chittagong, Bangladesh	Damage estimate not available
75	24–30 November, 1988	Khulna coast near Raimangal river, Bangladesh	4.4 m surge. 11,683 deaths in Bangladesh, 532 deaths in India 6,000 missing. 65,000 cattle killed. 15,000 deer killed. 9 royal Bengal tigers killed. Substantial crop damage.
76	7–8 October, 1990	Barisal, Bangladesh	150 fishermen missing. Substantial damage
77	16–18 December, 1990	Khulna coast, Bangladesh	4.4 m surge, 5683 deaths, 15,000 and 9 tigers killed, 65,000 cattle killed
78	25–30 April, 1991	Chittagong, Cox's Bazaar, Bangladesh	6–7.6 m surge. 140,000 deaths. 70,000 cattle killed. Great damage
79	31 May–2 June, 1991	Noakhali-Patakhali, Bangladesh	2.5 m surge, 300 deaths
80	16–21, Nov 1992	Teknoff, Bangladesh Coast	Damage estimation not available
81	21–25 Nov 1995	Coxbazar, Bangladesh	Damage estimation not available
82	26–29 October, 1996	Sundarban coast, Bangladesh	1.52–2.12 m surge, 9 deaths, 2000 fishermen missing, 15,000 cattle killed, 10,000 houses damaged
83	15–20 May, 1997	Chittogong, Bangladesh	4.55 m surge, 155 deaths
84	24–27 September, 1997	Noakhali-Chittogong coast, Bangladesh	3.03–4.55 m surge at Bhoala, 1.52–2.12 m surge at Barguna, 2.42–3.03 m surge at Galachipa, 67 deaths. At Khagrachhari, 16 villages and a part of the district town went under 1.82–2.42 m surge.
85	4–9 Nov 1997	Bangladesh coast	3.0 m surge, substantial damage
86	17–21 May 1998	Bangladesh coast	16 deaths

Table 6.22: Observed water levels (tide + surge) in meters at six locations in Bangladesh (ALI, 1980b)

Date	Khulna	Barisal	Sandwip	Chittagong	Chandpur	Companigonj
May 12. 1965	–	2.84	2.90	–	2.53	2.21
May 31. 1965	2.25	2.44	3.73	–	3.80	7.13
Oct 11. 1967	2.59	–	–	2.92	–	8.75
Oct 24. 1967	2.44	–	–	1.89	–	7.61
May10. 1968	–	–	2.78	3.38	–	4.74
Oct 10. 1969	2.61	–	7.21	3.20	4.27	4.63
Oct 23. 1970	3.02	3.47	–	–	4.74	4.21
Nov.12. 1970	–	2.67	3.86	5.58	4.09	5.58
Sep. 30. 1967	3.08	3.04	–	–	5.03	4.21
Oct. 20. 1976	–	4.64	3.00	3.17	3.54	5.02

Table 6.23. Some pertinent details for storm surges at Chittagong, Bangladesh (FLIERL and ROBINSON, 1972)

Date	Storm speed ($km \cdot h^{-1}$)	Maximum observed wind speed ($km \cdot h^{-1}$)	Astronomical tide (m)	Observe sea level (m)	Maximum surge (m)
Oct 11, 1960	20	161	1.5	6.0	4.5
Oct 31, 1960	38	193	0.0	6.6	6.6
May 9, 1960	38	161	1.2	4.8	3.6
May 30, 1960	22	161	0.6	–	–
May 29, 1960	40	209	0.3	–	–
Nov. 9, 1965	42	161	1.2	–	–
Dec. 15, 1965	32	161	0.3	–	
Nov. 13, 1970	20	161	1	6.0–9.0	4.2–7.2

been developed for storm surges on the coast of Bangladesh. Probably the first model is by DAS (1972) for the coasts of India and Bangladesh, and he simulated the surge dues to the November 1970 cyclone. This was extended by DAS et al. (1974). They investigated the effect of the central pressure drop and the speed of movement of the cyclone. Nomograms were given for the peak surge for three different tracks. This work will be considered under the subsection Storm Surges in India. FLIERL and ROBINSON (1972) also developed a liner linear model specifically for the coast of Bangladesh. A nomogram for practical purpose was also prepared.

ISLAM (1971) discussed the storm surge protection problem in Bangladesh. He mentioned the construction of various types of raised platforms (Machan, Killa., etc.) for people and animals. KIBRIA (1980) discussed the planned delta works to protect the Bangladesh coast from storm surges.

DUBE et al. (1984b, 1985b, 1985c, 1986a, 1986b) and SINHA et al. (1983, 1985, 1986) developed several models to simulate the surges associated with serve severe cyclonic storms hitting the coast of Bangladesh. Their models are confined to the northern shelf of the head Bay region with southern open Sea boundary at 19° N. Curvilinear coastal boundary treatment analogous to that used by Johns et al. (1981) was utilized by them. Experiments were carried out to determine the optimum grid resolution, which turned out to be 30 km in the E-W and

8–20.5 km in the N–S directions (varying because of the coordinate transformation). Authors attempted several problems including the computation of inland inundation using continuously deforming shoreline model and the impact of Meghna river discharge on storm surges. In the absence of the observed reliable data on storm surges it was difficult to compare the results, however limited comparisons with observed peak surge were given.

Fig. 6.33 and 6.34 show respectively the computed peak surge along the Bangladesh associated with November 1970 Chittagong cyclone and the temporal variation of predicted sea surface elevation at Maijdi. The impact of inclusion of the river and its discharge on the peak surge and on the temporal evolution of surge is clearly seen from these experiments.

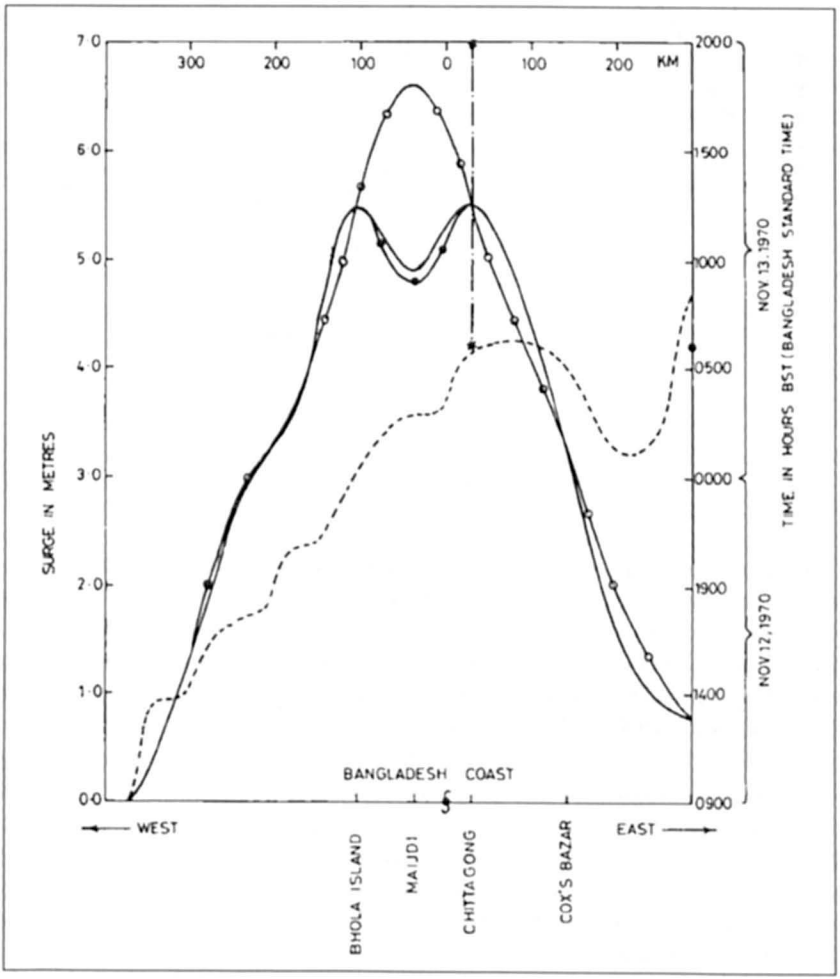

Fig. 6.33: Maximum predicted sea - surface elevation and its time of occurrence along the Bangladesh coast. § = place of landfall; • = time of landfall (on the time axis); - = peak surge envelope (BRM1) with discharge; - - - = time of occurrence (BRM1); -•-•- = peak surge envelop (BRM2) without discharge; -o-o- = peak surge envelope (MWR) without river; *-.-.-* = observed range of sea - surface elevation in excess of predicted tide (DUBE et al., 1986b)

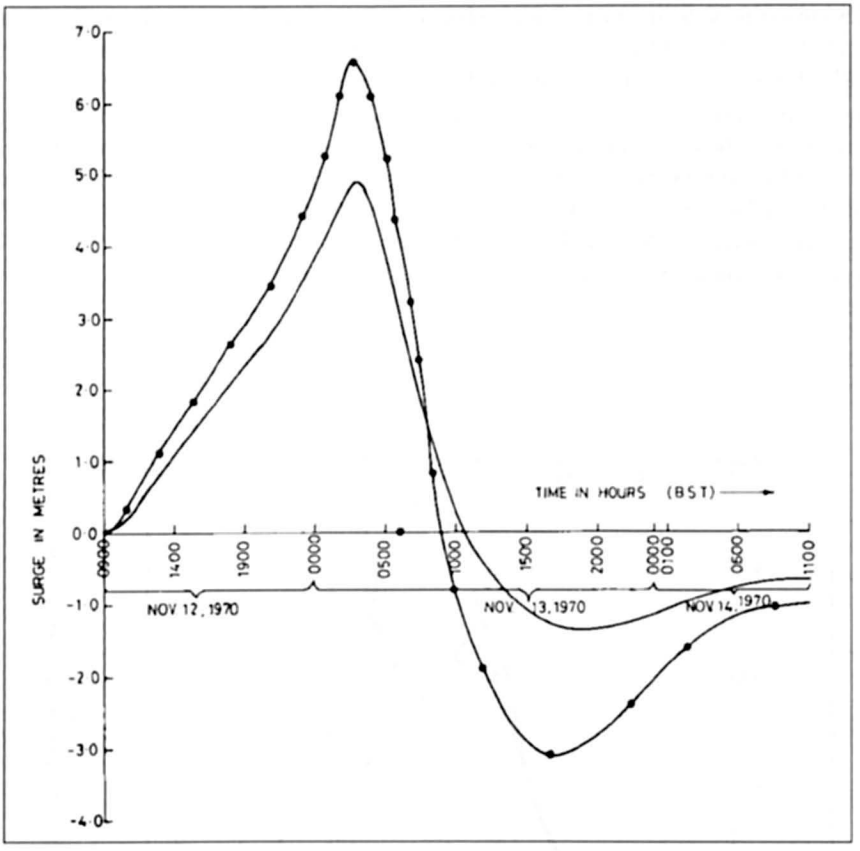

Fig. 6.34: Time variation of the predicted sea – surface elevation at Maijdi. • = time of landfall (on time axis); ___ = BRM1 (with discharge); –•–•– = MWR (without river). (DUBE et al., 1986b)

Considering the complexities of the Bangladesh coastline with numerous inlets, offshore islands and chars, the smooth curves of the model coast resulting from the curvilinear coordinate transformation appear to be a quite limitation of these models. Recognizing this shortcoming, JOHNS et al. (1985) developed a model for the Head Bay region using rectangular Cartesian coordinates. The southern open boundary of the model was at 19° 33' N, the grid size 17.6 km E–W by 19.8 km N–S, and five idealized river models, each of uniform depth and width and length 200 km were included to represent the main channels in the Ganges Delta. The model was nested with in a large curvilinear model of the whole Bay (JOHNS et al., 1981), which provided boundary input of tide and surge. The model was used to study the tide-surge interaction in the Bay of Bengal for details refer to section 4.5.2.

A detailed numerical storm surge prediction model for the Bangladesh region was developed by FLATHER (1994). The formulation used by the author allows the delta to be included in a much more complete and realistic manner. This was achieved by a modification in the standard depth-averaged equations with a numerical scheme in which the solution of one-dimensional equations for narrow channels and two-dimensional equations for the open sea are combined within a unified computational framework. In this manner author was able to realistically model the complex coastal area and the Gangetic Delta. Using the scheme earlier designed by FLATHER and HEAPS (1975), the model also allows the inland inundation.

The model was used to investigate the storm surges generated by November 1970 and April 1991 cyclones. Hindcast and "forecast" simulations of April 1991 event was described using forcing derived from a semi analytical cyclone model with data supplied by the Joint model with data supplied by the Joint. Typhoon Warning Center (JTWC). The results show that the timing of cyclone landfall and its coincidence with high tide determine the areas worst affected by flooding.

ALI et al. (1997b) studied the backwater effect of tides and storm surges on fresh water discharge through the Meghna estuary. In another study ALI et al. (1997a) used a two-dimensional model to study in detail the interactions between river discharge, storm surges and tidal interactions in the Meghna river mouth in the Bangladesh. The study considers the interactions mostly in terms of flow across the river mouth under the three forcing, individually and in different combinations of them. The model has been able to produce some interesting features of the interaction between three forcing in the mouth of Meghna estuary. It is shown by the authors that river discharge and tidal flow across the river mouth act both positively and negatively depending on the tidal phase, positively during the high tide and negatively during low tide. The result is also found true for the combination of all three forces. In most of the cases, river discharge is found to act in opposition to the storm surges. The interaction between river discharge and storm surges is shown to be dependent on their relative magnitudes. However, in respect of the total elevation in the estuarial region, river discharge tends to increase the surge height.

Recently HENRY et al. (1997) used a finite element model to study the tides and storm surges in offshore waters of the Meghna estuary. The model reproduced tidal elevations well at the four coastal sites used for model verification and simulated surge elevations at the coast with acceptable accuracy.

(b) East Coast of India

India is prone to storm surges on both its east and west coast although the frequency and severity of surges is greater on the east coast. Some important storm surges (form the point of view of loss of life) on the Bay of Bengal coast of India are listed in Table 6.24. List, which is based on various sources, might not be totally correct. Also, in this list, several minor surges in which less than 100 people were killed are excluded.

Some pertinent information on six storm surges at Saugor Island (in the northwestern part of the Bay of Bengal) during the period 1948–55 is given in Table 6.25. This table also compares the observed surges with those computed using simple empirical formulae (JANARDHAN, 1967).

RAO and MAZUMDAR (1966) and RAO (1968) used empirical relations to calculate storm surges on the east coast of India, south of 17° N. Topography near the shore and wind waves were also included in the calculations. Based on these calculations, RAO (1968) classified the east coast of India (and the coasts of Bangladesh and Burma for comparison into three types. These results are summarized in Table 6.26. In this table, the values listed under "storm surge amplitude" pertain to a storm with winds up to 40m · s –1. The values listed under "total water level" include the peak surge plus the wind waves.

Classification of types A, B, and C is as follows. For a type A coastline, the maximum total water level is less than or equal to 2 m during storm surge events, for type B the amplitude is between 2 and 5 m, and for type C the amplitude is greater than 5 m. This classification is shown in Fig 6.35, for the east and west coasts of India (the west coast of India will be

Table 6.24: List of storm surges along east coast of India (1681–1999)

No.	Date	Location	Damage
1	10 November, 1681	Nagapattinam, Tamilnadu, India	14,000 deaths
2	18 April, 1700	Visakhapatnam, Andhra Pradesh, India	Several ships lost at sea. No estimate of number of deaths available
3	December, 1706	Coringa, Andhra Pradesh, India	No exact estimate of the number of deaths, except a statement that people in great number were lost
4	18 December, 1709	Coastal Ramnad, Tamilnadu, India	Extensive inundation of coastal Ramnad. Major surge. Deaths in thousands
5	7–12 October, 1737	Mouth of Hoogly River, West Bengal, India	12 m surge (probably includes tide and wind waves). Surge penetrated 100 km inland through the Hoogly River. 300,000 deaths in India and Bangladesh (could be a slight exaggeration)
6	2 October, 1747	Madras, Tamilnadu, India	Extensive damage, no estimate of deaths
7	31 October, 1752	Madras, Tamilnadu, India	Extensive damage, no estimate of deaths
8	30 December, 1760	Pondicherry, Tamilnadu, India	Several ships destroyed. 11,000 deaths
9	31 October, 1763	Madras, Tamilnadu, India	Extensive damage, no estimate of deaths
10	13 October, 1779	Masulipatnam, Andhra Pradesh, India	3.63 surge, 20,000 deaths
11	20 May, 1787	Coringa, Andhra Pradesh, India	20,000 deaths. Coastal inundation due to storm surges
12	December, 1789	Near Coringa, Andhra Pradesh, India	3 major waves in the surge. Several ships lost. 20,000 deaths. Inundation of the whole city of Coringa of 1 to 2 m.
13	10 December, 1807	Madras, Tamilnadu, India	Extensive destruction in Madras, no estimate of deaths
14	11 May, 1811	Madras, Tamilnadu, India	Extensive destruction in Madras, no estimate of deaths
15	2 May, 1820	Near Madras, Tamilnadu, India	No estimate of deaths
16	8 May, 1820	Nellore District, Andhra Pradesh, India	Inundation. No estimate of deaths
17	27 May, 1823	Balasore, Orissa, India	Inundation up to 10 km inland. Several ships and whole villages disappeared
18	31 October, 1831	Balasore, Orissa, India	2.112–4.5 m surges. Extensive inundation. 22,000 deaths. 50,000 cattle lost. This might have been the same storm that also generated at surge at Barisal, Bangladesh.
19	10 May, 1832	Coringa, Andhra Pradesh, India	Extensive damage at Coringa
20	October, 1832	Balasore, Orissa, India	More violent storm than in 1823 (No. 16) but the surge was less destructive
21	21 May, 1833	Sagar Island/24 Paraganas, West Bengal, India	3 m surge. 50,000 deaths. 100,000 cattle lost
22	16 November, 1839	Between Visakhapatnam and Narsapur/Coringa, Injaram, Andhra Pradesh, India	Over 6 m surge. 20,000 deaths
23	22 May, 1843	Masulipatnam, Andhra Pradesh, India	Extensive damage
24	October, 1854	Mouth of Hoogly River, West Bengal, India	Up to 12 m water level increase near Calcutta and environs. 50,000 deaths
25	21–27 April, 1859	Near Nagapatnam, Tamilanadu, India	No estimation of deaths.

Table 6.24 (continued)

No.	Date	Location	Damage
26	2–5 October, 1864	Near Contai, West Bengal, India	Up to 12 m surge. Flooded up to 13 km on either side of the Hoogly River. 80,000 deaths.
27	1–2 November, 1864	Masalipatnam, Andhra Pradesh, India	About 130 km long stretch was subjected to surges up to 3.93 m. Surge penetrated up to 27 km inland. 30,000 deaths
28	1 November, 1867	East of Calcutta, West Bengal, India	1.8 m surge. Damage at Port Canning. 13 m surge at Hatia, Bhola Islands
29	4 November, 1870	Viskhapatnam, Andhra Pradesh, India	Lower parts of the town flooded. Also whole of Anakapalle town flooded. 7 deaths
30	1 July 1872	Near Cuttack, Orissa, India	Extensive damage, no estimate of deaths
31	13–16 October, 1874	Mouth of Hoogly, West Bengal, India	3049 deaths
32	7–8 October, 1876	Near Bhimilipatnam, Andhra Pradesh, India	Extensive damage, 30 deaths
33	6–8 December, 1878	Kakinada, Andhra Pradesh, India	Local storm surge and inundation
34	19–23 September, 1885	Cuttack (False Point) Orissa, India	7 m surge. 5,000 deaths by drowning. 300 deaths by falling trees. 50,000 houses destroyed. 10,000 cattle lost
35	6–15 September, 1882	South Orissa coast, India	Extensive damage
36	2–16 November, 1886	Madras coast, India	No estimation of deaths.
37	21–28 May, 1887	False Point, Orissa, India	Major surges
38	21–26 September, 1887	Calcutta, West Bengal, India	No estimation of deaths.
39	13–20 September, 1988	False Point, Orissa	No estimation of deaths.
40	21 November, 1988	Madras, Tamilanadu, India	No estimation of deaths.
41	24–27 October, 1909	Near GopalPur, Orissa, India	Extensive damage, no estimation of deaths.
42	20–24 September, 1911	Kaningapatnam, Andhra Pradesh, India	Extensive damage, no estimation of deaths
43	18–29 September, 1916	West Bengal coast, India	Extensive damage, no estimation of deaths
44	21–23 November, 1916	Near Cuddalore, Tamilanadu, India	Extensive damage, 300 deaths
45	12–20 May, 1925	Masulipatnam, Andhra Pradesh, India	The surge penetrated up to 6 km inland, 80 deaths.
46	29 Oct–1 Nov, 1927	Nellore, Andhra Pradesh, India	629 deaths, Considerable damage due to surge
47	14–19 Nov, 1933	Ongole, Andhra Pradesh, India	Moderate surge inundated low-lying areas
48	25–28 October, 1936	Masulipatnam, Andhra Pradesh, India	Surge penetrated up to 6 km inland. Destruction of agriculture due to saline water intrusion
49	21–25 Nov, 1938	Machilipatnam, Andhra Pradesh, India	2 m surge. Railway bridge washed away. Extensive damage to waterworks due to saline water intrusion
50	14–16 October, 1942	Contai, West Bengal, India	5 m surge at Midnapore (64 km upstream in Hoogly River) 15,000 deaths
51	13–23,May 1943	South of Madras, Tamilanadu, India	Extensive damage, low-lying areas inundated

Table 6.24 (continued)

No.	Date	Location	Damage
52	29–31 October, 1943	Kalingapatnam, Andhra Pradesh, India	Surge combined with floods in River Vamsadhara caused great damage
53	15–21 October, 1945	Masulipatnam, Andhra Pradesh, India	Up to 3.03–4.54 m surges penetrated 24 km inland
54	30 November, 1952	South of Nagapattinam, Tamilnadu, India	1.21 m surge penetrated 8 km inland. 400 deaths
55	6–14 October, 1955	Kalingapatnam, Andhra Pradesh, India	Surge up to 1.7 m
56	28 Nov–2 Dec, 1955	Tanjavore District, Tamilnadu, India	Surges up to 5 m penetrated 16 km inland. 500 deaths
57	29 May–1 June, 1956	Near Calcutta, West Bengal, India	Inundation in Midnapore District. Damage to agriculture due to saline water intrusion
58	21 October, 1963	Cuddalore, Tamilnadu, India	Almost 7 m surge
59	3–8 November, 1964	Madras coast, India	Low-lying areas of Madras city flooded
60	20–23 Dec, 1964	Tondi (Rameswaram Island), Tamilnadu, India	3–6 m Surge. 1,000 deaths
61	1–3 November, 1966	North Madras coast, India	Tidal bore flooded a large area of Madras city, 30 deaths, 3 ships grounded
62	8–11 October, 1967	Puri, Orissa, India	Water levels up to 9 m. 1000 deaths. 25 km inland inundation.
63	2–8 December, 1967	Nagapattinam, Tamilnadu, India	Moderate surges. 7 deaths
64	7 November, 1969	Kakinada, Andhra Pradesh, India	3.1 m surge. 900 deaths
65	26–30 October, 1971	Paradip, Orissa, India	4–5 m surge. The surge penetrated 25 km inland. 10,000 deaths
66	10 September, 1972	Barua, Orissa, India	3.4 m surge. 0.8 m tide
67	22 September, 1972	Gopalpur, Orissa, India	Inundation in Puri District
68	15–23 November, 1972	South of Nellore, Andhra Pradesh, India	Minor Surge
69	6–12 October, 1973	Chandbali, Orissa, India	Mild surge in river estuaries caused saline water intrusion in the coastal areas of north Orissa and West Bengal. 100 deaths
70	3–9 November, 1973	Near Paradip, Orissa, India	3–4.5 surge, Saline water inundation in Basudevpur and Uttar Sumiti
71	12–23 December 1968	Near Nagapattinam, Tamilanadu, Inia	7 deaths, Tidal waves caused severe damage in coastal districts of Ramanathapuram
72	13–20 August, 1974	Contai, West Bengal, India	3 m surge. Inundation of low-lying areas of Digha and Juneput. 7 deaths
73	11 September, 1976	Contai, West Bengal, India	2.5 m surge. 1.4 m tide. 40 deaths.
74	14–20 Nov, 1977	Chirala, Andhra Pradesh, India	Peak surge 5.0 m, Tide 0.3 m. Divi and surroundings totally inundated. 10,000 deaths
75	24 November, 1978	Between Kilakkarai and Rochemary Island, Tamilnadu, India	3–5 m surges on the coasts of Tamilnadu and Sri Lanka. Extensive damage on the northeast coast of Sri Lanka. 1000 deaths in Sri Lanka. 10 deaths in India
76	12 May, 1979	Kavali, Andhra Pradesh, India	3 m surge. 0.6 m tide. 700 deaths
77	1–4 June, 1982	Between Paradip and Chandbali, Orissa, India	2 m surge along the Orissa and West Bengal coasts. Peak surge of 4.8 m 35 km north of Dhamra harbour. 245 deaths.

Table 6.24 (continued)

No.	Date	Location	Damage
78	9–14 November, 1984	Near Sriharikota, Andhra Pradesh, India	524 deaths, extensive damage
79	20 September, 1985	Close of Puri, Orissa, India	2 m surge. Inundation lasted for 3 days. Substantial damage
80	16 October, 1985	Near Balasore, Orissa, India	Up to 4 m surge. Damage due to saline water inundation
81	13–19 October, 1987	North of Ongole, Andhra Pradesh, India	Moderate surge. 17 deaths. Substantial damage
82	31 October – 3 November, 1987	Nellore, Andhra Pradesh, India	50 deaths. 26,000 cattle killed. Substantial damage
83	23–27 May, 1989	Near Balasore, Orissa, India	3–6 m surge, 71 deaths, 2625 cattle killed, extensive damage in West Bengal and Orissa
84	4–7 November, 1989	Kavali, Andhra Pradesh, India	3–4 m surge caused destruction in Nellore and Kavali. 69 deaths
85	4–11 May, 1990	Mouth of Krishna River, Andhra Pradesh, India	4–5 m surge. 967 deaths. 600,000 houses destroyed. 21,600 cattle killed. 3,500,000 poultry killed. 42,700 goats and sheep killed. Substantial damage to agriculture
86	11–17 Nov, 1992	Sri Lanka, and Tutikorin, India	1–2 m surge at Tuticorin, 170 killed, 160 missing
87	1–4 December, 1993	Near Karaikal	1–1.5 m surge, 111 killed
88	29–31 Oct, 1994	Madras, India	1–2 m surge, 304 killed, 100, 000 huts damaged, 60,000 hectares crops dama-
ged			
89	6–10 Nov, 1995	Gopalpur, Orissa, India	1.5 m, 96 killed, 2,84,253 hectares crops damaged
90	12–16 Jun, 1996	Visakhapatnam, India	179 killed, 13,378 hectares of crops damaged
91	5–7 Nov, 1996	Kakinada, India	2–3 m surge, 978 killed, 1375 missing , 647554 houses damaged, 1.74 lakh hectares crops damaged
92	17–21 Nov, 1998	Visakhapatnam, India	16 deaths. Damage estimation not available

Table 6.25. Storm surge at Saugor Island, India, during 1948–55 (JANARDHAN, 1967)

Date	Distance of storm center to Saugor Island (km)	Observed peak surge (m)	Computed peak surge (m)	State of tide at time of peak surge
Aug. 14, 1948	306	0.34	0.43	High
Aug. 15, 1948	402	0.43	0.40	Low
July 25, 1951	306	0.85	0.98	Low
Aug. 05, 1952	418	0.34	0.34	High
Aug. 03, 1953	306	0.46	0.46	High
Aug. 30, 1955	217	0.46	0.46	High

considered in the next subsection). The storm surge considered here is the piling up of the water due to wind stress. The inverse barometer effect is not included here, since according to RAO (1968), it does not exceed 0.5 m anywhere on the east coast of India.

Table 6.26: Maximum possible storm amplitudes and total water levels (surge + wind waves) at selected locations on the east coast of India. The hypothetical storm has a wind speed of 40 $m \cdot s^{-1}$. A, total water level <2 m; B, 2–5 m; C, >5 m. A few locations in Bangladesh and one in Burma are included for comparison (RAO, 1968)

Location	Favorable Wind direction	Storm surge amplitude (m)	Storm surge + Wind wave (total water level) (m)	Classification
Dhanushkodi	NNE	4.8	8.2	C
Rameswaram	SE	6.8	11.3	C
Pamban	NNW	4.4	7.3	C
Devipatnam	E	4.5	7.5	C
Adirampatnam	SSE	5.1	8.5	C
Point Calimere	SSE	4.2	7.0	C
Nagapattinam	E	1.5	2.5	B
Karikal	E	0.3	1.3	A
Madras	ENE	1.5	2.5	B
Nizampatnam	SW	4.5	7.4	C
Mouth of Krishna River	SE	1.6	2.7	B
Narasapur	S	1.7	2.9	B
Sacromento Shoals (outer sand banks)	SSE	1.4	2.3	B
Kakinada (outer sand banks)	E	0.6	1.0	A
Visakhapatnam	SE	0.7	1.2	A
Kalingapatnam	E	1.1	1.8	A
Gopalpur	SE	0.9	1.5	A
Mouth of Devi River	SE	0.8	1.3	A
False point	SE	1.9	3.2	B
Balasore	SE	3.0	5.0	C
Mouth of Hoogly River	S	6.5	10.8	C
Mouth of Matla River	S	5.0	8.4	C
Mouth of Baleswar River (Bangladesh)	S	6.9	11.5	C
Mouth of meghna river (Lakhichar Island, Bangladesh)	SSE	8.0	13.4	C
Cox Bazaar (Bangladesh)	WSW	3.2	6.3	C
Moth of Faaf River (Burma)	SW	3.2	5.3	C

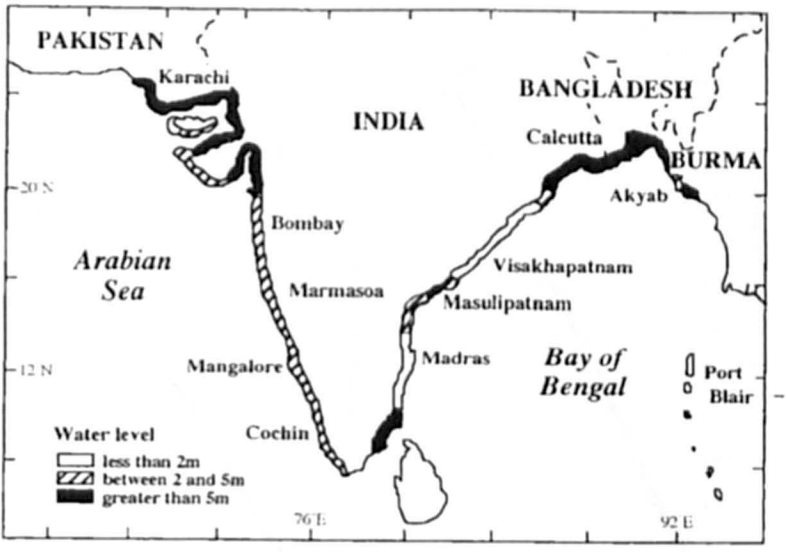

Fig. 6.35: Classification of the Bay of Bengal and the Arabian Sea coasts of India (RAO, 1968)

This classification into types A, B, and C has been verified to certain extent by comparison with actual data (Table 6.27). Thus, type C belts are the most prone to major storm surges. It can be seen from Fig 6.35 that there are four such belts on the coasts of the Indian subcontinent (RAO, 1968). Two are as follows.

1) The coastal belt around the head of the Bay Bengal, approximately to the north of 20° N. The frequency of cyclones is high here and the storm tracks are usually favorable for generating maximum surges, especially in the Sunderbans.
2) South Coromandel coast around the Palk Bay. Although the frequency of storms striking this region is somewhat smaller than for the first belt, the major storms that strike this coast usually produce major surges.

The other two belts are on the west coast of the subcontinent and will be considered in he next subsection.

There is a short, type C belt near Nizampatnam Bay. The Andhra cyclone of November 1977 produced major surges in this general area and killed several thousand people. The east coast of India, between 14 and 16.5° N, is in the type B category. Also, the Coromandel coast between point Calimere and karikal falls into this category.

GHOSH (1977) used the SPLASH model (JELESNIANSKI, 1972) for the east coast of India. He prepared nomograms for calculating peak surges based on pressure drop, radius of maximum winds, vector motion of the storm, and bathymetry offshore. The nomograms were prepared separated for the northern part (where the slope of the shelf is small) and for the remaining part of the coast (where the slope is large). A separate nomogram is presented to include the tidal effects on the northern part of the coast where the tidal range is large. Two typical nomograms prepared in this manner are shown in Fig. 6.36.

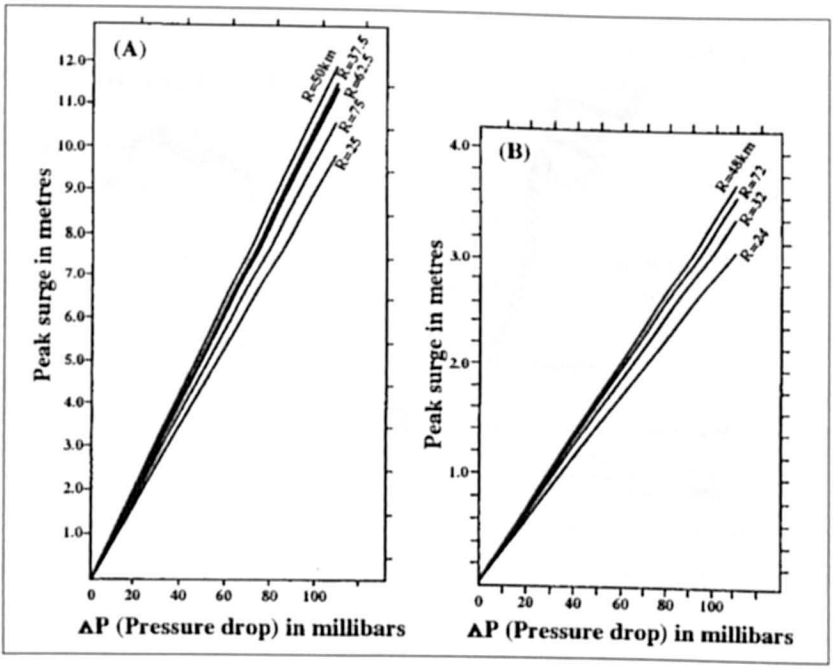

Fig. 6.36: Nomogram of peak storm surge as a function of pressure drop and radius of maximum winds for the (A) northern part and the (B) southern part of the east coast of India (GHOSH, 1977)

Table 6.27: Relationship between type of coastline and occurrence of storm surges on the coast of India. A, surge + wind wave amplitudes <2 m; B, 2–5 m; c, >5 m. Data are mainly for the period 1949–66. (RAO, 1968)

Type of coast	Intensity of storm	No. of storms that affected the coast	No. of storms that caused major storm surges
A	Moderate	13	–
	Severe	12	–
B	Moderate	19	–
	Severe	6	4
C	Moderate	1	–
	Severe	3	3

DAS (1972) used a numerical model to compute storm surges in the Bay of Bengal, which is probably the first numerical model developed for this area. DAS et al. (1974) extended this model to simulate the storm surge due to the cyclone of November 13, 1970, which caused great loss of life and destruction in Bangladesh. They used a two-dimensional linear model and telescoping grids. The grid scheme used for three different types of tracks is illustrated in Fig. 6.37. Nomograms for the storm surge as a function of the storm intensity and speed of movement of the storm are given (for the three tracks shown in Fig. 6.37, in Fig. 6.38).

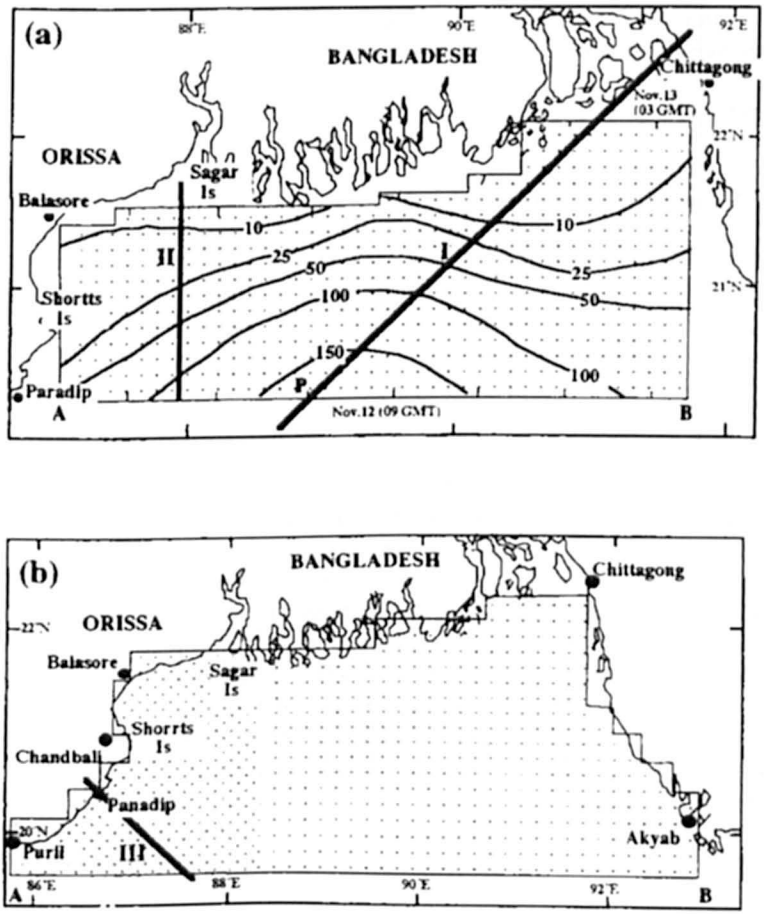

Fig. 6.37: (a) Grids for storms moving northeast (I) and north (II). Contours represent water depth (meters). (b) Grid for storms moving northwest (III) (DAS et al., 1974)

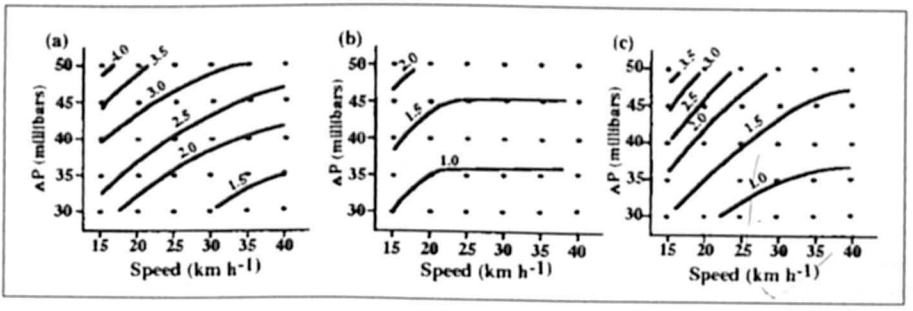

Fig. 6.38: Storm surge amplitude (meters) as a function of storm intensity (millibars) and speed 'c' of storm movement for the (a) northeast track (I), (b) northward track (II) and (c) northwest track (III) of Fig. 6.37 (DAS et al., 1974)

The relationship between the storm surge amplitude η and the storm intensity Δp and speed of movement of storm c was expressed as

$$\eta = A_0 \Delta p + A_1 (\Delta \Delta p)^2 + A_2 c \qquad (6.69)$$

Table 6.28. Numerical values of the constants A_0, A_1, and A_2 of eq. 6.69 for the three different tracks shown in Fig. 6.37 (DAS et al., 1974)

Track	A_0 ($\times 10^2$)	A_1 ($\times 10^4$)	A_2 ($\times 10^2$)
Northeast	9.59	−0.91	−4.60
North	2.88	3.08	−1.20
Northwest	8.24	−1.60	−5.15

The numerical values of the constants A_0, A_1, and A_2 are listed for the three different tracks (shown in Fig. 6.37) in Table 6.28. Theseauthors concluded that linear superposition of tide and surge would overestimate the water level by about 1 m.

DAS (1980) included nonlinear advective terms and improved the model of DAS et al. (1974), and the computational area was also enlarged. This model, which includes the tide-surge interaction in a more realistic manner, gave water levels that agreed better with observed levels. NATARAJAN and RAMANATHAN (1980) developed a nonlinear finite-element model and used the same computational area and storm tracks as in DAS et al. (1974)

In a series of papers JOHNS et al. (1981, 1982, 1983a, 1983b, 1985); DUBE et al. (1981, 1982); DAS et al. (1983); DUBE and SINHA (1982) and SINHA et al. (1993) have studied various aspects of storm surge modelling and prediction along the east coast of India. In all these modelling studies the treatment of the coastal boundaries involve a procedure leading to realistic curvilinear representation of the east coast of India, the details of which are described in Chapter 2.

In an attempt to simulate the surge generated by the devastating 1977 Andhra cyclone (Fig. 6.39) JOHNS et al. (1981) used three different numerical models. All the three models considered by the author's are fully nonlinear and based on the vertically integrated equations. The analysis area in the first model (designated M_1) includes the entire Bay of Bengal north of 6° N and utilizes a curvilinear boundary treatment to represent both western and eastern sides of the Bay. The second model (M_2) is a coastal zone model extending along the east coast of India with curvilinear treatment of the coastline. The third model (M_3) that again covers the entire Bay of Bengal uses conventional techniques based on the orthogonal straight-line segments to represent the coastline. Each of these models predict a maximum surge elevation along the Andhra coast in the range of 4–5 m. This compares well with the available observation. However, M_1 produced the surge elevation in excess of 6 m at the head of the Bay, which was unrealistic and is not seen in the results of M_2. Interesting analysis of the differences in the response obtained from each model has been made. The difference between responses of M_1 and M_2 in the head Bay is attributed by the author's to the funnelling effect of the converging coastline towards the north. Subsequently DUBE et al. (1981) performed numerical experiments, using M_1 with number of alternative cyclone models, to further investigate the phenomenon of large sea surface elevations in the head Bay. Contrary to the earlier explanation given by JOHNS et al. (1981), the authors attribute the anomalous surge produced at Contai in the head Bay to the choice of the cyclone

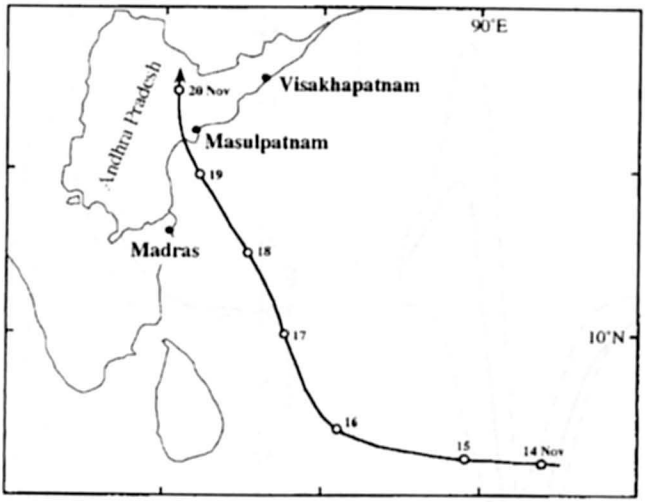

Fig. 6.39: Track of Andhra cyclone: 14–20 November 1977 (JOHNS et al., 1981)

model which gives significantly strong winds at greater distances from the centre of the cyclone.

Frequently, the lateral boundaries in numerical storm surge prediction models are taken to be vertical sidewalls through which no flux of water is allowed. In actuality, however, the water will usually move continuously inland and the use of idealized vertical sidewalls may lead to misrepresentation of the surge development. Recognizing this short coming of earlier models, JOHNS et al. (1982) developed a model which used a continuously deforming lateral fluid boundary instead of using the conventional solid wall boundary at the coast. The model is an extension of the earlier transformed coordinate coastal zone model wherein the coastal topography is included to route the storm surges over the land. As a result of the movement of the coastal boundary with changing water level the horizontal grid deforms with time and the undisturbed water depth at each grid point is recomputed at every time step. Numerical experiments were performed by the authors with different sea-floor slopes and with a fixed boundary version of the model. A comparison of the results slow that the moving boundary model gives a reduced surge response at the initial coastline position than that in fixed boundary model. Further, fixed boundary model yields a significantly greater maximum inland intrusion as compared with deforming coastline model. Calculations based on fixed boundary model also show that the predicted maximum inland inundation occurs some 5 hours earlier than in moving boundary model. The differences decrease as the seabed slope at the coast is increased. Seaward recession of the coastline, following the peak surge is also simulated. Fig. 6.40 gives the variation of the coastline displacement and sea surface elevation at initial position of coastline along two stations of Andhra Coast with seabed slope of 2×10^{-4}.

JOHNS et al (1983 a) developed a fully three-dimensional coastal zone storm surge model and applied it to the 1977 Andhra cyclone. The model employed a highly sophisticated turbulent energy closure scheme due to JOHNS (1978). The model was developed with the surmise that the shallow water evolution of the surge response may be significantly different in three-dimensional model because of the full representation of the vertical current structure. It was also thought that the sea-surface surge response would be critically dependent on

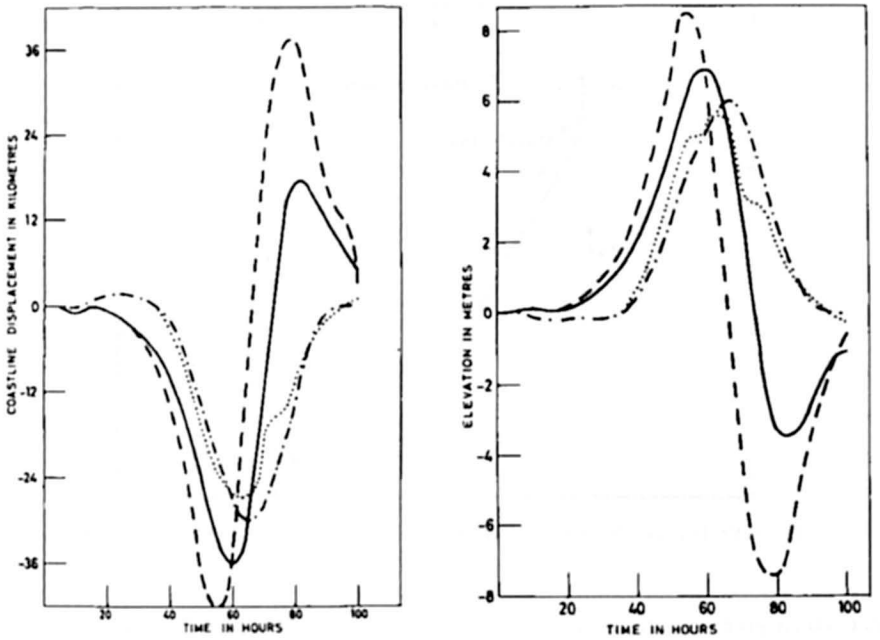

Fig. 6.40:(a) Variation of coastline displacement with $S = 2 \times 10^{-4}$ calculated from MD and MF. Kavali (MD) -; Kavali (MF) - - -; Divi (MD) -.-.-; Divi (MF) ..., (b) Variation of sea surface at initial position of coastline with $S = 2 \times 10^{-4}$ calculated from MD and MF. Kavali (MD) -; Kavali (MF) - - -; Divi (MD) -.-.-; Divi (MF) ..... .

the value chosen for the bottom roughness parameter in the three-dimensional model. Simulations of the Andhra cyclone using two-and three-dimensional models were carried out. The results of their experiment are illuminating.

They found a remarkable qualitative and quantitative similarity between the two simulations, suggesting that details of the dissipative mechanism and vertical current structure were unimportant. They further conclude that if the vertical current structure is not a primary concern, it does not appear worthwhile replacing the depth-averaged procedure by a more complicated three-dimensional model.

Since the coastal surge elevations are effectively dependent upon the near coastal bathymetry, a desirable feature of storm surge simulation schemes is the ability to incorporate increased resolution adjacent to the coastline. This was achieved by JOHNS et al. (1983 b) by introducing an additional transformation of the offshore coordinates in their earlier coastal zone model (JOHNS et al., 1981). This version of the model was used to determine the influence of model resolution and nearshore bathymetry on the computed surge proper resolution of the near shore bathymetry was found to be crucial in determining the storm induced sea surface elevation, one of the interesting results identified by the authors pertain to a northward propagating component of the computed surge response which is found to have the characteristics of a coastally trapped wave. Thus the total response is determined by the contribution from direct wind stress together with the northward propagating component.

For the east coast of India, the phenomenon of alongshore propagation was further identified in a model developed to investigate tide-surge interaction in the Bay of Bengal (JOHNS

et al., 1985). Clear evidence is shown by the authors to the northeasterly propagation in the case of both the 1982 Orissa surge and the 1977 Andhra surge.

Coastal trapping of the energy is implied and the locally shallow water suggests that nonlinear aspects of the propagation process are important. Moreover, the trapped waves cannot have the form of a Kelvin wave, since this is necessarily right bounded, and must, instead, have the form of a topographically trapped edge waves. These findings were further illuminated by JOHNS and LIGHTHILL (1993). They used a simple theoretical model with uniform shelf slope to investigate the formation of anomalous sea-surface elevations remote from the position of landfall of the generating cyclone.

DAS et al. (1983) used the stretched coordinate model of JOHNS et al. (1983b) to simulate the surge generated by the 1982 Orissa cyclone. JARREL et al. (1982) made one of the most comprehensive studies of storm surges in the Bay of Bengal. They developed five models for the Sri Lanka/ India/ Bangladesh coastlines, two models for the Myanmar /Thailand coastline and one for the Andaman Islands region. The analysis areas of the models cover the coastline and the water area up to and slightly beyond the continental shelf. Based on population centers, a total of 16 tropical cyclone impact points were chosen (Table 6.29). The maximum wind speed in the calculations varies from 55 to 130 knots. The directions from which the cyclones could realistically approach the impact points are given in Table 6.29. A total of 258 runs were made for the 16 impact points. Tidal constituents M_2, S_2, N_2, K_1, O_1 and S_a were included in the models. Model provided surge heights in the case of 1977 Andhra cyclone are shown in Fig. 6.41. These model-simulated surges along the Andhra coast are in good agreement with limited available observations. GHOSH et al. (1983) applied the "SPLASH" model to compute the surge associated with 1977 Andhra and two other cyclones. They obtained a peak surge elevation of 5.7 m about 50 km to the right of the landfall. This is in good agreement with earlier calculation of JARREL et al. (1982).

Table 6.29: Angles of cyclone approach (with respect to the coast line) to be modelled for the individual impact points (JARREL, LEWIS and WHITAKER, 1982)

Impact Point	Direction from which storm approaches
Trinconamalee (Sri Lanka)	SE through NE
Jaffna (Sri Lanka)	SE through NE
Negapatam (India)	SE through NE
Pondicherry (India)	SE through NE
Madras (India)	SSE through ENE
Masulipatnam (India)	SSE through ENE
Coconada (India)	S through ENE
Vishakhapatanam (India)	SSW through ESE
Berhampur (India)	SSW through ESE
Puri (India)	SSW through SE
Calcutta (India)	SW through SE
Port Blair (Andaman Is.)	S
Chittagong (Bangladesh)	SW through S
Bassein (Burma)	S through W
Rangoon (Burma)	SSE through SSW
Phuket (Thailand)	Only ESE

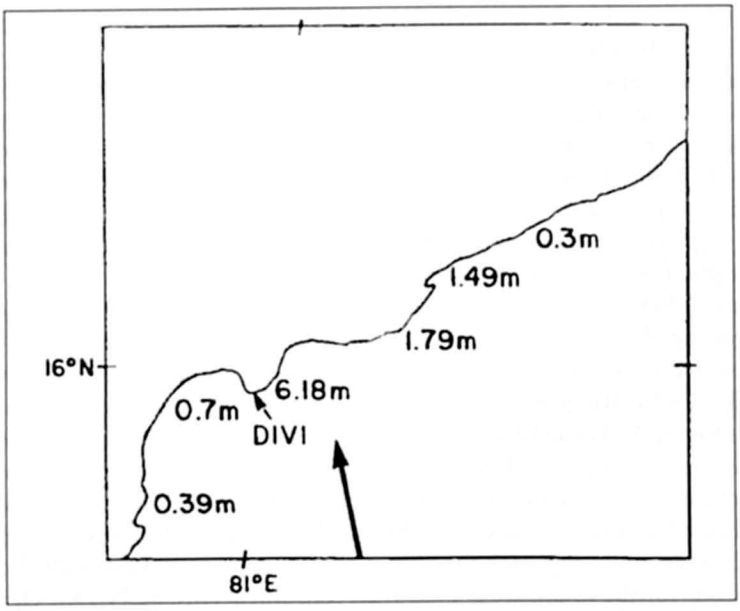

Fig. 6.41: Storm surge height distribution along the east coast of India for the November 1977 Andhra cyclone (JARREL, LEWIS and WHITAKER, 1982)

Advent of powerful personal computers has set up a trend to run storm surge models in real time on PC-based workstations in an operational office. Recognizing this DUBE et al. (1994) describe a real time storm surge prediction system for the east coast of India. The forecasting system proposed by the authors is based on the vertically integrated numerical storm surge models that were developed earlier by the group (JOHNS et al., 1981; 1983 b; DUBE et al., 1985 b). Surface winds associated with a tropical cyclone are derived from a dynamic storm model (JELESNIANSKI and TAYLOR, 1973). The only meteorological inputs required for the model are the positions of the cyclone, pressure drop and radii of maximum winds at any fixed interval of times. The model can be run in a few minutes on a PC in an operational office. The system is operated via a terminal menu and the output consists of the two-dimensional and three-dimensional views of peak sea surface elevations with the facility of zooming the region of interest. One of the significant features of this storm surge predication system is its ability to investigate multiple forecast scenarios to be made in real time. This has an advantage because the meteorological input needed for surge prediction can be periodically updated with the inflow of data on fast telecommunication links. The model has extensively been tested with severe cyclonic storms, which struck the east coast of India during the period 1960–1990. The model results reported for three case studies (June 1982 Orissa cyclone; November 1977 Andhra Cyclone and May 1990 Andhra Cyclone) are in very good agreement with the available observations and estimates of the surge. In Figs. 6.42 and 6.43 we show respectively the track of May 1990 Andhra cyclone and model computed peak surge envelope along the east coast of India. Detailed case studies by using this model may be seen in DUBE and GAUR (1995). This version of the model was tested in near real time during the cyclone periods of 1992–1993 (DUBE and GAUR, 1995). Operational feasibility test of the model is presently undergoing at India Meteorological Department.

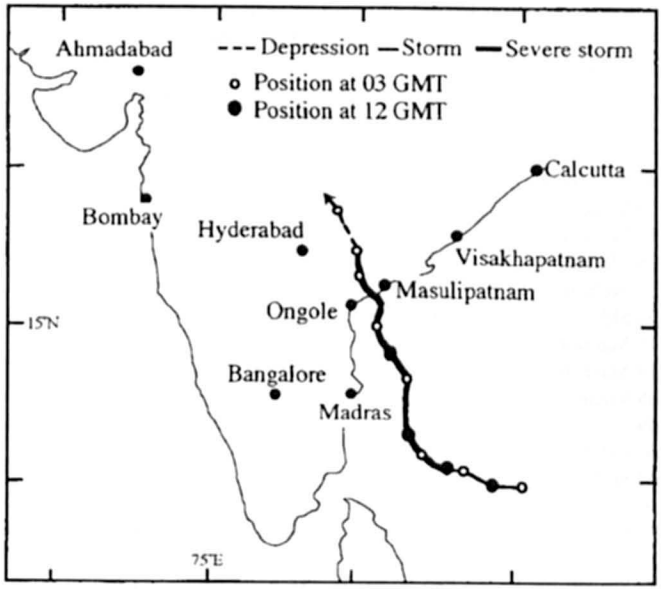

Fig. 6.42: Track of Andhra cyclone; 5–11 May 1990 (DUBE et al., 1994)

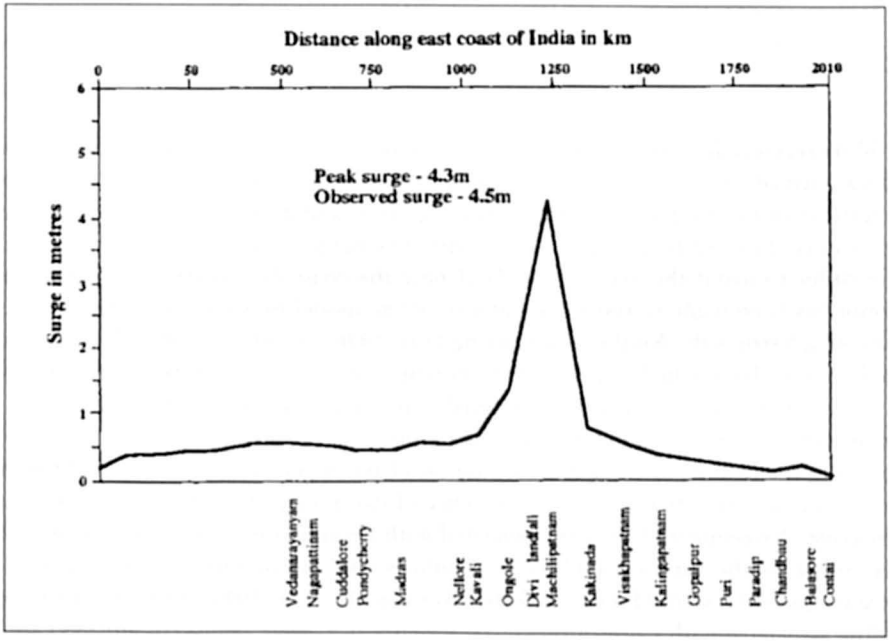

Fig. 6.43: Peak surge envelope associated with 1990 Andhra cyclone (DUBE et al., 1994)

Table 6.30: Severe cyclonic storms having potential of producing significant surges along the Andhra coast during 1895 to 1996

No.	Cyclone	ΔP (mb)	R (km)	Landfall Lat (N)	Maximum Wind Speed (knots)
1	1895 Kakinada	35	18	17.2	70
2	1906 Vizag	25	15	17.9	60
3	1921 Nellore	30	15	14.3	60
4	1925 Machili	60	20	16.1	108
5	1927 Nellore*	80	25	14.3	100
6	1940 SH	30	22	14.0	60
7	1945 Machili	50	19	16.3	90
8	1949 Machili*	60	25	16.3	110
9	1965 Vizag	30	15	17.9	62
10	1969	45	25	16.7	96
11	Kakinada*	30	15	13.8	80
12	1972 SH*	30	15	16.1	70
13	1976 Machili	28	15	14.8	60
14	1976 Kavali	80	40	15.8	135
15	1977 Divi*	26	15	14.8	55
16	1977 Kavali	60	35	14.8	100
17	1979 Kavali*	60	25	14.0	102
18	1984 SH*	26	15	14.4	50
19	1987 Nellore	26	15	15.9	50
20	1987 Machili	70	20	14.8	110
21	1989 Kavali*	80	40	15.7	136
22	1990 Divi*	30	25	13.0	75
23	1994 Madras*	35	20	16.7	90
	1996 Kakinada*				

More recently RAO et al., (1997) developed a location specific high-resolution model for Andhra coast of India, on the lines similar to that of DUBE et al. (1994). One of the important features of the model is that it uses more accurate and detailed bathymetry for the offshore waters of the Andhra Coast. A simple drying scheme has also been included in the model in order to avoid the exposure of land near the coast due to strong negative surges. Attempt has been made to test the reliability of the model by validating it for various cyclones, which struck the Andhra coast during 1891–1996. Table 6.30 list the 23 cyclones identified by the authors, which appear to have potential of producing a peak surge of more than 1m. In Table 6.31, the computed and observed peak surges and their locations of landfall have been listed for eleven cyclones for which post-storm survey surge information could be procured from the records of India Meteorological Department. Authors have used the model results to calculate the frequency of occurrence of storm surge heights at different locations of the coast. Assessment of the risk associated with a major storm surge for a given location is also made by the authors (Table 6.32). Authors also use an empirical formula given by FREEMAN and MEHAUTE (1964) and latter also used by ALI (1996), to estimate the inland flooding associated with storm surges.

Table 6.31: Comparison of observed and computed peak surge amplitude and their locations

	Surge (m)		Location of peak surge	
Cyclone	Observed/ Reported	Computed	Observed	Computed
1927 Nellore	3.0	3.07	North of Nellore	Nellore
1949 Machili	2.5	2.093	Machilipatnam	10 km N of Machilipatnam
1969 Kakinada	2.6	2.82	Kakinada	Kakinada
1972 SH	0.8–1	1.23	Sriharikota	Sriharikota
1977 Divi	5.0	4.93	Divi	Divi
1979 Kavali	3.0	3.3	Kavali	10 km North of Kavali
1984 SH	2.0	2.4	Sriharikota	Sriharikota
1989 Kaval	3–4	3.8	40 km N of Kavali	48 km N of Kavali
1990 Divi	4.5	4.41	Divi	Divi
1994 Madras	1–1.5	0.83	Madras	20 km North of Madras
1996 Kakinada	1.5	1.6	Kakinada	Kakinada

Table 6.32: Risk (%) of exceedence of storm surge heights at Divi (Zone 'G')

Years	Surge height (m)				
	≥ 1	≥ 2	≥ 3	≥ 4	≥ 5
10	50	22	20	18	8
20	75	40	36	34	16
50	97	92	67	65	36
160	99.9	99.4	89	87	59
200	99.99	99.99	98.8	98.5	83.9

Before ending this subsection we may like to refer few other storm surge studies, which have been carried out for the east coast of India. Interested readers may refer to the works of KUMAR et al. (1995), MATHEW et al. (1996), HENRY et al. (1997), MURTY and DUBE (2000), and DUBE et al. (1998, 1999a, 2000a, 2000b).

(c) Myanmar

Storm surges affecting Myanmar are to much less extent in comparison with Bangladesh and India. However, whenever a severe cyclone struck the coast of Myanmar it leaves severe damage and casualties mostly due to strong winds and storm surge floods. During the period 1884 to 1999 the Myanmar coast was affected by eleven severe cyclonic storms of which seven were associated with significant surges. Table 6.33 lists the impact of these cyclones (THAW, 1998).

During April 22–26, 1936, a severe storm struck the Kyaukpyu area and killed about 2000 people and over 7,000 cattle. Another cyclone that caused heavy loss of life and pro-

Table 6.33: Losses of lives and properties due to severe cyclone during 1884–1998

Sr. No.	Year	Month	Day	Wind Speed in m.p.h.	Damage to crop	Loss of Lives	Loss of Cattle	No. Of homes damaged	Total loss in Kyats	Point of landfall
1	1884	May	14–17	100	–	100	–	–	200,000,000	Sittwe
2	1936	April	22–26	80–100	–	2000	7000	–	200,000,000	Kyaukpyu
3	1948	October	5–8	80–100	–	–	–	–	100,000,000	Sittwe
4	1952	October	22–24	60–80	–	4	–	–	10,000,000	Sittwe
5	1967	May	7–10	80–100	–	–	–	–	30,000,000	Kyaukpyu
6	1967	October	22–24	80	–	172	656	–	100,000,000	Sittwe
7	1968	May	4–7	130	–	1037	17 537	57 663	800,000,000	Sittwe
8	1975	May	5–7	80–100	–	304	10 191	246 700	776,500,000	Pathein
9	1978	May	14–17	80–100	–	–	–	–	20,000,000	Kyaukpyu
10	1982	May	2–5	80–100	–	31	63	–	38,000,000	Gwa
11	1994	May	1–2	100–120	787 acres	10	150	2874	78,000,000	Maungdaw

perty cross the Myanmar coast near Sittwe on May 7, 1968. The cyclone generated a surge of more than 4 m with loss of more than 1000 human lives. The storm surge due to the May 1975 cyclone killed 304 people and more than 10,000 cattle and destroyed about 28,000 houses (LWIN, 1994a). In recent past a severe cyclonic storm crossed the coast of Myanmar near Maungdaw on 2 May 1994. Storm surge of 3.26 m and loss of 10 lives in addition to some damages were reported (THAW, 1998). The peak surge envelope for May 1994 cyclone is shown in Fig. 6.44.

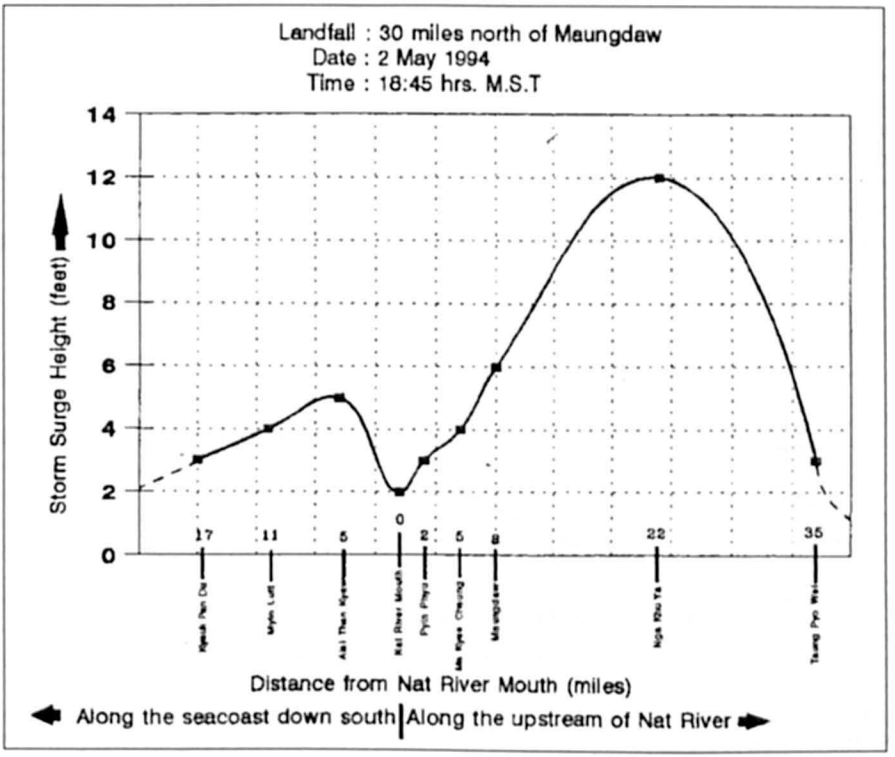

Fig. 6.44: Storm surge envelope of May 1994 severe cyclone storm in Myanmar (LWIN, 1994 a)

In Myanmar, tidal and storm surge data are available at about 10 stations beginning with 1966. The list of the tide gauges available along the coast of Myanmar is shown in Table 6.34. Rakhine coast and Deltaic region are the most favorable places for storm surge inundation. The available surge data during the last 35 years are shown in Table 6.35(a, b). Based on the available data THAW (1998) points out following salient features of storm surges affecting the Myanmar coast

(i) For narrow coastal areas where there is no estuary, storm surge occurred on both sides of the point of landfall. But it was higher and more extensive on the onshore wind region.

(ii) For coastal strip close to Deltaic region, the storm surge entered through estuaries over the delta, which is not directly struck by the high onshore winds of cyclone. The Pathein cyclone of May 1975 and Maungdaw cyclone of May 1994 are the examples. The storm surge due to the May 1975 event penetrated at least 100 km into the river system and

Table 6.34: List of available observed tidal data along the coast of Myanmar

Name of Station	Latitude	Longitude	Data available since
Kyaukpyu	19.25	93.33	1973
Thandwe	18.28	94.21	1968
Pathein	16.46	94.56	1973
Yangon	16.46	96.10	1953
Yangon River Mouth (Elephant Point)	16.35	96.12	1968
Mawlamyine	16.30	97.37	1965
Amherst	16.05	97.34	1967
Dawei	14.06	98.13	1972
Myeik	12.26	98.36	1966
Kawthoung	09.58	98.35	1966

caused inland flooding (LWIN, 1980). The distribution of the maximum surge along the Ayeyarwady River for the cyclone of May 1975 is given in Fig. 6.45 (CHO, 1980). The highest surge was recorded 80–90 kilometers inland Duration of storm surge was longest where water logged. It was about 25–30 km inland (Fig. 6.46).

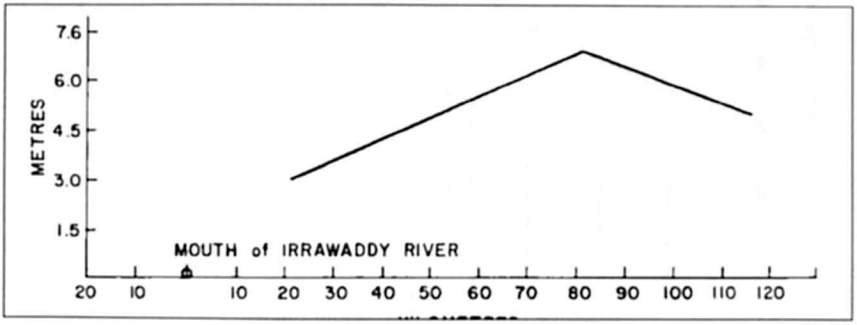

Fig. 6.45: Distribution of the maximum surge along the Ayeyarwady River for the storm of May 5–8, 1975. The ordinate is the surge amplitude and the abscissa is the distance along the river (CHO, 1980)

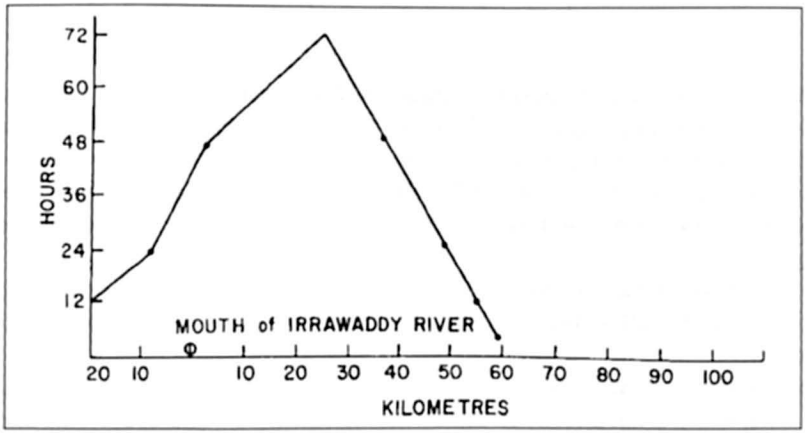

Fig. 6.46: Surge duration versus distance along the Ayeyarwady River for the storm of May 5–8, 1975 (CHO, 1980)

(iii) For deltaic coastal strip covered by many estuaries and islands, storm surge occur with winds, which may be offshore to the general coastline. In the case of 1968 Sittwe cyclone the strong offshore easterly winds have brought in water mass from the underlying surface and inundated the whole of the area.

ODD (1980) studied the storm surges generated by May 1975 cyclone in the Ayeyarwady Delta Area of Myanmar making use of hydraulic and numerical models. He concluded that the surge amplitudes as well as the amplitude of the semidiurnal tide increase rapidly east of China Bakir because of the shallowness and funnel shape of the Gulf of Martaban.

Table 6.35 (a): List of computed and observed surge heights for rakhine coast

Year	Station	ΔP (mb)	C ($km \cdot hr^{-1}$)	Computed Surge (m)	Observed Surge (m)	E
1967	Sittwe	25	10	1.85	1.80	+0.08
1967	Sittwe	22	10	1.66	NA	NA
1968	Sittwe (Kyaukpyu)	50	11	4.05	4.25	−0.20
1976	Thandwe	20	10	1.42	NA	NA
1978	Kyaukpyu (Myabon)	34	8	2.78	NA	NA
1994	Maungdaw	43	36	3.26	3.08	+0.18

NA = Not Available

Table 6.35 (b): List of computed and observed surge heights for deltaic coast

Year	Station	V_{max} (kt)	H_c (m)	H_0 (m)	E
1975	Pathein	140	2.75	3.00	−0.25
1982	Latputta	60	0.48	0.60	−0.12
1982	Gwa	120	3.75	3.70	+0.05

LWIN (1980) developed an analytical and empirical prediction model, which is based on the combination of Miyazak's and Fletcher's equations. The empirical formula developed by LWIN (1980) relates the peak surge h (cm) with the maximum sustained wind Vm (ms^{-1}) and the angle between the normal to the coast and the direction of the moment of the storm θ. The relation is

$$h = (A + B \cos \theta) V_m^2$$

where A and B are numerical constants, whose values are determined from the historical records. The values of A and B are:

(i) For Rakhine coast; A = 0.0563, B = 0.0744

(ii) For the Deltaic coast; A = 0.1264, B = 0.0864.

Two precomputed nomograms, one for shallow water corresponding to deltaic coast and the other for deep water corresponding to Rakhine coast were also constructed by the author. These nomograms are given in Fig. 6.47a and 6.47b.

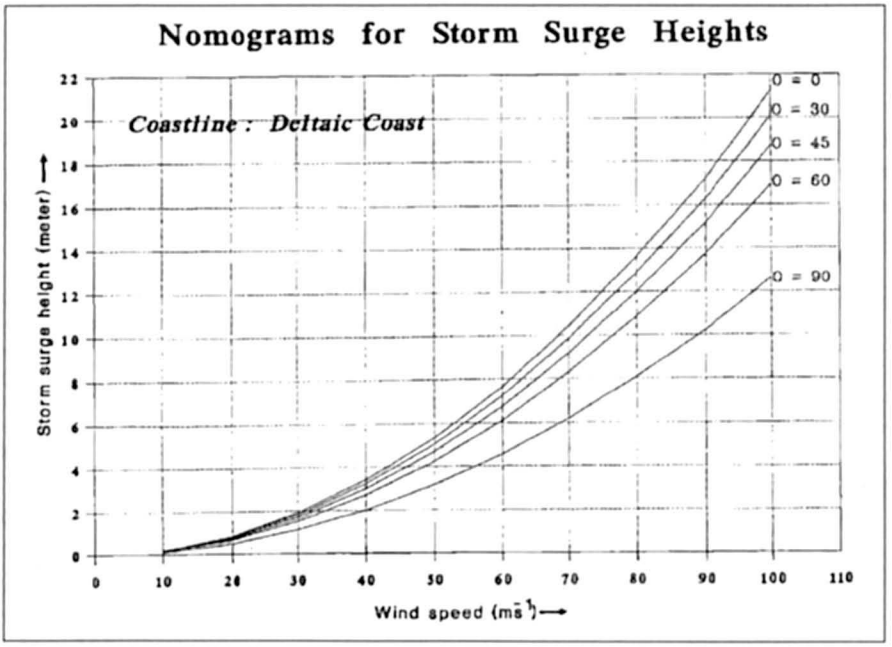

Fig. 6.47a: Nomograms for storm surge heights (deltaic coast) (Lwin, 1994b)

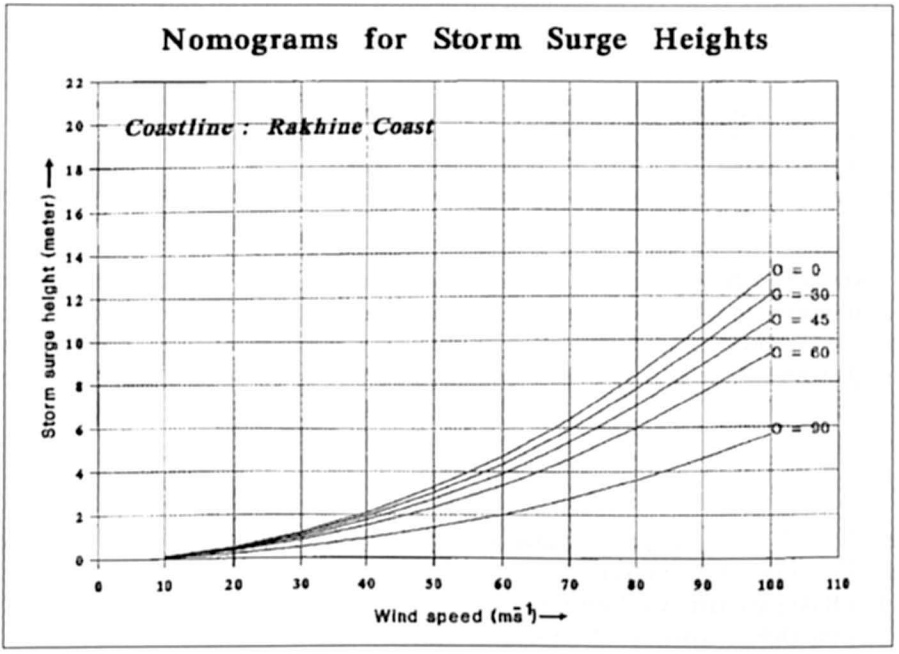

Fig. 6.47b: Nomograms for storm surge heights (Rakhine coast) (Lwin, 1994b)

As already maintained JARREL et al. (1982) developed two models for the Myanmar/ Thailand coastlines. Analysis area of the models included the coastline and offshore region up to and slightly beyond the continental shelf. Three tropical cyclone impact points based on the population were chosen: Two in Myanmar (Pathein and Yangon) and one in Thailand (Phuket). Authors performed several runs for these impact points to assess the storm surge threat in the coastal regions of Myanmar and Thailand.

DUBE et al. (1984a) used a vertically integrated storm surge model to simulate the surge generated by May 1975 Pathain cyclone. Their model is based on fully nonlinear equations and cover the whole Bay of Bengal extending from 6° N to 22.5° N and the western and eastern sides of the analysis area are the east coast of India and Myanmar-Malaya coasts respectively. Their model produced the maximum surge in the range of 3 to 5 m in the deltaic region of Myanmar right from the mouth of Ayeyarwady to the extreme northern regions of the Gulf of Martaban. This is good agreement with the available observations.

Attempts have also been made to predict storm surges in Myanmar using different empirical and statistical techniques. The detailed review of these methods is given by LWIN (1994b). LWIN (1994a) and THAW (1998) give the detailed review of the present status of storm surge fore coasting in Myanmar.

DUBE (1998b) applied a coastal zone vertically integrated numerical storm surge model to Myanmar. He performed several simulation experiments by using the data of severe cyclonic storms hitting the coastal regions of the Myanmar. He compared the simulated sea surface elevation with observations from local tide gauges where ever possible or with post storm survey estimates. The results of the experiments are in general in good agreement with reported values along the deltaic region of Myanmar. The computed peak surge envelope for May 1982 Gwa cyclone is shown in Fig. 6.48.

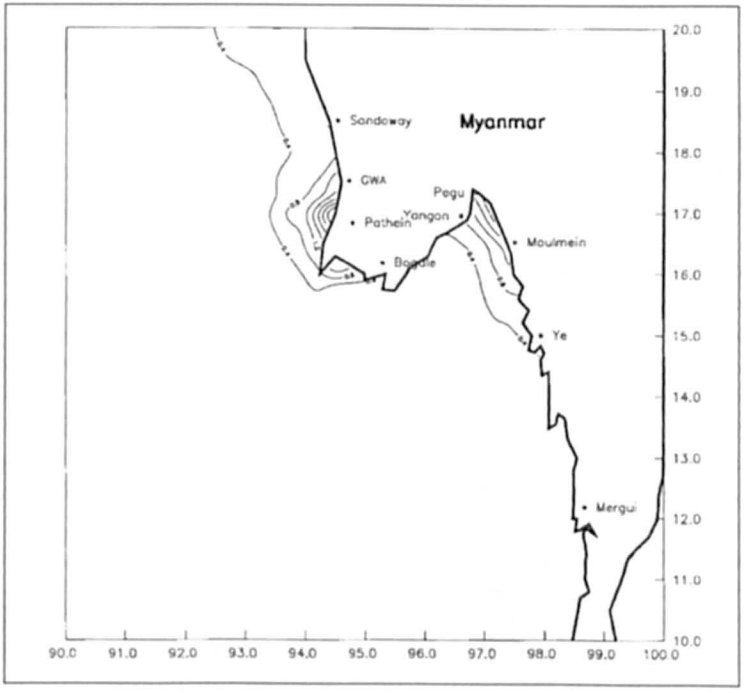

Fig. 6.48: Computed peak surge for May 1982 Gwa cyclone (DUBE, 1998b)

(d) Sri Lanka

Storm surges are not frequent in Sri Lanka; however major surges occurred in association with December 1964 and November 1978 cyclone. December 1964 Trincomalee/Rameswaram cyclone was one of the severest storm that affected Sri Lanka and extreme southern India peninsula. Batticoloa cyclone of November 1978 also affected southeast coast of India besides causing extensive loss of life and property in the coastal regions of east coast of Sri Lanka Table 6.36 lists the severe cyclonic storms, which formed in the Bay of Bengal during 184–1999 and crossed Sri Lanka coast. It may be seen from the table that east and north Sri Lanka coast are the most vulnerable coast for the landfall of tropical cyclones.

Table 6.36: Severe cyclonic storms of Sri Lanka

No.	Date	Location	Damage
1	8–10 March, 1907	Eastern coast of Sri Lanka	Damage estimation not available
2	17–24 December, 1964	Near Trincomalee	Damage estimation not available
3	17–24 November, 1978	Near Batticaloa	2 m surge, 915 deaths 100,000 houses damaged, At Kalkudah, the sea had entered land to distance of about 1.5 km.
4	11–17 November, 1992	Eastern coast of Sri Lanka	4 deaths, 29,116 houses damaged

Study of the storm surges in Sri Lanka has not attracted many workers. Only studies that came to our notice are by JARREL et al. (1982), RAO et al. (1994), DHARAMRATNA (1996) and CHITTIBABU (1999).

JARREL et al. (1982) developed models for Sri Lanka as a part of their major study to evaluate storm surge threat in the Bay of Bengal. They selected Trincomalee and Jaffna as the tropical cyclone impact points on the northeast coast of Sri Lanka. Several numerical experiments were performed by the authors for the cyclones of varying wind speeds approaching Trincomalle and Jaffna from SE through NE. This study may probably be considered as one of the most comprehensive study to assess the impact of storm surges on the coast of Sri Lanka.

RAO et al. (1994) developed a coastal zone numerical model to simulate storm surges and currents arriving Sri Lanka and Southern Indian Peninsula. The model is based on the conventional depth averaged equations and cover an analysis area extending from 2° N to 20° N and 72° E to 86° E. Experiments are carried out to simulate the surges generated by the December 1964 and November 1992 cyclones. The 1964 Rameswaram cyclone crossed the Sri Lanka coast about 50 km north of Trincomallee on 22 December at about 0600 UTC, Moving north westward it crossed the Sri Lanka and struck the Indian coast about 30 km to the south of Tondi on December 23 at 0600 UTC. Surges therefore occurred both on the northeast coast of Sri Lanka and southeast coast of India in association with this cyclone.

The track of the cyclone is shown in Fig. 6.49 computed maximum sea surface elevations for the landfall of the cyclone in Sri Lanka and later in India are shown in Fig. 6.50. A peak surge of 3.7 m is predicted at about 50 km north of Trincomalee (Sri Lanka) while near Tondi (India) a peak surge of 5.6 m is predicted. This is in agreement with the reported flooding and surge in the region (RAO and MAZUMDAR 1966). Very recently CHITTIBABU (1999) used the model developed by RAO et al. (1994) to simulate the surge generated by November 1978

Batticoloa cyclone. Model computed contours of peak surge elevations for the east coast of Sri Lanka and southeast coast of India are given in Fig. 6.51.The simulated surges are in good agreement with the reported maximum surge values (SRINIVASAN et al., 1978).

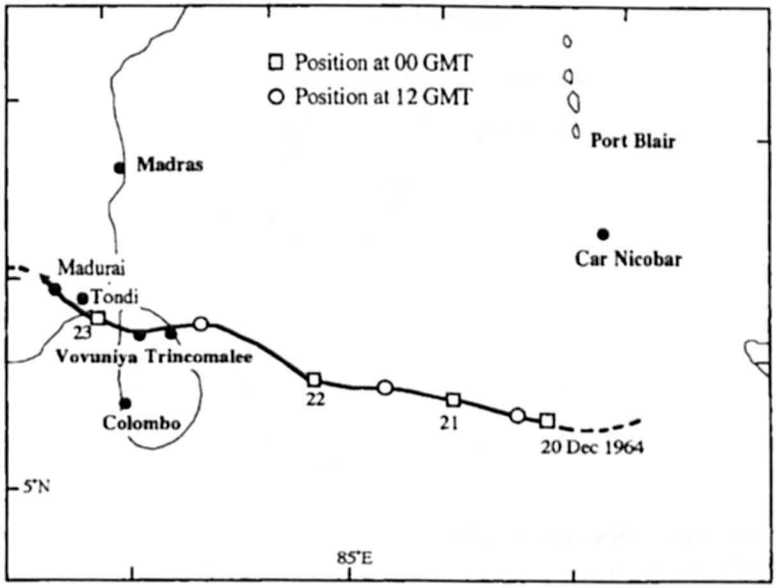

Fig. 6.49: Track of December 1964 Rameshwaram cyclone (RAO et al., 1994)

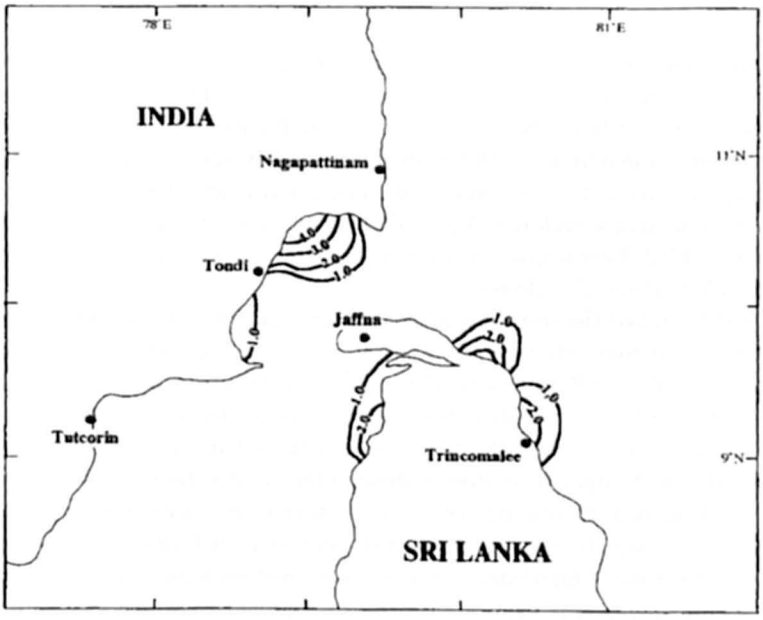

Fig. 6.50: Computed maximum sea surface elevations for the landfall of the cyclone in Sri Lanka and later in India (RAO et al., 1994)

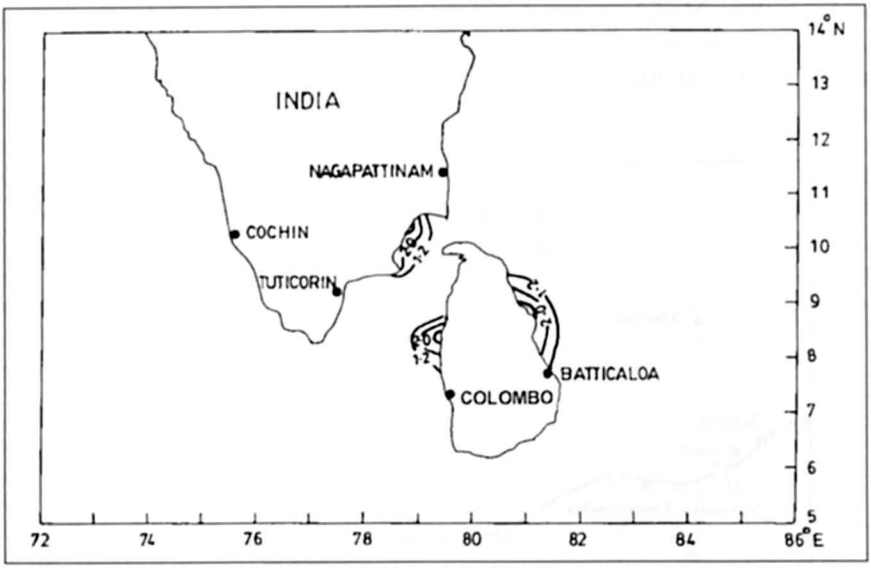

Fig. 6.51: Computed peak surge associated with November 1978 Batticoloa cyclone of Sri Lanka (CHITTIBABU, 1999)

DHARMARATNA (1996) presented the nomograms based on the model output of JELESNIANSKI (1972) for predication of the storm surges on the entire east coast of Sri Lanka. He applied these nomograms to successfully compute the surge associated with 1978 Batticoloa cyclone.

6.3.2 Arabian Sea

Although more cyclones occur in the Bay of Bengal than the Arabian Sea, there are several records of severe cyclonic storms hitting the Gujarat and the North Maharashtra regions of the west coast of India. Number of cyclones in the Bay of Bengal over a given period is about four times the number in the Arabian Sea; however, only about one quarter of the Bay of Bengal storms mature into severe storms, whereas about 40 % of the Arabian Sea storms can become severe cyclones. A partial list of major storm surges on the Arabian coast of India during 1782–1999 is given in Table 6.37. Table shows that the Gujarat coast is the most vulnerable to tropical cyclones.

RAO (1968) studied the storm surges on the Arabian Sea coast of India (and Pakistan). Classification of this coast into types A, B, and C is given in Fig 6.35. Previously, it was mentioned that on the Bay of Bengal coast of the subcontinent, there are two dangerous zones (type C). On the Arabian coast, also, there are two dangerous zones. The first one includes the Konkan coast to the north of 18° N and the coastal belt around the Gulf of Cambay.

In this belt, the frequency of storms striking the coast is low. This may be seen from Fig. 6.52, which provide the landfall of cyclonic storms on a district-wise basis. Here, the tidal range is quite large (e. g., 8 m at Mumbai. and 11 m at Cambay). Unless peak surge occurs close to the time of high tide, no major water level oscillations may occur in this belt. It should be emphasized that, even though the Arabian Sea coast experiences major storm surges much less frequently than the Bay of Bengal coast, the reason there are two dangerous belts in the manner of the classification into types A, B, and C. This classification does not

Table 6.37: List of Storm surges along west coast of India (1618–1999)

No.	Date	Location	Damage
1	May 15, 1618	Mumbai coast Maharastra, India	2000 deaths, many vessels lost in Bombay port
2	20–21 April, 1782	Near Surat, Gujarat coast, India	Major storm surge in Gulf of Cambay, several Thousands killed, several ships grounded
3	April 18, 1847	Laccadive islands, India	1000 deaths, huge storm wave swept over several of the Laccadive islands
4	May, 1851	32 km west of Karachi	Major storm surge Karachi and environs
5	30 October–2 November, 1854	Bombay coast, India	1000 deaths
6	6–14 June, 1920	Veeraval, India	Major storm surge in Gulf of Cambay
7	9–13 June, 1964	Naliya, India	2 m storm surge at Kandla, 1.5 m at Okha, 1 m at Navlakhi, 27 killed, extensive damage
8	19–24 October, 1975	Porbandar, Saurashtra, India	85 deaths, several thousand houses damaged
9	31 May–5 June, 1976	Mahua, India	87 deaths, 4500 cattle died, extensive damage
10	13–23 November, 1977	Karwar, India	72 deaths, major storm surge Karwar and environs
11	4–9 November, 1982	Veeraval, Gulf of Cambay	542 deaths, 1,50,332 cattle killed, 12624 pucca houses and 54549 kutcha buildings destroyed. Storm surge – 3.5 m at Mangral, 2 m at Diu, 2 m at Veraval, 3 m at Jafarafad
12	12–15 Nov., 1993	North Gujarat and Sindh coast	50 fishermen missing
13	17–20 June, 1996	Between Kodiar and Diu, India	5–6 m storm surge near Bharuch. Gulf of Cambay are affected by storm surge of height 3–5 m. 47 killed. 30,000 houses destroyed
14	8–11 June, 1998	Kandla, Gulf of Kutch	550 killed, 150 kmph winds, great destruction

include the frequency of occurrence. It only deals with the maximum water level to be expected in the event of major storms, however infrequently they may occur.

The second dangerous belt stretches from Dwarka (India) to Karachi (Pakistan). This region includes the extensive marshy areas (mostly unpopulated) known as the "Rann of Kutch." In this belt, also, the frequency of storm is low and the tracks are not usually favorable for major surge development. However, on rate occasion when they do occur, storm surges several meters in amplitude could result.

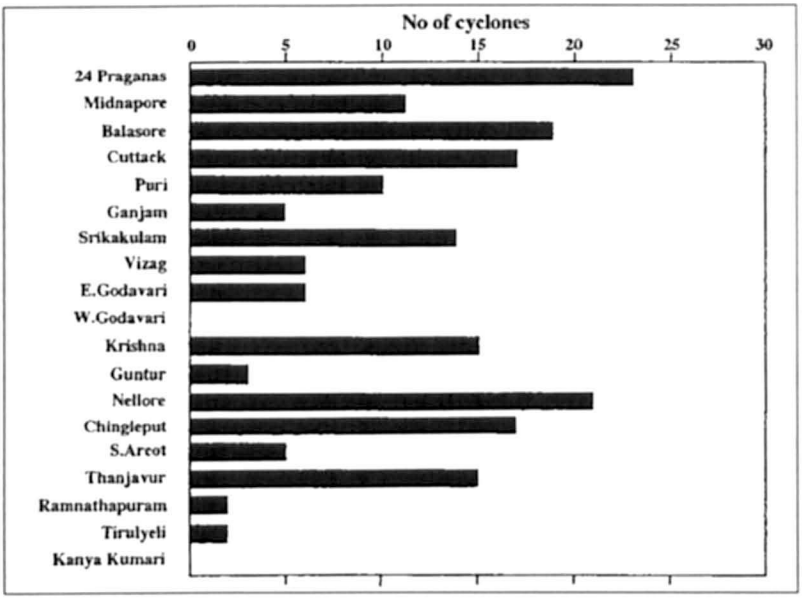

Fig. 6.52: The frequency of storms striking the west coast of India (DUBE et al., 1997)

RAO (1968) mentioned that the extensive marshlands of the Rann of Kutch are subject to large storm surges with the onset of the strong westerlies of the southwest monsoon season. The entire west coast of India south of 18° N falls into the type B category. In this area, also, the frequency of storms is low (Fig. 6.52). Also, the tracks are not generally favorable for major surge development. The coast around the Kathiawar Peninsula between Diu and Dwarak belongs to the type B category. The major surge amplitudes that can occur here are about 1.5 m and are about half the tidal range here. In this area the frequency of storms is high, but usually they are not intense (not of hurricane strength).

The peak storm surge amplitudes, maximum total water level (surge + wind waves), and the classification (into type A, B, or C) at several locations on the west coast of India and the coast of Pakistan are listed in Table 6.38. The track of the Kutch cyclone of June 1964 and the areas where surges occurred are shown in Fig. 6.53 Modeling of storm surges in the North Indian Ocean has attracted more attention to the Bay of Bengal, very few modelling studies have been carried out for the west coast of India.

GHOSH et al. (1983) have run the "SPLASH" model of JELESNIANSKI (1972) to determine storm surge envelope for the November 1982 cyclone. The peak surge computed by them is in good agreement with available estimates from observations. DUBE et al. (1985a) appears to be the among the first to use a two-dimensional fully nonlinear coastal zone numerical model to study the storm surges on the west coast of India. Their model covers an analysis area lying between 10° N and 23.2° N and between 67.8° E and 76° E. Orthogonal straight-line segments represent the coastal boundary of the west coast of India, which has the advantage of representing the Gulf of Cambay. This model has been used to simulate the surge generated by the 1975 Porbandar cyclone (Fig. 6.54a). The predicted maximum surge elevation at Porbandar compares well with the actual observations. The distribution of the predicted maximum sea surface elevations (peak surge envelope), observed surge and the time of occurrence along the Gujarat coast are given in Fig. 6.54b. It is interesting to note from the figure that the predicted peak surge of 2.2 m at Porbandar is in good agreement with the post storm

Table 6.38: Peak surge amplitude and maximum water level; (surge + wind wave) that can occur for storm with maximum winds of 40 $m \cdot s^{-1}$ on the Arabian Sea coast of the Indian subcontinent. Classification: B, total water level 2–5 m; C, > 5 m. (RAO, 1968)

Location	Favorable wind direction	Peak surge amplitude (m)	Maximum value of total water level (m)	Classification
Muthan Point (Nagercoil)	SW	1.4	2.3	B
Cochin	W	1.6	2.7	B
Calicut	WSW	2.1	3.5	B
Mangalore	WSW	1.8	3.0	B
Bhatkal	WSW	2.7	4.5	B
Panjim	WSW	1.7	2.8	B
Devgad	WSW	1.5	2.5	B
Ratnagiri	W	1.8	3.0	B
Harnaf	WSW	1.7	2.8	B
Mouth of Rajpuri River (Murud)	W	3.1	5.2	C
Mouth of Patel Ganga River	W	4.3	7.2	C
Bombay	W	1.5	4.5	B
Agashi Bay	W	4.2	7.0	C
Dahapu	W	4.0	6.7	C
Bulasar Kheri	W	4.5	7.5	C
Suvali Point	WSW	3.3	5.5	C
Mindola	WSW	5.2	8.7	C
Mal Bank	S	4.3	7.2	C
Mahuva Road	SE	2.0	3.4	B
Jafarabad	SSE	3.1	5.2	C
Diu	SSE	2.2	3.7	B
Veeraval	SW	1.5	2.5	B
Porbandar	SSW	1.6	2.7	B
Dwarka	SW	1.6	2.7	B
Balachin	W	5.1	8.5	C
Rann of Kutch	WSW	3.9	6.5	C
Wair Creek	SSW	4.0	6.7	C
Mouth of Indus River	S	3.0	5.0	C
Karachi	S	3.5	5.8	C

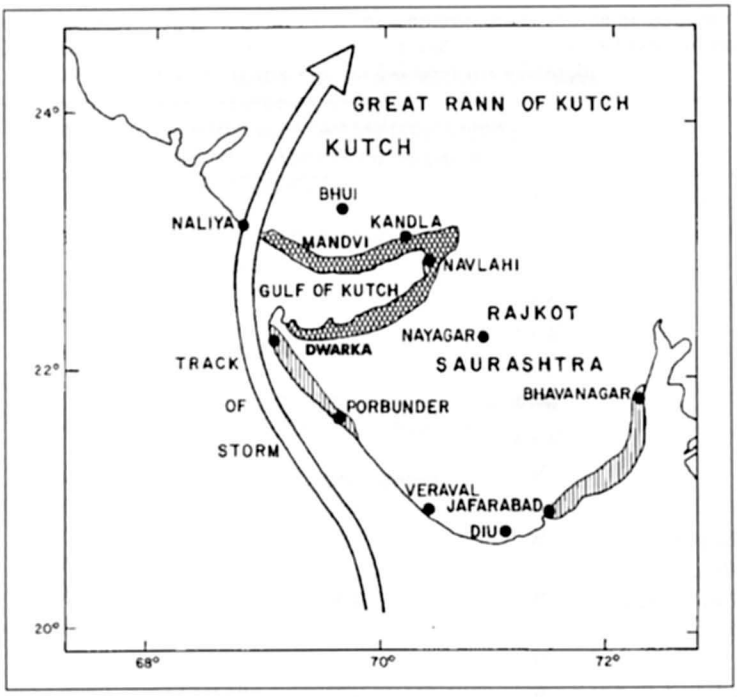

Fig. 6.53: Track of the Kutch cyclone of June 1964 on the west coast of India. Single – hatched area is affected by minor surges; double – hatched areas are affected by major surges (RAO, 1968)

survey estimated sea-surface elevation of 2.7 m (GHOSH 1981). A slightly lower elevation produced by the model has been attributed by the authors to the contribution due to astronomical tides, which was not accounted in the model. At approximately the time of the landfall of the cyclone, the predicted value of astronomical tides was 63 cm. No other observation on the sea surface elevation was, however, available to make a comparison of the observed and predicted surge along this part of the Gujarat coast.

SINHA et al. (1984) used the numerical model developed DUBE et al. (1985 a) to simulate the surge induced by November 1982 Gujarat cyclone. During the period of this event, the estimated heights of water level above normal tide was collected during the post storm survey at certain ports (RAMA SASTRY et al., 1984). Model computed maximum surge height was found to be in good agreement with the estimated values at Veraval, Diu and Jafrabad (Fig. 6.55). However, at Mangral, which is about 80 km to the left of the landfall, the predicted value is much lower than the estimated one, for which the authors could give no satisfactory explanation.

More recently CHITTIBABU et al. (2000) developed a high-resolution location specific model for Gujarat coast. Model has been used to simulate surges associated with recent cyclones hitting the coast of Gujarat.

The coastal area of Pakistan is occasionally affected by severe cyclonic storms, which form in the Arabian Sea. A partial list of severe cyclonic storms during the period 1891–1999 which made landfall on Pakistan coast is given in Table 6.39, Data on storm surges associated with these tropical cyclones are not available. However numerical simulation experiment performed by CHITTIBABU (1999) using the information available for June 1999 cyclone shows that the cyclone could have generated a minor surge on the Sind coast of Pakistan.

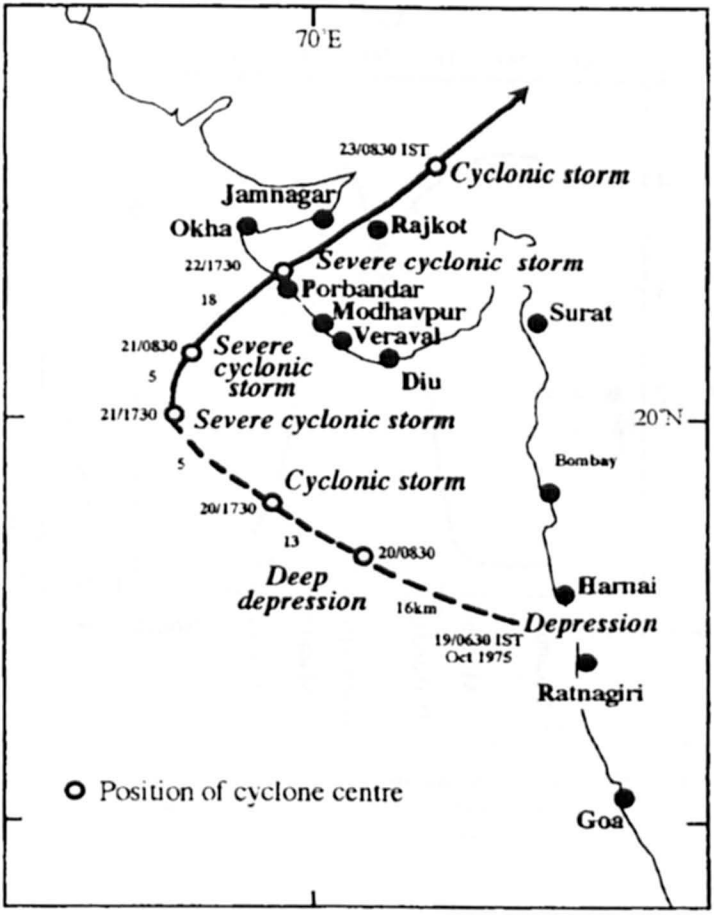

Fig. 6.54a: Path of Porbandar cyclone (DUBE et al., 1985a)

Table 6.39: List of severe cyclonic storms in Pakistan and rest of the Arabian Sea

No.	Date	Location	Damage
1	May 1851	32 km west of Karachi	Major storm surge Karachi and environs
2	25 April–5 May 1901	Makran coast	Damage estimation not available
3	7–14 May 1902	Near Karachi	Damage estimation not available
4	11–16 June 1902	Near Karachi	Damage estimation not available
5	4–6 June 1907	Near Karachi	Damage estimation not available
6	18–20 June 1920	South of Karachi	Damage estimation not available
7	5–9 June 1994	Saudi Arabian Coast	Damage estimation not available
8	15–20 Nov. 1994	Somali coast	Damage estimatio not available

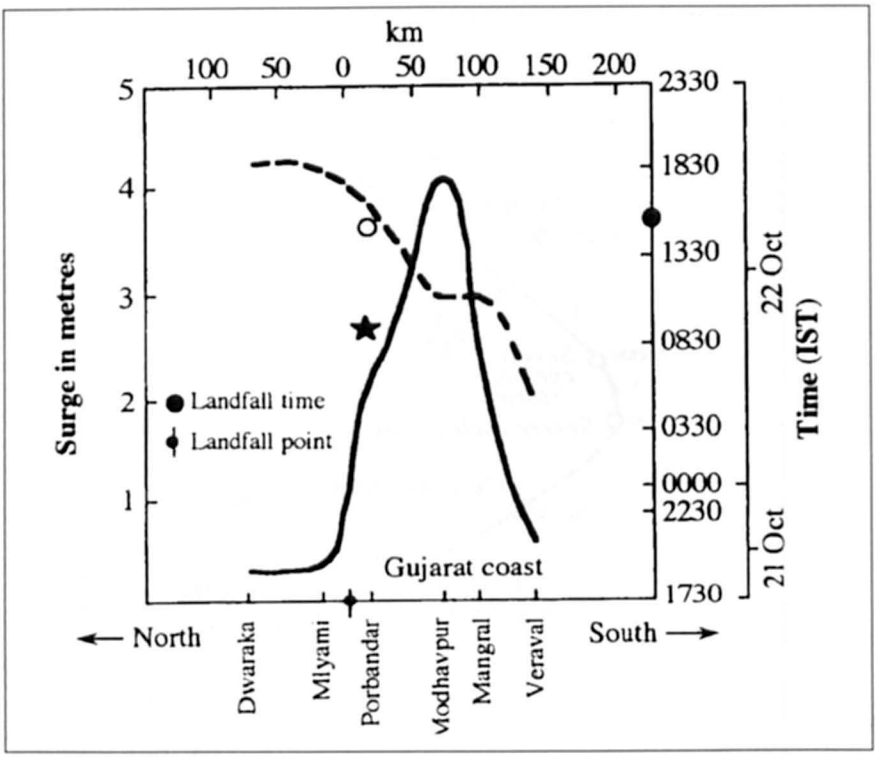

Fig. 6.54b: Maximum sea – surface elevation and time of occurrence along Gujarat coast: –, peak surge envelope; - - -, time of occurrence of peak surge; *, observed storm generated surge; °, observed time of occurrence of peak surge (DUBE et al., 1985)

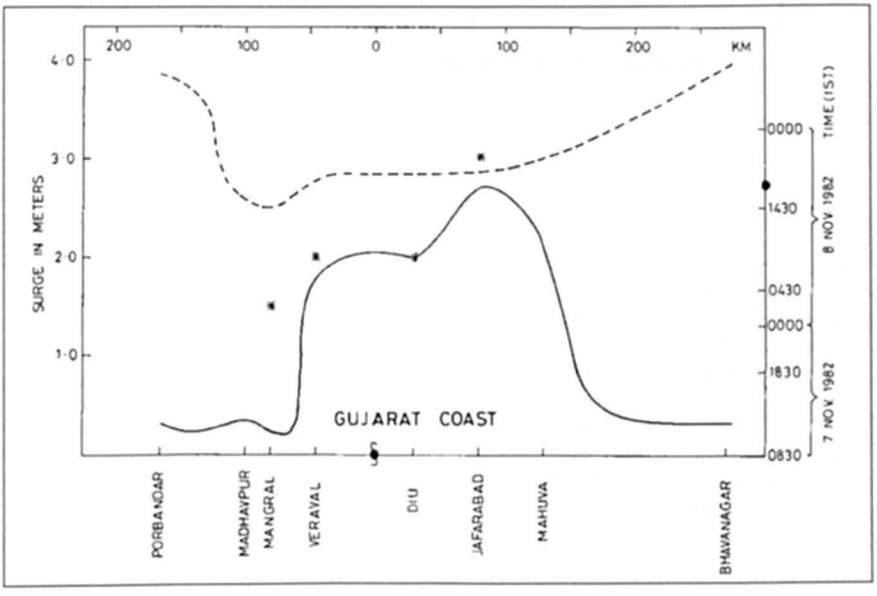

Fig. 6.55: Maximum sea surface elevation and time of occurrence along Saurashtra coast (SINHA et al., 1984)

6.4 South West Indian Ocean

6.4.1 Storm Surges in Malagasy Republic (Madagascar)

Figure 6.56 shows a geographical map of Madagascar. Figure 6.57 shows the tracks of cyclones that influence Morondava und Fort-Dauphin. Table 6.40 lists some pertinent data about cyclones for the period 1975 to 1992.

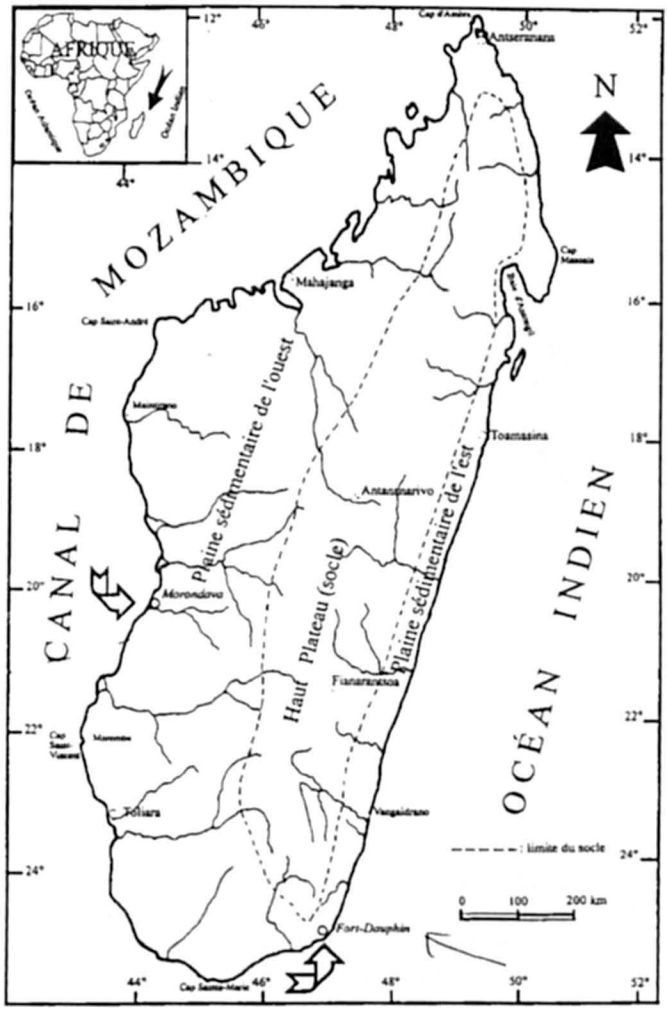

Fig. 6.56: Geographical map of Madagascar.

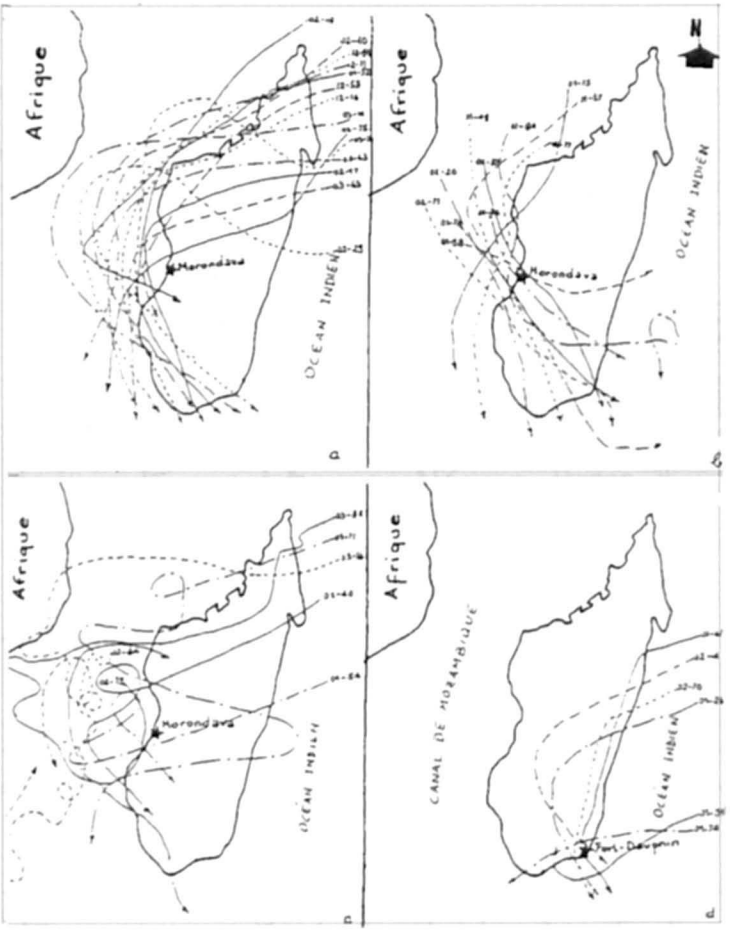

Fig. 6.57: Track of cyclones that influence Morondava and Fort-Dauphin, (a) cyclones from the Indian ocean influencing Morondava, (b) cyclones from the Mozambique channel influencing Morondava, (c) cyclones with complex trajectories influencing Morondava, (d) cyclones influencing Fort-Dauphin (BATTISTINI, 1964).

Earlier, it was mentioned that tropical cyclones travel nearby and sometimes traverse Malagasy Republic. The only study this author could find on the storm surges in this region is by LACOUR (1935). In principle, storm surges could occur along the long east and west coasts of this island (about 1500 km in length). However, favourable cyclone tracks usually generate surges on the east coast of this island, where the tidal range is small (less than 80 cm).

Storm surges appear to be more frequent on the east coast than on the west coast. Also, surges on the east coast are more important south of Tamtave than north of it. Although surges are more frequent on the east coast the amplitudes usually are rather small (20 cm or less). However, the March 1927 event near Tamtave was a major surge and caused some destruction. Major surges could occur at Tuléar on the sourthern part of the west coast (e.g., the event of January 1933). DAS et al. (1978) stated that cyclonic storms in the Island of La Réunion in the South Indian Ocean often produced exceptionally heavy rain accompanied by surges of 4.6 m have been reported from this island.

Table 6.40: Cyclones affecting Madagascar (RASOANILANA, 1997)

Date	Name	Wind Speed (KPH)	Central Pressure (hPa)
23–24 Dec 1974	Adele		
2–21 Jan 1975	Camille	200	–
1 Feb	Fernande	200	–
12–29 Jan 1976	Danae	240	965
27 Mar–10 April 1976	Gladys	100	–
23 Jan 1977	Domitile	120	992
28 Jan–5 Feb 1977	Emilie	130	980
17 Feb–3 Mar 1977	Herves	108	986
23–25 Jan 1978	Georgia	96	992
10–13 Feb 1978	Irena	200	985
16–31 Dec 1978	Angele	194	958
4–12 Feb 1979	Dora	–	–
10–13 Jan 1980	Gudule	68	1002
28 Dec 1980	Edwige	–	998
Ist Jan 1981			
17–25 Feb 1981	Iadine	180	991
31 Jan–5 Feb 1982	Electre	95	997
16–27 Mar 1982	Justine	135	957
9–16 Jan 1984	Elinah	–	–
5–10 Jan 1984	Caboto	43	–
18 Jan–2 Feb 1984	Domoins	100	–
1985–1986	Alifredy	58	–
	Berobia	58	–
	Gista	120	–
	Honorine	120	–
1987–1988	Calidera	–	–
	Doaza	–	–
9–17 Jan 1989	Calasanjy	133	980
1989	Iana	150	–
16–19 Feb 1991	Cynthia	113	979
25 Dec 1991	Bryna	65	1002
10 Jan 1992			

6.5 South East Indian Ocean

By South East Indian Ocean, we mean the northern part of the West Coast of Australia, which is subjected to storm surges generated by tropical cyclones, HUBBERT et al. (1991) numerically modelled. Tropical cyclone generated storm surges on the northern part of the Australian coastline. Fig. 6.58 shows the tracks of four hurricanes that made a landfall in the study area. Out of these hurricanes Jason Winifred and Aivu struck the Pacific coast of Australia (these will be considered in section 6.6) and Hazel made landfall on the Indian Ocean coast of Australia. In this section, we will consider only the Indian Ocean coast.

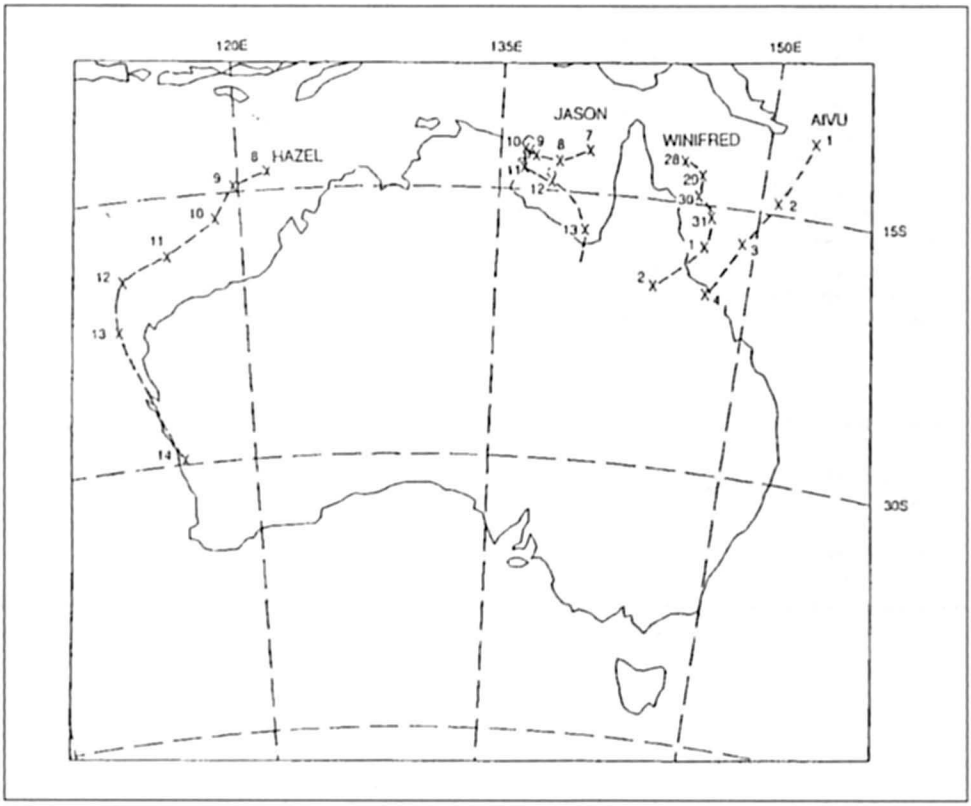

Fig. 6.58: Tracks of the four tropical cyclones (Winifred, Aivu, Jason and Hazel) used in this study. 00 UTC times and dates are shown (HUBBERT et al., 1991)

6.5.1 Numerical Model and Results

The two-dimensional depth-averaged model of HUBBERT et al. (1990) was used in conjunction with HOLLAND'S (1980) analytical-empirical model to derive the atmospheric pressure and wind fields at sea level. This model requires only the positions of the hurricane centre, the cyclone intensity and the radius of maximum winds (RMW).

The error in the numerical model for the prediction of surge elevations is 0.1 m to 0.2 m and the arrival times of the surge waves on the coast have atmost an error of one hour. The model includes such second order effects as coastally trapped edge waves.

When a tropical cyclone moves with the coast on the left (Southern Hemisphere) near to the propagation speed of a coastally trapped wave, resonant amplification of the sea surface elevation can occur, which is referred to by JELESNIANSKI (1967) as "Resurgence". This is a particular problem for the West Coast of Australia, where conditions for such resonant amplification are met. FANDRY et al. (1984) showed that the resulting surface elevation could propagate for thousands of kilometres and can cause inundation even at vast distances.

Hurricane Hazel attained a lowest central pressure of 936 hPa as it approached Carnarvon with an RMW of 30 km. As Hazel moved obliquely towards the coast, a region of positive surge developed first. A region of negative surge then formed and moved ahead of the amplifying positive surge wave, with the zero line staying slightly ahead of the cyclone position.

Fig 6.59 shows the contours of the water level at time of maximum surge at the Carnarvon. Significant amplification of the surge wave occurred in Shark Bay with amplitudes greater than 3 m. A second branch continued to propagate down the coast, resonating with the

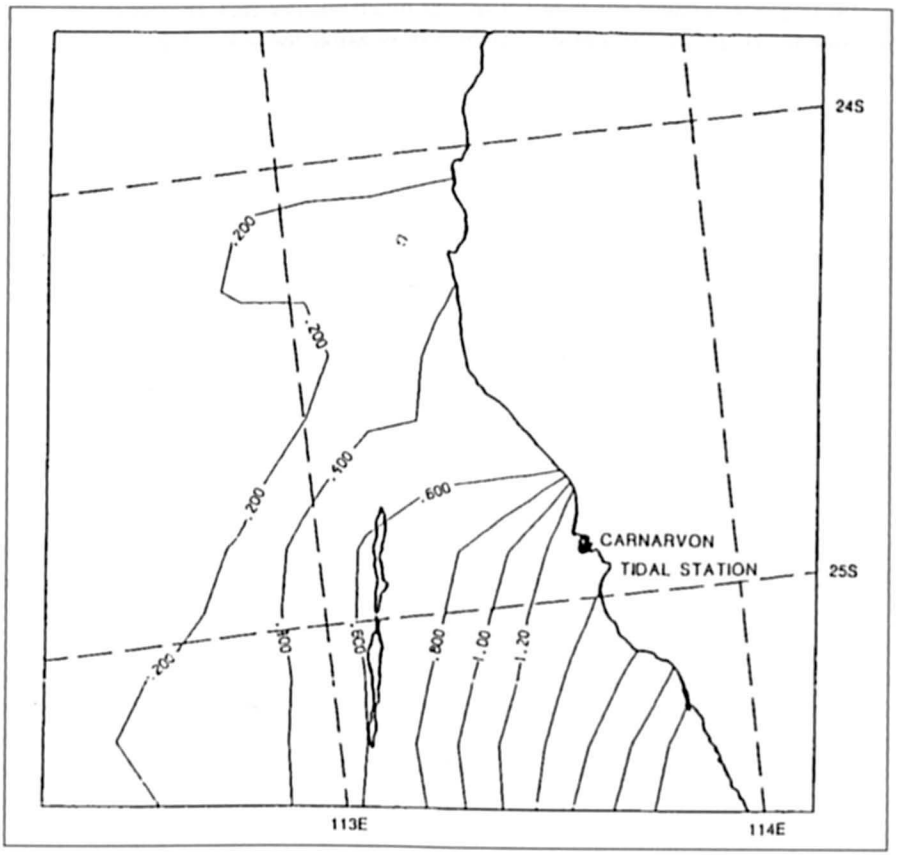

Fig. 6.59: Model results at the time of peak Carnarvon surge for tropical cyclone Hazel (14 UTC, 13 March 1979): (a) Sea surface elevations (m), and (b) depth – integrated currents (cms^{-1}) (HUBBERT et. al., 1991)

developing Hazel. After the cyclone rapidly weakened after landfall, the second branch evolved into a freely propagating coastally trapped wave, with amplitude of about 10 cm. Table 6.41 summarises the errors.

Table 6.41: Errors in the results of the numerical model for hurricane Hazel

	Surge amplitude (m)			Time of Max. Surge		
	Observed	Computed	Error	Observed	Computed	Error
Carnarvon	1.3	1.3	0.0	1400	1400	0.0
Geraldton	0.7	0.6	–0.1	2100	2100	0.0

Table 6.41 shows that model results are quite accurate. However, the amplitude of the negative surge computed for Carnarvon was much greater than the observed value. Next, the authors made another simulation with a cyclone similar to Hazel but approaching the coast in a perpendicular direction near Carnarvon. Consistent with the analytical study of FANDRY et al. (1984), the maximum surge of 0.8 m was much smaller than the observed surge of 1.3 m, implying that resonant amplification was responsible for some of the surge at Carnarvon.

6.6 South West Pacific Ocean

By southwest Pacific, we mean the east coast of Australia and the coastlines of New Zealand.

6.6.1 New Zealand

Severe storm surges generally do not occur on the coasts of New Zealand. GILMOUR (1963) reported a surge of 0.78 m at Bluff Harbour; AGNEW (1966) found surges of up to 0.8 m on the west coast of the North Island during July 1965. Two cyclones in April 1972 produced surges up to 0.3 m on the east coast of New Zealand (PICKRILL, 1972). HEATH (1979) mentioned that due to the windy climate of New Zealand, departures from isostatic equilibrium are quite common.

Although storm surge amplitudes are small on the New Zealand coast, they cause considerable erosion (GIBB, 1976, 1977), e.g. in the Bay of Plenty on the west coast of the North Island and all along the east coast of the North Island (north of Auckland).

HEATH (1979) studied three storm surges: April 9–10, 1968, on the east coast of the North Island, July 30–August 1, 1975, on the east coast of the South Island, and September 11–13, 1976, on the west coast of the North Island. These three are the major storm surge events in New Zealand during the period 1968–78. The maximum surge in these events was about 0.6 m.

6.6.2 Australia

HOPLEY and HARVEY (1979) studied storm surges in Australia. They questioned the accuracy of the 12.2 m surge in Bathurst Bay in 1899 (WHITTINGHAM, 1958) and the 7.01 m surge at Groote Eylandt in 1923 (WHITTINGHAM, 1958). However, they mentioned that several surges with amplitudes greater than 3 m occur in eastern Queensland. Gulf of Carpentaria, and western Australia. These authors used the JELESNIANSKI (1972) scheme to compute the amplitudes of the surges. The maximum surge height h_c was calculated from

$$h_C = h_S \frac{V_P}{87} F_D \tag{6.70}$$

where, h_s is the precomputed surge height based on cyclone parameters (see the SPLASH model of JELESNIANSKI 1972), V_p is a correction factor based on maximum wind field and pressure drop, and F_D is a depth correction factor for local bathymetry.

Surge amplitudes are generally small on the Australian coastline, with the highest levels usually occurring on the Queensland coast, particularly south of Fraser Island. Storms moving parallel to the west and east coasts of Australia produce edge waves. It is observed that these edge waves tend to amplify the crest of the surge waves on the west coast of Australia, whereas on the coast of Queensland, they tend to amplify the trough. Negative surges also predominantly occur on the Queensland coast.

Storm surge profiles at several locations along the Australian coast are shown in Fig. 6.60. The maximum surge (3 m) in this diagram was at Townsville due to Cyclone Althea during December 22–25, 1976. HOPLEY and HARVEY (1979) analysed the contributions form the forerunner, effects of wind stress and pressure gradients, and semi-diurnal tides to the total

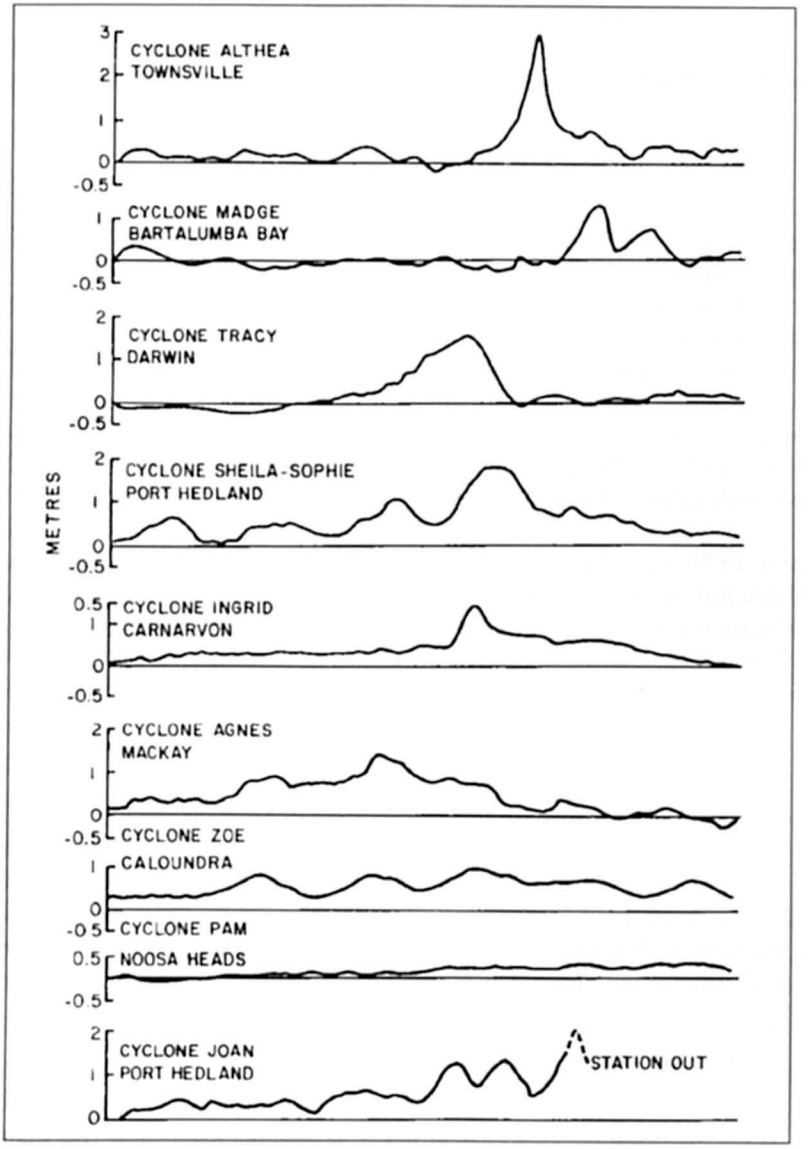

Fig. 6.60: Storm surge profiles at some locations due to selected hurricanes on the coast of Australia. Total length of the abscissa is 72 h, with the exception of cyclone Tracey, for which it is only 18 h. (HOPLEY and HARVEY, 1979)

water level during storm surge events for six regions of Australia. These results are summarised in Table 6.42.

These authors also calculated the peak surge occurrence probability curves for 19 locations around the northern coast of Australia. Brisbane and Noosa have the lowest surge risk. Two locations with the greatest surge risk are Townsville and Karumba. These results, however, change somewhat when one superimposes the tide on the surge. The greatest risk will then be at Miller Bay, followed by Carnarvon, Townsville, and Centre Island. These surge risk results are summarized in Table 6.43.

Table 6.42: Percentage contribution of various factors to the total water during storm surge events in Australia (HOPLEY and HARVEY 1979)

Region	No. of surges analyzed	Forerunner	Wind and pressure	Semidiurnal	24-h diurnal tide	Other sources
South Queensland	22	40.4	31.5	14.1	10.0	4.0
North Queensland	28	27.1	29.1	23.8	10.9	9.1
Gulf of Carpentaria	15	29.1	44.1	3.9	23.8	–
Northwest (Broome-Darwin)	4	15.7	31.4	37.2	4.7	9.0
Central Western Australia (Port Hedland Carnarvon	8	50.3	25.5	9.7	5.8	8.7
Southwest Australia	7	74.5	14.7	1.3	3.2	6.3

* Without Melville Bay.

Table 6.43: Maximum surge heights (m) that can occur in 10,100, and 1000 yr at any point along a 100-km coastline centered at specific locations on the coast of Australia (HOPLEY and HARVEY, 1979).

Station	10 yr	100 yr	1000 yr
Brisbane	0.15	0.43	0.73
Noosa	0.20	0.50	0.83
Bundaberg	1.40	2.80	4.15
Gladstone	1.30	2.50	3.78
Mackay	1.40	2.40	3.40
Townsville	1.45	3.25	4.90
Cairns	1.03	1.78	2.55
Thursday Island	1.25	2.50	3.70
Weipa	0.60	1.30	2.00
Karumba	2.25	3.20	4.15
Center island	1.41	2.22	3.00
Milner Bay	1.40	2.25	3.15
Melville Bay	1.50	2.40	3.30
Darwin	1.65	2.30	2.90
Wyndham	1.50	2.73	3.60
Broome	1.10	1.75	2.38
Port Hedland	1.50	2.78	3.70
Carnarvon	0.80	1.46	2.10
Geraldton	0.60	1.15	1.64

NELSON (1975) listed 30 major tropical cyclones that caused surges of amplitudes of at least 0.5 m on the north coast of Australia during the period 1880–1970. Hurricane Tracey of December 25, 1974, did great damage near Darwin. DAS et al. (1978) pointed out that although the central pressure was as low as 955 mb and wind gusts attained 200 $km \cdot h^{-1}$, the peak surge was only 1.6 m. RUSSEL (1898) reported that storm surges passing over the Bass Strait. These surges contained waves with periods of about 26 min. Similar phenomena occurred in Lake George. TRONSON and NOYE (1973) developed the statistical models for the Adelaide area were considered.

MACKEY and WHITTINGHAM (1956) studied the storm surges at Port Hedland on the northwest coast of Australia for the events of November 14–20, 1955, and February 24–March 2, 1956. The observed and predicted tides and the observed surge for the latter case are shown in Fig. 6.61.

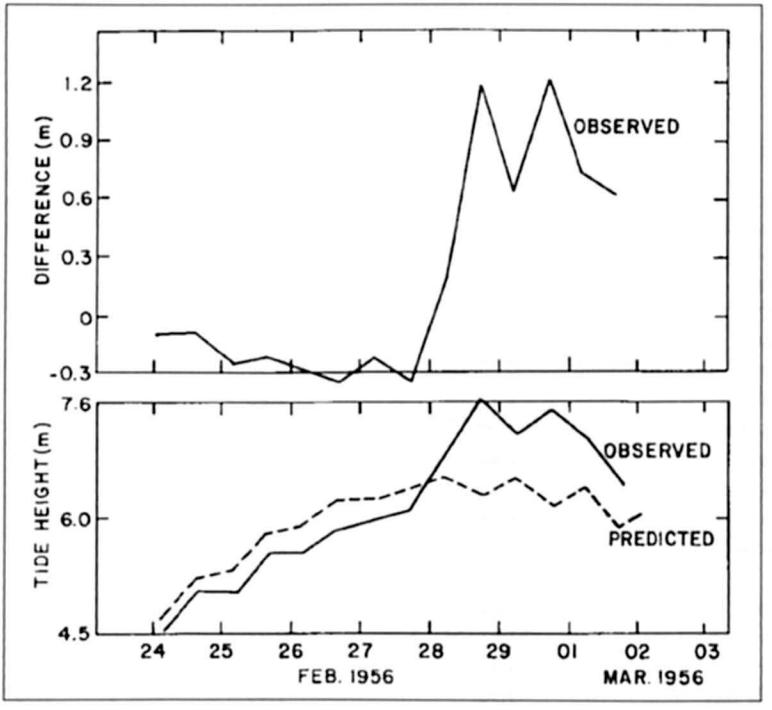

Fig. 6.61: Observed surge (top) and observed and predicted tides (bottom) at Port Hedland on the northwest coast of Australia during February 24–March 2, 1956 (MACKEY and WHITTINGHAM, 1956)

HUBBERT et al. (1991) numerically modelled the storm surges from three tropical cyclones on the East Coast of Australia. The tracks of Jason, Winifred and Aivu have been shown in Fig. 6.58.

Fig. 6.62 shows the surface pressure field for Winifred derived from the HOLLAND's (1980) model and Fig. 6.63 shows the surface wind field computed from the same model. Fig. 6.64 shows the surge amplitude for hurricane Winifred. Fig. 6.65 shows the surge amplitude for hurricane Aivu, whereas Fig. 6.66 similar results for hurricane Jason. Table 6.44 lists the errors in the results of the numerical model.

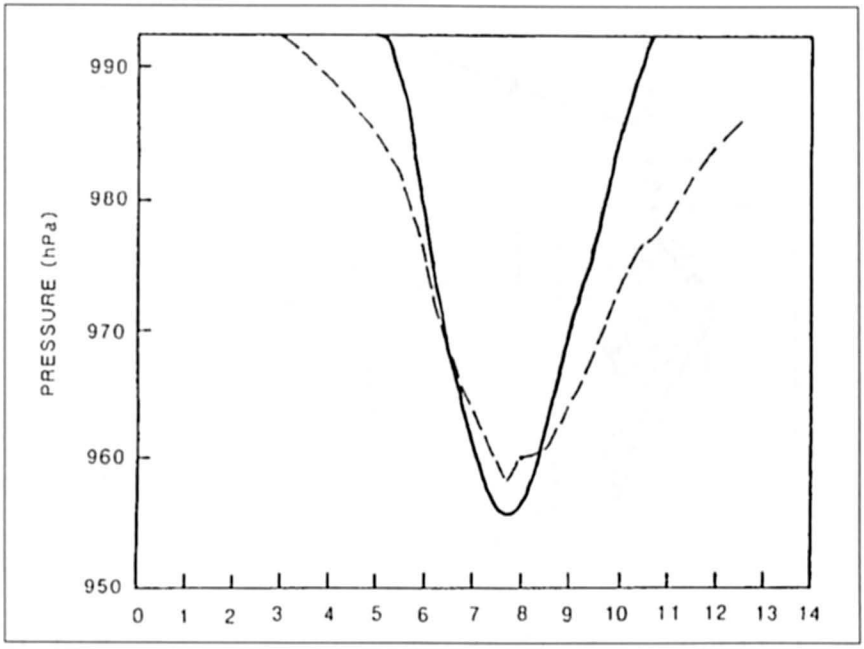

Fig. 6.62: Surface pressures and wind speeds for tropical cyclone Winifred (solid lines) compared with observations (broken lines) at Cowley Beach (just north of the cyclone landfall point) (HUBBERT et al., 1991)

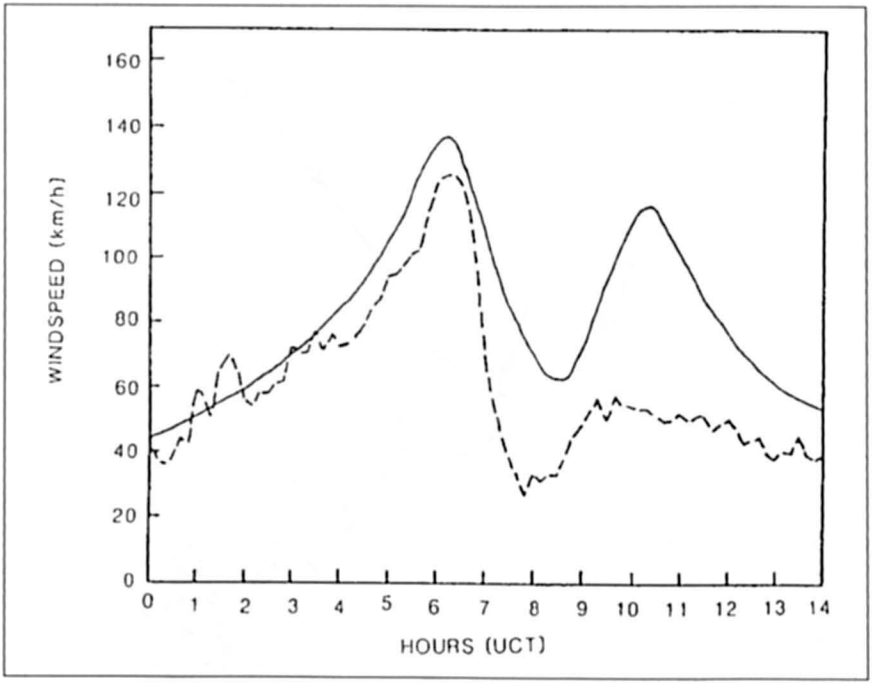

Fig. 6.63: Surface pressures derived from the Holland model for tropical cyclone Winifred (solid lines) compared with observations (broken line) at Cowley Beach (just north of the cyclone landfall point) (HUBBERT et al., 1991)

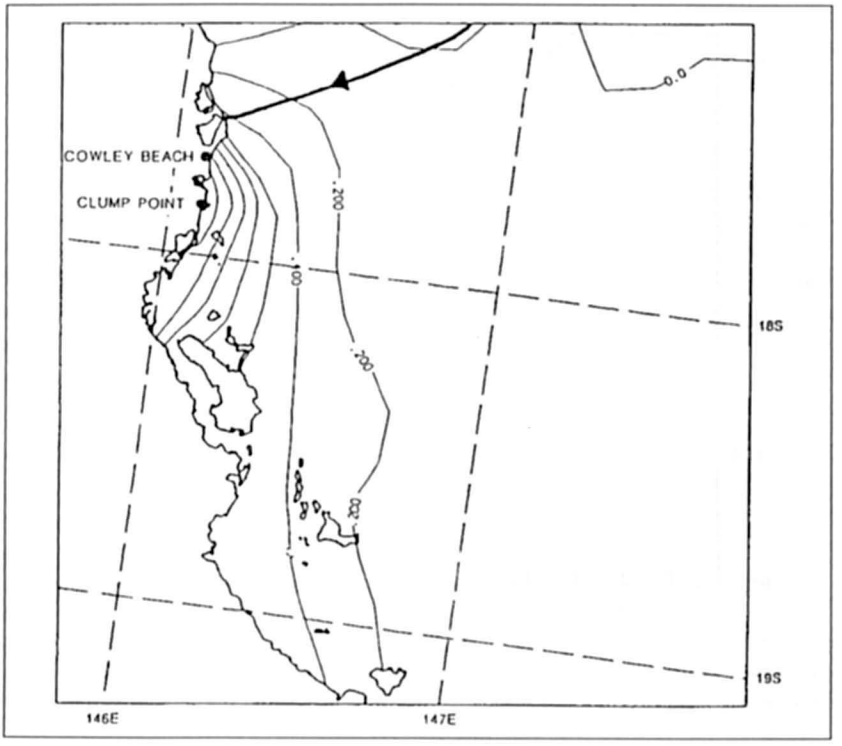

Fig. 6.64: Surge amplitude for hurricane Winifred (HUBBERT et al., 1991)

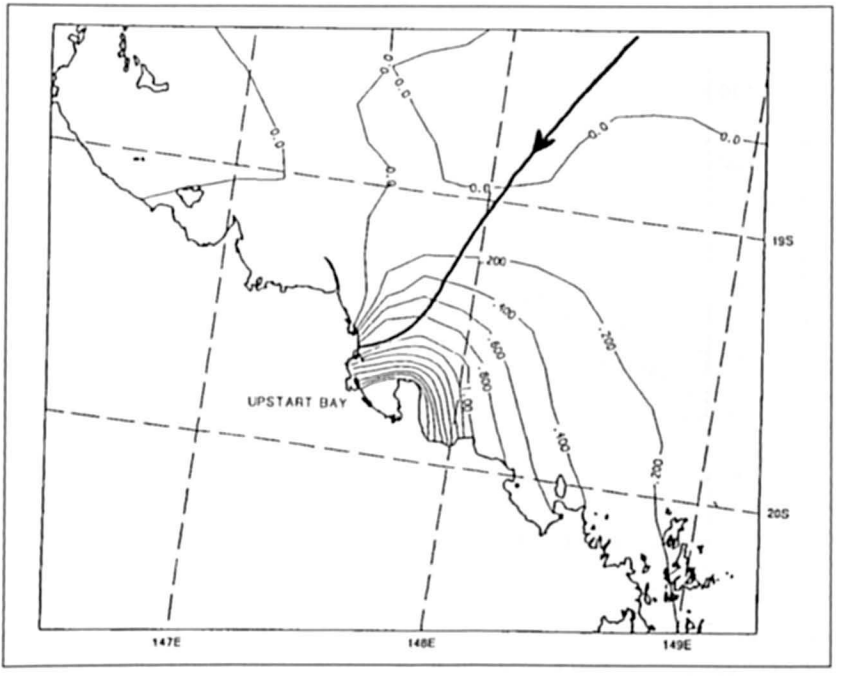

Fig. 6.65: Model results at landfall of tropical cyclone Aivu (00 UTC, April 3, 1989): Sea surface elevation (m) together with Aivu's track (HUBBERT et al., 1991)

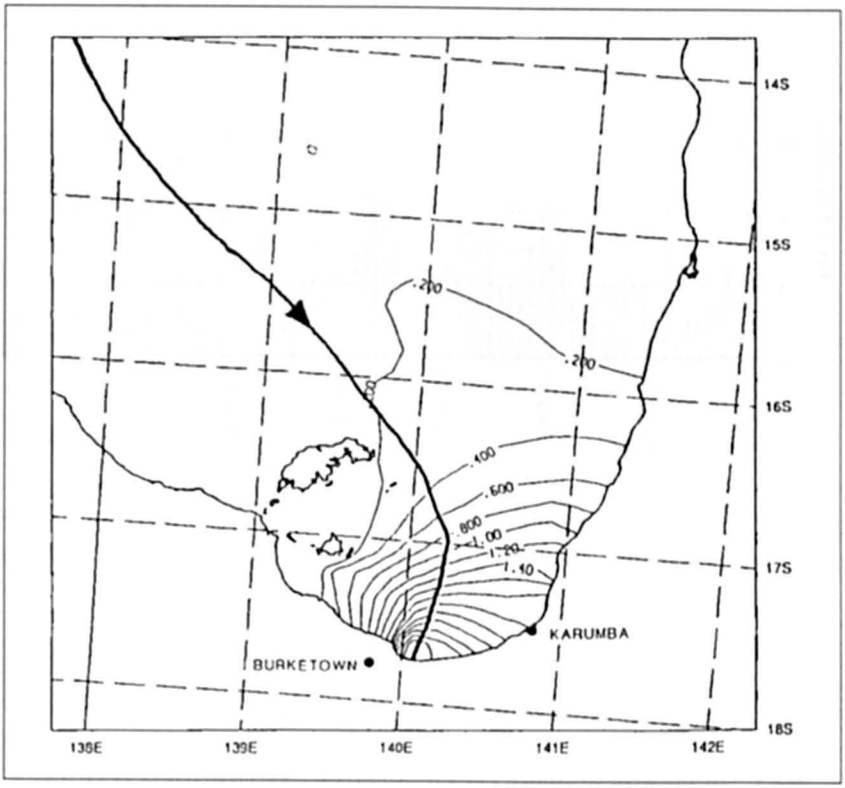

Fig. 6.66: Surge amplitude for hurricane Jason (HUBBERT et al., 1991)

Table 6.44: Errors in the results of the numerical model

		<-------- Surge Amplitude (m) -------->			Arrival Time of Peak Surge		
Cyclone	Location	*Observed*	*Computed*	*Error (m)*	*Observed*	*Computed*	*Error (H)*
Winifred	Clumppoint	1.6	1.5	–0.1	0900	0900	0
Aivu	Upstart Bay	2.8	2.5	–0.3	0000	0100	1
Jason	Karumba	2.0	1.9	–0.1	0500	0400	–1
Jason	Burketown	3.5	3.3	–0.2	0500	0500	0

Fig. 6.67 shows the histogram of the number of cyclones in the southwest Pacific for the period 1920 to 1994 (BLONG, 1997) while it appears that there might have been a slight increase during 1970–1980, since then the numbers have decreased.

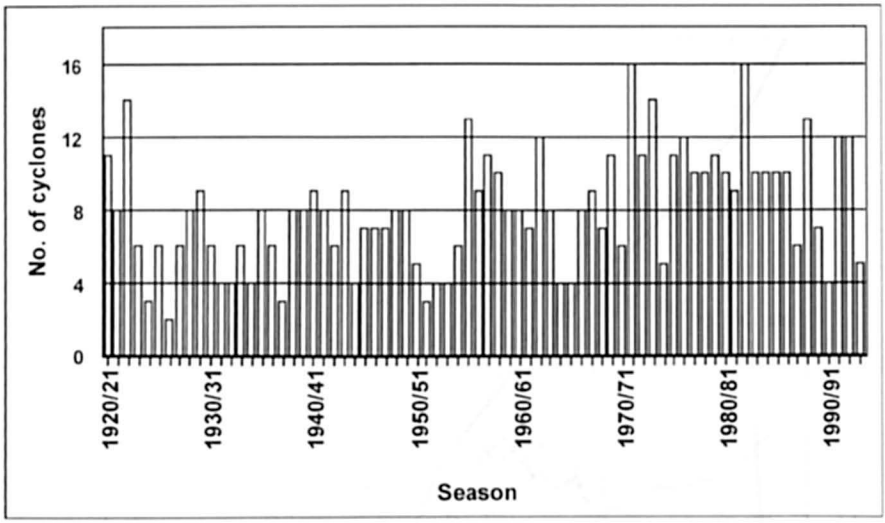

Fig. 6.67: Tropical cyclones in the South West Pacific seasonal occurrence – 1920/21 to 1993/94 (BLONG, 1997)

6.7 Western Tropical Pacific

6.7.1 Marianas, American Samoa, Solomon Islands, and Tonga

REDFIELD and MILLER (1957) mentioned that near the island of Mille in the Marianas, a storm surge of 12–15 m occurred in 1905 due to a build up of the surge in a lagoon 25 nautical miles (46 km) long.

GALLAGHER (1973) studied the nonlinear distortion produced to the tidal regime due to openings of restricted depth. He showed that the tides in the Pala Lagoon in American Samoa and the Main Lagoon on Christmas Island (in the latter case, very severely) are distorted. Similar behaviour is expected for other long waves such as storm surges and tsunamis.

GROVER (1967) studied storm surges in the Solomon Islands, which is a rare phenomenon there. Cyclones forming in the Coral Sea region and intensifying in the area south and east of the Solomons could cause surges occasionally. The storm surge of January 1952 caused some destruction on the west coast of Guadalcanal and at Malaita. The amplitude of the surge (at the time of low tide) at Honiara was about 3.5 ft (1.07 m). Winds greater than 85 $mi \cdot h^{-1}$ (137 $km \cdot h^{-1}$) were recorded there during this event.

The surge caused serious erosion in a swath 60 m wide. Interesting topographic changes took place in the coastal waters. GROVER (1967) mentioned that some villages that withstood severe tsunamis during a half-century period were obliterated by this surge.

A major storm surge occurred during March 3–4, 1982, in Tonga Island in the South Pacific (which is located about 4025 km northeast of Sydney, Australia), and the surge amplitude was at least 1.3 m (The Citizen, March 4, 1982, Ottawa, Ont.). Winds up to 276 $km \cdot h^{-1}$ coupled with the surge caused great devastation and killed several people.

LUICK et al. (1997) studied storm surges in the so-called Pacific forum region. Fig. 6.68 shows a geographical and climatological map of the area (MCLEAN, 1995). The South Pacific region consists of the following island, nations: Cook Islands, Federated States of Micronesia, Fiji, Kingdom of Tonga, Marshall Islands, Nine, Papua New Guinea, Republic of Kiribati, Republic of Nauru, Solomon Islands, Tuvalu, Vanuatu, Western Samoa.

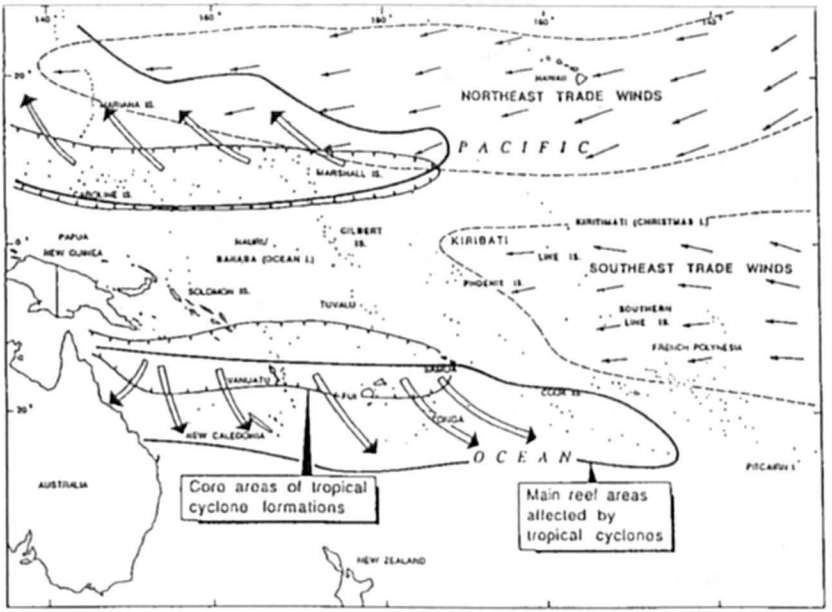

Fig. 6.68: Geographical and climatological map of the Western tropical Pacific area (MCLEAN, 1995)

The nations mainly in the western part e.g. Federated States of Micronesia (FSM) and Fiji, are subject at periodic intervals to tropical cyclones and the storm surges that are produced by them. Even though the lack of extensive continental shelves precludes the development of large amplitude surges such as those that occur in the Bay of Bengal and the Gulf of Mexico, nevertheless, moderate surges are generated. The inundation from such surges could cause problems in small islands with increased coastal erosion and salt-water intrusion into coastal aquifers.

Because of the complex topography (several small islands interspersed over a large area), traditional finite-difference models are not very applicable. Instead more sophisticated irregular triangular grid models are being developed to include not only realistic bathymetry but also the state of the tide. These finite element models were discussed earlier in chapter 3.

A map of the South Pacific Forum region (Fig. 6.69) gives the locations of the eleven SEAFRAME gauges in the region operated by National Tidal Facility (NTF) of Australia. These gauges use acoustic signals and have a precision of about 1 mm as compared to an accuracy of about 1 cm for the more traditional gauges. These gauges were placed to monitor the relative sea level changes that may be caused by the Green house warming.

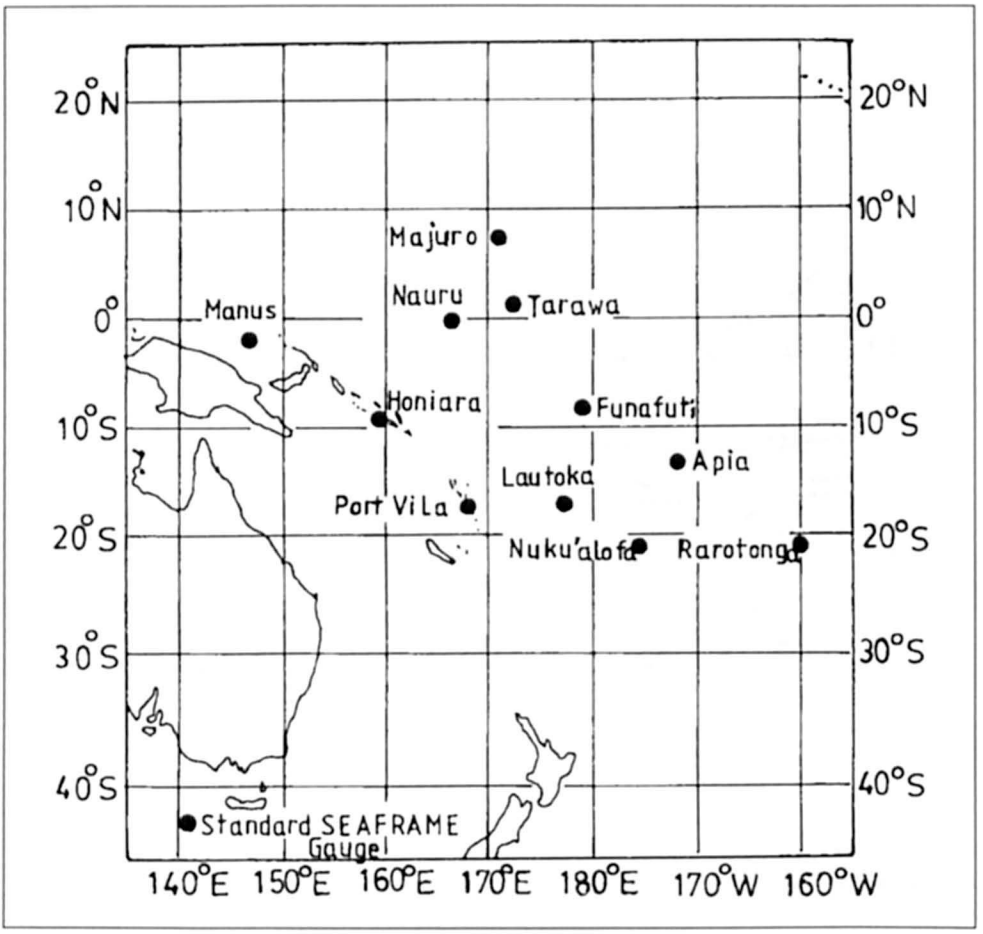

Fig. 6.69: Location of the SEAFRAME gauges in the Pacific operated by the National Tidal Facility of Australia (source: National Tidal Facility)

However, these gauges record all forms of long gravity waves, such as tides, storm surges and tsunamis. Storm surges up to one metre have been noticed occasionally in the residuals of these tide gauge records.

Fig. 6.70 shows the areas north and south of the equator where the tropical cyclones form. There is a clear break at the equator where there are none due to the absence of the Coriolis force.

Tropical cyclones in the South Pacific tend to form in the "monsoon trough" between 10°–15° S in the western South Pacific. During El Nino years the monsoon trough shifts to the cast onto the Central Pacific. Very few cyclones intensify south of 20° S (due primarily to increasing westerlies in the upper troposphere).

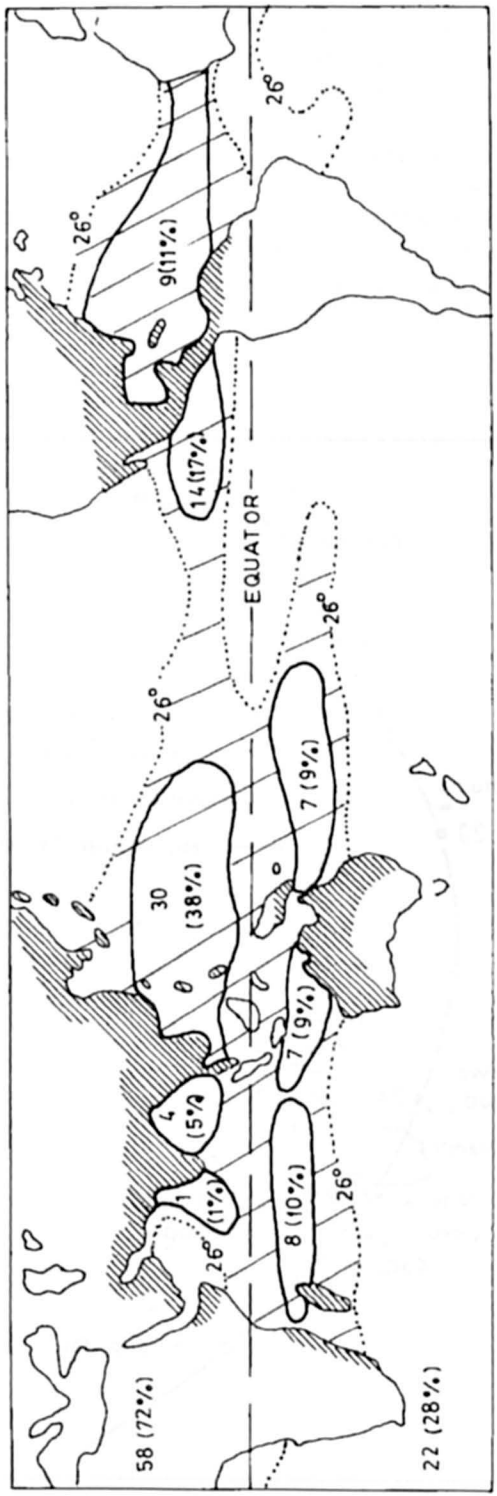

Fig. 6.70: Areas of tropical cyclone occurrence (GRAY, 1975). Land areas affected by cyclone are shown hatched (LUICK et al., 1997)

In the Southwest Pacific, tropical cyclones typically continue to intensify as they move southwards from their points of origin, decaying over cooler subtropical water. More than half however decay prior to reaching 30° S, while a third of tropical cyclones in the southwest Pacific eventually become extra-tropical depressions.

It is known (MURTY, 1984) that looking down the track of movement of a tropical cyclone, peak surges occur to the right of the track in the northern hemisphere and to the left in the southern hemisphere.

Fig. 6.71 shows the track of Hurricane Bebe of 1972. Even though the track is over Viti Levu, there is no coast against which the tangential wind stress can push water to the left of the track and pile it up. On the other hand, depending upon the strength of the wind field a surge could occur on the island, Vanua Levu.

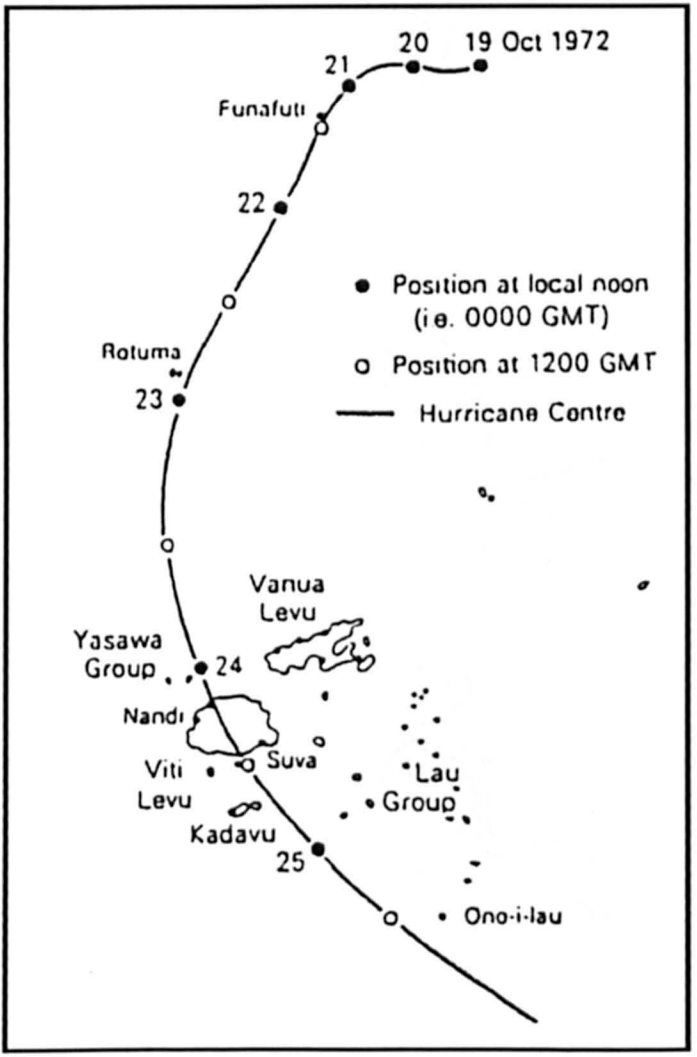

Fig. 6.71: Track of Hurricane Bebe October 1972 (from New Zealand Meteorological Service)

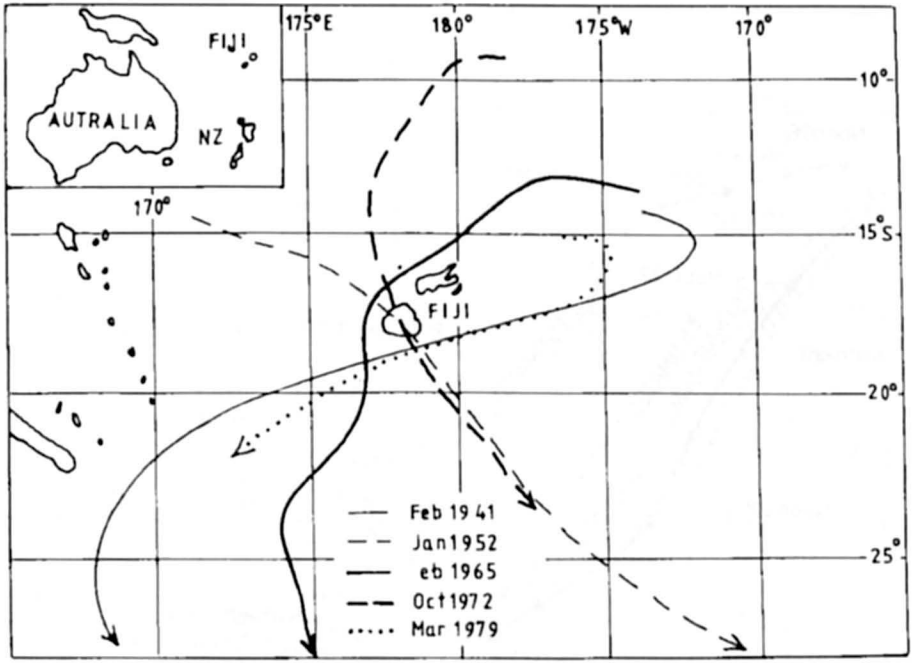

Fig. 6.72: Tracks of severe hurricanes in the Fiji area between 1940 and 1979 (from Fiji Meteorological Service)

The tracks of five hurricanes near Viti Levu are shown in Fig. 6.72. Again using the above rule of thumb, only the track for February 1965 should generate a peak surge on Viti Levu, depending upon the strength of the wind field.

Figs. 6.73 and 6.74 respectively show the tracks of hurricanes, Oscar (24th February to 2nd March 1983) and Meli (24th to 28th March 1979) impinging on the coastlines of Fiji.

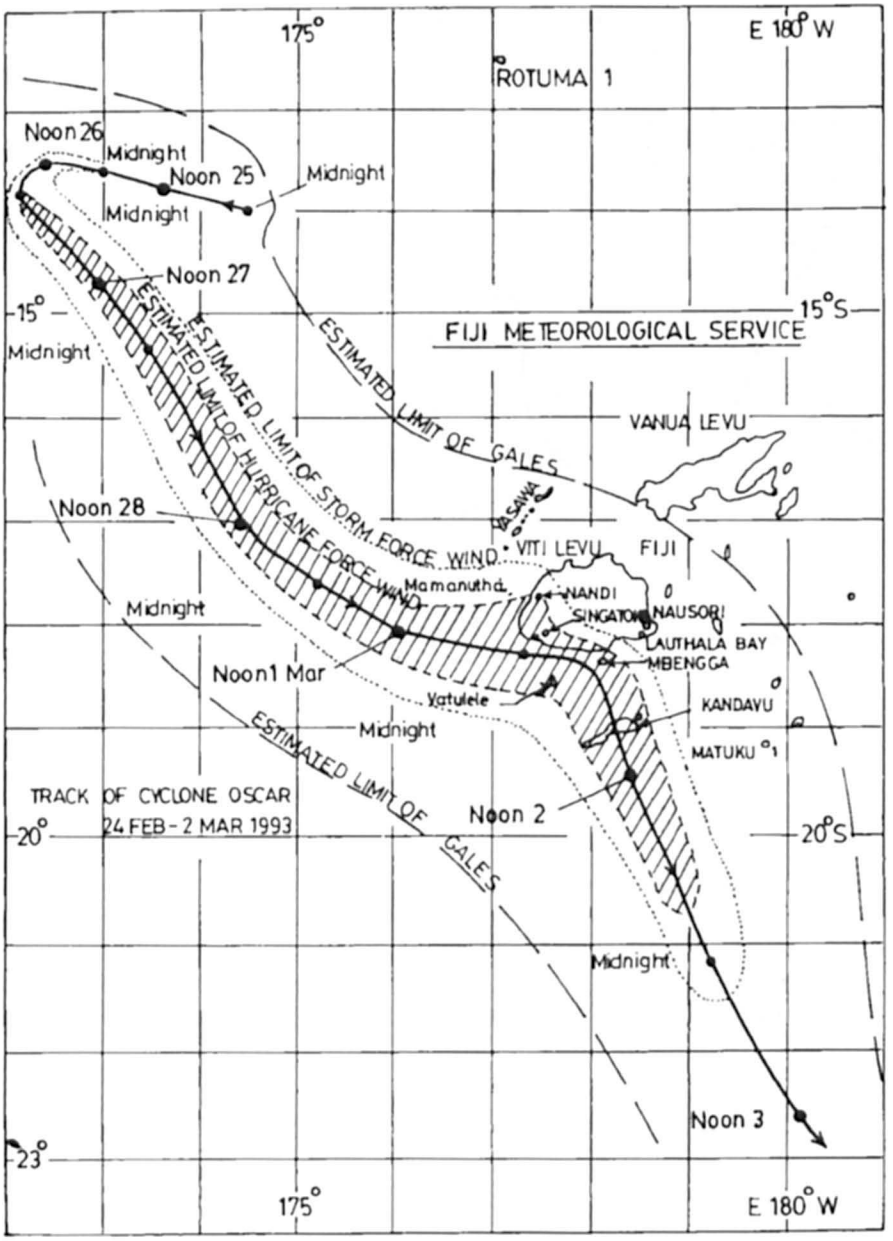

Fig. 6.73: Track of tropical cyclone Oscar, 24 February–2 March 1983 (Fiji Meteorological Service)

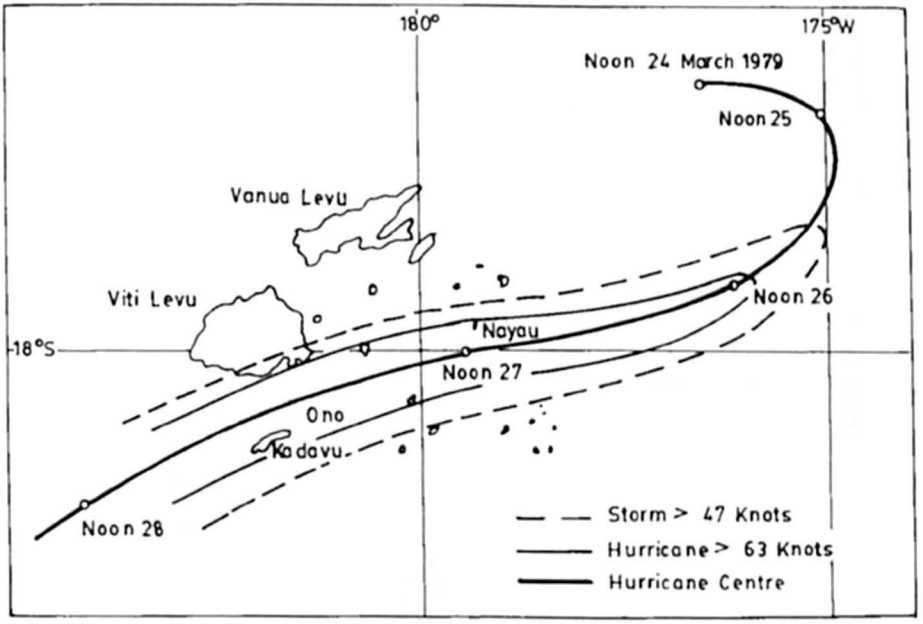

Fig. 6.74: Track of hurricane Meli and associated winds, March 1979 (Fiji Meteorological Service)

During 15–16 January 1996, a minor storm surge occurred in Tonga and was recorded on the SEAFRAME as shown in Fig. 6.75. The following information can be deduced from an examination of this figure.

Total residual or storm surge ~0.33 m.

Wind set-up (residual adjusted for the atmosphere pressure effect) ~0.18 m.

Inverse barometer effect = 0.33–0.18 m = 0.15 m. Pressure drop ~15hPa (hecto Pascals).

The wind set-up can be estimated roughly from the following simple calculation.

$$\frac{\partial \eta}{\partial x} = \frac{\varrho_\alpha}{\varrho} \frac{C_D W^2}{gD} \qquad (6.71)$$

η = amplitude of the surge (m)
x = coordinate perpendicular to the shoreline
ϱ_a = density of air = 1.25 kg/m^3
ϱ = density of sea water = 1.026 x 10^3 kg/m^3
C_D = drag coefficient = 2.8 x 10^{-3} (dimensionless)
g = gravity = 9.8 m/s^2
D = average depth of the water = 10 m
W = wind speed = 35 m/s

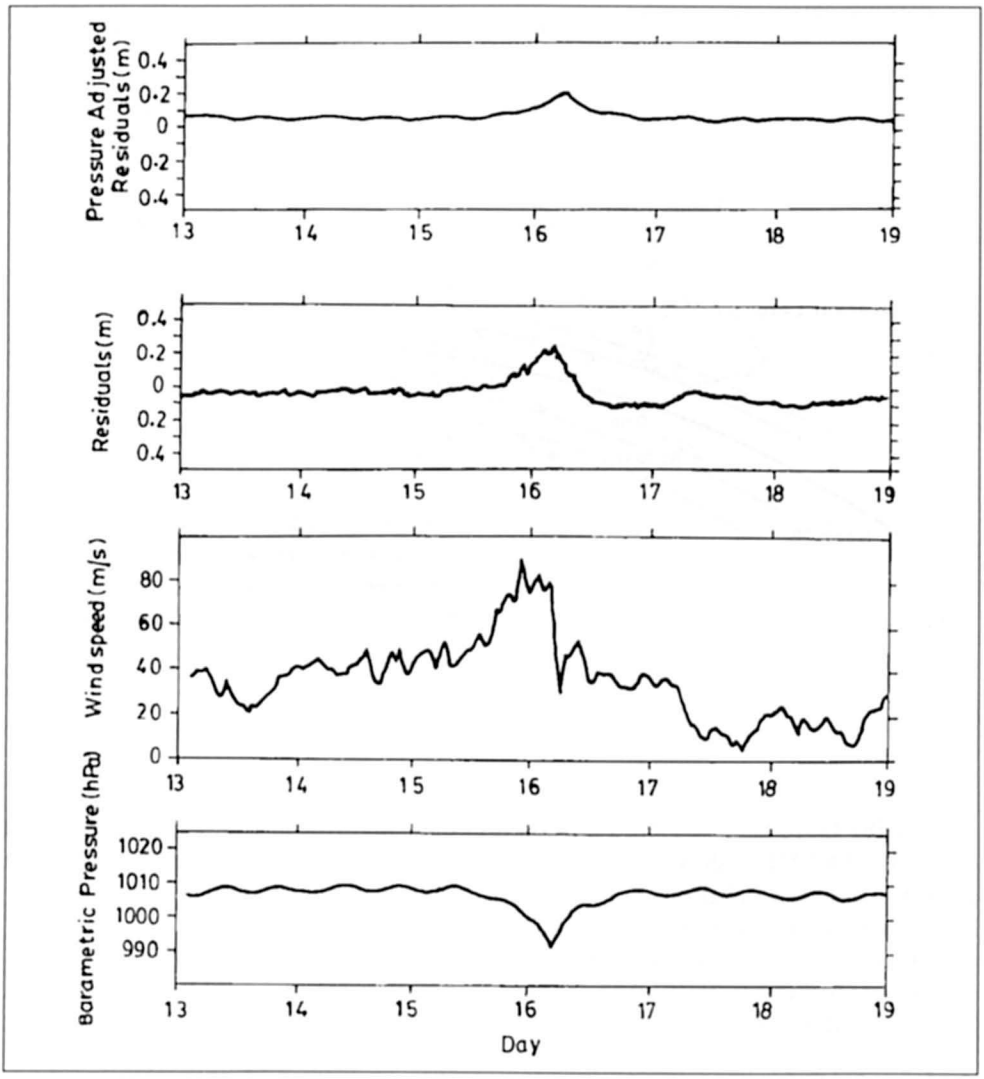

Fig. 6.75: Wind gust, barometric pressure, adjusted residual and residual at Tonga SEAFRAME gauge for January 1996

Using these values, we get

$$\frac{\partial \eta}{\partial x} = 0.42 \times 10^{-4} \tag{6.72}$$

Assuming a fetch of 5 km, one can write.

$$\eta = \frac{\partial \eta}{\partial x} = 0.42 \times 10^{-4} \times 5 \times 10^{3}\,\mathrm{m} = 0.21\mathrm{m} \tag{6.73}$$

The amplitude of the wind set-up computed from the simple formula is 0.21 m, which compares reasonably well with the observed wind set-up of 0.18 m. A numerical model will yield a better agreement. Fig. 6.76 shows the incidence of tropical cyclones for the study area and surroundings (CARTER et al., 1991). Table 6.45 lists the general level of threat from various hazards in the study area whereas Table 6.46 gives the incidence of tropical cyclones in the South Pacific.

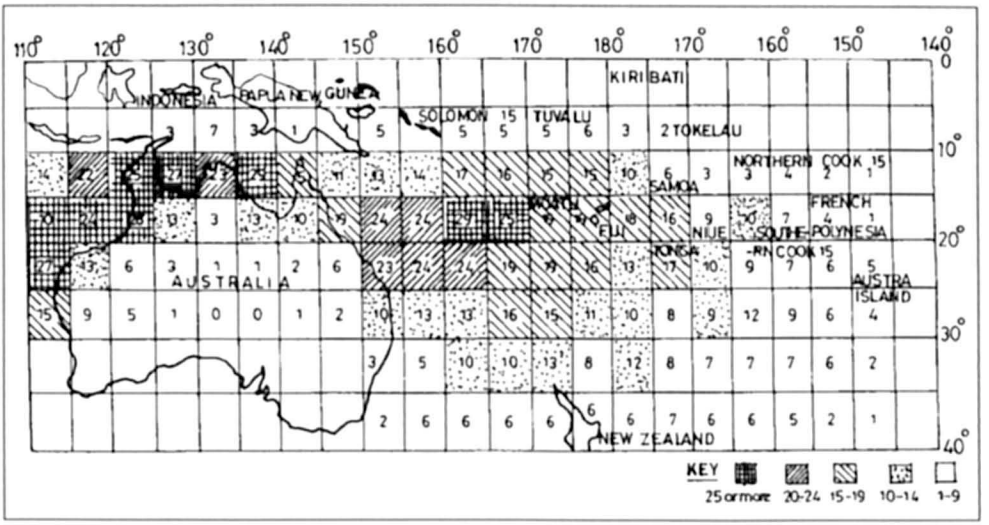

Fig. 6.76: Average decadal incidence of Tropical cyclones in 5-degree latitude – longitude squares. West of 150 east based on data for 1959–1975, East of the Longitude on data for 1969–1979 (CARTER et al., 1991)

Table 6.45: General level of threat (CARTER et al., 1991)

	Cooks	Fiji	Solomons	Tonga	Vanuatu	W. Samoa	Kiribati	PNG
Cyclone	M	H	H	H	H	M	L	L
Drought	H	M	L	M	L	L	H	M
Earthquake	L	M	H	H	H	M	L	H
Flood	L	H	H	M	H	H	L	H
Landslide	L	H	H	L	H	H	L	H
Tsunami	M	H	H	H	H	H	L	H
Volcanic Eruption	–	–	H	H	H	L	–	H

L = Low M = Medium H = High

Table 6.46: Incidence of Tropical Cyclones in the South Pacific (CARTER et al., 1991)

Year	Cooks	Fiji	Solomons	Tonga	Vanuatu	W. Samoa	PNG
1960	1	–	–	2	1	–	–
1961	–	–	–	1	1	1	–
1962	1	–	–	–	–	–	–
1963	2	–	–	1	2	–	–
1964	–	3	–	1	1	1	–
1965	–	1	–	–	–	–	–
1966	–	1	2	–	–	1	–
1967	1	1	1	–	–	–	–
1968	–	–	1	–	2	1	–
1969	–	–	1	1	–	–	–
1970	–	3	–	1	–	–	–
1971	–	–	1	1	1	–	–
1972	1	1	1	1	4	–	–
1973	–	3	2	1	–	–	–
1974	–	1	–	1	1	1	–
1975	–	2	–	–	1	1	–
1976	1	–	–	–	1	2	–
1977	–	1	–	1	3	–	1
1978	–	3	1	1	1	–	–
1979	–	1	1	1	1	–	–
1980	–	3	–	–	–	–	–
1981	1	1	–	–	2	–	–
1982	–	1	1	1	1	–	–
1983	2	2	–	–	–	–	–
1984	–	–	–	–	–	1	–
1985	–	3	–	–	3	–	1
1986	2	2	1	–	1	–	–
1987	1	1	–	–	1	–	–
1988	1	–	1	–	3	–	–
1989	1	–	–	–	1	1	–
Total	15	34	14	15	32	10	2

6.8 Western Pacific Ocean

Under this heading we will include: China, Japan, South Korea, Philippines, Vietnam and Thailand.

6.8.1 China

Storm surges up to 6 m can occur occasionally on the coast of China, with surges up to 2–3 m occurring quite frequently. TSENG-HAO and SHIH-ZAO (1975) used a numerical model to compute storm surges in the Po Hai Sea. JIN-CHUAN and GUANG (1979) developed empirical techniques for hourly predictions of surges due to typhoons on the southeastern coast of China. Their study involved predictions for the following tidal stations: Shacheng, Sansha, Xiamen, Dongshan, Shantou, and Shanwei. The total number of surges considered by them was more than 1000. They used the empirical formulae thus developed operationally since 1977. The hourly predicted and observed surges at three locations due to typhoon 7908 of August 2, 1979 are compared in Table 6.47. JIN-CHUAN and GUANG (1979) gave surge profiles for the 24 most important storm surges on the southeastern coast of China during the 1970's. Five of these profiles are given in Fig. 6.77–6.81. C. Tseng-Hao and F. Shih-Zao (unpublished data) developed numerical models for storm surge prediction on the east coast of China.

Table 6.47: Predicted and observed storm surges at three locations in China due to Typhoon 7908 of August 2, 1979 (JIN-CHUAN and GUANG, 1979)

	Storm surges (cm) at					
	Shantou		Xiamen		Chongwu	
Time (h) GMT	Observed	Predicted	Observed	Predicted	Observed	Predicted
05	95	106	84	105	78	99
08	158	163	88	107	61	75
10	201	223	91	95	47	65
11	187	199	92	87	35	60
14	66	100	27	43	21	40

KENTANG (2000) studied the damage from storm surges in China since 1990. He mentions that storm surges are the number one marine hazard in China. Since 1990, 62 typhoons made a landfall on the coast of China. Three events, one in 1992, the second one in 1994 and the third one in 1997 were particularly disastrous. The direct economic losses from these events were about 1.7, 2.6 and 3.8 billion US Dollars. In average year between 1989–1991 the economic loss is much less and is about 0.7 billion US Dollars.

Fig. 6.82 shows the tracks of these three typhoons and Table 6.48 lists the damage. The author suggests the following counter measures:

1. Raise the society's awareness and public education about storm surge hazard
2. Work out a plan for building new sea walls
3. Improve and perfect the available warning and disaster relief command system and
4. Develop an insurance service in order to promptly mitigate the loss caused by severe storm surge disaster events.

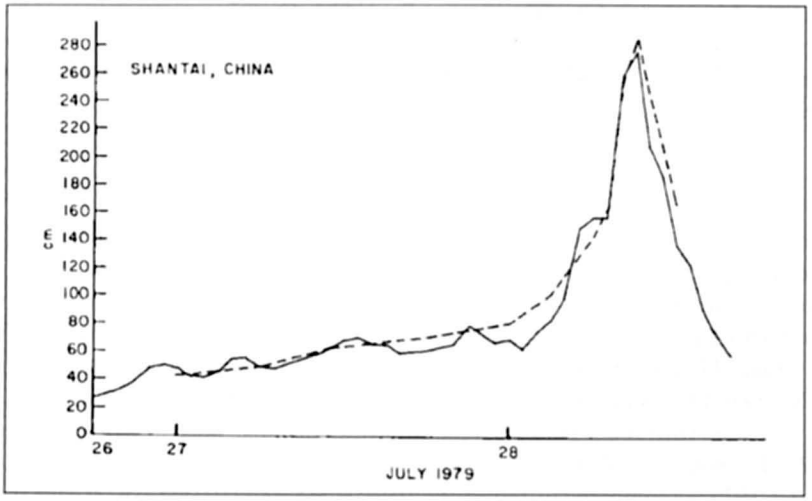

Fig. 6.77: Observed (solid line) and computed (broken line) surges at Shantow, China during July 26–29, 1979 (JIN-CHUAN and GUANG, 1979)

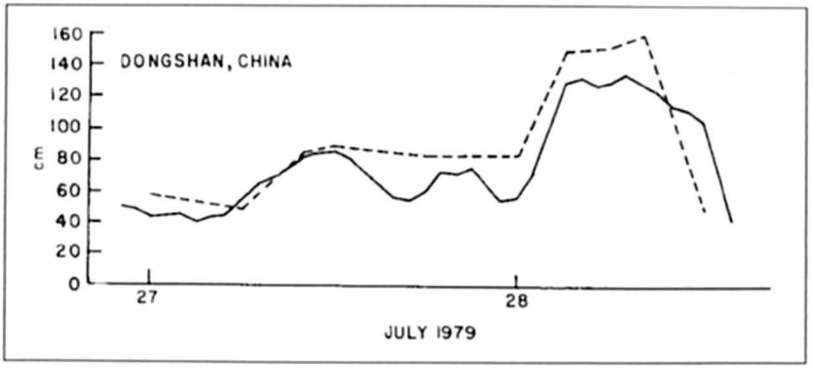

Fig. 6.78: Observed (solid line) and computed (broken line) surges at Dongshan, China during July 27–28, 1979 (JIN-CHUAN and GUANG, 1979)

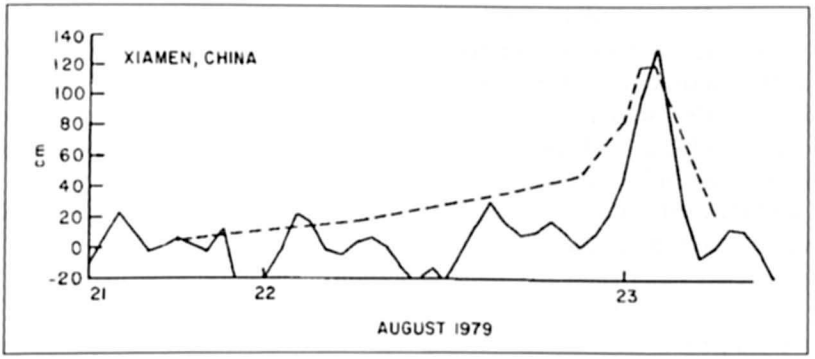

Fig. 6.79: Observed (solid line) and computed (broken line) surges at Xiamen, China during August 21–23, 1979 (JIN-CHUAN and GUANG, 1979)

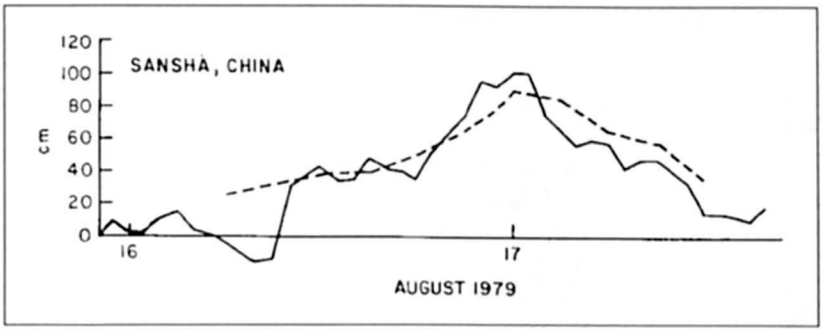

Fig. 6.80: Observed (solid line) and computed (broken line) surges at Sansha, China during August 16–17, 1979 (JIN-CHUAN and GUANG, 1979)

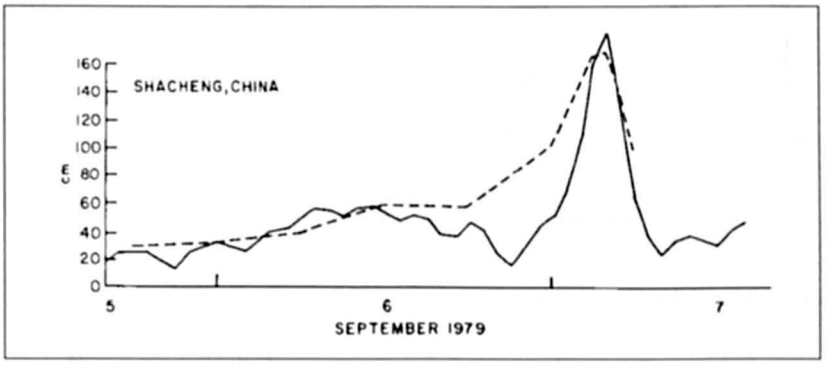

Fig. 6.81: Observed (solid line) and computed (broken line) surges at Shacheng, China during September 5–7, 1979 (JIN-CHUAN and GUANG, 1979)

Table 6.48: Damages of three severe storm surge disaster events (KENTANG, 2000)

		destroyed wall and bank (km)			killed and missing people (number)			direct economic loss (billion yuan, RMB)		
Name of typhoon		Polly	Fred	Winnie	Polly	Fred	Winnie	Polly	Fred	Winnie
Name of disaster		9216SSD	9417SSD	9711SSD	9216SSD	9417SSD	9711SSD	9216SSD	9417SSD	9711SSD
Province or city	Fujian	203.3		*	12		0	0.92		*
	Zhejiang	546.3	520.7	922	114	1216	46	3.15	17.76	18.6
	Shanghai	*		~15	0		7	*		0.6
	Jiangzu	77.7		260	10		17	0.32		3.0
	Shandong	299		85	57		159	4.15		11.5
	Hebei							0.32		
	Tijanjin	44.4			0			0.40		
Total		1170.0	520.7	1282	193	1216	229	9.26	17.76	33.7

(Note: * stands for the much less damage of the item and is not counted in the total)

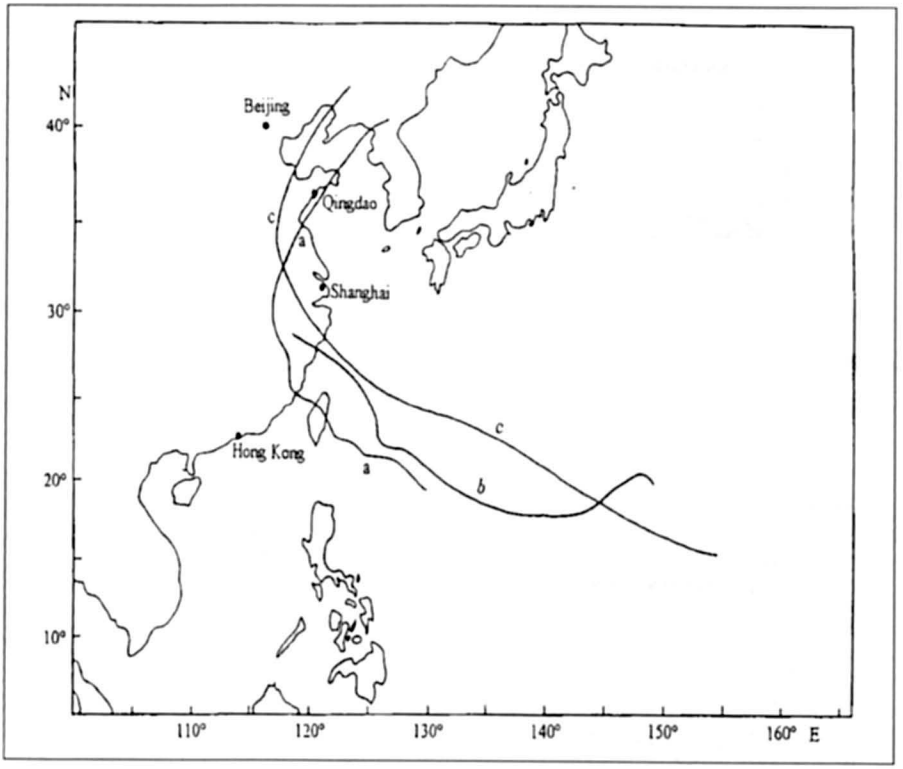

Fig. 6.82: Tracks of the three typhoons in the text (a) Polly, (b) Fred, (c) Winnie (KENTANG, 2000)

Surges in Shanghai Harbour

QIN et al. (1994) numerically simulated tides and storm surges in Shanghai harbour and vicinity by including non-linear tide-surge interaction, as opposed to the traditional method in which tides and surges are linearly super-imposed. They simulated the surges from 16 tropical cyclones hitting Shanghai during the period 1949 to 1990. For the tidal simulations, 63 tidal constituents were included.

Fig 6.83 shows the computational domain. Figs 6.84 to 6.86 respectively show the typhoon tracks for 1949–1959, 1960–1979 and 1980–1990. Fig 6.87 compares the computed water levels for Gloria (1949) and Marge (1951). For results for all the other typhoons, we refer the reader to the original paper. Table 6.49 lists the relative errors for all the simulations. Even though the method used here is not necessarily better in every single simulation; in an overall sense the method used here yielded better results than the traditional method.

Table 6.49: Root-mean-square-errors in the neighbouring high water level using the traditional method and the proposed method incorporating nonlinear surge-tide coupling (QIN et al., 1994)

TC No.	TC Name	Traditional method (cm)	Proposed method (cm)
4906	Gloria	9.0	46.5
5116	Marge	24.7	21.0
5410	Grace	42.5	34.6
5612	Wanda	44.5	20.5
5907	Sarah	29.5	29.5
6014	Carmen	48.5	38.8
6207	Nora	37.6	22.4
7008	Billie	45.0	37.6
7308	Iris	40.0	14.5
7413	Mary	33.0	21.1
7910	Judy	40.2	28.7
8114	Anges	39.2	28.1
8310	Forrest	29.9	23.5
8615	Vera	26.7	22.2
8913	Lola	33.9	25.9
9015	Abe	8.7	17.8

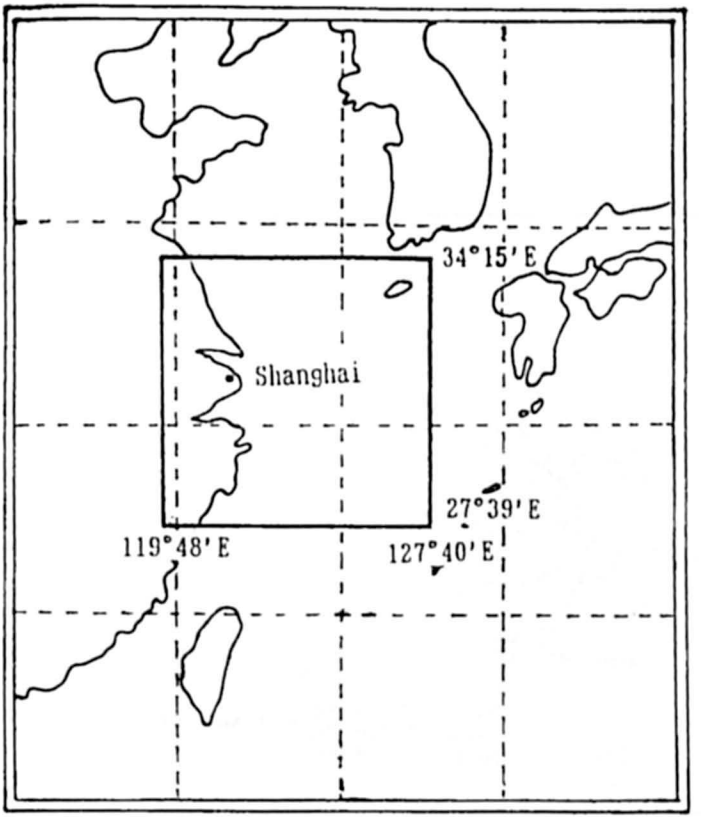

Fig. 6.83: Computational domain (QIN et al., 1994)

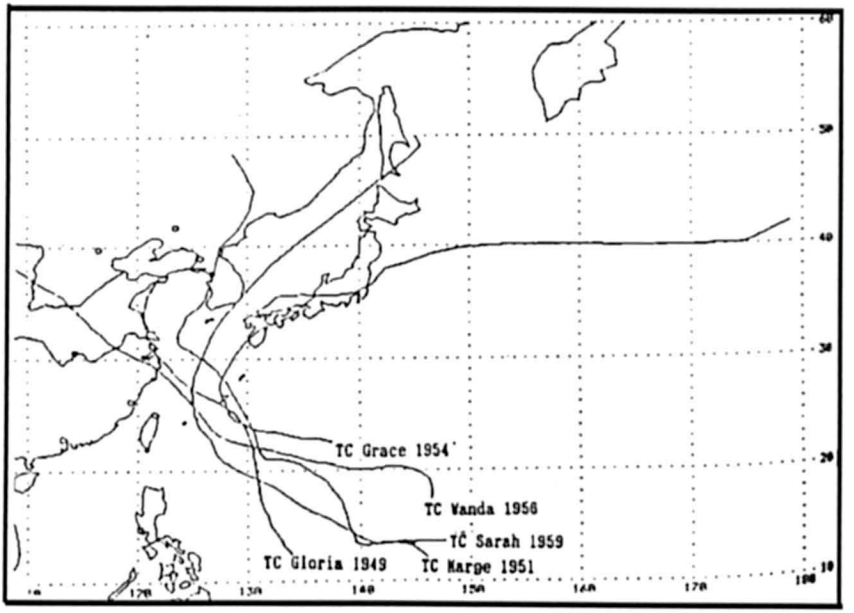

Fig. 6.84: Tracks of tropical cyclones for 1949–1959 (QIN et al., 1994)

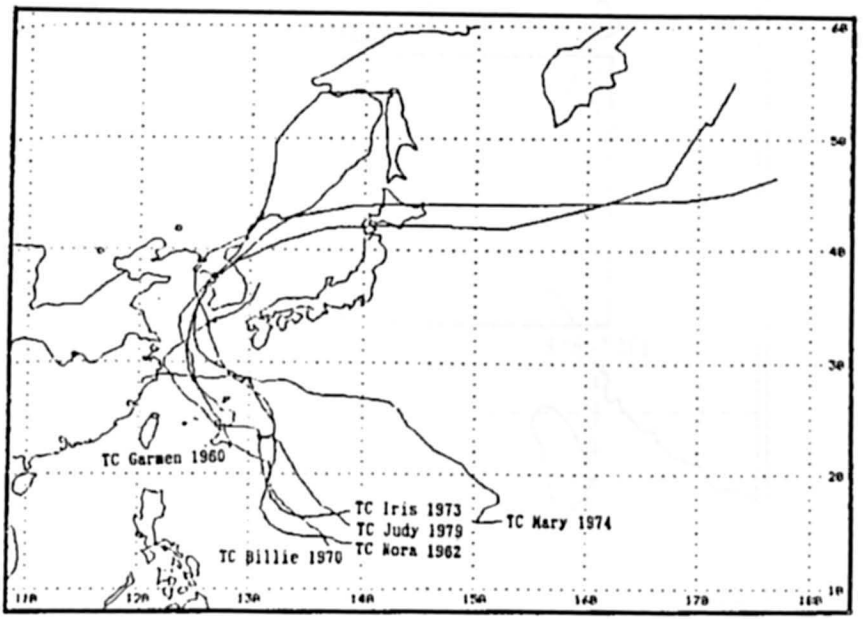

Fig. 6.85: Tracks of tropical cyclones for 1960–1979 (QIN et al., 1994)

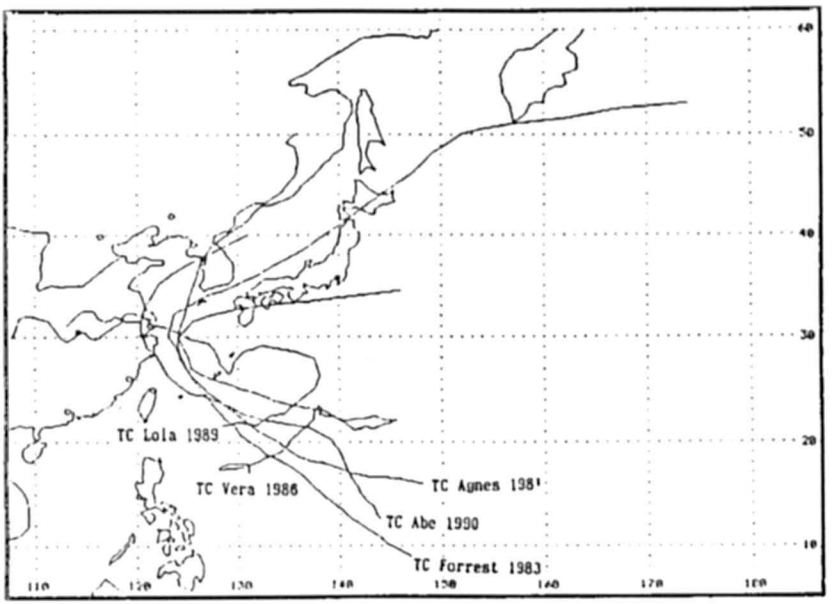

Fig. 6.86: Tracks of tropical cyclones for 1980–1990 (QIN et al., 1994)

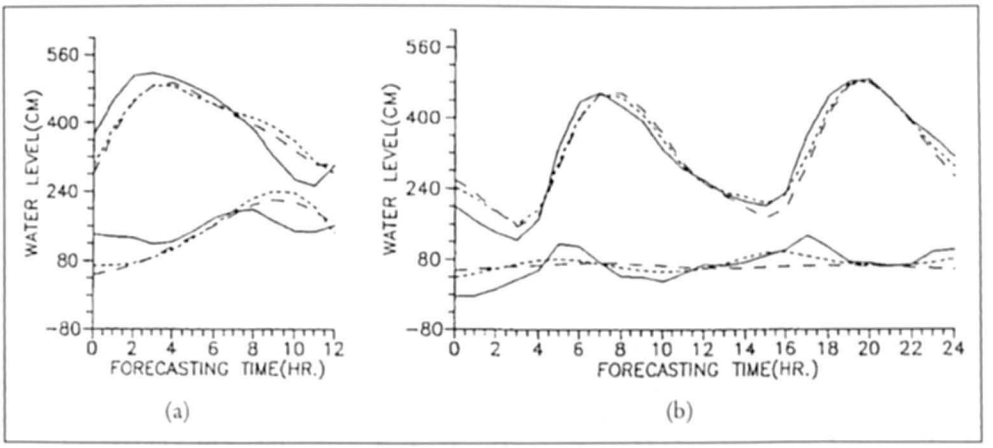

Fig. 6.87: (a) Surge and water level process curves caused by TC Gloria 1949 for Wuson. Legend: solid lines – observed, dashed lines – simulated (longer for the traditional method, shorter for the proposed method); top case for total water-level, bottom case for storm surges (b) same as above except those caused by TC Morge 1951 (QIN et al., 1994)

Surges in Hong Kong

Storm surges are reasonably severe in Hong Kong (CHAN and WALKER, 1979) have described three different types of surges and the empirical formulae for predicting them. The return periods for surges of different amplitudes (BELL, 1961), computed using Gumbel's methods and using data from maximum hourly winds, are listed in Table 6.50. SILVESTER (1971) studied storm surges in Hong Kong and developed empirical relations. The pressure deficits and observed storm surges at North Point, Hong Kong Harbour, for seven different typhoons are listed in Table 6.51.

Table 6.50: Return periods for extreme storm surges in Hong Kong (BELL, 1961)

Surge amplitude (m)	Return period (Yr)	Surge amplitude (m)	Return period (Yr)
1.6	10	2.4	200
1.8	20	2.7	500
2.0	50	2.9	1000
2.2	100		

Table 6.51: Observed storm surge amplitudes and pressure deficits in typhoons that affected Hong Kong (North Point) (SILVESTER, 1971)

Typhoon	Date	Pressure deficit (mb)	Observed surge amplitude (m)
Wanda	Sept. 1962	61	0.62
Faye	Sept. 1963	17	0.17
Viola	May 1964	21	0.21
Ida	Aug. 1964	38	0.39
Ruby	Sept. 1964	45	0.46
Sally	Sept. 1964	24	0.24
Shirley	Aug. 1968	44	0.45

LAU (1980b) used the SPLASH model to compute storm surges at North Point and in Tolo Harbour for events of tropical cyclone passages across the northern part of the South China Sea. This study used 93 historical storms during the period September 1906–June 1976 that generated storm surges in Hong Kong. The standard storm of the SPLASH model gives an open-coast peak surge of 1.92 m at North Point. Nomograms for the surge height at North Point are given in Fig. 6.88–6.92, respectively, as a function of the central pressure of the storm, storm direction, storm speed, radius of maximum winds, and distance of nearest approach of storm.

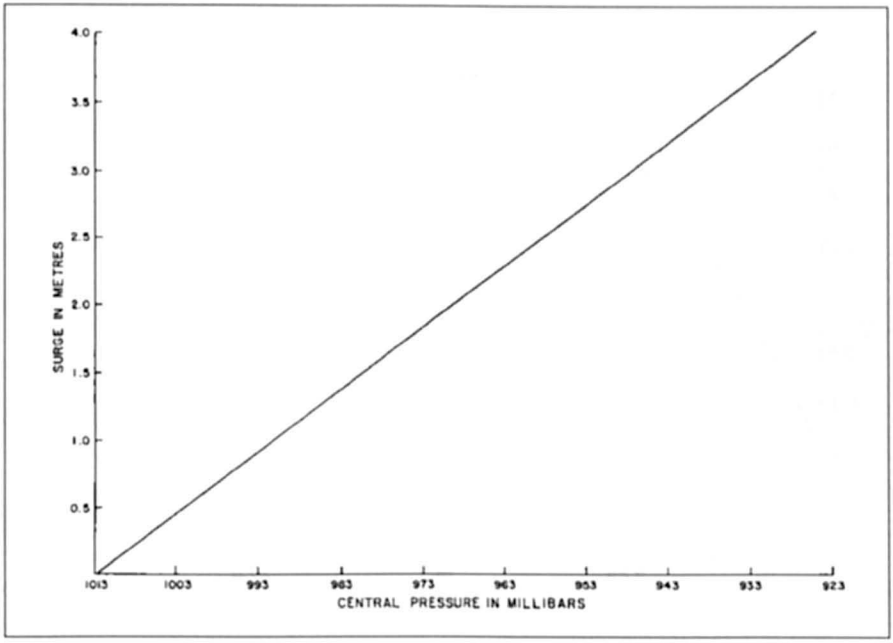

Fig. 6.88: Surge amplitude versus central pressure of storm for North point in Hong Kong harbour (LAU, 1980b)

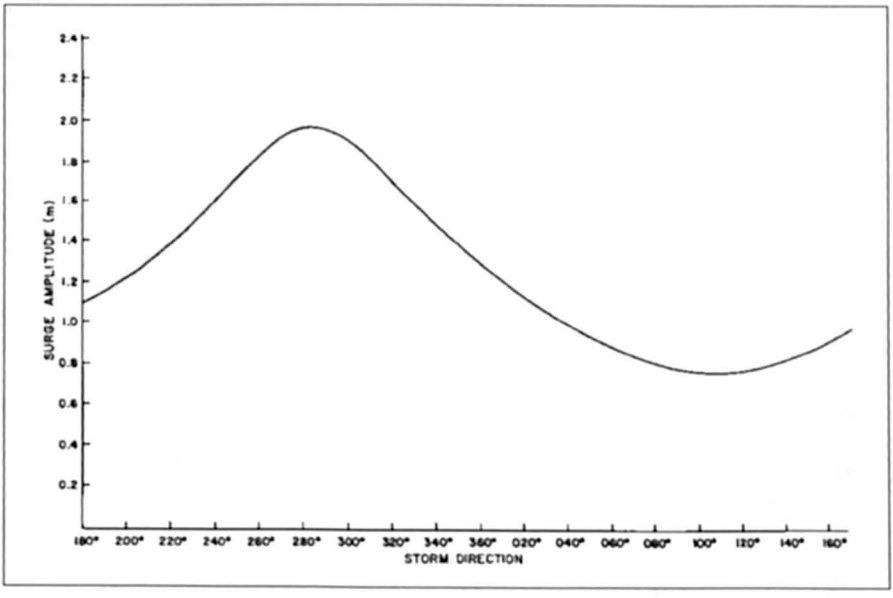

Fig. 6.89: Surge amplitude versus storm direction in 360° compass bearing for North point in Hong Kong harbour (LAU, 1980b)

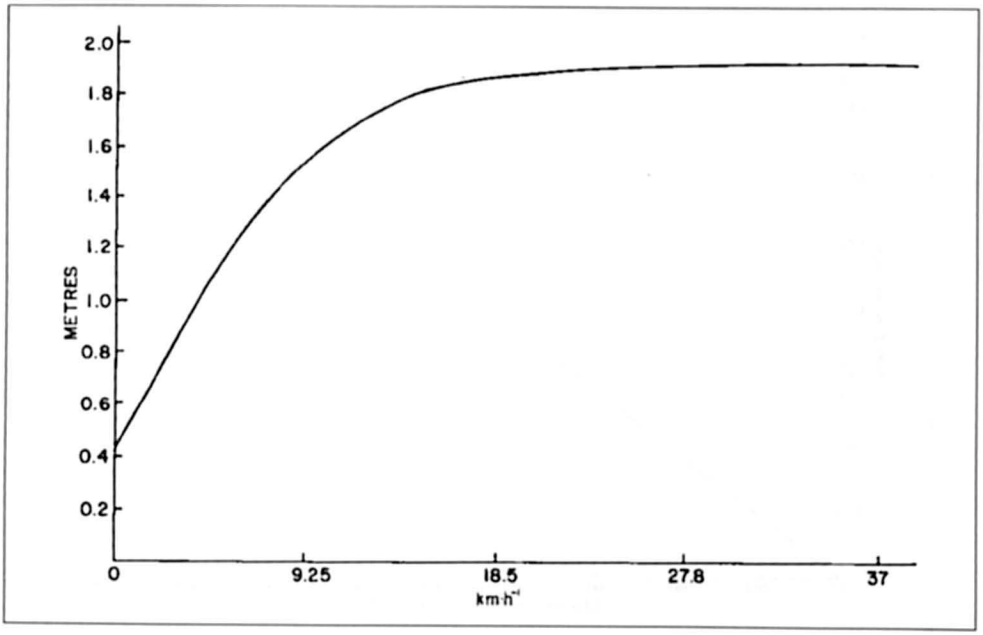

Fig. 6.90: Storm surge amplitude versus storm speed for North point in Hong Kong harbour (LAU, 1980b)

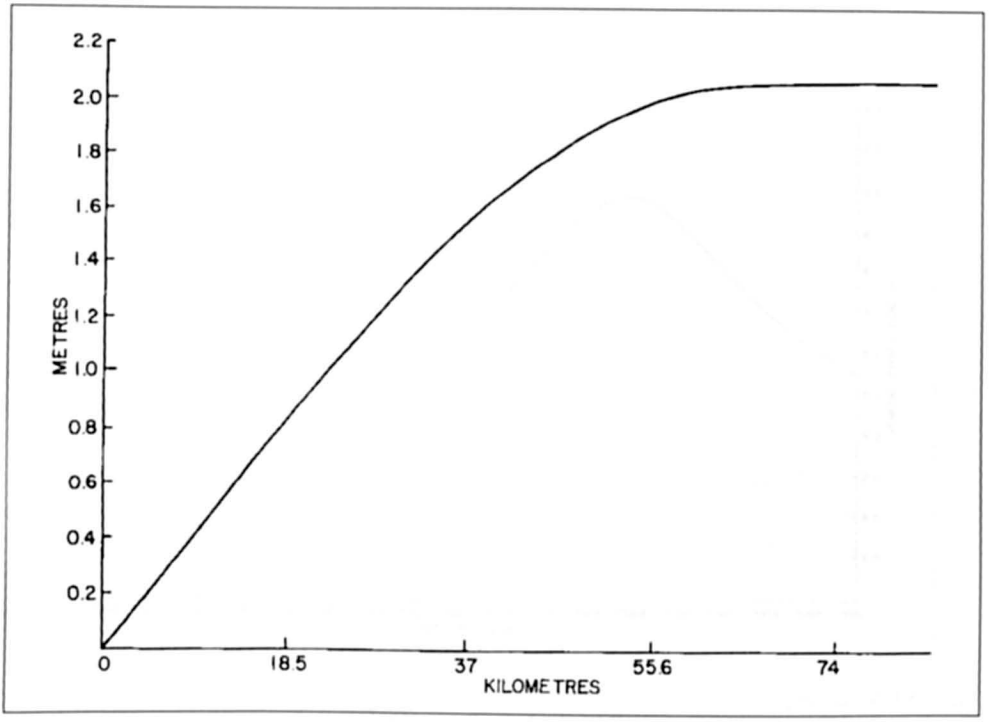

Fig. 6.91: Storm surge amplitude (ordinate) versus radius of maximum winds (abscissa) for North point in Hong Kong harbour (LAU, 1980b)

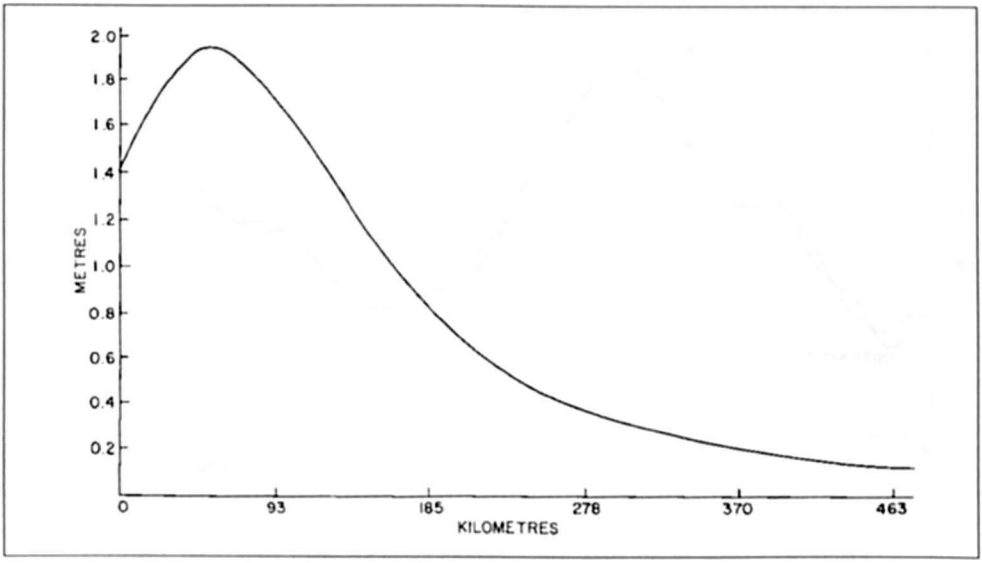

Fig. 6.92: Storm surge amplitude (ordinate) versus distance from the nearest approach of storm for North point in Hong Kong harbour (LAU, 1980b)

LAU (1980a) mentioned that the storm surge problem is getting worse in Hong Kong with more and more people crammed into reclaimed low-lying areas. A typhoon surge on September 2, 1937, killed 11000 people, and several villages around Tolo Harbour were destroyed. Typhoon Wanda of September 1, 1962, killed 127 people. LAU (1980a, 1980b) summarised the empirical relations developed by CHENG (1967) and CHAN (1976). He also included a table from PETERSON (1975) in which joint probabilities for certain combinations of tides and surges at Tolo Harbour and North Point were listed. Finally, LAU (1980a) developed a series of numerical models for computing surges in different areas of Hong Kong and environs. Observed and computed water levels at Tai Po Kau due to Typhoon Elaine of October 29–30, 1974, are compared in Fig. 6.93. Computed and observed water levels at Tai Po Kau due to Typhoon Elsie of October 14–15, 1975, are compared in Fig. 6.94.

DAS et al. (1978) mentioned that storm surges occur at the rate of three to four per year in Hong Kong Harbour. Thirty-five surges with amplitudes from 0.2 to 1.8 m occurred there during 1954–64 (CHENG, 1967). Typhoon Wanda of September 1962 produced a surge of about 3.2 m at Tai Po Kau (farther inland from Hong Kong Harbour), whereas the peak surge in Hong Kong Harbour was 1.8 m.

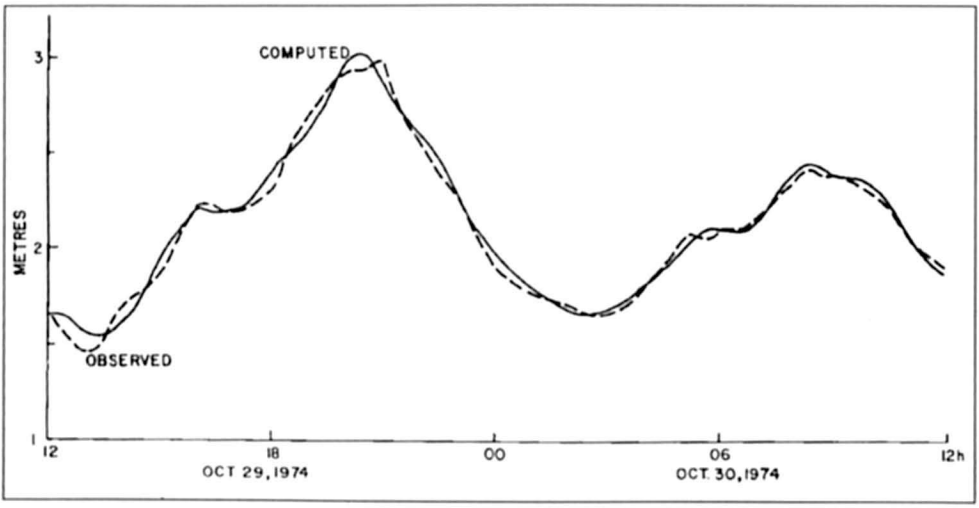

Fig. 6.93: Computed (solid line) and observed (broken line) water levels at Tai Po Kau due to Typhoon Elaine of October 29–30. 1974. Time is Hong Kong Standard Time (LAU, 1980a)

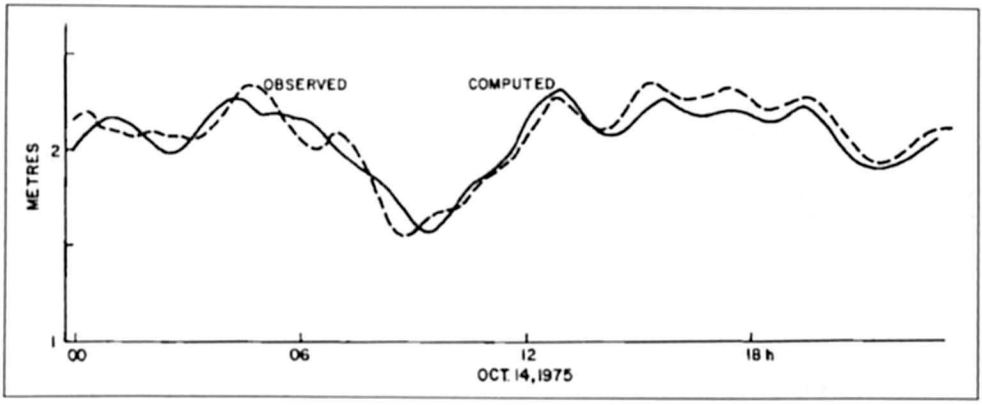

Fig. 6.94: Compared (solid line) and observed (broken line) water levels at Tai Po Kau due to Typhoon Elsie of October 14–15, 1975. Time is Hong Kong Standard Time (LAU, 1980a)

6.8.2 Japan

Storm surges in the bays on the coast of Japan are slightly less severe than, for example, in the Bay of Bengal and the Gulf of Mexico but they cause great damage and loss of life when they strike the densely populated coasts of Tokyo Bay, Osaka Bay, Ise Bay, etc. Table 6.52 and 6.53 list the important storm surges in Japan. MIYAZAKI (1975) mentioned that storm surge records in Japan generally exhibit three features: the forerunner, the main surge, and the resurgence. The surge profiles at Nagoya and Toba along the coast of Ise Bay due to the typhoon of September 26–27, 1959, are given in Fig. 6.95. Forerunners with amplitudes of 20–30 cm can be seen. Resurgences with periods of about 7 h can also be seen. MIYAZAKI (1975) also estimated the return periods of surges with different maximum amplitudes at six locations in Japan. These results are summarised in Table 6.54.

Table 6.52: Storm surges in Japan during the period 1900–73 with maximum amplitudes in excess of 2 m. Highest level includes surge and tide (MIYAZAKI, 1975)

Date	Affected Area	Peak surge (m)	Highest level (m)	Meteorological extreme values: Central pressure (mb)	Wind ($m \cdot s^{-1}$)	Location
Oct. 1, 1917	Tokyo Bay	2.3	3.1	950.4	SSE 40.0	Tokyo
July 18, 1930	Ariake Sea	2.5	–	954.6	ENE 30.6	Tomie
Sept. 21, 1934	Osaka Bay	3.1	3.2	954.3	S 48.4	Osaka
Sept. 1, 1938	Tokyo Bay	2.2	–	978.6	S 31.0	Tokyo
Sept. 3, 1950	Osaka Bay	2.1	2.5	964.3	NE 33.4	Kobe
Aug. 17, 1956	Ariake Sea	2.4	4.2	968.4	SE 27.0	Saga
Sept. 26, 1959	Ise Bay	3.4	3.9	958.5	SSE 37.0	Nagoya
Sept. 16, 1961	Osaka Bay	2.5	2.9	937.3	SSE 33.3	Osaka
Sept. 25, 1964	Osaka Bay	2.1	2.6	983.5	S 27.1	Sumoto
Sept. 10, 1965	Osaka Bay	2.2	–	966.0	SSE 38.8	Sumoto
Aug. 21, 1970	Tosa Bay	2.4	3.1	962.3	SW 35.8	Ashizuri

Table 6.53: Severe damage caused by storm surges in Japan during the period 1900–73 (MIYAZAKI, 1975)

Date	Affected Area	Highest sea level (m)	Peak surge (m)	Lives Lost	Houses destroyed or swept away
Oct. 1, 1917	Tokyo Bay	3.0	2.1	1324	60 175
Sept. 13, 1927	Ariake Sea	3.8	0.9	439	2211
Sept. 21, 1934	Osaka Bay	3.1	2.9	3036	92 323
Aug. 27, 1942	Inland Sea	3.3	1.7	1158	102 374
Sept. 17, 1945	South Kyushu	2.6	1.6	3121	115 984
Sept. 3, 1950	Osaka Bay	2.7	2.4	534	120 923
Oct. 14, 1951	South Kyushu	2.8	1.0	943	72 648
Sept. 27, 1959	Ise Bay	3.9	3.4	5098	156 676
Sept. 16, 1961	Osaka Bay	3.0	2.5	200	54 782

Table 6.54: Return periods of storm surges in Japan (MIYAZAKI, 1975).

Location	Maximum Surge observed (m)	Return period (yr) for surges with peak amplitude of at least: 0.5 m	1.0 m	2.0 m
Tokyo	2.1	1.0	8	35
Yokohama	1.1	1.4	19	–
Nagoya	3.4	0.6	3	15
Osaka	3.1	0.7	3	10
Kobe	2.2	1.0	6	30
Beniya (on the Ariake Sea)	2.5	–	7	17

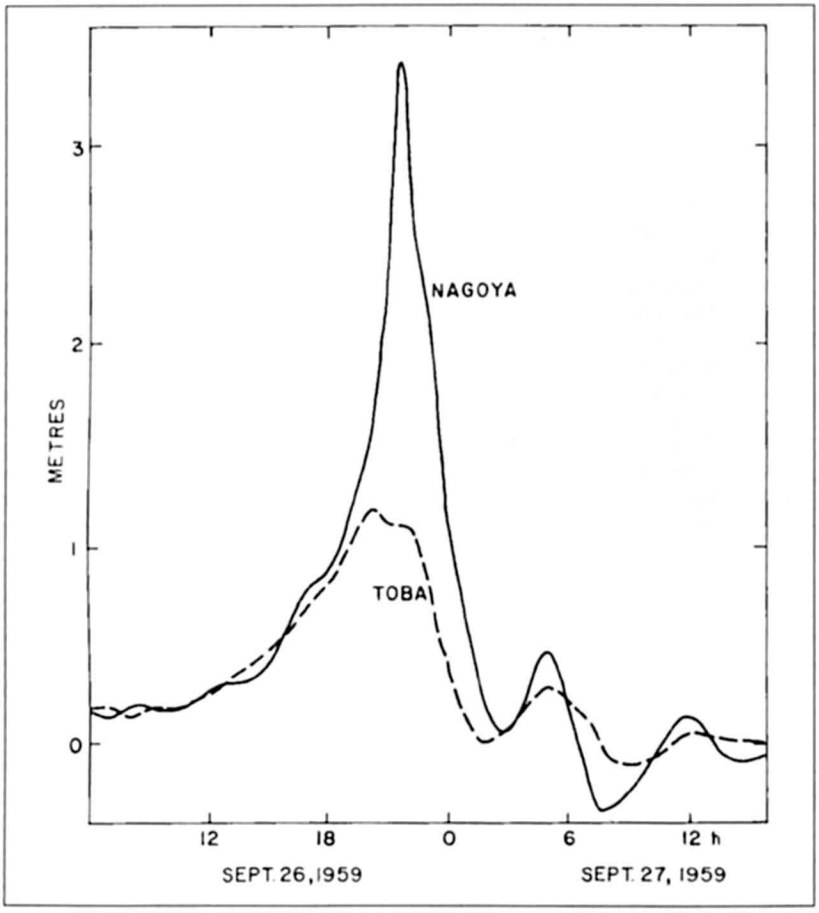

Fig. 6.95: Storm surges at Nagoya and Toba on Ise Bay, Japan, due to the typhoon of September 26–27, 1959. Note the forerunners and the resurgences in addition to the main surge (MIYAZAKI, 1975)

Unusual storm tracks can occur in the Japan area. The track of typhoon Orchid of September 1980 is illustrated in Fig. 6.96. This track is remarkable because it shows three loops. NAKAYAMA (1972) described the telemeter system for the tsunami and storm surge warning service provided by the Japan Meteorological Agency. As of 1972 there were a total of 60 coastal tide gauge stations in this system. Next, storm surge events will be considered in several different bays along the coast of Japan, beginning with Tokyo Bay and proceeding southwest. Note that the storm surge problem on the west coast of Japan (facing the Sea of Japan) is less severe than along the Pacific coast of Japan.

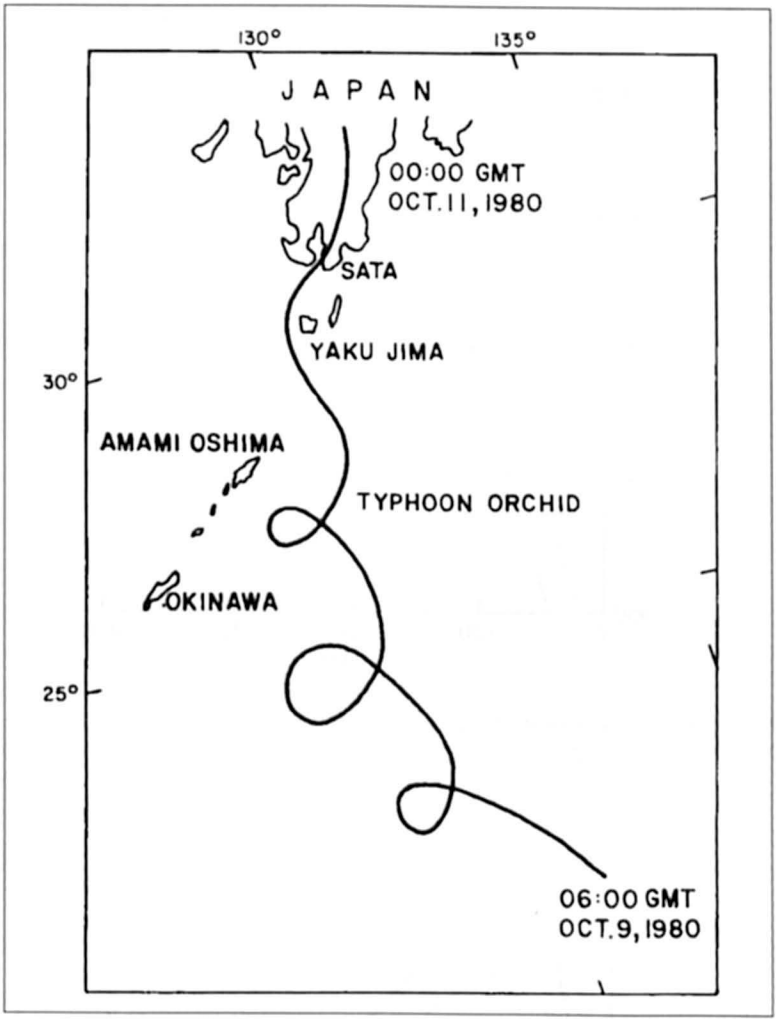

Fig. 6.96: Track of typhoon Orchid during October 9–10, 1980 (JOINT TYPHOON WARNING CENTER, 1981)

MIYAZAKI et al. (1961) used numerical models to compute the storm surges in Tokyo Bay, Ise Bay, and Osaka Bay. They reconstructed the meteorological forcing terms for the Ise Bay typhoon of September 1959. The pressure-distance and wind-distance relations are shown in Fig. 6.97 and 6.98, respectively.

Simulations were made for the following cases: (1) surge in Ise Bay due to the Ise Bay typhoon of September 1959, (2) surges in Tokyo Bay due to the typhoon of October 1, 1917, and Typhoon Kitty of September 1949, and (3) surges in Osaka Bay due to the Muroto typhoon of September 1934 and Typhoon Jane of September 1950.

The horizontal distribution of the storm surge amplitudes in Tokyo Bay due to the typhoon of October 1917 is given in Fig. 6.99. Computed and observed surges at Kishiwada and Osaka due to Typhoon Jane are compared in Fig. 6.100. The spectrum of the storm surge at Kobe due to Typhoon Jane is shown in Fig. 6.101.

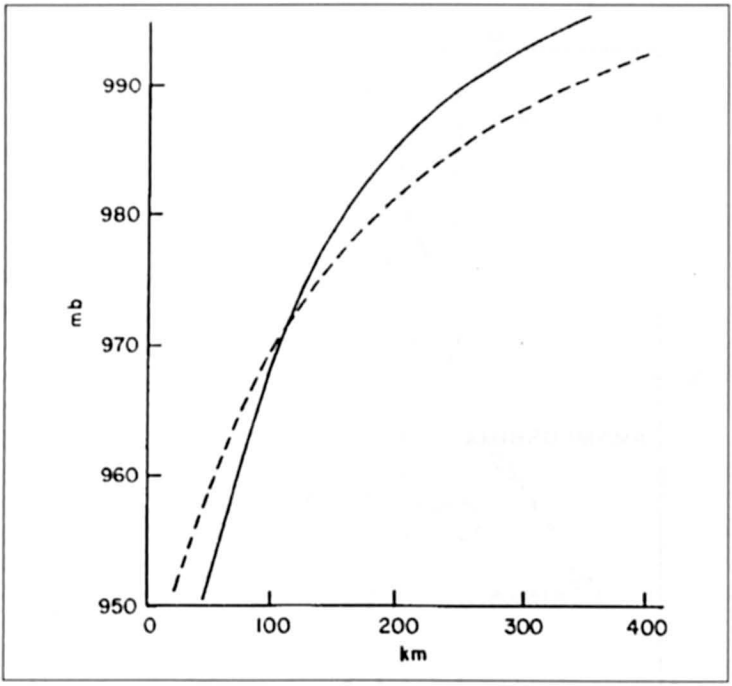

Fig. 6.97: Atmospheric pressure versus distance from the typhoon center for the Ise Bay typhoon of September 1959. Solid curve is obtained using Fujita's formula and the broken curve is from Takahasi's formula (MIYAZAKI et al., 1961)

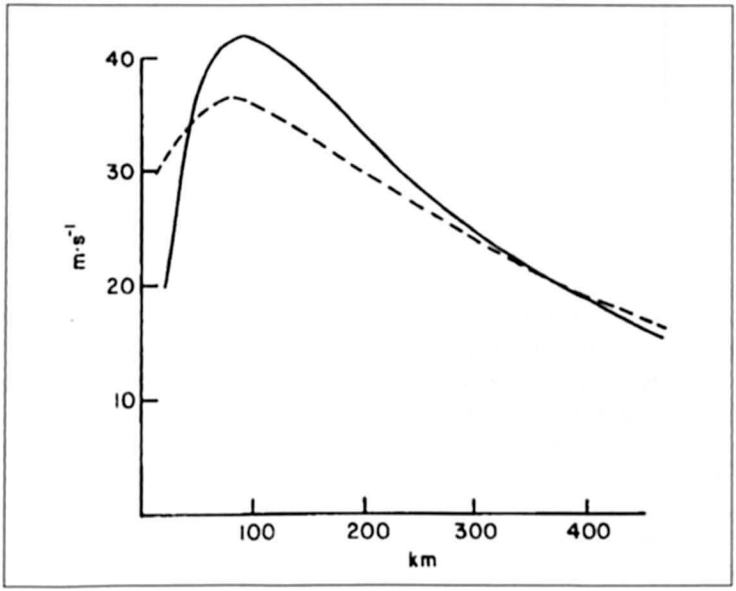

Fig. 6.98: Wind speed versus distance from the typhoon center for the Ise Bay typhoon of September 1959. Solid curve is from Fujita's formula and the broken curve is from Takahasi's formula (MIYAZAKI et al., 1961)

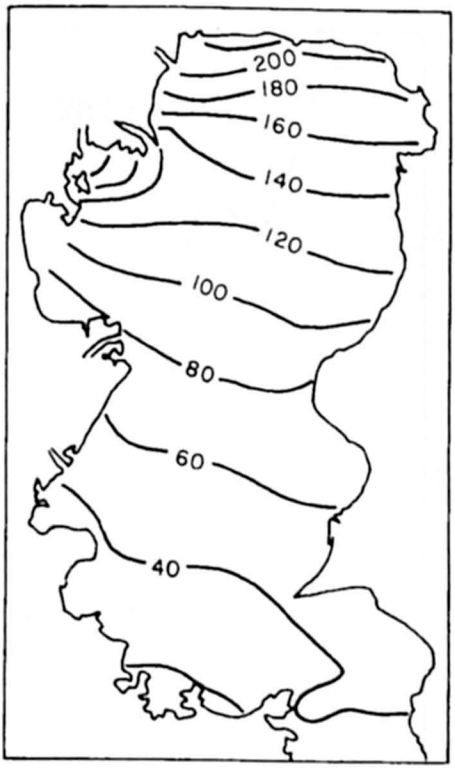

Fig. 6.99: Distribution of storm surge heights (centimeters) in Tokyo Bay at 04:00 on October 1, 1917 (MIYAZAKI et al., 1961)

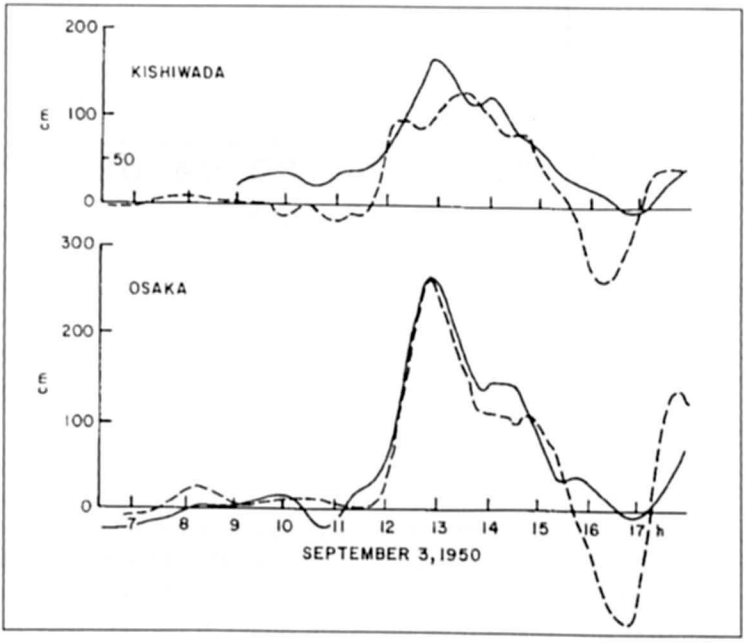

Fig. 6.100: Observed (solid line) and computed (broken line) storm surges at Kishiwada and Osaka due to typhoon Jane of September 1950 (MIYAZAKI et al., 1962)

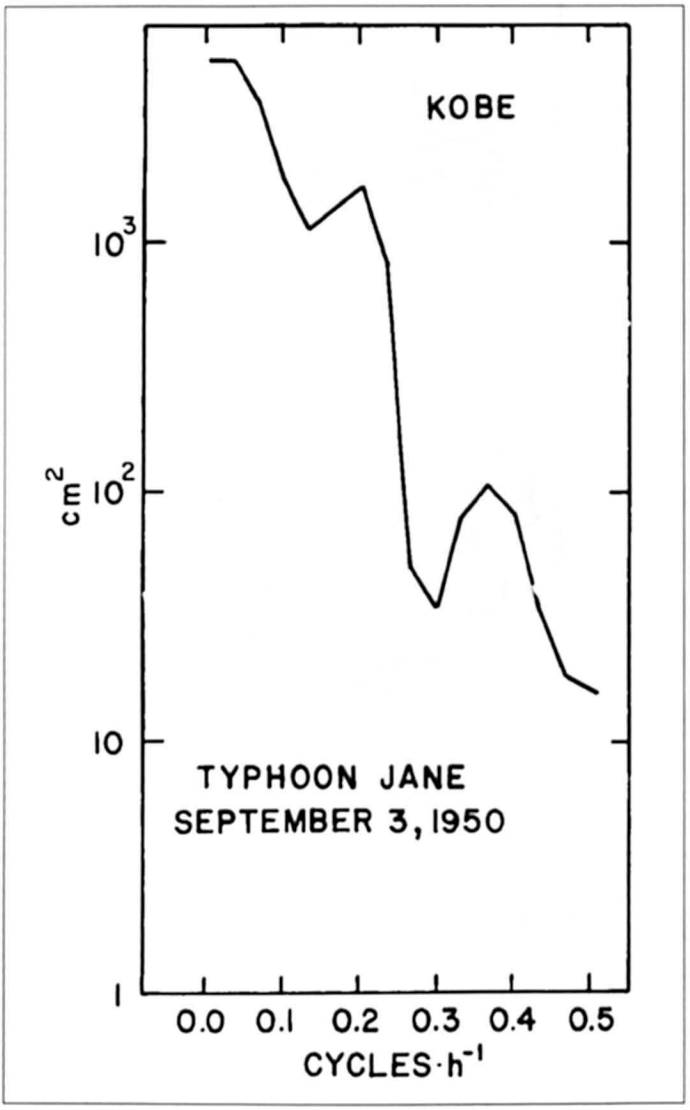

Fig. 6.101: Power spectrum of the storm surge at Kobe due to Typhoon Jane of September 3, 1950 (DAS et al., 1978)

ITO et al. (1965) developed a two-dimensional numerical model for storm surges in Tokyo Bay and the outer shelf using multiple grids. They also studied the problem of tide-surge interaction and the influence of a dyke (with an opening) in Tokyo Bay (north of a line connecting Kawasaki and Kisarazu) on the storm surges in the bay. They simulated the surges due to the October 1, 1917, typhoon and also due to the Ise Bay typhoon of September 1959.

They found the following empirical relation for the maximum water level max in that part of the bay protected by the dyke:

$$\eta_{max} = a + m \log A \qquad (6.74)$$

where, A is the cross-sectional area of the opening, a is a constant that depends on the point of observation, and m is another constant almost independent of location.

Runs were made with the numerical model for openings with widths of 20 m to 2 km and also for a case of two openings, each 0.5 km wide. The results tend to show that the maximum surge amplitudes in the inner bay (i.e. protected by the dyke) decrease when a dyke is present. Also, the maximum surge amplitude decreases for smaller widths of the opening (Fig. 6.102). The problem of tide-surge interaction has already been discussed in section 4.5.8.

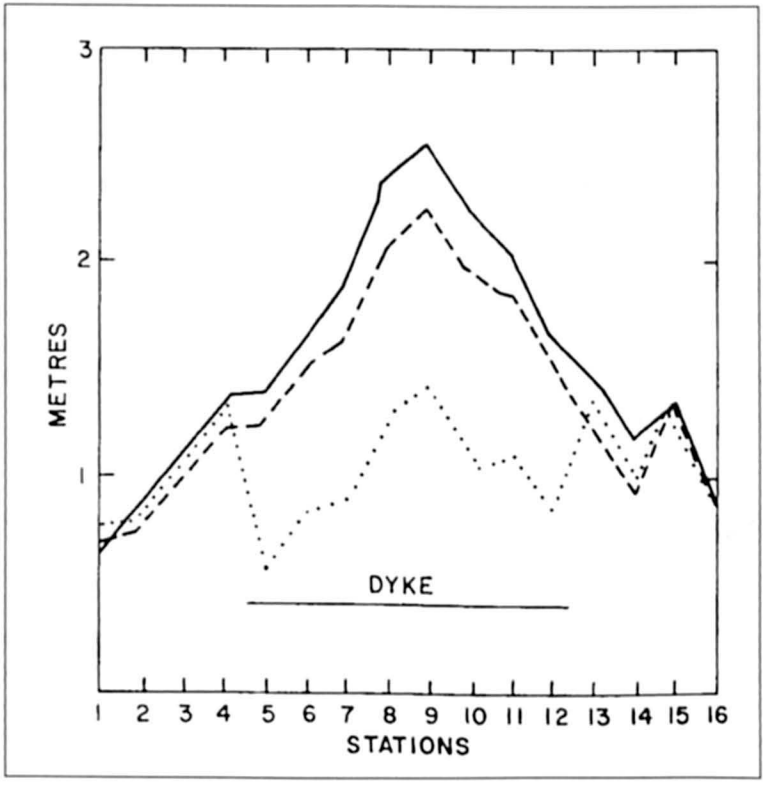

Fig. 6.102: Computed envelope of peak storm surge in Tokyo bay after the construction of a dyke. Solid line: without dyke; broken line: with dyke having an opening of 2 km dotted line with dyke having an opening of 0.5 km width, Stations: 1. Kurihama, 2. Yokosuka; 3. Yokohama; 4. Kawasaki South; 5. Kawasaki North; 6. Tokyo; 7. Urayasu; 8. Funabashi; 9. Chiba,; 10. Goi; 11. Anegasaki; 12. Narawa; 13. Kisarazu; 14. Futtusu; 15. Isone; 16. Kaiho II (ITO et al., 1965)

KAWAHARA et al. (1980) used a finite-element model to compute storm surges in the Surugawan Bay due to the typhoon (No. 6626) of September 24, 1966. The maximum surge produced was about 1 m. After the disastrous storm surge of September 1959 in Ise Bay, a breakwater was constructed in the inner part of the bay to protect the Nagoya district.

(NAKAMURA et al. 1964). These authors also performed hydraulic model tests. The tests showed that the breakwater will not significantly alter the tide but will reduce the surge considerably in the inner part of the bay.

The Muroto typhoon of September 21, 1934, caused major storm surges in Lake Biwa (northeast of Osaka). The southern portion of this lake is very shallow with an average depth of only 3.4 m. Surges up to 2.4 m in amplitude were generated (NOMITSU, 1935).

MIYAZAKI (1955) studied storm surge in the Kobe Harbour. During the period 1925–54, a total of at least 34 storm surges occurred in this harbour. The Muroto typhoon of September 21, 1934, produced a surge of amplitude 2.2 m. Typhoon Jane of September 3, 1950, produced a surge of 1.7 m; the Makurazaki typhoon of September 18, 1945, as well as another typhoon on September 26, 1954, produced surges up to 1.5 m.

MIYAZAKI (1955) gave the following return periods for surges of amplitude 1.0, 1.5, 2.0, and 2.0 m in Kobe harbour: 5, 24, 105, and 455 yr. Of a total of 32 storm surges studied, 22 were caused by tropical cyclones and the remaining 10 were caused by extratropical cyclones. Further, any surges with amplitudes greater than 0.8 m were exclusively produced by tropical cyclones.

Osaka bay is frequently subjected to severe storm surges. The Muroto typhoon of September 21, 1934, killed 2593 people and 110,000 houses were destroyed in Osaka alone. The central pressure of this typhoon was the lowest ever recorded at a land station (912 mb). Wind velocities of up to 60 $m \cdot s^{-1}$ created maximum water level of 4.6 m, and surges with amplitudes of up to 2.3 m inundated large areas (MATSUO, 1934). Osaka Harbour (and several others) was heavily damaged and individual ships of up to 3145 t in weight were carried ashore by the surge. The total weight of the ships carried ashore in Osaka Harbour was about 23,000 t. The envelope of maximum surge amplitude at several locations along Osaka Bay due to Typhoon Nancy of 1961 is shown in Fig. 6.103.

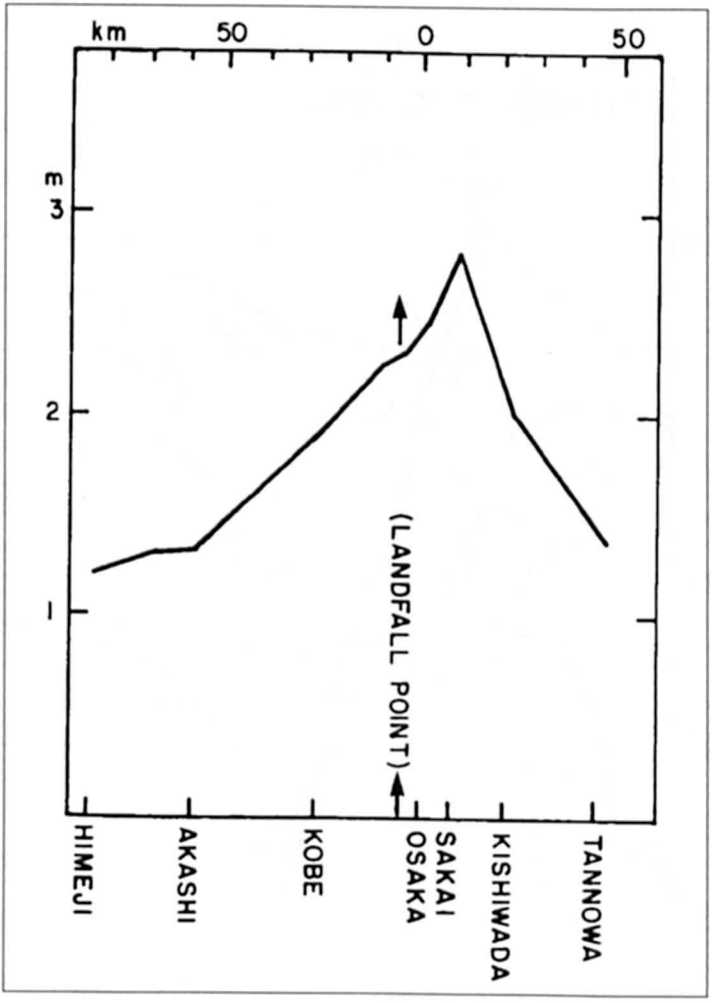

Fig. 6.103: Peak surge envelope at stations along Osaka Bay due to Typhoon Nancy of 1961 (DAS et al., 1978)

HAYAMI et al. (1955) performed hydraulic model experiments to study the propagation of a storm surge as a bore in the rivers and canals near Osaka City and concluded that the embankment under construction (1955) would provide some protection but not total protection from storm surges. MUROTA (1963) also performed hydraulic model studies for Osaka bay and concluded that construction of breakwater would actually increase the amplitudes of storm surges due to increased seiche action. UNEO (1981) used SPLASH and also a numerical model to simulate the storm surge of August 21, 1970, in Tosa Bay, which produced surges up to 2 m in amplitude. He also used a two-layer model to include the effect of stratification.

MINATO (1998) numerically simulated storm surges in Tosa (Fig. 6.104) making use of the three-dimensional terrain following Princeton Ocean Model (POM) with horizontally uniform stratification in the area of Tosa bay. Finer Resolution in the vertical direction and stronger stratification generates slightly greater peak surges.

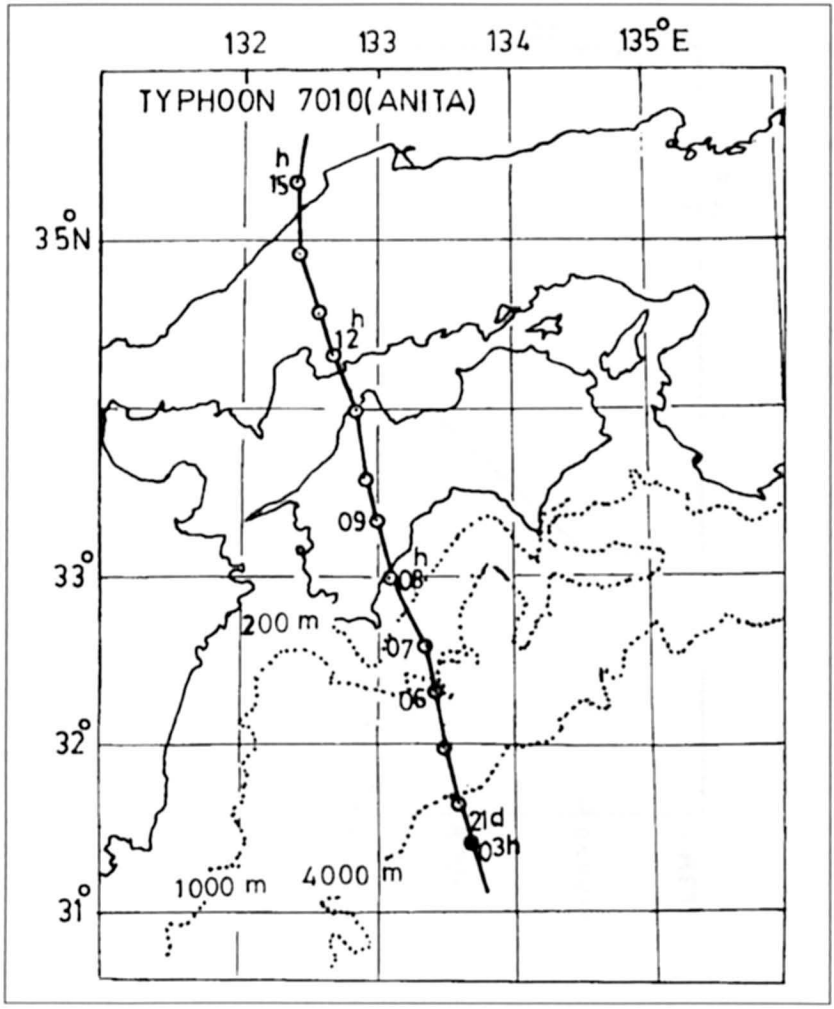

Fig. 6.104: Typhoon 7010 track (MINATO, 1998)

6.8.3 South Korea

Storm surges are not a serious problem in the Sea of Japan. Hence, the west coast of Japan and the east coast of Korea are not prone to major storm surges. However, storm surges occur in the Yellow Sea and the Po Hai Sea. Thus, storm surges on the west coast of Korea deserve attention.

On the southern part of the Korean peninsula, the tidal range in the Yellow Sea is about 4 m and it increases to about 10 m in the northern part (AN, 1980). The typhoons that pass over Korea are usually less severe than those that affect Japan.

The observed storm surge at Inchon (tidal range here is about 7 m) during August 30–31, 1979, due to Typhoon Billie is shown in Fig. 6.105. The track of this typhoon is shown in Fig. 6.106. AN (1980) used a two-dimensional numerical model to simulate this storm surge. The range (trough to crest) of the storm surge at Inchon was about 1.4 m. At Mokpo and Kunsan;

the range was only about 0.4 m. On July 29, 1965, a storm that struck the west coast of Korea generated an unusually large surge of 5.2 m (DAS et al., 1978).

CHOI (1987) developed numerical models for tides and surges in the Yellow Sea with application to South Korea. OH et al. (1988) studied storm surges due to typhoons passing through the south sea of Korea. Making use of data from eight tidal stations, they showed that surges have greater amplitudes generally for the western stations as compared to eastern stations also negative surges are more predominant for the western area.

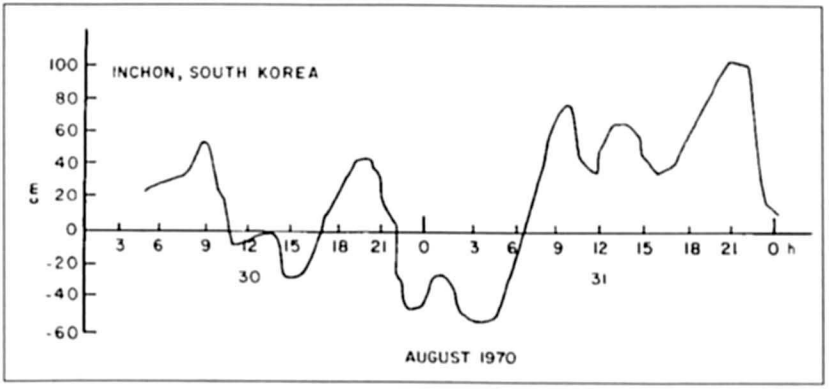

Fig. 6.105: Storm surge at Inchon, South Korea during August 30–31, 1970, due to Typhoon Billie. Time is Korean Standard Time (AN, 1980)

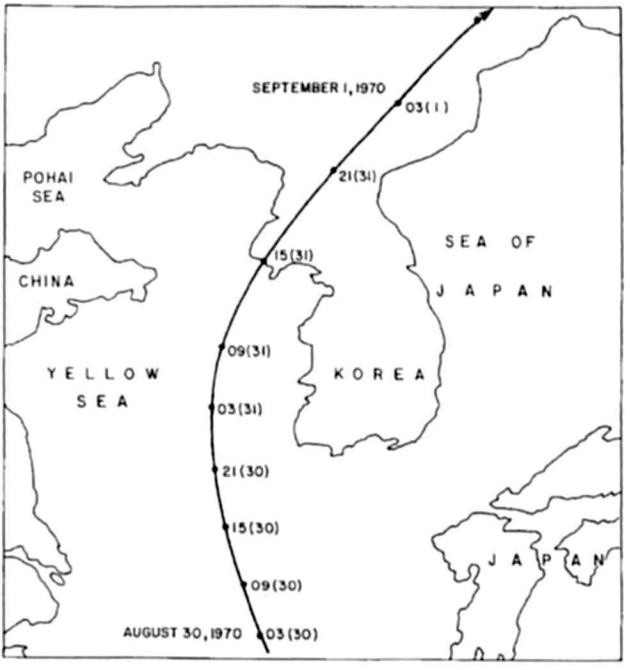

Fig. 6.106: Track of Typhoon Billie during August 30– September 1, 1970. Time is Korean Standard Time. Numbers in the parentheses are the dates (AN, 1980)

SHIN (1994) studied storm surges on the coast of South Korea. Table 6.55 lists the typhoons for the period 1904 to 1983. Fig. 6.107 shows the tracks of the typhoons coming from various directions. Table 6.56 lists the frequency and percentage of typhoon approach from different directions. Table 6.57 lists the peak surge amplitudes at various locations.

Table 6.55: The temporal distribution of the major storms around the Korean Peninsular during the years 1904–1983

Year	May	Jun.	Jul.	Aug.	Sep.	Oct.	Total	Year	May	Jun.	Jul.	Aug.	Sep.	Oct.	Total
1904				2			2	1945			1	2	1		4
1905			1	1	1		3	1946			1	2			3
1906				1	1	1	3	1947							0
1907			2		1		3	1948			1	1	2		4
1908				1			1	1949		1	2	1			4
1909				2			2	1950		2	1	3	2		8
1910			1				1	1951				1	1	1	3
1911			2	1	1	1	5	1952		1	1	1	1		4
1912			1				1	1953		1	1	1			3
1913			1				1	1954				1	2		3
1914		1	2	1	2		6	1955			2		1		3
1915			1	1	1		3	1956				1	3		4
1916				1	1		2	1957		1		1			2
1917				1	2		3	1958					1		1
1918			1	2			3	1959			2	1	4		7
1919				3	1		4	1960			1	2			3
1920							0	1961	1		1	1	1	1	5
1921					2		2	1962			1	2	1		4
1922			2		2	1	5	1963		1	1	1			3
1923		1	1	2			4	1964			3	1			4
1924			1	3			4	1965			1	2			3
1925			3	1	1		5	1966				2	1		3
1926			1	2			3	1967			1				1
1927				1	1		2	1968			1	1	1		3
1928					2		2	1969					1		1
1929				1			1	1970			2	2			4
1930			2	1			3	1971				2	1		3
1931			2	1			3	1972			2	1	1		4
1932				2			2	1973			2	1			3
1933			3	1	2		6	1974			2	1	1		4
1934			1	1	1		3	1975			1	1			2
1935				1	1		2	1976			3	2	1		6
1936			1	2	1		4	1977				1	1		2
1937			1		1		2	1978		1		2	1		4
1938				1	1		2	1979				2			2
1939			1	1			2	1980			1	1	1		3
1940			2	1	2		5	1981		2	1		2		5
1941			1	2			3	1982				3	1		4
1942			1	3			4	1983					1		1
1943			3	1			4	Total	1	12	72	94	63	5	247
1944				1			1								

Table 6.56: The frequency and percentage of storms, which were grouped by their routes

Group	Frequency	Percentage (%)
S	58	23
W	48	17
E	34	14
WE	27	11
CWEN	27	11
CWES	21	9
CWN	17	7
Others	20	8
Total	247	100

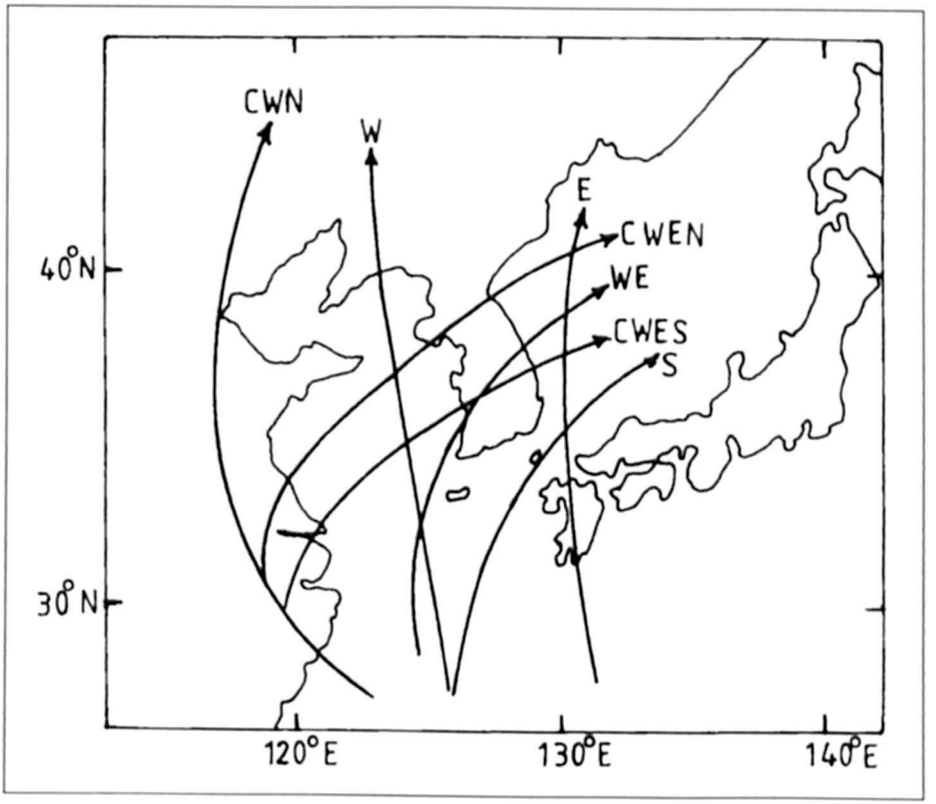

Fig. 6.107: Schematic representation of typhoon tracks (SHIN, 1994)

Table 6.57: Maximum tidal deviation at each station during the years 1957–1970 (SHIN, 1994)

Year	Cheju		Taehuksan do		Mokp'o		Kunsan		Inch' on		Yosu		Chinhae		Pusan		Ulsan	
	Date	Ht.	Date	Ht.	Date	Ht.	Date	Ht.	Date	Ht.	Date	Ht.	Date	Ht.	Date	Ht.	Date	Ht.
1959					7-Feb	120	5-Dec	90	19-Dec	70			18-Sep	*110				
1960					19-Jan	60							21-Mar	80				
1961					6-Feb	70	17-Dec	140	29-Aug	80			4-Apr	80				
													17-Dec					
1962					16-Nov	80	7-Mar	110	10-Apr	80								
1963					25-May	57	5-Dec	95	7-Jul	62			3-Jan	40				
													20-Jun					
1964	21-Aug	60			2-Apr	58	12-Jan	62	21-Aug	73			7-Apr	40			21-Dec	60
													12-Aug					
1965	6-Jun	60			10-Jan	48	18-Mar	58	10-Jan	88	6-Jun	82	2-Jan	40	2-Jan	27		
1966	22-Aug	*102	14-Oct	53	18-Mar	54	6-May	95	27-Jul	79	*24 Aug	110	17-Apr	40	Sep	26	11-Sep	40
																	3-Jul	
1967	27-Jan	34	8-Oct	98	15-Apr	54	8-Apr	32	14-Dec	87	30-Apr	70	11-Dec	40	29-Nov	29	3-Sep	30
													21-Aug	40				
1968	6-Dec	43	3-Sep	78	12-Mar	59	28-Jul	66	2-Jan	71	16-Mar	70	28-Nov		12-Dec	28		
													27-May	50				
1969	16-Apr	39	19-Oct	73	28-Mar	62	28-Apr	65	12-Jun	53	25-Apr	40	31-Oct		24-May	28		
															6-Jun			
1970	30-Aug	*69	30-Aug	*112	30-Aug	*92	12-Jan	98	31-Aug	*79	30-Aug	88	31-Aug	*40	30-Jan	30	6 Jul	30
																	16-Aug	

* Tidal deviation caused by typhoon. ____ Same month

6.8.4 Philippines

Philippines is an archipelago of about 7,100 islands located between the South China Sea and the Pacific Ocean and the Southeast Asian continental shelf (BROWN et al., 1991). Its coastline of 17,460 km makes it particularly vulnerable to storm surges as it lies in the path of destructive typhoons.

During the period 1907–31, there were 43 significant storm surges in the Philippines (DAS et al., 1978). A storm of October 15–16, 1912, struck the towns of Leyte and Cebu and apparently caused 9-m surges at Sogod Norte in the Lisayan Islands. Typhoon Irma of October 24–26, 1981, caused major surges and destroyed one village.

Storm surges occur in the Sulu Sea, which is a water body on the southeastern corner of the South China Sea. Surges up to 1.22 m in amplitude and with periods of up to 75 min occur in this water body (HAIGHT, 1928).

Fig. 6.108 shows the various regions of Philippines considered in the study by BROWN et al. (1991). Fig. 6.109 shows the intensity map of strongest typhoons in Philippines. The intensity shown is the maximum wind speed in meters per second (mps) from any typhoon during this thirty year period. The historical distribution of storm surges around Philippines is shown in Fig. 6.110.

Table 6.58 lists the annual average landfall of typhoons in the regions shown in Fig. 6.108 whereas Tables 6.59 and 6.60 respectively show the probability of landfall of typhoons per year (in percent) and probability of at least one typhoon-crossing region. The average monthly frequency of typhoons for the period 1980 to 1989 is shown in Table 6.61. Tables 6.62 and 6.63 respectively list the vulnerability levels by region of typhoon hazards and annual typhoon damage and casualties.

Table 6.58: Annual average landfall of typhoons per region (BROWN et al., 1991)

Region	Latitude	Annual Average
Batanes (Region II)	19–22N	1.7
Northern Luzon (Regions I & II)	16–19N	2.7
Bicol and Quezon (Regions IV & V)	13–16N	1.9
Visayas (Regions VI & VII)	10–13N	1.9
Mindanao (Regions X, XI & XII)	7–10N	1.0
Total		9.2

Source: Philippine Atmospheric, Geophysical and Astronomical Services Administration (PAGASA)

Table 6.59: Probability of landfall of typhoons per year (in percent) (BROWN et al., 1991)

At least one	100
2 or more	100
3 or more	100
4 or more	100
5 or more	94
6 or more	77
7 or more	71
8 or more	64
9 or more	48
10 or more	39

Source: PAGASA

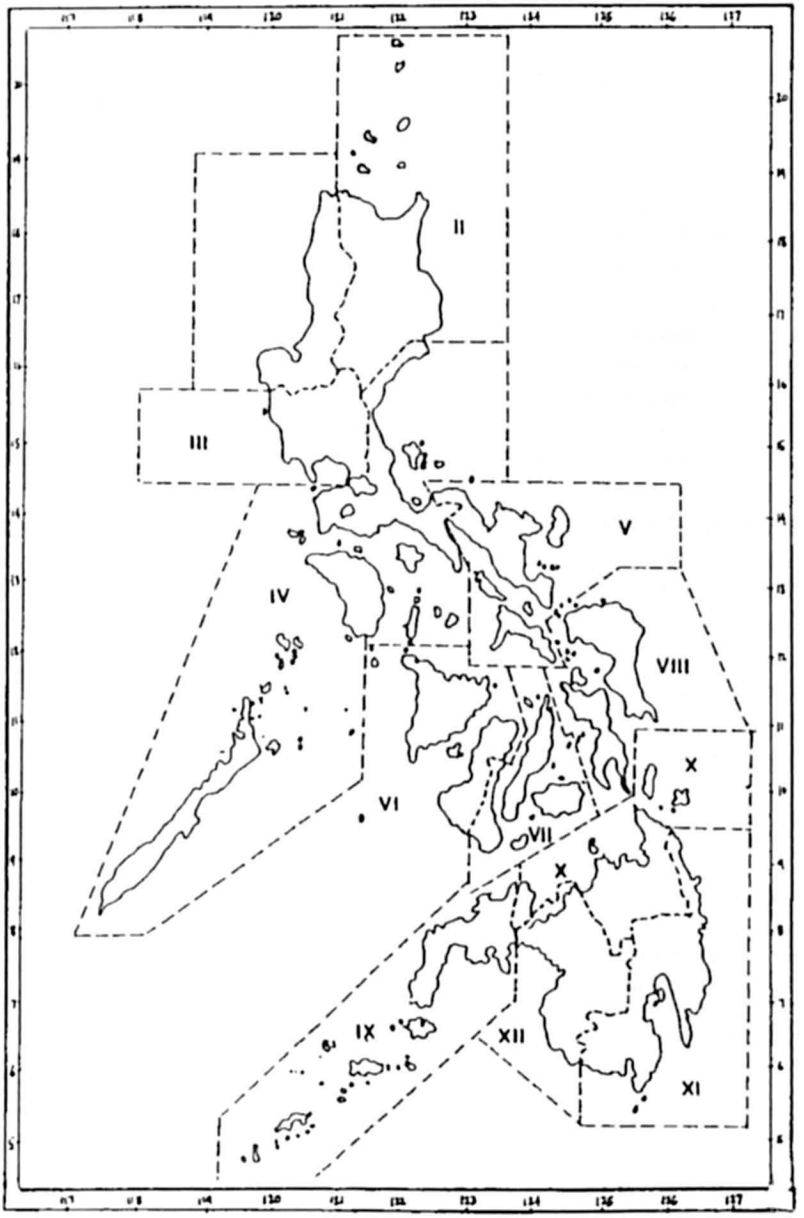

Fig: 6.108: Various regions of Philippines from the point of view of typhoons (BROWN et al., 1991)

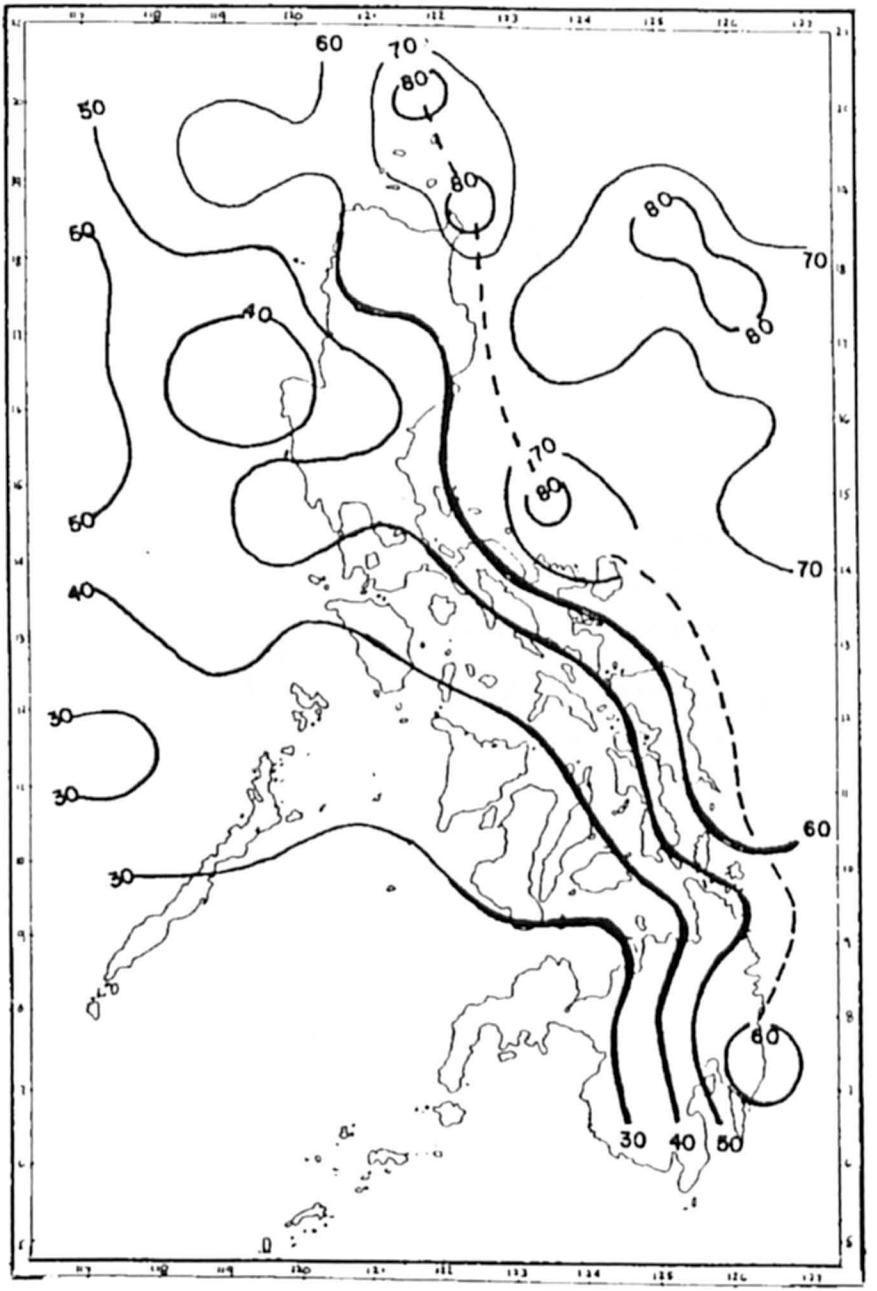

Fig. 6.109: Intensity (mps) of strongest typhoon, which passed every degree latitude – longitude square from 1960–1989 (BROWN et al, 1991)

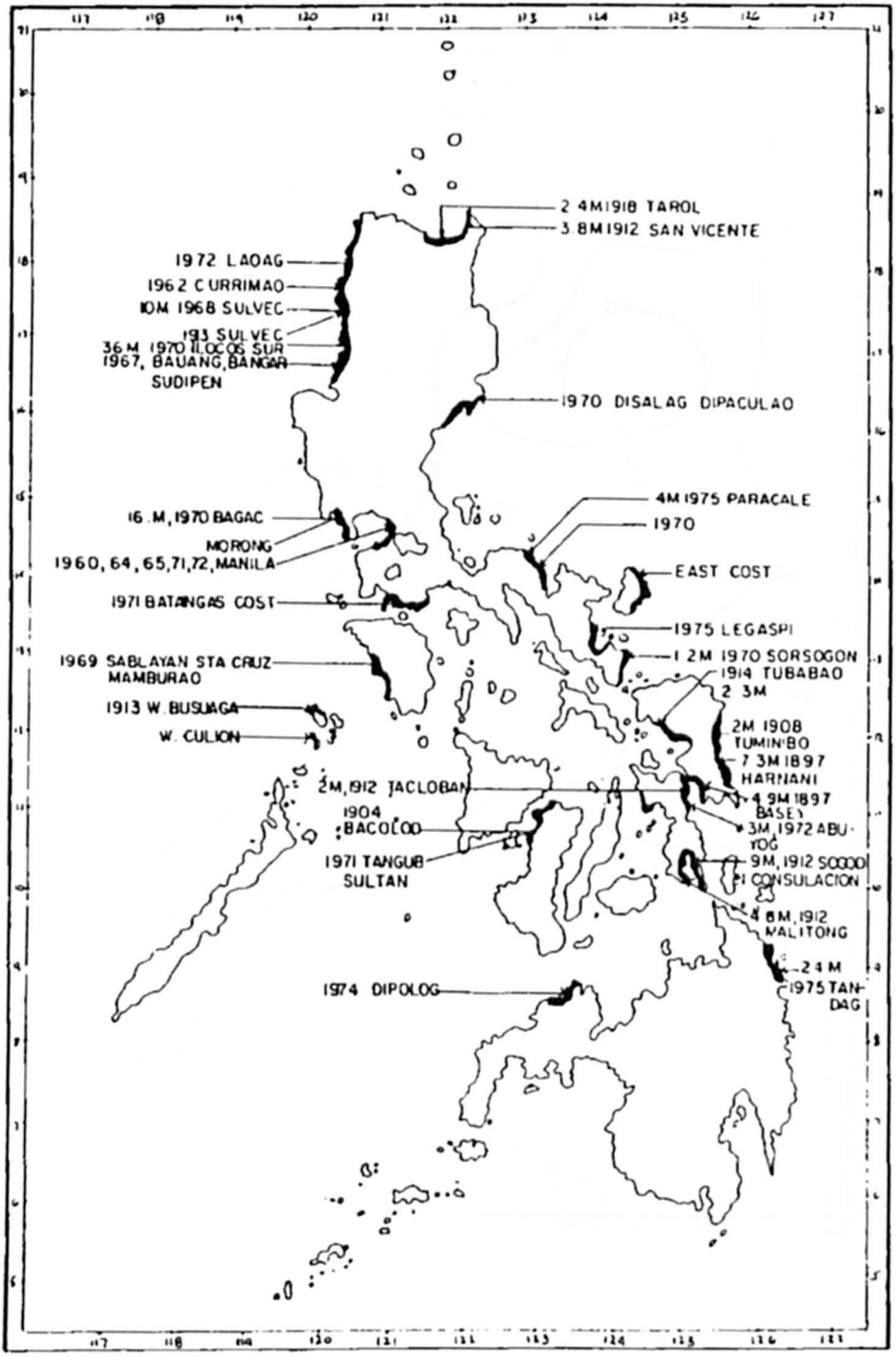

Fig. 6.110: Historical storm surges in the Philippines (BROWN et al., 1991)

Table 6.60: Probability of at least one typhoon crossing a region (BROWN et al., 1991)

Region	Probability (%)
Batanes (Region II)	90
Northern Luzon (Regions I & II)	87
Bicol and Quezon (Regions IV & V)	74
Visayas (Regions VI & VII)	87
Mindanao (Regions X, XI & XII)	58

Source: PAGASA

Table 6.61: Average monthly frequency of typhoons (1980–1989) (BROWN et al., 1991)

Months	Average frequency of typhoons	Probability of at least one typhoon making landfall (in percent)	Average frequency of making landfall
January	0.4	23	0.4
February	0.3	3	0.1
March	0.3	10	0.3
April	0.2	5	0.2
May	0.8	20	0.3
June	1.7	48	0.6
July	3.6	58	1.1
August	3.1	74	1.2
September	2.6	74	1.4
October	3.4	55	1.3
November	2.2	84	1.7
December	1.6	48	0.6
Total	20.2	100	9.2

Source: PAGASA

Table 6.62: Vulnerability levels by region for typhoons hazards (BROWN et al., 1991)

Region	High Winds	Floods	Storm Surge
National Capital	H	H	L
I	H	M	M
II	M	H	M
III	H	H	M
IV	H	M	H
V	H	H	H
VI	M	M	M
VII	M	L	M
VIII	H	M	H
IX	L	L	L
X	H	H	H
XI	M	M	L
XII	n.a	H	n.a
Cordillera[A/]	H	n.a	n.a

n.a. Not Applicable
A/ Prior to 1989, CAR was part of Region I
Source: Table composed by consultants

Table 6.63: Annual typhoon damage and casualties (BROWN et al., 1991)

	Billions of Pesos	(in Lives Lost current Prices)
1980	1.4	143
1981	1.3	484
1982	1.6	337
1983	0.5	126
1984	5.8	1979
1985	2.7	211
1986	1.7	171
1987	4.0	1020
1988	8.7	429
1989	4.5	382
Total	32.2	5282
Average	3.2	528

Source: Office of Civil Defense (OCD)

6.8.5 Vietnam

Storm surges occur on the east coast of North Vietnam and on the east and south coasts of South Vietnam. NICKERSON (1971) used SPLASH models to study these surges. One of the worst storm surges in human history occurred in 1881 in which about 300,000 people were killed in the area surrounding Haiphong (LACOUR, 1917c).

IMAMURA and TO (1997) studied storm surges and other natural disasters in Vietnam for the period subsequent to 1997. Fig. 6.111 shows the cost of natural and human made disasters in Vietnam for this period whereas Fig. 6.112 shows the damage due to typhoons. Fig. 6.113 shows the areas affected by floods and storm surges. Fig. 6.114 shows the tracks of typhoons Andy and Cecil in 1995, which devastated Central Vietnam. Fig. 6.115 shows the dyke system of Vietnam for protection against storm surge inundation and floods.

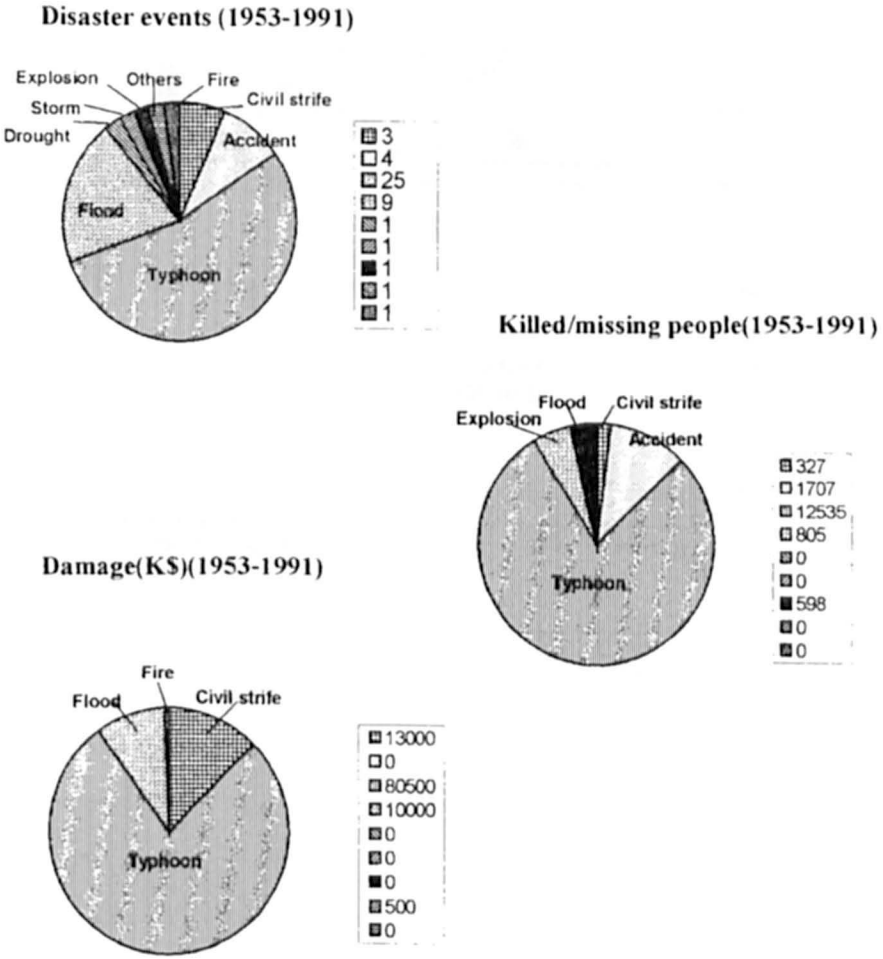

Fig. 6.111: Estimated damage caused by man-induced and natural disasters in Vietnam (1953–1991) (IMAMURA and TO, 1997)

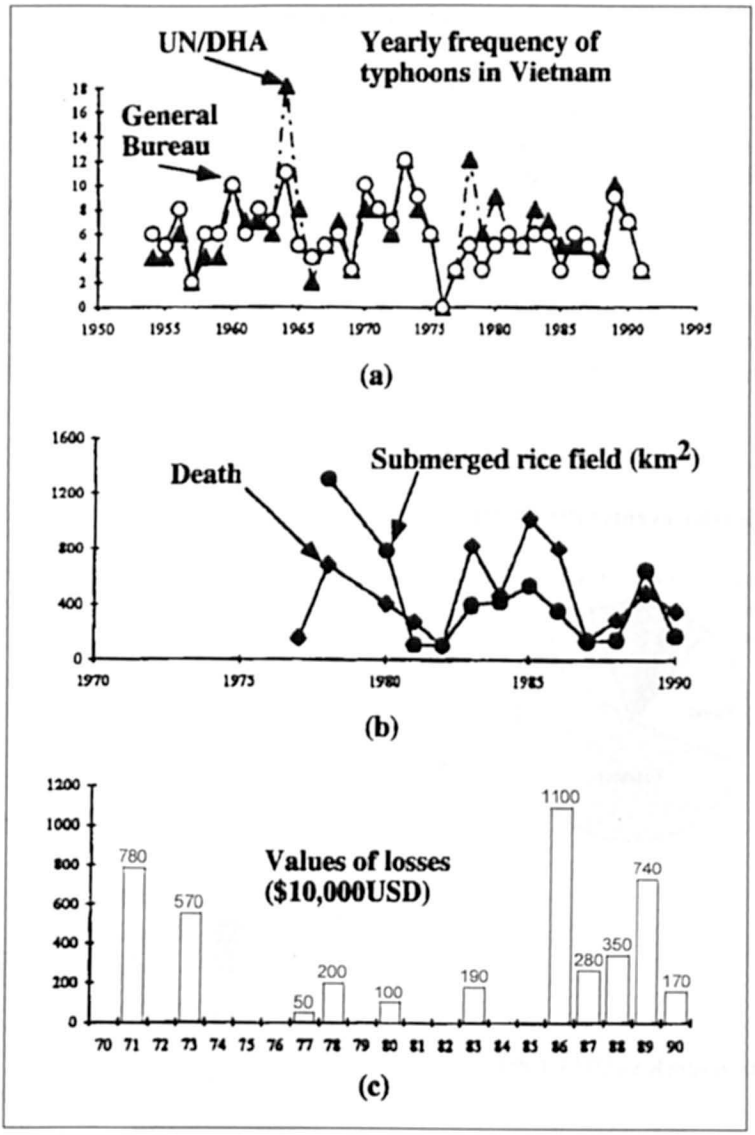

Fig. 6.112: (a) Frequency of typhoons and (b) flood damage death, submerged rice field, and (c) value of losses (IMAMURA and TO, 1997)

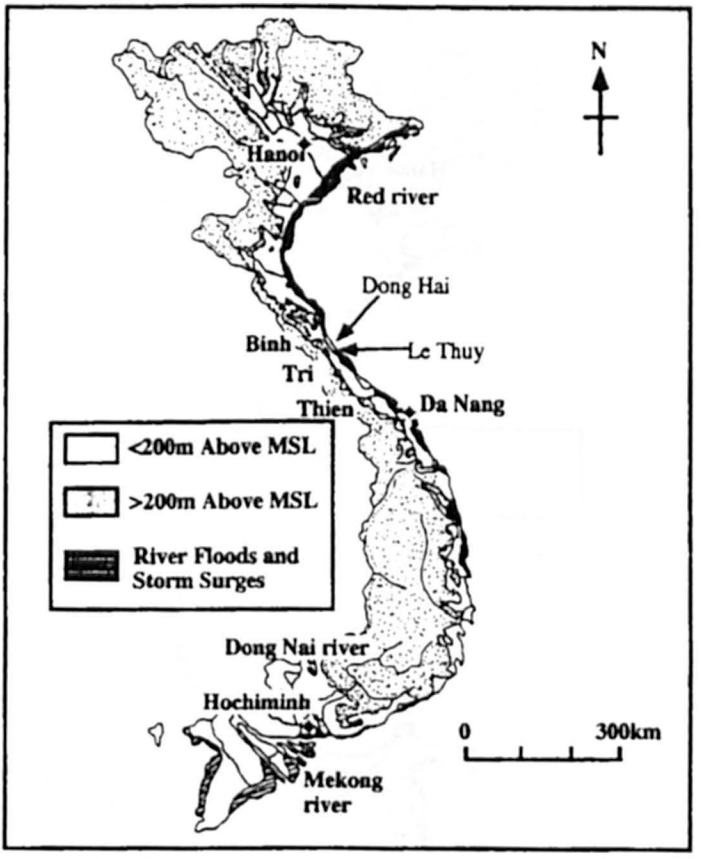

Fig. 6.113: Topography of Vietnam with elevation above sea level and areas damaged by river floods and storm surges shown by the horizontal shades (IMAMURA and TO, 1997)

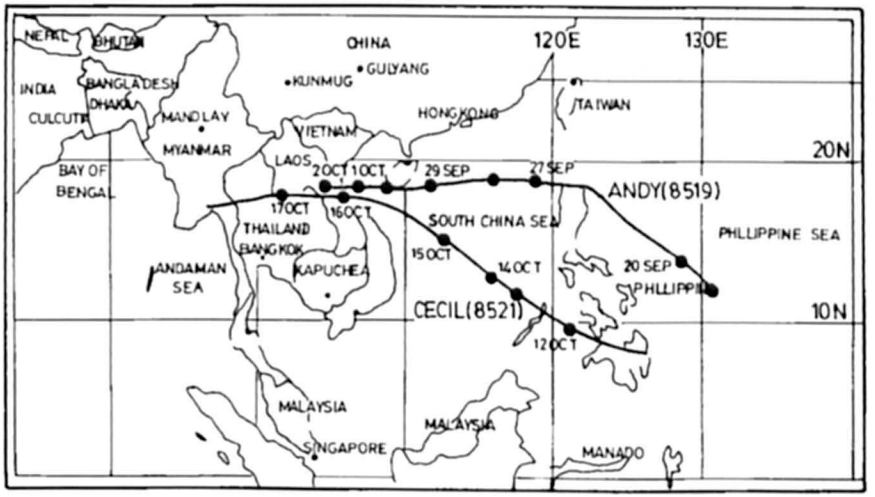

Fig. 6.114: Map of Vietnam, located in eastern Indo-China and the route of typhoons, Andy and Cecil in 1985, which devastated central Vietnam (IMAMURA and TO, 1997)

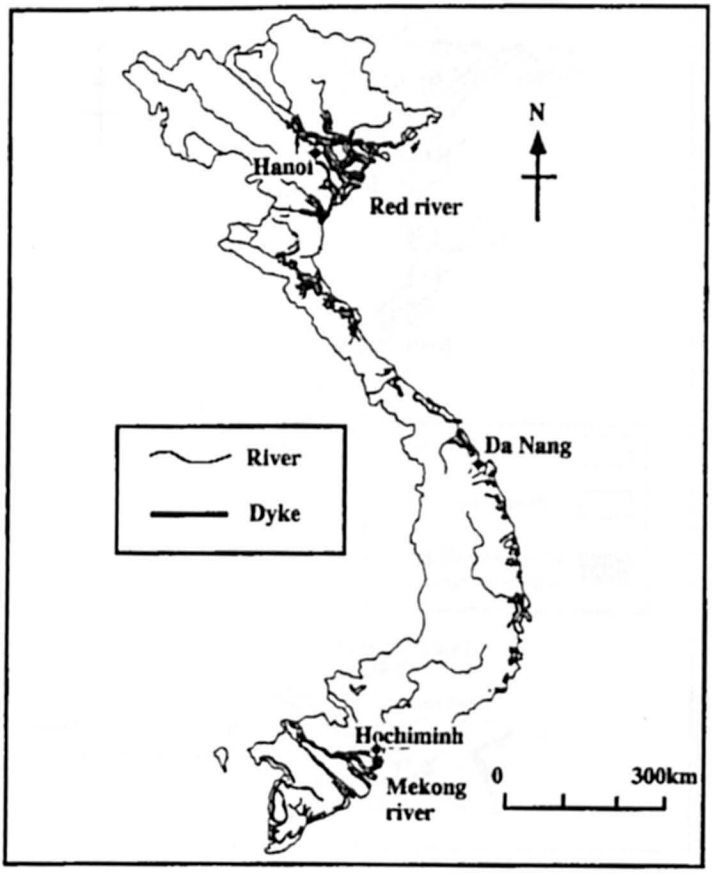

Fig. 6.115: Dike system in Vietnam along river and coasts. The system started more than 2000 years ago (IMAMURA and TO , 1997)

Table 6.64 compares the frequency of typhoons in various Southeast Asian countries. Table 6.65 and 6.66 respectively show the monthly frequency of typhoons during the period 1954 to 1991 and those that struck various districts.

Table: 6.64: Frequency of typhoons in the Southeast Asian countries in 1985–1989 (IMAURA and TO, 1997)

Country	1985	1986	1987	1988	1989	Total
China	8	6	4	4	11	33
Philippines	4	6	5	5	7	27
Japan	10	2	3	4	4	23
Rep. Of Korea	8	3	2	0	1	14
Vietnam	2	1	3	2	4	12
Hong Kong	2	3	1	3	2	11
Thailand	1	1	2	0	1	5
Malaysia	0	1	0	2	0	3
Total	17	11	12	12	19	71

Table 6.65: Monthly frequency of typhoons in Vietnam in 1954–1991 (IMAURA and TO, 1997)

Period	Jan	Feb	Mar	Apr	May	Jun	Jul	Aug	Sep	Oct	Nov	Dec	Total	Average
1954–59	0	0	0	1	1	4	3	9	7	5	2	1	33	5.5/yr.
1960–69	0	0	0	0	1	6	8	15	17	9	8	1	65	6.5/yr.
1970–79	0	0	0	0	–	6	7	11	15	10	10	4	63	6.3/yr.
1980–89	0	0	2	1	1	6	5	5	9	21	5	0	54	5.4/yr.
1990–91	0	0	1	0	0	0	1	2	1	3	2	0	10	5.0/yr.
Total	0	0	3	2	3	22	24	42	48	48	27	6	225	5.9/yr.

Table 6.66: Monthly frequency of typhoons, which struck the district regions of Vietnam (1954–1991) (IMAMURA and TO, 1997)

Region	Jan	Feb	Mar	Apr	May	Jun	Jul	Aug	Sep	Oct	Nov	Dec	Total
Northern	0	0	0	0	0	15	24	28	22	7	1	0	97
Central	0	0	0	1	2	0	0	14	23	35	6	0	81
Southern	0	0	3	1	1	7	0	0	3	6	20	6	47
Total	0	0	3	2	3	22	24	42	48	48	27	6	225

6.8.6 Thailand

VONGVISESSOMJAI (1994) studied storm surges in the upper Gulf of Thailand. Table 6.67 lists the characteristics of historic cyclones for this region. Fig. 6.116 shows the position of the inter tropical convergence zone (ITCZ) at three different times in the year and typhoon approach directions. Fig. 6.117 shows the typhoon tracks for the month of October for the period 1961 to 1970 whereas Fig. 6.118 shows the tracks of tropical cyclones for the period 1952 to 1974. The recurrence interval of maximum wind velocity and central pressure index for cyclones affecting the Gulf of Thailand is shown in Fig. 6.119.

Table 6.67: Historical cyclone characteristics (VONGVISESSOMJAI, 1994)

No.	Year, Month, Date		Name	CPI or P_0 (millibars)	Max. Velocity U_{max} (mph)	Forward Speed, V_F (miles/hr)	Radius, R (nautical miles)
1	1952	Oct 21–22	VAE	990	53	14.97	6.7
2		Oct 24–25	TRIX	998	44	17.27	60
3	1960	Oct 3–4	–	992	52	3.45	8.4
4	1962	Jul 12–13	–	990	53	18.45	10.6
5	1966	Jun 17–18	–	–	–	12.67	–
6		Oct 25–26	–	990	48	9.21	49
7	1967	Jun 16–27	–	978	62	12.67	140
8		Oct 5–6	–	996	49	11.52	16
9		Oct 9–10	–	998	44	17.27	90
10		Nov 10–11	–	–	–	12.67	–
11	1968	Sep 5–6	BESS	992	44	2.3	115
12		Oct 21–22	HESTER	998	46	11.52	10
13		Jun 24–25	–	998	46	6.91	7.5
14		Sep 20–21	–	992	51	12.67	57
15		Nov 2–3	–	1000	45	16.12	10
16	1970	Sep 20–21	–	994	52	13.82	20
17		Oct 25–26	KATE	1000	27	13.82	314
18		Nov 29–30	RUTH	1000	42	11.52	32
19	1972	Jun 3–4	NAMIE	990	48	6.91	123
20		Sep 6–7	–	990	49	4.61	16
21		Sep 18–19	–	–	–	–	–
22		Dec 4–5	SALLY	994	50	5.76	5
23	1973	Nov 12–13	–	1002	38	5.76	4
24		Nov 17–18	THELMA	998	45	5.76	39
25	1974	Oct 9–10	–	1002	34	6.91	15
26		Nov 5–6	–	998	45	13.82	60

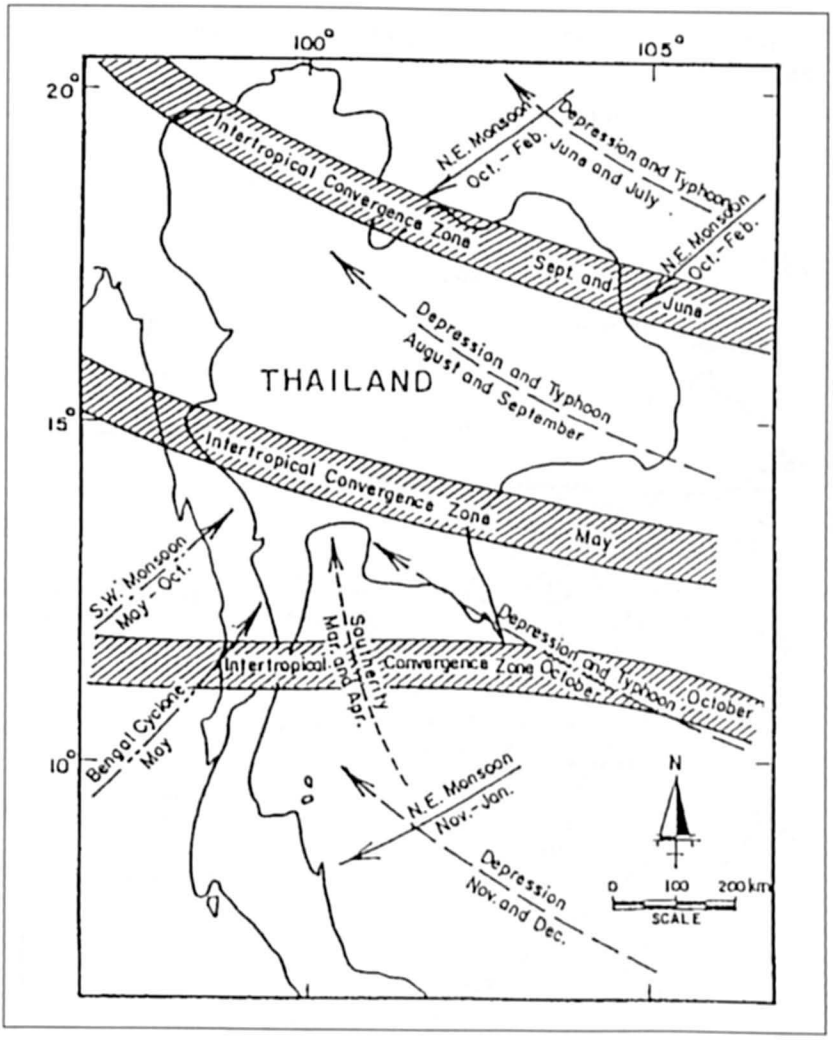

Fig. 6.116: Monsoon and storm tracks in Thailand (VONGVISESSOMJAI, 1994)

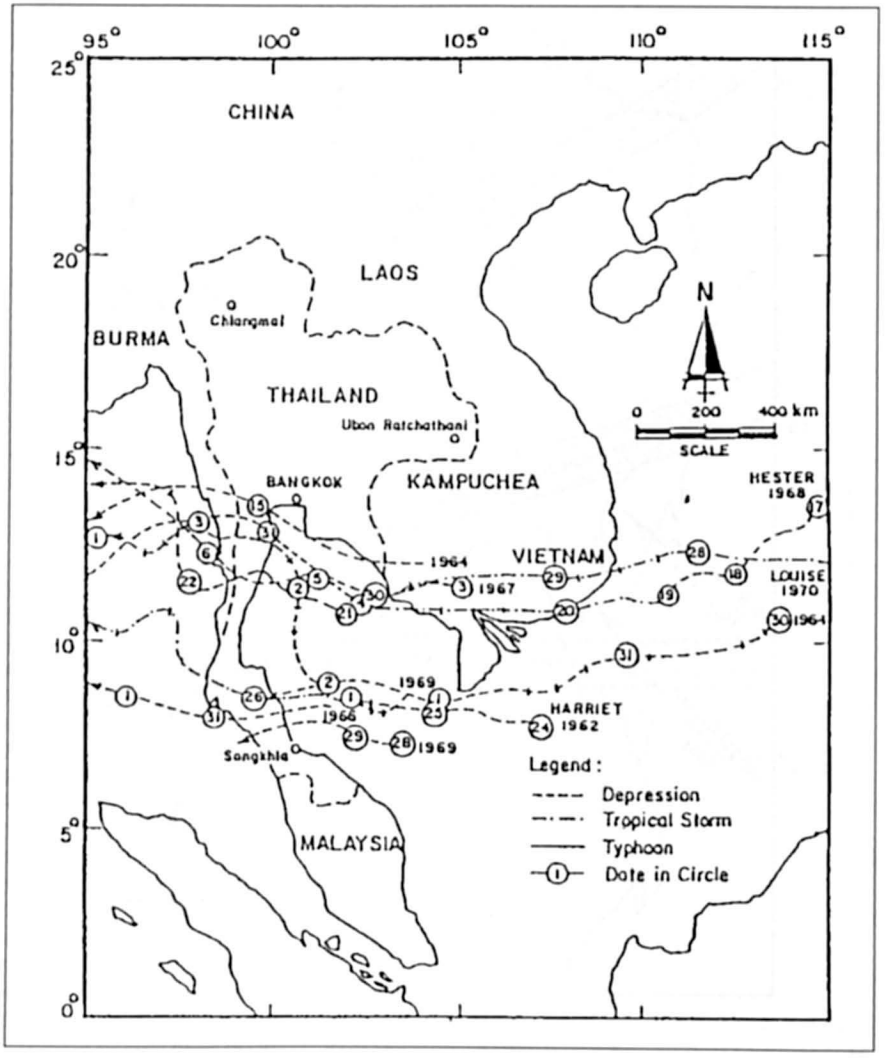

Fig. 6.117: Tracks of cyclones over the Gulf of Thailand in October 1961 to 1970 (VONGVISESSOMJAI, 1994)

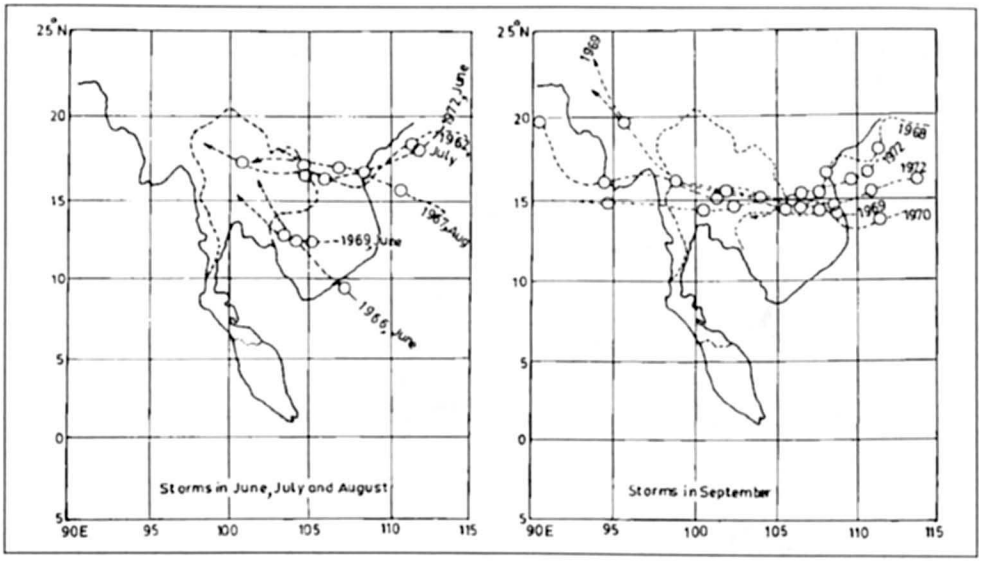

Fig. 6.118: Tracks of tropical cyclones over the Gulf of Thailand and its vicinity between 1952–1974 A. D. Encircled numbers are the positions of storm centers at 7 am on the days shown (VONGVISESSOMJAI, 1994)

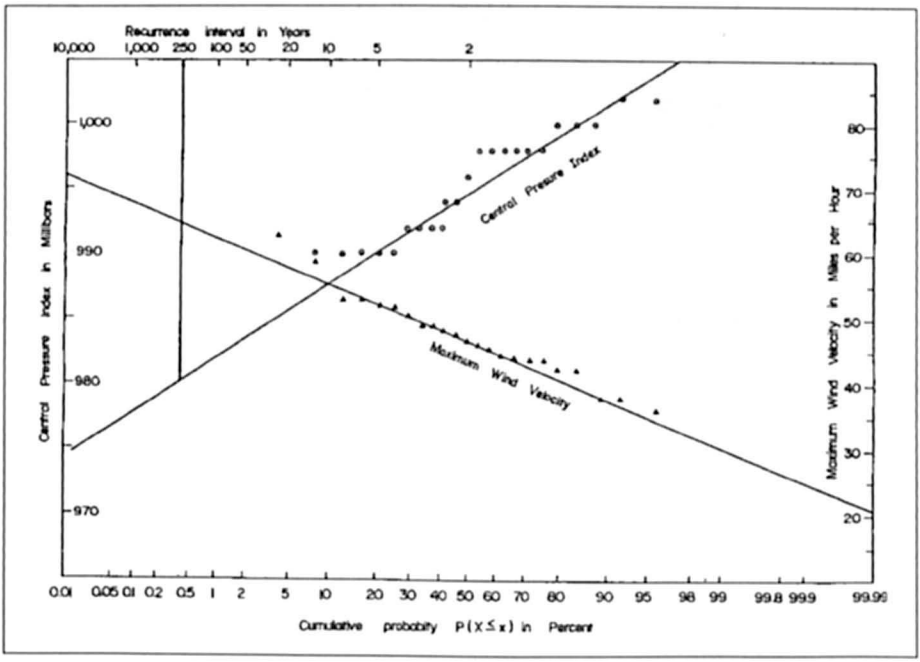

Fig. 6.119: Recurrence interval of cyclone characteristics for the Gulf of Thailand (VONGVISESSOMJAI, 1994)

Fig. 6.120 shows the wind field for the probable maximum cyclone (PMC) for the Gulf of Thailand. Figs. 6.121 and 6.122 respectively show the peak surge and maximum wind wave at Aophai for the PMC and a 250 year typhoon.

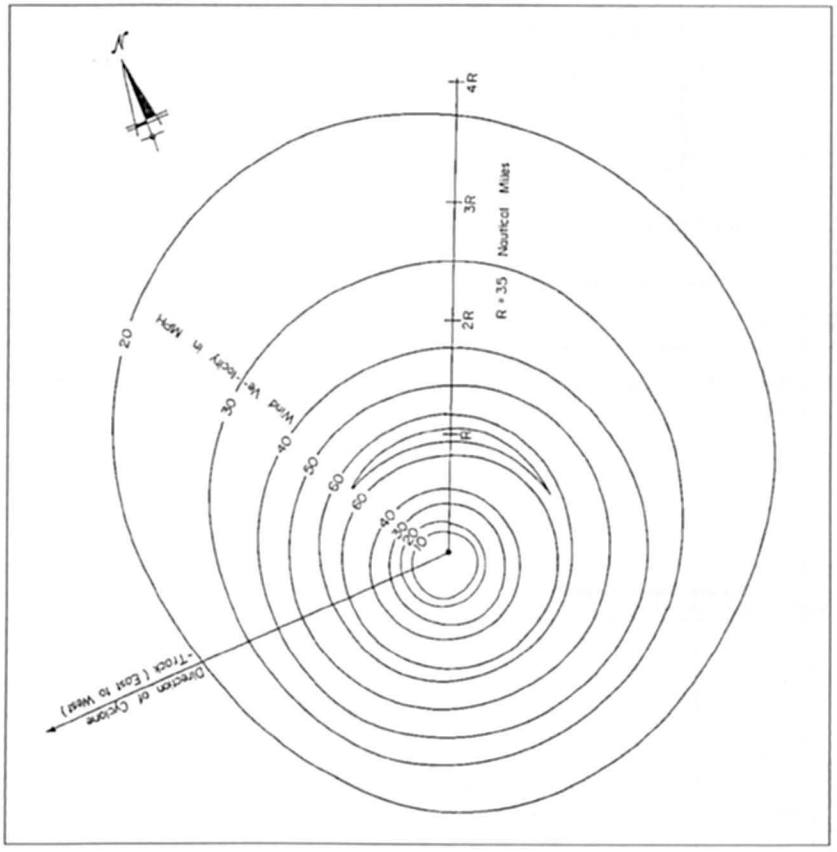

Fig. 6.120: Wind field of the probable maximum cyclone for the Gulf of Thailand (VONGVISESSOMJAI, 1994)

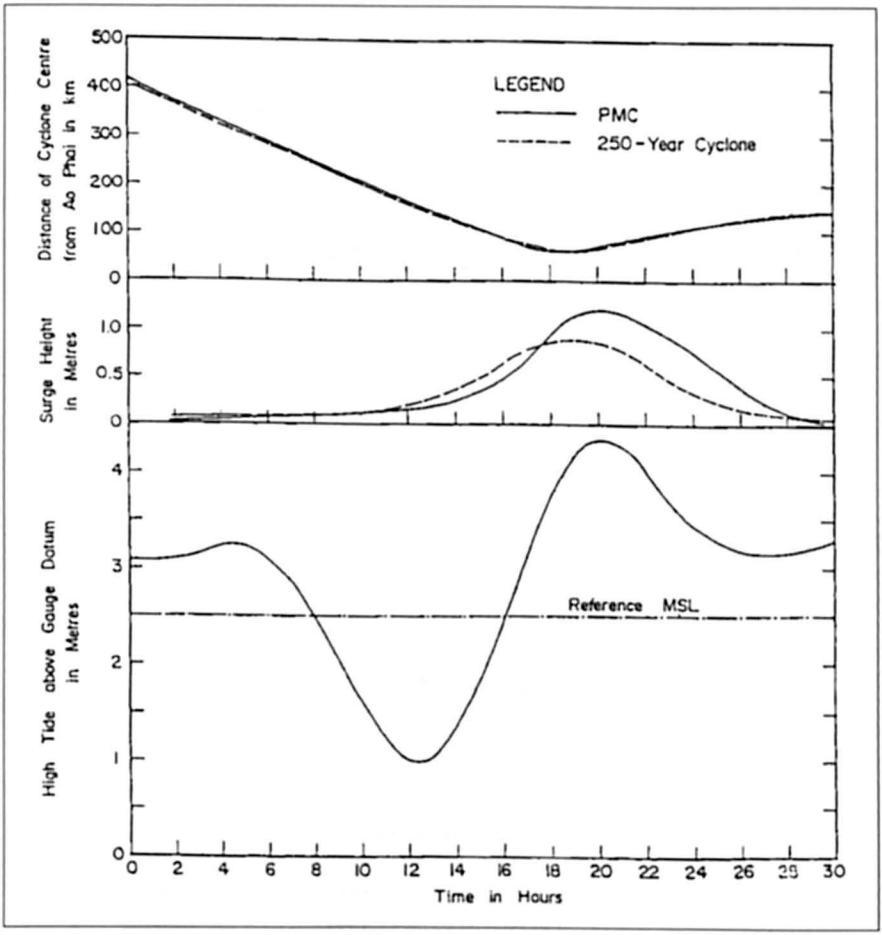

Fig. 6.121: Probable maximum cyclonic surge (PMC & 250 year) and high tide at Ao Phai (VONGVISESSOMJAI, 1994)

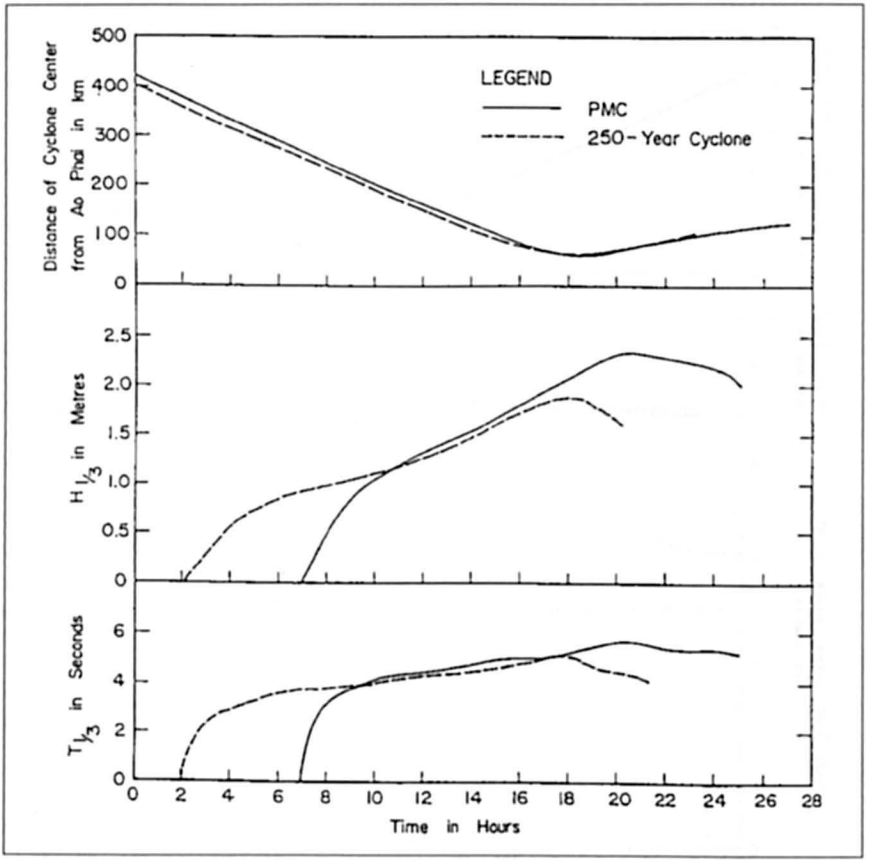

Fig. 6.122: Probable maximum wind wave (PMC & 250 year) at Ao Phai (VONGVISESSOMJAI, 1994)